



Centre for Sensors, Instruments and  
Systems Development  
UNIVERSITAT POLITÈCNICA DE CATALUNYA  
Shaping light to your needs

## DOCTORAL THESIS

FOR OBTAINING THE DOCTORAL DEGREE IN THE FIELD OF OPTICAL  
ENGINEERING FROM THE  
**UNIVERSITAT POLITÈCNICA DE CATALUNYA**  
DEPARTMENT OF OPTICS AND OPTOMETRY

---

**Development of new methodologies for the clinical, objective  
and automated evaluation of visual function based on the  
analysis of ocular movements. Application in visual health**

---

Author:

**CLARA MESTRE FERRER**

Supervisors:

Dr. JAUME PUJOL RAMO

Dr. JOSSELIN GAUTIER

Terrassa, 2019

## **Supervisors' certificate**

Dr. **Jaume Pujol Ramo**, professor at the Universitat Politècnica de Catalunya (UPC), and Dr. **Josselin Gautier**, postdoctoral researcher at the University of California

### **CERTIFY**

that the work reported in the thesis entitled

**Development of new methodologies for the clinical, objective and automated evaluation of visual function based on the analysis of ocular movements. Application in visual health**

which is submitted by Clara Mestre Ferrer in fulfilment of the requirements for the degree of Doctor by the Universitat Politècnica de Catalunya (UPC) has been carried out under our supervision within the framework of the PhD program in Optical Engineering of the same university.

Jaume Pujol Ramo

Josselin Gautier

Terrassa, 2019

Terrassa, 2019

## Acknowledgments

I feel deeply grateful to all people who have surrounded me during the last three years. To express my most sincere feelings, I would like to thank them in Catalan except those who could not understand my words.

Jaume, gràcies per haver confiat en mi des de molt abans de començar el doctorat. Aquell camí que em vas plantejar a tercer de carrera i que llavors em quedava tan lluny s'està a punt d'acabar. Gràcies per donar-me l'oportunitat d'aprendre al teu costat i crèixer, tant professionalment com personalment. Sempre m'he sentit recolzada, i això ha sigut vital per seguir mirant endavant en els moments difícils.

Josselin, thanks for your exhaustive guidance. You settled the basis from which my knowledge of ocular movements has grown. Thank you for devoting part of your time in France and California to supervise my work despite of the distance. I guess it is not easy to keep connected to the work that is being done at 9500 km, and I really appreciate your effort.

Voldria agrair especialment al Fernando la seva ajuda per posar a punt els muntatges de la tesi i, sobretot, per estar sempre disposat a donar-me un cop de mà amb qualsevol cosa. També vull agrair al Carles la seva ajuda en diversos moments de la tesi. Has sigut un gran predecessor. Gracias Ana y Tommaso por ser tan buenos compañeros en este viaje. Nuestras risas han sido muy útiles. Gràcies, Marta, per tot el què hem compartit durant més de set anys dins a la universitat, a la feina, i també a fora. Gràcies a tots els companys del dRC i del CD6 per tenir una paciència infinita amb mi i estar sempre disposats a participar en múltiples sessions de mesura.

I would like to thank Harold Bedell for his generous collaboration in two studies of this thesis. I have learned a lot from our insightful discussions. Undoubtedly, I thank Rowan Candy for opening the door of her lab and her hospitality during those three months. I would like to thank her for giving me the opportunity to come back to Bloomington for a post-doc. I know it will be a great opportunity for me. I feel fortunate to know what will come in the future even before closing the PhD stage.

Aquesta tesi tampoc hauria estat possible sense la família i amics que m'han recolzat sempre.

Gràcies als meus pares per haver-me educat des de petita en la cultura de l'esforç, per transmetre'm que cal lluitar per aconseguir el que un vol. Estic convençuda que sense aquests valors hauria tirat la tovallola fa temps. Si sóc on sóc és en gran part gràcies a vosaltres. Gràcies també per donar-me sempre totes les facilitats que heu tingut al vostre abast, per creure en mi en tot moment i, per què no dir-ho, per aguantar el meu mal humor i poques paraules els vespres dels dies difícils.

## Acknowledgements

---

Gràcies, Anna, per ser la millor germana gran que podria tenir. Gràcies a tu i al Jepi per escoltar-me, animar-me, donar-me suport i per treure'm de casa quan, molt encertadament, heu cregut que necessitava una mica d'aire. Per molt lluny que vagi sempre us sentiré a prop.

Gràcies a totes les amigues que hi han sigut durant tot aquest temps, han confiat en mi i m'han ajudat a seguir mirant endavant.

Quan hi ha qui confia en tu, és més fàcil fer-ho bé.

Moltes gràcies! Thank you!

# Contents

<b>Contents .....</b>	<b>ix</b>
<b>List of figures .....</b>	<b>xiii</b>
<b>List of tables.....</b>	<b>xxiii</b>
<b>1. Introduction .....</b>	<b>1</b>
<b>2. Goals of the thesis.....</b>	<b>5</b>
<b>3. Structure of the thesis .....</b>	<b>7</b>
<b>4. State of the art .....</b>	<b>9</b>
4.1. General concepts and fundamental laws .....	9
4.1.1. Positions of gaze.....	9
4.1.2. Listing's law.....	9
4.1.3. Donders' law .....	10
4.1.4. Hering's law of Equal Innervation .....	10
4.1.5. Sherrington's law of Reciprocal Innervation .....	11
4.2. The oculomotor system .....	11
4.2.1. The extraocular muscles.....	11
4.2.2. Action of individual muscles.....	12
4.3. Binocular vision .....	14
4.3.1. Fusion, diplopia and retinal correspondence.....	14
4.3.2. Fixation disparity.....	16
4.3.3. Stereopsis .....	17
4.3.4. Binocular dysfunctions.....	17
4.4. Eye movements .....	19
4.4.1. Saccades .....	19
4.4.1.1. Metrics and dynamics of saccades .....	21
4.4.1.2. Latency .....	23
4.4.1.3. Corrective saccades .....	24
4.4.1.4. Neural control.....	25

4.4.2.	Vergence eye movements.....	28
4.4.2.1.	Stimuli to vergence movements .....	28
4.4.2.2.	Interactions between vergence and accommodation .....	30
4.4.2.3.	Dynamics of vergence .....	31
4.4.2.4.	Latency .....	33
4.4.2.5.	Neural control.....	34
4.4.2.6.	Saccade-vergence interactions .....	36
4.4.3.	Smooth pursuit .....	37
4.4.3.1.	Dynamics of smooth pursuit.....	38
4.4.3.2.	Latency .....	39
4.4.3.3.	Effect of prediction.....	39
4.4.3.4.	Neural control.....	39
4.4.4.	Fixational eye movements.....	41
4.4.4.1.	Tremor.....	42
4.4.4.2.	Drift .....	43
4.4.4.3.	Microsaccades .....	44
4.4.5.	Vestibular-Optokinetic eye movements .....	46
4.5.	Eye tracking techniques .....	47
4.5.1.	Electro-oculography .....	48
4.5.2.	Scleral search coils .....	49
4.5.3.	Video oculography .....	50
4.5.3.1.	Pupil and limbus detection .....	50
4.5.3.2.	Pupil-corneal reflection technique.....	51
4.5.3.3.	Dual Purkinje image eye-tracker .....	53
4.5.4.	Scanning Laser Ophthalmoscopy .....	54
<b>5.</b>	<b>Methodology and results.....</b>	<b>55</b>
5.1.	Study 1. Robust eye tracking based on multiple corneal reflections for clinical applications .....	55
5.1.1.	Introduction .....	55
5.1.2.	Methods.....	59
5.1.2.1.	Experimental methodology .....	59
5.1.2.2.	Image processing.....	60
5.1.2.3.	Gaze estimation .....	62

5.1.2.4.	Evaluation.....	64
5.1.2.5.	Statistical analysis .....	65
5.1.3.	Results .....	65
5.1.4.	Discussion .....	68
5.1.4.1.	Light sources configurations .....	68
5.1.4.2.	Normalization of the pupil-glint vectors .....	71
5.2.	Study 2. An automated and objective cover test to measure heterophoria.....	75
5.2.1.	Introduction .....	75
5.2.2.	Methods.....	78
5.2.2.1.	Subjects .....	78
5.2.2.2.	Materials and instrumentation .....	79
5.2.2.3.	Experimental procedure .....	80
5.2.2.4.	Eye-tracker data processing.....	82
5.2.2.5.	Statistical analysis .....	85
5.2.3.	Results .....	86
5.2.3.1.	Differences between 1-eye and 2-eyes methods .....	86
5.2.3.2.	Repeatability of ET method .....	87
5.2.3.3.	Agreement between CT, TH and ET methods .....	89
5.2.3.4.	Effect of motor ocular dominance on phoria.....	91
5.2.4.	Discussion .....	92
5.2.4.1.	Differences between 1-eye and 2-eyes methods .....	92
5.2.4.2.	Repeatability of ET method .....	93
5.2.4.3.	Agreement between CT, TH, and ET methods .....	95
5.2.4.4.	Effect of motor ocular dominance on phoria.....	97
5.3.	Study 3. Characteristics of saccades during the near point of convergence test .....	99
5.3.1.	Introduction .....	99
5.3.2.	Methods.....	101
5.3.2.1.	Subjects .....	101
5.3.2.2.	Instrument and visual stimulus.....	101
5.3.2.3.	Experimental procedure .....	102
5.3.2.4.	Eye movement data analysis .....	103
5.3.2.5.	Statistical analysis .....	104
5.3.3.	Results .....	105

## Contents

---

5.3.4.	Discussion .....	111
5.3.5.	Appendix A .....	114
5.3.5.1.	Correction of vertical eye-position traces .....	114
5.3.5.2.	Modification of the Engbert-Kliegl (E-K) algorithm .....	115
5.3.6.	Appendix B .....	116
5.4.	Study 4. Effects of stimulus' predictability on the vergence facility test: a preliminary study .....	123
5.4.1.	Introduction .....	123
5.4.2.	Methods .....	124
5.4.2.1.	Subjects .....	124
5.4.2.2.	Instrumentation and visual stimulus .....	126
5.4.2.3.	Experimental procedure .....	127
5.4.2.4.	Data analysis .....	128
5.4.3.	Results .....	131
5.4.4.	Discussion .....	136
6.	<b>Conclusions and future work .....</b>	<b>141</b>
7.	<b>Dissemination of results .....</b>	<b>145</b>
7.1.	Journal publications .....	145
7.2.	Papers in submission .....	145
7.3.	Oral presentations in conferences .....	145
7.4.	Poster presentations in conferences .....	145
8.	<b>References .....</b>	<b>147</b>

## List of figures

Figure 1.1. Schematic representation of the visual sensory pathway. F: fixation point. f: foveae. LGN: lateral geniculate nucleus. Source: (Schwartz, 2009).....	1
Figure 4.1. (A) Listing's plane and the axes of rotation of the eye (X,Y,Z). (B) Orientations of the eye when they rotate to secondary and tertiary positions and obey Listing's law. In tertiary positions, the eyes appear to rotate around the visual axis due to false torsion. Source: (Leigh & Zee, 2015). ....	10
Figure 4.2. Anterior (A) and superior (B) views of the extraocular muscles. Source: Modified from (Levin et al., 2011). .....	12
Figure 4.3. Orientation of the vertical rectus muscles (A) and the oblique muscles (B) in the orbit. Source: (Von Noorden & Campos, 2002). .....	13
Figure 4.4. Primary, secondary and tertiary actions of extraocular muscles. Source: Modified from (Carpenter, 1988). .....	14
Figure 4.5. Relative lines of direction. F, principal visual direction. N, secondary visual direction. When the eye rotates, the principal visual direction shifts accordingly to the new position of the fovea. Source: Modified from (S. B. Steinman, Steinman, & Garzia, 2000). ....	15
Figure 4.6. Schematic representation of the horopter and the Panum's fusional area. Source: (S. B. Steinman et al., 2000).....	16
Figure 4.7. (A) Duration versus magnitude (amplitude) of human saccadic eye movements. Source: (Bahill et al., 1975). (B) Typical velocity profiles of horizontal saccades ranging from 5 to 80°. Vertical bars represent $\pm 1$ standard deviation (SD). The small SD indicates that saccades were very reproducible. Source: (Collewijn et al., 1988a).....	22
Figure 4.8. Saccadic main sequence. Peak velocity versus magnitude (amplitude) of human saccadic eye movements. Source: (Bahill et al., 1975).....	22
Figure 4.9. Frequency histogram of 486 saccadic latencies. Source: (Noorani & Carpenter, 2016).	24
Figure 4.10. Human saccades of different sizes. The beginning of each movement is at time zero. Overshoot for lower amplitude saccades and undershoot for larger amplitude ones can be seen. Source: (Carpenter, 1988). .....	25
Figure 4.11. (A) The cerebral areas involved in the control of saccades are shaded in red. The brainstem (shaded in gray) is enlarged in panel (B) with a sagittal view. The different brainstem areas	

---

## List of figures

---

that control saccadic movements are represented schematically. V1: primary visual cortex. PPRF: paramedian pontine reticular formation. MLF: medial longitudinal fasciculus.....	26
Figure 4.12. Schematic representation of the neural pathways involved in the control of a rightward horizontal saccade. Red: excitatory circuit. Green: Inhibitory circuit. PPRF: Paramedian pontine reticular formation.....	27
Figure 4.13. Example of the firing rate of different neurons that control saccadic movements. Source: (Kandel, Schwartz, Jessell, Siegelbaum, & Hudspeth, 2013). .....	28
Figure 4.14. Simplified block diagram of a model of accommodation (upper branch) and vergence (lower branch) systems and their interactions proposed by Schor (1992). .....	31
Figure 4.15. (A) Phase plane plot showing peak velocity versus amplitude for a single vergence movement. A: amplitude of the fast component; $V_p$ : vergence peak velocity. Source: (Hung et al., 1994). (B) Main sequence of accommodative vergence elicited by three different stimuli (Aligned, Monoc Line and Binoc Line), disparity vergence (Disparity), and vergence responses to both disparity and blur cues (Blur + Disparity). The error bars show the SD of the means between subjects for Aligned and Disparity responses. SD for other conditions were similar but not shown for clarity. Source: (Maxwell et al., 2010). .....	32
Figure 4.16. (A) Response to a predictable stimulus. Vergence precedes the target jumps (arrows). (B) Response to an unpredictable stimulus. Vergence follows the target jumps. Source: Modified from (Kumar et al., 2002).....	34
Figure 4.17. (A) The cerebral areas involved in the control of vergence movements are shaded in red. The brainstem (shaded in gray) is enlarged in panel (B) with a sagittal view. The different brainstem areas that control vergence are represented schematically. V1: primary visual cortex. MT: medial temporal visual area. MST: medial superior temporal visual area. NRTP: nucleus reticularis segmenti pontis.....	35
Figure 4.18. Demonstration of pursuit velocity saturation, which becomes evident with target velocities above 93°/s. Source: (Meyer, Lasker, & Robinson, 1985).....	38
Figure 4.19. Sagittal view of the brainstem with the main areas involved in the control of smooth pursuit. The cerebral areas that project to these regions are represented in Figure 4.20. NRTP: nucleus reticularis segmenti pontis. DLPN: dorsolateral pontine nucleus.....	40

Figure 4.20. Schematic representation of the neural pathways involved in the control of smooth pursuit. Red: pathway involved in smooth pursuit initiation. Blue: pathway involved in sustaining smooth pursuit. DLPN: Dorsolateral pontine nuclei. N RTP: Nucleus reticularis tegmenti pontis... 41
Figure 4.21. (A) Horizontal eyes position of a normal person versus time. The small-amplitude, high-frequency component is tremor; the large and slow excursions are drift; microsaccades are numbered from 1 to 4. LE: left eye. RE: right eye. Source: Modified from (Schulz, 1984). (B) Schematic representation of how fixational eye movements carry the retinal image across the photoreceptors. Tremor is the high-frequency movement superimposed on slow drifts (curved lines). Microsaccades are represented with straight lines. The diameter of the patch of the fovea shown here is 0.05 mm. Source: (Pritchard, 1961). ..... 42
Figure 4.22. Main sequence of saccades in free-viewing conditions (blue) and microsaccades during fixation conditions (red). Source: (Otero-Millan et al., 2008). ..... 45
Figure 4.23. Bright (A) and dark (B) pupil images. Source: (Morimoto, Koons, Amir, & Flickner, 2000). ..... 51
Figure 4.24. (A) Schematic representation of the basic principle of the pupil-corneal reflection technique. K: Linear distance between the center of curvature of the cornea and the center of the pupil. $\theta$ : angle of rotation of the eye. Source: (Merchan et al., 1974). (B) Estimated separation between the corneal reflection and the center of the pupil as a function of the angle of rotation. Parameters used: radius of curvature of the cornea of 7.7 mm and anterior chamber depth of 3.5 mm..... 52
Figure 5.1. Setup. (A) EVA system. Once the patient sits, the head of the machine goes down and adjusts its position according to the patient's height. (B) Frontal view of the optical modules. (C) Schematic representation of the optical module; the eye-tracker is shaded in dark gray while the vision and autorefractometer subsystems are represented in light gray. (D) Lateral view of the system. (E) Right (top) and left (bottom) eye images captured with the system..... 60
Figure 5.2. Histogram of the number of RANSAC iterations with the original algorithm (5 points, solid), choosing 5 points and distributing them spatially (5 points - distributed, dotted), considering a subset of 6 points without constraints about distribution (6 points, dashed) and considering 6 points and distributing them spatially (6 points – distributed, dotted-dashed). ..... 61
Figure 5.3. Eye images with the tested light sources configurations. ..... 62

---

## List of figures

---

Figure 5.4. Percentage of images averaged for all participants in which each glint is occluded. The corresponding occluded glints are represented in black in the schemes below the bars. Error bars show $\pm 1$ SD.....	67
Figure 5.5. Median vertical accuracy in degrees without normalizing the pupil-glint vectors (empty circles) and applying the normalization (solid circles). Each configuration of light sources is represented in the schemes below the bars, where active and inactive LEDs are represented in white and black, respectively. Error bars show the IQR. Bars correspond to the relative improvement of vertical accuracy due to the normalization.....	68
Figure 5.6. Percentage of images averaged for all participants in which there were five or more visible glints for the configurations (A) <i>12 glints</i> , (B) <i>8 glints</i> , and (C) <i>8 lowest glints</i> . Error bars show $\pm 1$ SD.....	70
Figure 5.7. (A) Schematic representation of the experimental setup. (B) Visual stimulus. The central target has been enlarged for the sake of visibility. The other eight stimuli were identical and used to calibrate the eye-tracker.....	80
Figure 5.8. Test sequence.....	81
Figure 5.9. Examples of the movements of both eyes during the performance of the cover test. (A) Example of a subject with no fixation disparity. During the binocular calibration and the binocular period of the cover test both visual axes cross exactly at the target. As the subject has an esophoria, the LE turns right when it is occluded. Note that this scheme might not represent the most typical condition in which zero fixation disparity generally is accompanied by a small phoria. (B) Example of a subject with eso fixation disparity. In binocular viewing conditions the visual axes cross in front of the target. When the LE is occluded, it turns right to its heterophoric position and the RE refixates the target. This scheme illustrates the most physiologically plausible condition, in which esophoria occurs with eso fixation disparity. (C) Example of a subject with exo fixation disparity. In binocular viewing conditions the visual axes cross behind the target. When the LE is occluded, it turns right to its heterophoric position and the RE makes a leftward movement to refixate the target. Like (A), this scheme does not represent the most typical condition, as an exo fixation disparity generally is associated with an exophoria.....	84
Figure 5.10. Ocular traces from a representative observer during the performance of the cover test. Horizontal RE and LE positions are represented with blue and orange lines, respectively. Periods of LE occlusion are shaded in orange and periods of RE occlusion are shaded in blue. The non-shaded	

areas correspond to binocular fixation periods. The inset panel zooms in on the eye traces during a RE occlusion period and shows how the RE stabilizes on its heterophoric position. ..... 86

Figure 5.11. Agreement between ET phoria measurements obtained with the *1-eye* and *2-eyes* methods. (A) Phoria measurements obtained with the 1-eye and 2-eyes methods, averaged across sessions and participants. \*\*  $p<0.01$ . (B) Magnitude (absolute value) of phoria measurements obtained with the *1-eye* and *2-eyes* methods, averaged across sessions and participants. In (A,B) circles are means and error bars represent 95% within-subject bootstrapped confidence intervals of the mean. (C) Bland and Altman plot showing the differences between *1-eye* and *2-eyes* ET phoria measurements as a function of the mean of both methods. The solid line represents the mean difference between methods. The dashed lines show the 95% limits of agreement. The inset in (C) shows the same plot, rescaled along the y-axis..... 87

Figure 5.12. Repeatability of the ET method. (A) Phoria measurements obtained with the ET *2-eyes* method in the first and second sessions, averaged across participants. (B) Magnitude (absolute value) of ET *2-eyes* phoria measurements obtained in the first and second sessions, averaged across participants. In (A,B) circles are means and error bars represent 95% within-subject bootstrapped confidence intervals of the mean. (C) Bland and Altman plot showing the differences between the two sessions as a function of the mean of them. The solid line represents the mean difference between methods. The dashed lines show the 95% limits of agreement. The inset in (C) shows the same plot rescaled along the y-axis. .... 88

Figure 5.13. Agreement between CT, TH, and ET methods. (A) Phoria measurements obtained with the CT, TH and ET methods. CT and TH results are averaged across participants and ET results are averaged across sessions and participants. (B) Magnitude (absolute value) of phoria measurements obtained with the CT, TH and ET methods, averaged across participants for the CT and TH, and across sessions and participants for the ET. Circles are means and error bars represent 95% within-subject bootstrapped confidence intervals of the mean. \*  $p<0.05$ ; \*\*\*  $p<0.001$ ..... 89

Figure 5.14. Agreement between the three pairs of methods. Bland and Altman plots comparing the CT with the TH (A), the CT with the ET (B), and the TH with the ET (C). The solid lines represent the mean difference between methods. The dashed lines show the 95% limits of agreement. The best fitting regression line through each pair of data is shown in red..... 90

Figure 5.15. Difference between the phoria measured in the right and left eyes as a function of motor ocular dominance. (A) Magnitude (absolute value) of phoria measured separately in the right and left eyes with the ET *2-eyes* method, averaged across sessions and participants. Circles are means and

error bars represent 95% within-subject bootstrapped confidence intervals of the mean. ** $p<0.01$ . (B) Difference between the magnitudes of phoria measured in the RE and in the LE as a function of motor ocular dominance. Circles are means and error bars represent 95% confidence intervals of the mean.....	91
Figure 5.16. Ocular traces of a non-cooperative patient during two occlusions periods. Horizontal RE and LE positions are represented with blue and orange lines, respectively. The LE occlusion period is shaded in orange and the RE occlusion period is shaded in blue. The non-shaded areas correspond to binocular fixation periods. In the LE occlusion, a 1.80 PD esotropia of the RE would have been measured with the <i>I-eye</i> method although the displacement of the RE is due to a leftward saccadic movement of both eyes. ....	93
Figure 5.17. Comparison of published intersession repeatability results of different methods. Repeatability results of cover test, modified Thorington test, and eye tracking methods are represented with blue circles, red squares, and orange stars, respectively. Mean differences are plotted against the SD of the differences. Filled symbols correspond to signed mean and SD of the differences and empty symbols correspond to absolute mean and SD of the differences. Data extracted from (Antona et al., 2011; Babinsky et al., 2015; Hirsch & Bing, 1948; Johns et al., 2004; Morris, 1960). ....	94
Figure 5.18. (A) Main sequence on a log-log scale as a function of the viewing distance. The color code exposes the tendency for greater saccade amplitudes and peak velocities at shorter viewing distances. (B) Saccade amplitude as a function of vergence demand. The black line corresponds to the least-squares regression fit, which is shown only for illustrative purposes ( $R^2=0.48$ ). (C) Amplitude distribution of saccades detected during convergence (top) and divergence (bottom) periods. The black vertical lines at amplitude = $10^\circ$ show that most saccades had an amplitude smaller than $1^\circ$ and can therefore be presumably considered to be equivalent to fixational microsaccades in terms of size, even though the fixation target in our experiment was not stationary. ....	106
Figure 5.19. Polar histogram of the saccade directions (gray sectors). The directions of saccades during convergence and divergence periods are shown with green and orange lines, respectively. Zero and 90 degrees indicate rightward and upward saccades, respectively.....	107
Figure 5.20. (A) Histogram of the difference in saccade direction between the two eyes (direction of the right eye minus direction of the left eye) in degrees. An angular difference of $0^\circ$ means that the two eyes moved in the same direction, whereas $\pm 180^\circ$ means that the saccade had opposite directions in the two eyes. (B) Histograms of the between-eye differences in saccade direction during	

convergence (top) and divergence (bottom). Note that the vertical axes are scaled logarithmically in panel (B) to emphasize the numbers of saccades that differed in direction in the two eyes. ....	108
Figure 5.21. Distribution of the right (panels (B) and (D)) and left (panels (A) and (C)) eyes directions for the directionally non-conjugate saccades as a function of the direction of the concurrent vergence movement (convergence: panels (A) and (B); divergence: panels (C) and (D)). The unfilled distributions limited by the solid lines are the directions of saccades which differed in the two eyes by more than $\pm 45^\circ$ , while the areas shaded in color represent the directions of saccades which differed in the two eyes by more than $\pm 90^\circ$ . ....	109
Figure 5.22. Saccade rate of each subject averaged across the three repetitions as a function of the direction of the concurrent vergence movement. The bars in the right subplot represent the mean saccade rate of all subjects. Error bars correspond to $+1$ SD. ....	109
Figure 5.23. (A) Saccade rate over time averaged across subjects and the three repetitions (black line). The shaded area corresponds to $\pm 1$ standard error of the mean (SEM). The right axis and the red line represent the target distance. (B) Saccade rate over time averaged across the three repetitions for a representative subject (Subject 8) who showed a decreased saccade rate at the closest target distance (black line). The right axis and the red line represent the target distance. This participant did not report diplopia during any of the three repetitions of the test. (C) Saccade rate over time averaged across the three repetitions for a representative subject (Subject 2) who showed an increased saccade rate at the closest target distance (black line). The right axis and the red line represent the target distance. ....	110
Figure 5.24. Vertical traces of a representative observer (Subject 5) who exhibited an upbeat vertical nystagmus (slow downward drift interrupted by upward saccades). Positive and negative values mean upward and downward movements, respectively. The right axis and the red line represent the target distance. ....	113
Figure 5.25. (A) Vertical right eye position of Subject 10 during convergence (gray line) and divergence (black line) periods of dynamic calibration as a function of the viewing distance. The red line corresponds to the fitted function according to Eq. (5.11) ( $a=-0.44$ cm, $b=-4.4^\circ$ , $R^2=0.96$ ). (B) Vertical vergence exhibited by the same subject during the first repetition of the NPC test before (gray line) and after (black line) correction of the vertical traces. The shaded area corresponds to the period when the subject reported diplopia. The large spike in the two vertical vergence traces before time = 20 s might be an artifact associated with the loss of fusion. ....	115
Figure 5.26. (A) Horizontal (black) and vertical (gray) eye position of Subject 5 during a 5-second period of the NPC test. During this period the observer exhibited six saccades, which are identified	

with numbers. (B) Horizontal (black) and vertical (gray) components of eye velocity during the same period of the NPC test. (C) Plot of the trajectory in velocity space. The ellipse used as the criterion to identify saccades is represented in gray. Its horizontal and vertical center is at 6.60 and 0 °/s, respectively. The six saccades showed considerably higher velocities than the median velocity during the 5-second period. ....	116
Figure 5.27. (A) Main sequence on log-log scale as a function of the viewing distance. The color code exposes the tendency for greater saccade amplitude and peak velocity at shorter viewing distances. (B) Saccade amplitude as a function of vergence demand. The black line corresponds to the least-squares regression fit, which is shown only for illustrative purposes ( $R^2=0.40$ ). (C) Amplitude distribution of saccades detected with the clustering method (top) and with the modified version of the E-K algorithm (bottom). ....	118
Figure 5.28. Polar histogram of the saccade directions (gray sectors). The direction of saccades during convergence and divergence periods is shown with green and orange lines, respectively. Zero and 90 degrees indicate rightward and upward saccades, respectively. ....	118
Figure 5.29. (A) Histogram of the difference in saccade direction between the two eyes (direction of the right eye minus direction of the left eye) in degrees. An angular difference of 0° means that the two eyes moved in the same direction, whereas ±180° means that the saccade had opposite directions in the two eyes. (B) Histograms of the between-eye differences in saccade direction during convergence (top) and divergence (bottom). Note that the vertical axes are scaled logarithmically in panel (B) to emphasize the numbers of saccades that differed in direction in the two eyes. ....	119
Figure 5.30. Distribution of the right (panels (B) and (D)) and left (panels (A) and (C)) eyes directions for the directionally non-conjugate saccades as a function of the direction of the concurrent vergence movement (convergence: panels (A) and (B); divergence: panels (C) and (D)). The unfilled distributions limited by the solid lines are the directions of saccades which differed in the two eyes by more than ±45°, while the areas shaded in color represent the directions of saccades which differed in the two eyes by more than ±90°. ....	120
Figure 5.31. Saccade rate of each subject averaged across the three repetitions as a function of the direction of the concurrent vergence movement. The bars in the right subplot represent the mean saccade rate of all subjects. Error bars correspond to +1 SD. ....	121
Figure 5.32. Saccade rate over time averaged across subjects and the three repetitions (black line). The shaded area corresponds to ± 1 standard error of the mean (SEM). The right axis and the red line represent the target distance. ....	121

Figure 5.33. Example of the data analysis in a convergent and a divergent transition. The black square wave function in the upper plot represents the vergence demand. The two vertical green lines represent the moments when the patient pressed the key to report single vision. The two horizontal dashed lines in the lower plot represent the velocity thresholds used to determine the onset of convergence and divergence movements, respectively. Positive vergence positions and velocity correspond to convergence and negative vergence positions and velocity correspond to divergence.

129

Figure 5.34. (A) Mean vergence latency at each experimental condition. (B) Mean vergence latency as a function of the vergence direction. (C) Mean vergence latency as a function of the direction of phoria. (D) Mean vergence latency as a function of the subjects' expertise. (E) Mean latency exhibited by esophoric and exophoric participants as a function of the direction of the vergence transitions. Error bars in panels (A) and (B) show  $\pm 1$  within-subjects' SD. Error bars in panels (C), (D) and (E) show  $\pm 1$  SD. \*\* Statistically significant ( $p<0.01$ )..... 132

Figure 5.35. (A) Mean time to peak velocity at each experimental condition. (B) Mean time to peak velocity as a function of the vergence direction. (C) Mean time to peak velocity as a function of the direction of phoria. (D) Mean time to peak velocity as a function of the subjects' expertise. (E) Mean time to peak velocity exhibited by esophoric and exophoric participants as a function of the direction of the vergence transitions. Error bars in panels (A) and (B) show  $\pm 1$  within-subjects' SD. Error bars in panels (C), (D) and (E) show  $\pm 1$  SD. \* Statistically significant ( $p<0.05$ )..... 134

Figure 5.36. (A) Mean response time at each experimental condition. (B) Mean response time as a function of the vergence direction. (C) Mean response time as a function of the direction of phoria. (D) Mean response time as a function of the subjects' expertise. (E) Mean response time exhibited by esophoric and exophoric participants as a function of the direction of the vergence transitions. Error bars in panels (A) and (B) show  $\pm 1$  within-subjects' SD. Error bars in panels (C), (D) and (E) show  $\pm 1$  SD. \* Statistically significant ( $p<0.05$ ). \*\* ( $p<0.01$ ). \*\*\* ( $p<0.001$ ). ..... 135

Figure 5.37. Median perceptual predictability scores given to each experimental condition. A score of 1 means a totally predictable condition while 5 means totally random. Error bars show  $\pm 1$  interquartile range. \*\* Statistically significant ( $p<0.01$ ). \*\*\* ( $p<0.001$ ). ..... 136

Figure 5.38. Latency (A), time to peak velocity (B), and response time (C) as a function of the perceptual predictability score attributed to each randomness condition. The only significant correlation was shown by the time to peak velocity in condition 3. ..... 137



## List of tables

Table 4.1. Classification of saccades proposed by Leigh & Zee (2015).....	20
Table 5.1. Median (interquartile range; IQR) of the horizontal and vertical accuracies in degrees for different configurations .....	66
Table 5.2. Median (IQR) of the horizontal and vertical accuracies in degrees for different configurations when the pupil-glint vectors were normalized. ....	67
Table 5.3. Subjective break and recovery points averaged across the three repetitions of the NPC test ± SD for all subjects, and total number of saccades exhibited during the three convergence and divergence periods. ....	105
Table 5.4. Number of saccades that corrected or produced a horizontal disparity error; number of saccades that brought the right eye (RE) or the left eye (LE) closer to the target; and the dominant eye of each subject.....	111
Table 5.5. Number of saccades exhibited during convergence and divergence movements by each subject. ....	117
Table 5.6. Number of saccades that corrected or produced a horizontal disparity error; number of saccades that brought the right eye (RE) or the left eye (LE) closer to the target; and the dominant eye of each subject.....	122
Table 5.7. Age, expertise, refractive error of right eye (RE) and left eye (LE), phoria at 40 cm, vergence facility (VF) performed clinically at 40 cm, and stereopsis of the 37 participants. N: naïve; E: expert; negative values of phoria correspond to exophoria and positive values correspond to esophoria. ....	125
Table 5.8. Summary of the characteristics of the four experimental conditions.....	128
Table 5.9. <i>p</i> -values obtained with the mixed ANOVA with two within-subjects' factors (Randomness condition and Vergence direction) and two between-subjects' factors (Expertise and Phoria direction). *Statistically significant.....	131



# 1. Introduction

Visual perception involves a series of actions starting with the reception of light on the retina (Schwartz, 2009). Several structures in the ocular globes, their adnexa, and the nervous system are involved in the visual process (Figure 1.1). Anatomical integrity of all these structures is not enough for the visual cortex to create a satisfactory visual experience from the received information. Instead, the two ocular globes and their adnexa need to cooperate in a coordinated way. In this regard, the visual process can be divided into the *sensory* and *motor* stages (Von Noorden & Campos, 2002). The *sensory* aspect of the visual process entails the processes by which light goes through the refractive media of the eyes and reaches the retina, where it produces a series of physical and chemical reactions in the photoreceptors that, in turn, generate a neural signal that is transmitted along the rest of the visual pathway. This initial stage of the visual process represents the stimulus for the *motor* system, which triggers a series of responses in the inner and outer muscles of the eyes. Although for the purpose of this study the distinction between sensory and motor systems is made, it is also important to understand the visual system as a single sensorimotor unit as a whole. In particular, the oculomotor system cannot be seen as an independent entity as it is mostly governed by the feedback from the sensory system.

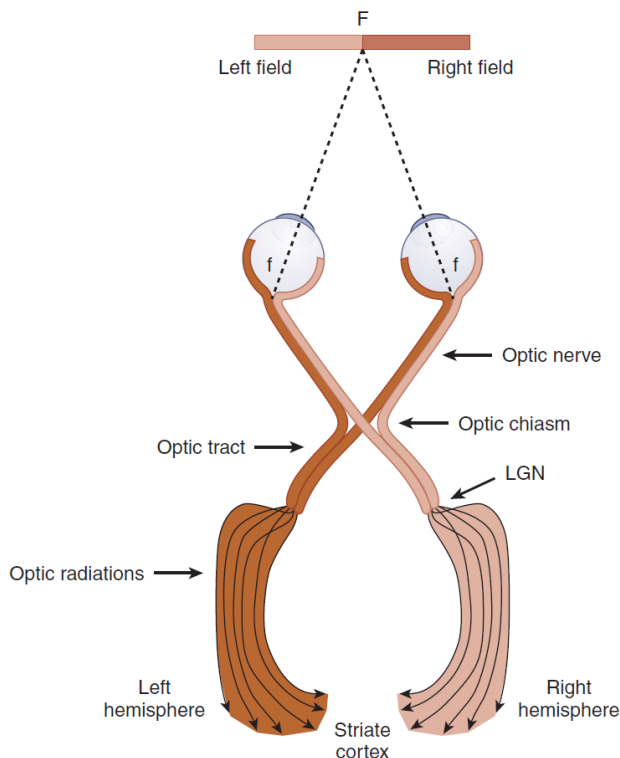


Figure 1.1. Schematic representation of the visual sensory pathway. F: fixation point. f: foveae. LGN: lateral geniculate nucleus. Source: (Schwartz, 2009).

One of the main tasks of the motor system is to generate the optimal conditions that allow the maintenance of binocular vision (Von Noorden & Campos, 2002). *Binocular vision* is the ability of the visual system to coordinate and integrate the information received separately from the two eyes into a single binocular percept (Evans, 2007; Julesz, 1971). Proper functioning of binocular vision also depends on sensory and motor aspects, besides the anatomical integrity of the visual system. *Sensory fusion* is the unification of visual excitations from the stimulation of corresponding retinal elements in the two eyes into a single visual image (Von Noorden & Campos, 2002). The main goal of *motor fusion* is to align the two eyes properly so that sensory fusion can be maintained. While the stimulus to sensory fusion is the excitation of corresponding retinal elements, the stimulus for the fusional eye movements driven by the motor fusion mechanism is the excitation of non-corresponding elements in the retinal periphery. At the highest level, binocular vision leads to *stereopsis*, which is the ability to order visual objects in depth.

Anomalies in either the sensorial or the motor aspect of binocular vision or in their interaction with other processes such as accommodation may lead to dysfunctions often associated with symptoms. Binocular dysfunctions are sometimes classified according to the type of ocular misalignment (Evans, 2007). Heterophoria, or phoria, is a deviation of the visual axes that only occurs in absence of a stimulus for sensory fusion. In contrast, strabismus is the condition by which one eye deviates manifestly even with a stimulus for sensory and motor fusion. Strabismus affects between 2 and 5% of the population (Friedman et al., 2009). The presence of phoria *per se* is not considered an abnormal condition. However, when its magnitude is higher than normal and the effort of the binocular system is not sufficient to compensate the deviation, it leads to a non-strabismic binocular dysfunction. The most common non-strabismic binocular dysfunction is convergence insufficiency. Its prevalence is estimated at 3-5% of the population (Rouse et al., 1999; Rouse, Hyman, Hussein, Solan, & Group, 1998; Scheiman et al., 1996), and it is associated with symptoms such as asthenopia, intermittent blur or diplopia or burning and tearing (Scheiman & Wick, 2014). Other examples of less prevalent non-strabismic binocular dysfunctions are excess of convergence, divergence insufficiency or excess of divergence. Nowadays, there is an emerging concern over the increase in visual symptoms and discomfort even for subjects with normal binocular vision, which is thought to be related to near sustained visual activities with computer and other small, handheld devices such as smartphones and tablets (Bababekova, Rosenfield, Hue, & Huang, 2011; Rosenfield, 2011).

Binocular vision is typically evaluated in optometric clinical practice after determining the patient's refractive status (Scheiman & Wick, 2014). The first tests are intended to assess the motor aspects of binocular vision. The evaluation often starts with the assessment of ocular alignment and

the measurement of the deviation if present. Then, the amplitude of fusional vergence is assessed. The near point of convergence test evaluates the nearest point on which the eyes can maintain binocular single vision and is considered a valuable test for the diagnosis of convergence insufficiency (Rouse, Hyman, et al., 1997). Besides assessing the maximum range (amplitude) of vergence, the ability to make fast and abrupt changes of fixation between far and close targets is also important for healthy binocular vision. The vergence facility test evaluates this ability. These are some examples of the tests used to evaluate motor binocular vision. Evaluation of the sensory status, which includes the evaluation of suppression and stereopsis, is especially important in cases of strabismus. The alterations of sensory fusion are much less severe, or non-existent, in non-strabismic binocular dysfunctions.

In essence, the tests to evaluate the motor aspects of binocular vision consist in eliciting eye movements and asking the patients to report when they perceive diplopia and/or single vision. In a conventional optometric clinical setting, all the above optometric tests evaluating binocular vision are run subjectively, as they depend on the answers of the patients or on the examiner's own criteria. This subjectivity leads to a considerable variability of the results, differences between examiners, and it is a potential source of error in the diagnostic of binocular dysfunctions (Antona, Barrio, Barra, Gonzalez, & Sanchez, 2008; Antona et al., 2011; Rainey, Schroeder, Goss, & Grosvenor, 1998). However, there exist instruments to determine the gaze position and measure ocular movements objectively, i.e. *eye-trackers*. Among a wide range of applications, eye-trackers have become a useful research tool for a variety of different disciplines such as neuroscience, psychology, industrial engineering, marketing and advertising or computer science (Duchowski, 2002). The first eye tracking systems date from the late 1800s, and were complex and invasive (Duchowski, 2017; Holmqvist & Nyström, 2011). Several techniques have been developed since then, but the method that probably leaded to the most significant grow in eye-trackers' popularity is the non-invasive one relying on the corneal reflection of one or several external light source(s).

Eye tracking systems have been widely used for research in the fields of ophthalmology, optometry and vision science. Initially, the first instruments of such have allowed to confirm the existence of most basic eye movements and document their characteristics (Yarbus, 1967). With the development of non-invasive techniques, other applications arose, such as the diagnostic of reading problems in children (Borsting, Rouse, Shin, Dold, & McClallen, 2007; Colby, Laukkanen, & Yolton, 1998). Other examples of more demanding applications are the use of eye-trackers to guide the laser during refractive surgery (Y. C. Lee, 2007), or to identify potential ocular signs that provide valuable information about severity or progression of neurodegenerative diseases such as Parkinson disease,

dementia with Lewy bodies, Huntington disease or Alzheimer disease (T. J. Anderson & MacAskill, 2013).

Currently, eye-trackers are seldom used in optometric clinical practice. However, it seems reasonable to think that the evaluation of motor fusion could better rely on eye tracking systems (Bedell & Stevenson, 2013; Martinez-Conde, 2006). Eye-trackers could bring a powerful advantage in the evaluation of binocular vision. They provide an objective measurement independent to the patients' answers and the criteria and expertise of the examiner, which could lead to a higher repeatability. More accurate measurements than those based on naked eye observations can be obtained. Temporal and dynamic characteristics of ocular movements can be analyzed in order to identify new oculomotor signs that help to diagnose binocular vision dysfunctions and/or to justify visual symptoms of subjects with normal binocular vision but high visual demands. Moreover, the integration of eye-trackers in virtual reality systems lead to the possibility to perform the tests automatically, i.e. using automatic setups controlled by computers with repeated stimuli and without examiner's intervention. Therefore, the variability of the results due to different testing conditions could be minimized, and the tests could be adapted to the patients' age or other characteristics.

Before the implementation of eye-trackers in general optometric clinical practice, both manufacturers and vision science researchers have to solve a long list of matters. On the one hand, manufacturers face the challenge to produce economical, user-friendly devices with suitable specifications for clinical applications. On the other hand, there is a wide field of research to make all the advantages listed above come true. The most part of this thesis will be essentially based on the analysis of particular characteristics of eye movements in clinically interesting situations, that is, during the performance of different tests to evaluate the oculomotor aspect of binocular vision. To do so, these tests have been performed in an automated setup and eye movements have been measured objectively with an eye-tracker.

The goals of this thesis and its structure throughout this document are detailed in the following two sections.

## 2. Goals of the thesis

The final objective of this thesis is to develop new methodologies for the clinical, objective and automated evaluation of visual function based on the analysis of ocular movements. This general goal is split into two main objectives:

1. The development of new methods for an eye tracking system based on multiple corneal reflections for clinical applications.

This initial goal is addressed in the first study of the thesis which, in turn, leads to two specific objectives:

- 1.1. To analyze the advantages of using multiple corneal reflections and determine the optimum arrangement of the light sources.
- 1.2. To propose methods to normalize the pupil-glint vectors in order to improve spatial accuracy.

By accomplishing this goal, a deep understanding of how video-based eye-trackers function was achieved. This allowed us to use a commercial research-purpose eye-tracker for the subsequent objectives not as a mere black box, but with full knowledge of its limits and characteristics. A third objective related to eye tracking methods was subsequently fulfilled in the third study of the thesis:

- 1.3. To propose methods to estimate the actual eye positions in the 3D world based on multiple calibrations and geometric extrapolation functions.
2. The analysis of ocular movements in clinically interesting situations for the objective and automated evaluation of binocular vision.

This goal is split into three specific objectives in order to cover three different binocular vision tests. Each specific objective is addressed in a different study.

- 2.1. To measure heterophoria with an automated *cover test* using an eye-tracker and validate the results against other clinical methods.
- 2.2. To analyze the characteristics of small saccades that occur during the *near point of convergence test* as a function of vergence demand, and to determine whether some saccadic features can be used as objective biomarkers to predict the results of this test.
- 2.3. To analyze the effect of stimulus' predictability on temporal characteristics of vergence movements in order to understand its impact on the results of the *vergence facility test*.



### **3. Structure of the thesis**

This thesis is structured in four studies. Each study is detailed in a different section after the State of the art chapter. They are written in a paper-like format, thus each of them include the following subsections: introduction, methods, results and discussion. In addition, the third study have two appendices which contain further details about the methodology and supplementary results.

The first study is focused on the first objective of the thesis: developing new and accurate eye tracking methods relying on multiple corneal reflections. The images taken with the hardware of an existing eye-tracker are used to evaluate the advantages of using multiple corneal reflections from multiple light sources and determine their optimal arrangement. Other methods are also proposed in order to optimize eye tracking accuracy.

The other three studies are more clinically focused and, instead of investigating methods to improve eye tracking accuracy, a commercial eye-tracker is the instrument used to measure ocular movements. Each study is focused on a different aspect of the assessment of binocular vision: the measurement of phoria, the assessment of the maximum convergence capability, and the evaluation of the dynamic abilities of convergence and divergence. Specifically, in the second study, an objective cover test in an automated setup is proposed and validated against two other clinical methods. The third study analyzes the characteristics of saccadic movements that occur during the near point of convergence testing. Without the registering of eye movements with an eye-tracker, it would not be possible to notice the existence of these small movements. This study explores the possibility of using some saccadic features as objective markers to predict the results of the near point of convergence test. As a particularly wide tracking range is required to track the eyes during the near point of convergence test, additional calibration methods to estimate accurately the 3D eye positions are proposed in the third study of the thesis. Finally, the fourth study inspects the effects of the stimulus' predictability on the latency and response time of vergence movements, which in the end impact the results of the vergence facility test.

After the four studies, global conclusions and related future works are suggested. Finally, a list of publications in which the results of this thesis have been disseminated and bibliographic references are provided.



## **4. State of the art**

This thesis is based on the assessment of binocular vision using eye tracking systems. The following subsections will review the most important concepts of these two fields that are relevant to this work. First, the general concepts of the human oculomotor system and binocular vision will be reviewed. Then, the characteristics of the different types of eye movements will be detailed. Finally, the last subsection of this chapter will include a review of the main eye tracking techniques, placing special emphasis on the corneal reflection method.

### **4.1. General concepts and fundamental laws**

#### **4.1.1. Positions of gaze**

The primary position of gaze is defined as the position of both eyes in binocular vision in which the head is erected and the eyes are fixating a point at infinity which lies at the intersection of the sagittal plane of the head and a horizontal plane passing through the center of the two globes (Myers, 1975).

Secondary positions of gaze involve rotation of the eyes around only one of the primary axes, i.e. a horizontal or vertical axis.

Tertiary positions of gaze are obtained by a simultaneous rotation around the horizontal and vertical axes.

#### **4.1.2. Listing's law**

Listing's law states that each movement of the eye from the primary position involves a rotation around a single axis lying in the Listing's plane. The Listing's plane is defined as a plane passing through the head and the center of rotation of the eyes that is perpendicular to the line of sight when the eyes are in primary position (Figure 4.1A). The axis is perpendicular to the plane that contains the initial and final positions of the line of sight. Listing's law implies that all eye movements from the primary position occur without torsion or cyclorotation with respect to the primary position. However, each movement is associated with a definite degree of false torsion (Von Noorden & Campos, 2002).

False torsion is the apparent cyclorotation of the eye associated with a change of direction of regard from the primary position to a tertiary position. It is present due to the fact that the vertical meridian of the eye remains vertical when the eye rotates to a secondary position but tilts with respect to vertical in any tertiary position (Figure 4.1B).

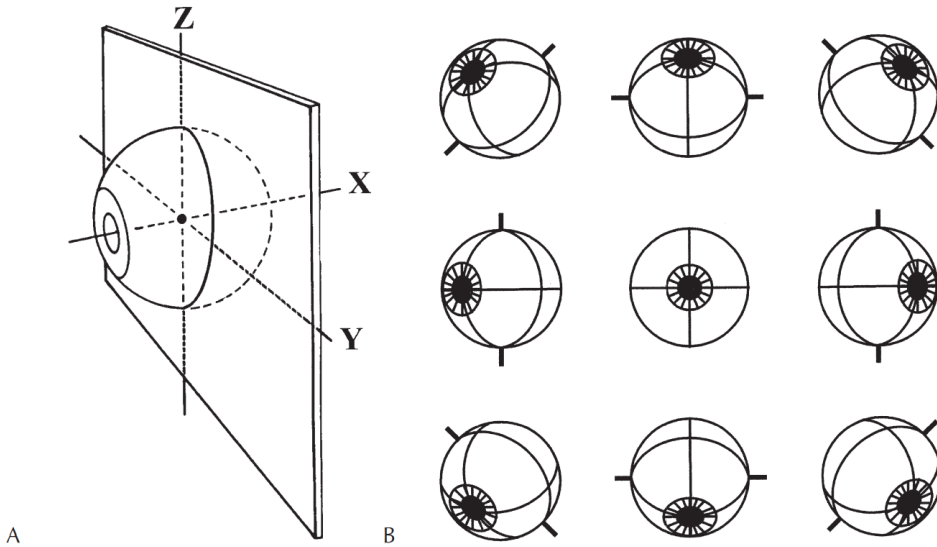


Figure 4.1. (A) Listing's plane and the axes of rotation of the eye (X,Y,Z). (B) Orientations of the eye when they rotate to secondary and tertiary positions and obey Listing's law. In tertiary positions, the eyes appear to rotate around the visual axis due to false torsion. Source: (Leigh & Zee, 2015).

Listing's law can also be expressed in terms of any initial eye position, not just primary position. If the eye starts to rotate from an eccentric position, the Listing's plane is no longer perpendicular to the line of sight; instead it is tilted in the same direction as the line of sight but only half as much. This relationship is called Listing's half-angle rule.

Listing's law allows to understand the organization of neural and mechanical factors in the control of 3D eye movements and it is also of importance to clinicians because it has implications for the optimal management of strabismus (A. M. F. Wong, 2004).

#### **4.1.3. Donders' law**

Donders' law suggests that the angle of tilt (or false torsion) for a given tertiary position of the eye is always the same irrespective of the path taken by the eye to reach that position. After returning to its initial primary position, the retinal meridian is oriented exactly as it was before the movement was initiated (Von Noorden & Campos, 2002). This law implies that the torsional orientation of the eye is fixed for a given horizontal and vertical position. The corollary is that one can retrieve a unique and single orientation of the eye for a targeted viewed object.

#### **4.1.4. Hering's law of Equal Innervation**

Hering's law of Equal Innervation states that whenever an impulse for the action of an eye movement is sent out to an extraocular muscle, the contralateral agonist muscle receives equal innervation. There

are separate neural controllers for conjugate and vergence movements and each eye receives an identical neural command from each controller. The agonist muscle is the one that produces the movement, while a movement in the opposite direction is caused by its antagonist muscle.

Hering's law applies only to extraocular muscles. There are no muscles in the human body that are functionally interrelated as are the pairs of muscles of the eye. However, the law applies to all normal eye movements, both voluntary and involuntary (Von Noorden & Campos, 2002).

Alternatively to Hering's law, Helmholtz stated that binocular coordination is a learned behavior based on independent neural control of each eye. A more detailed explanation about the controversy between Hering and Helmholtz hypotheses is given in section 4.4.2.6.

#### **4.1.5. Sherrington's law of Reciprocal Innervation**

Sherrington's law of Reciprocal Innervation states that whenever a muscle receives an impulse to contract, an equivalent inhibitory impulse is sent to its ipsilateral antagonist, which relaxes and lengthens. Reciprocal innervation is physiologically and clinically important since it explains why strabismus occurs following paralysis of an extraocular muscle and must be considered when surgery on the extraocular muscles is performed.

This law applies to all striated muscles of the body; thus, it is not limited to the extraocular ones (Von Noorden & Campos, 2002).

### **4.2. The oculomotor system**

This section reviews the final effector tissues that perform the actions dictated by the neural structures comprised in the oculomotor system. For the purpose of this thesis, this section focuses exclusively on the extraocular muscles, whose fundamental function is the maintenance of motor fusion.

#### **4.2.1. The extraocular muscles**

Humans have six extraocular muscles in each orbit: the medial rectus, the lateral rectus, the superior rectus, the inferior rectus, the superior oblique and the inferior oblique (Figure 4.2). All six muscles consist of striated muscle fibers with abundant elastic fibers (Jordan, Mawn, & Anderson, 2012).

The four rectus muscles take origin from a tendinous structure named the annulus of Zinn. The superior oblique muscle arises from the lesser wing of the sphenoid bone via a short, narrow tendon in the angle between the annulus of Zinn and the periorbita of the medial wall. The inferior oblique takes its origin from a small, shallow fossa in the floor of the orbit (Jordan et al., 2012).

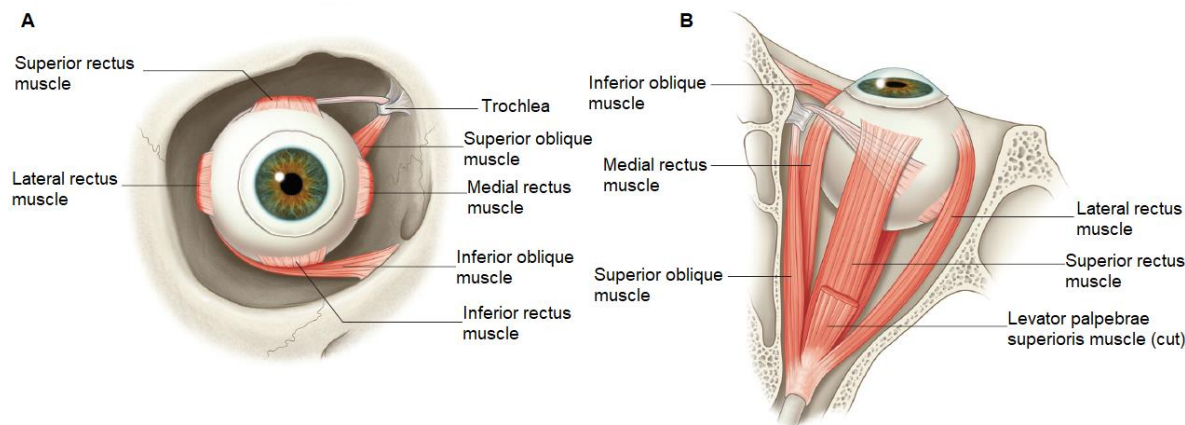


Figure 4.2. Anterior (A) and superior (B) views of the extraocular muscles. Source: Modified from (Levin et al., 2011).

The extraocular muscles insert into the eyeball via their thin, flat tendons, which blend into episclera and superficial sclera. Only the horizontal and vertical recti insert in front of the equator of the eyeball. Both obliques have their insertions behind the equator of the globe (Figure 4.2).

As far as innervation of the extraocular muscles is concerned, the abducens nerve (cranial nerve VI) supplies the lateral rectus. The inferior division of the oculomotor nerve (cranial nerve III) supplies the inferior rectus, the inferior oblique and usually the medial rectus. Meanwhile, the superior division of the oculomotor nerve (III) supplies the superior rectus, and occasionally the medial rectus besides the levator palpebrae superioris (the elevating muscle of the eyelid, which is not an extraocular muscle). Finally, the superior oblique is supplied by the trochlear nerve (cranial nerve IV).

The lateral branch of the ophthalmic artery supplies the lateral and superior rectus muscles, and the superior oblique muscle. The medial branch of the ophthalmic artery supplies the inferior and medial rectus muscles and the inferior oblique muscle. The inferior rectus muscle and the inferior oblique muscle receive additional blood supply from the infraorbital artery, and the medial rectus muscle also receives a branch from the lacrimal artery.

#### 4.2.2. Action of individual muscles

The eyeball has three degrees of freedom. It can rotate around each of these three axes, all going through the center of rotation. One is the anteroposterior or sagittal axis, coincident with the line of sight, while the other two are perpendicular to the line of sight and are assumed to lie in the Listing's plane; one is vertical, and the other is horizontal. The center of rotation of the eye is not fixed, it actually moves in a systematic way along a curved line fixed in space (Park & Park, 1933). In primary

position the center of rotation is located about 13.5 mm behind the apex of the cornea on the line of sight (Von Noorden & Campos, 2002).

The rotations of the single eye are termed *duction* movements. Rotations around the vertical axis are called adduction (nasalward rotation) and abduction (templeward rotation). Rotations around the horizontal axis are termed elevation (upward rotation) or depression (downward rotation). A combination of the horizontal and vertical rotations moves the globe into oblique positions (tertiary positions of gaze). Rotations around the anteroposterior axis are called exocycloduction (rotate the upper pole of the cornea templeward) and incycloduction (rotate the upper pole of the cornea nasalward).

Because of the configuration of the eyeballs and the way the extraocular muscles are oriented in the orbit, especially vertical recti and obliques (Figure 4.3), the muscles not only perform a single action, but also have secondary and tertiary actions. The actions of each extraocular muscle from the primary position are illustrated in Figure 4.4.

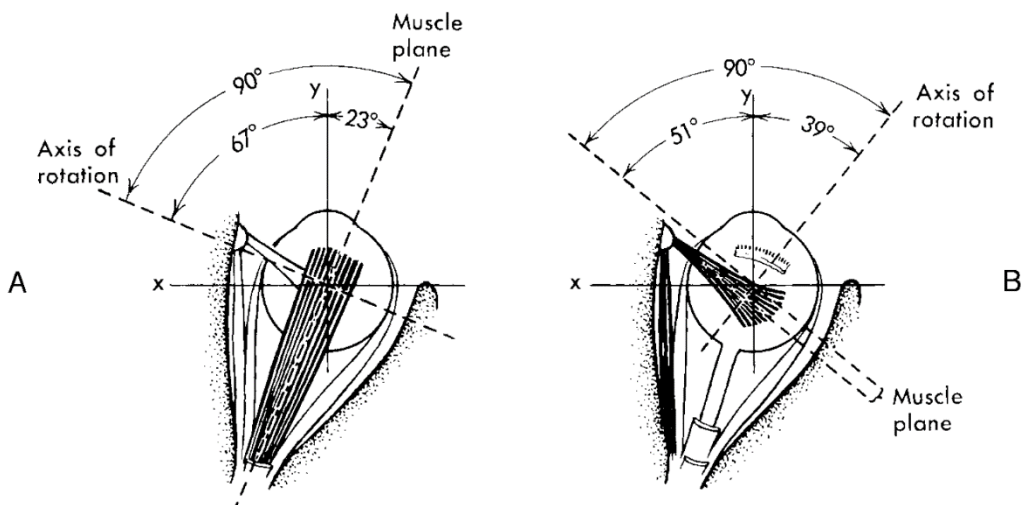


Figure 4.3. Orientation of the vertical rectus muscles (A) and the oblique muscles (B) in the orbit. Source: (Von Noorden & Campos, 2002).

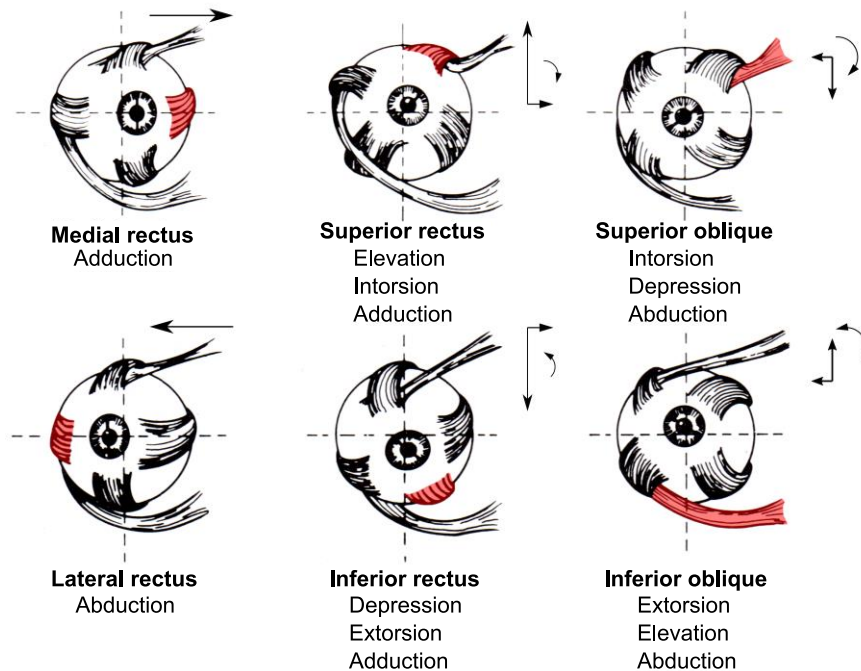


Figure 4.4. Primary, secondary and tertiary actions of extraocular muscles. Source: Modified from (Carpenter, 1988).

### 4.3. Binocular vision

Binocular vision is the ability of the visual system to coordinate and integrate the information received separately from the two eyes into a single binocular percept (Evans, 2007). As pointed out in the introductory chapter, the visual system should be considered a whole *sensorimotor* unit. However, distinction between sensory and motor components is usually made for the purpose of study. Basic concepts to understand binocular vision and a brief review of the most common binocular anomalies and the tests typically used for their diagnostic are introduced in the following subsections.

#### 4.3.1. Fusion, diplopia and retinal correspondence

When light reaches a retinal point, the stimulus is perceived not only with a certain color, brightness and shape, but it is also localized in a certain *direction* in visual space. Each retinal point has a directional value, which is an intrinsic and inherent property as are all the other properties that lead to sensations of color, brightness or shape (Von Noorden & Campos, 2002). The direction in which a retinal point localizes a stimulus is not absolute. Instead, it is relative to the principal visual direction, which corresponds to the fovea, the area of highest cone density and visual acuity of the retina (Figure 4.5). The stable relationship between the visual direction of the fovea and that of all other retinal areas allows the ordered perception of the visual field.

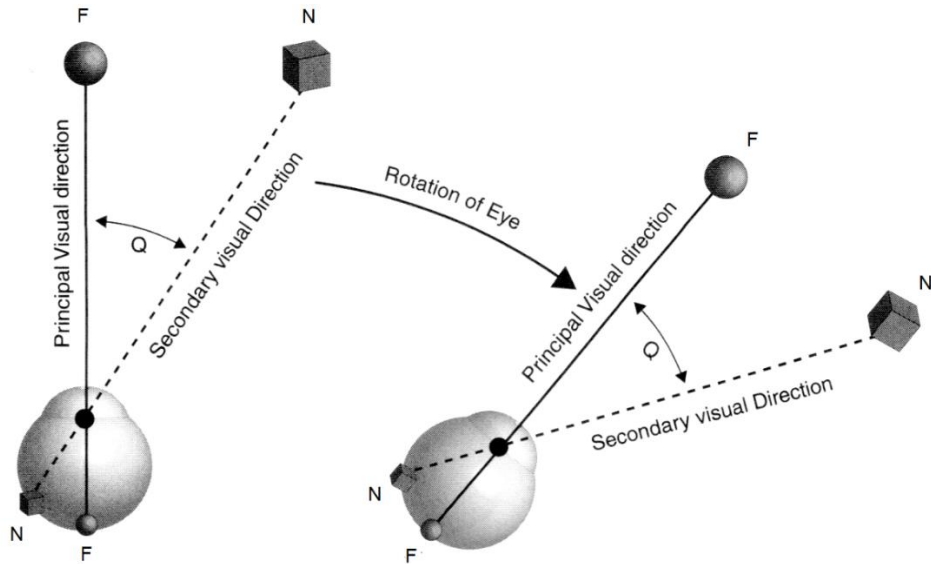


Figure 4.5. Relative lines of direction. F, principal visual direction. N, secondary visual direction. When the eye rotates, the principal visual direction shifts accordingly to the new position of the fovea. Source: Modified from (S. B. Steinman, Steinman, & Garzia, 2000).

Every retinal point has an associated point in the retina of the other eye with which it shares a common visual direction. Retinal points of the two eyes sharing a common visual direction are called *corresponding retinal points*. The common visual directions are also relative to the principal common visual direction of the two foveae.

*Sensory fusion* is the unification of visual excitations from corresponding retinal images into a single visual percept (Von Noorden & Campos, 2002). An object localized in the same visual direction by stimulation of the two retinas can only be perceived as one, single visual object. Thus, the stimulus to sensory fusion is the excitation of corresponding retinal points. When non-corresponding or disparate retinal points are stimulated simultaneously, the object is localized in two different visual directions at the same time. Thus, it is perceived double or in diplopia.

*Motor fusion* is the ability to align the eyes so that sensory fusion can be maintained. The stimulus to motor fusion is the stimulation of disparate retinal points, and the response is the movement of the two eyes in opposite directions, i.e. vergence movements. The characteristics of vergence movements are explained in detail in section 4.4.2. A motor response cannot exist when the images of an object stimulate the fovea of each eye.

For sensory fusion to occur, the images must be located on corresponding retinal points and must be sufficiently similar in size, brightness, and sharpness (Von Noorden & Campos, 2002). Otherwise, they may lead to *retinal rivalry*, which is the alternation in perception that occurs when

different images are presented in the two eyes, as dissimilar stimuli do not permit fusion (Blake & Logothetis, 2002).

#### 4.3.2. Fixation disparity

The *horopter* is defined as the locus of all object points that are imaged on corresponding retinal elements at a given fixation distance (Von Noorden & Campos, 2002) (Figure 4.6). By definition, all the points lying on the horopter curve are seen singly and all those points not lying on the curve are seen double. *Physiologic diplopia* is elicited by object points outside the horopter. Actually, there exists a certain tolerance and points slightly away from the horopter can be fused properly. The region in front and back of the horopter in which single vision is present is the *Panum's area of single binocular vision* or *Panum's fusional area* (Figure 4.6). The horizontal extent of these areas ranges between 2 and 20 min of arc (Duwaer & Van Den Brink, 1981; Fender & Julesz, 1967; Schor & Tyler, 1981). It depends on retinal eccentricity, being smaller near the fovea and increasing toward the periphery. The size is also modulated by stimulus characteristics such as size and complexity (Fender & Julesz, 1967; Kertesz, 1981) or spatial and temporal frequency (Schor & Tyler, 1981; Woo, 1974). Moreover, adjacent retinal regions interact (Kertesz, 1981), and Panum's fusional areas not only enlarge but also shift across the retina as a function of the stimulation (Diner & Fender, 1988).

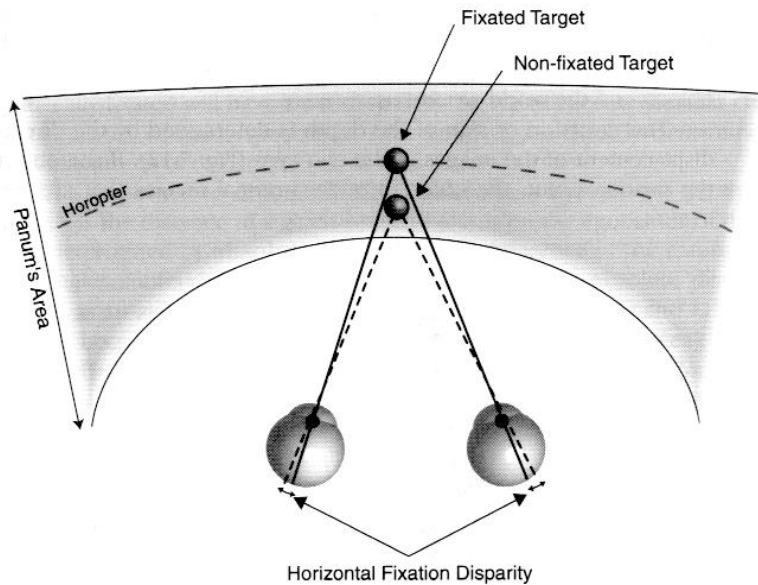


Figure 4.6. Schematic representation of the horopter and the Panum's fusional area. Source: (S. B. Steinman et al., 2000).

*Fixation disparity* is the condition by which an image displacement of the order of minutes of arc occurs within Panum's fusional area while fusion is maintained. There is controversy regarding

its clinical relevance. While in most cases the assessment of fixation disparity is not necessary for the diagnosis and management plan of binocular dysfunctions (Scheiman & Wick, 2014), it is useful to determine those patients who are likely to have symptoms (Sheedy, 1980; Sheedy & Saladin, 1977), and to determine the amount of prism to prescribe for the treatment of certain binocular disorders (Sheedy & Saladin, 1978).

#### **4.3.3. Stereopsis**

*Stereopsis* is the ability to order the visual objects in depth. It represents the most robust binocular cue to depth perception. The physiologic basis for stereopsis relies on the simultaneous stimulation of disparate retinal points within the Panum's fusional area (Figure 4.6). Due to the horizontal separation of the two eyes (the interpupillary distance), an object produces slightly different visual images in the two eyes. The two images can be fused because they lie within Panum's fusional area, and result in a three-dimensional percept (Von Noorden & Campos, 2002).

The direction of the perceived depth is determined by the direction of relative displacement of the images projecting in the two eyes (S. B. Steinman et al., 2000). If the two retinal images of a non-fixated object are in crossed or temporal disparity as in Figure 4.6, the object is perceived in front of the fixation point. Conversely, the object is perceived farther from the fixation point when the two retinal images are in uncrossed or nasal disparity.

The *stereoacuity* is the smallest disparity beyond which no stereoscopic effect is produced, in other words, it is the smallest depth difference a person can see. Stereoacuity is highly dependent on the method used to measure it, but a threshold of 15 to 30 seconds of arc obtained in clinical tests is generally considered as optimum (Von Noorden & Campos, 2002).

Although stereopsis can occur only in binocular vision, a sense of depth persists in monocular vision as a result of experience. Examples of monocular depth cues are relative size, linear perspective, interposition, distribution of lights and shadows or motion parallax (Schwartz, 2009).

#### **4.3.4. Binocular dysfunctions**

Sensory and motor systems must be adequate for normal binocular vision to be present, as well as physical integrity of all the structures of the visual system. An anomaly in any of these elements may cause a binocular dysfunction (Evans, 2007).

Anomalies in the motor system may lead to strabismic or non-strabismic binocular dysfunctions, depending on the manifestation of an ocular deviation. The main non-strabismic binocular dysfunctions are convergence insufficiency, divergence insufficiency, convergence excess,

divergence excess, fusional vergence dysfunction, basic esophoria and basic exophoria. There is considerable disparity regarding the prevalence of non-strabismic binocular disorders published by different authors, although general consensus is that convergence insufficiency is the most prevalent one (Cacho-Martínez, García-Muñoz, & Ruiz-Cantero, 2010).

All these dysfunctions except fusional vergence dysfunction are associated with a high latent ocular deviation (phoria), which only occurs in absence of a stimulus for sensory fusion. In this sense, convergence insufficiency is related to high exophoria at near; divergence insufficiency is related to high esophoria at distance; convergence excess is associated with high esophoria at near; divergence excess with high exophoria at distance; and basic esophoria and basic exophoria are related to high esophoria and exophoria, respectively, at both distances (Scheiman & Wick, 2014). Another sign of exophoric conditions is the difficulty with fusion through base-out (BO) prisms, which stimulate convergence movements. Conversely, esophoric conditions are associated with the difficulty with fusion through base-in (BI) prisms, which stimulate divergence movements. Convergence insufficiency is usually accompanied by receded near point of convergence (Rouse et al., 1997). Although fusional vergence dysfunction is not associated with high values of phoria, it is related to difficulty with fusion through both BI and BO prisms.

Several tests are performed in clinical optometric practice to evaluate the motor aspect of binocular vision, which is the most impaired in non-strabismic binocular dysfunctions (Evans, 2007; Scheiman & Wick, 2014). Next, the most relevant tests for the scope of this thesis will be briefly reviewed. Notice that additional tests might be performed as a function of the patients' symptoms to validate the diagnosis.

The starting point is the assessment of size and direction of the phoria. The most common test to do so is the *cover test*. It consists in covering the patients' eyes in turn while the examiner observes whether the eyes move. In this instance, the amount of the deviation, which is the magnitude of phoria, can be measured with a prism bar. Other methods to measure the phoria are the Maddox rod, the modified Thorington test, or the von Graefe technique (Rainey et al., 1998; Sanker, Prabhu, & Ray, 2012). Advantages and disadvantages of some of these methods are detailed in section 5.2.1.

The *fusional vergence amplitude* can be assessed either with a prism bar or with the rotary prisms of the phoropter. In both methods, the test consists in increasing the vergence demand by increasing progressively the prism power until the patient reports diplopia. Then, the prism power is decreased progressively until the patient recovers single vision. BI prisms are used to assess negative fusional vergence (divergence), and BO prisms are used to measure positive fusional vergence

(convergence). The repeatability of the positive fusional vergence measurement is low, and both methods are not interchangeable (Antona et al., 2008).

The *near point of convergence test* assesses the nearest point on which the eyes can converge. It is determined by asking the patient to maintain fixation on an object placed in the midline while it is moved toward the patient's eyes. The object is generally an accommodative target or a penlight (Scheiman et al., 2003). The near point of convergence test is a very valuable test for the diagnosis of convergence insufficiency (Rouse et al., 1997).

Finally, the *vergence facility test* assesses the ability to make rapid repetitive vergence changes over an extended period of time (Scheiman & Wick, 2014). It is generally performed by alternating flipper prisms of 3 prism diopters (PD) BI and 12 PD BO to elicit divergence and convergence movements, respectively (Gall, Wick, & Bedell, 1998). Patients are asked to look at a target and try to fuse it as fast as possible. The vergence facility is typically measured as the number of cycles per minute that can be fused. One cycle corresponds to an alternation of BI and BO prisms.

Anomalies in the sensory system might be the result of a loss of quality of the optical image in one or both eyes, a difference in image size between the two eyes, or anomalies of the visual pathway or cortex (Evans, 2007). Anomalies in the motor system, especially those associated with strabismus, may lead to adaptations and anomalies in the sensory system in order to lessen the symptoms caused by the motor dysfunction. Examples of these sensory anomalies are suppression, abnormal retinal correspondence, eccentric fixation, or amblyopia (Evans, 2007; S. B. Steinman et al., 2000; Von Noorden & Campos, 2002).

## 4.4. Eye movements

There are six types of eye movements used for bringing the image of an object of interest onto the fovea or maintaining foveal fixation. They can be classified as saccades, vergence, smooth pursuit, fixational eye movements, vestibulo-ocular reflex and optokinetic nystagmus.

In the following subsections, the characteristics of these different types of eye movements are detailed. A special emphasis is put on saccades and vergence movements since they are the most relevant types of eye movements concerning binocular vision.

### 4.4.1. Saccades

Saccades are fast movements of the eyes bringing the object of interest to the most sensitive region of the retina, i.e. the fovea. They are conjugate, accurate, high-velocity and ballistic eye movements

(Bahill & Stark, 1979). In general, they are considered voluntary movements. However, saccades include a range of behaviors that encompass also involuntary shifts of fixation, quick phases of vestibular and optokinetic nystagmus and the rapid eye movements that occur during rapid eye movement (REM) sleep (Leigh & Zee, 2015). A classification of saccades proposed by Leigh & Zee (2015) is presented in Table 4.1.

Table 4.1. Classification of saccades proposed by Leigh & Zee (2015).

Classification	Definition
Volitional saccades	Voluntary saccades made as part of purposeful behavior.
Predictive, anticipatory	Saccades generated in anticipation of or in search of the appearance of a target at a particular location.
Memory-guided	Saccades generated to a location in which a target has been previously present.
Antisaccades	Saccades generated in the opposite direction to the sudden appearance of a target after being instructed to do so.
To command	Saccades generated on cue.
Reflexive saccades	Saccades generated to novel stimuli (not necessarily visual) that unexpectedly occur within the environment.
Express saccades	Very short latency saccades that can be elicited when the novel stimulus is presented after the fixation stimulus has disappeared.
Spontaneous saccades	Seemingly random saccades that occur when the subject is not required to perform any particular behavioral task.
Scanning saccades	Consecutive saccades used to extract a particular piece of information from a complex visual environment in which there are many potential targets.
Quick phases	Quick phases of nystagmus generated during vestibular or optokinetic stimulation or as automatic resetting movements in the presence of spontaneous drift of the eyes.

Saccades have become a valuable research tool in a wide range of disciplines in neuroscience beyond control of eye movements, such as many aspects of cognition (memory, attention, motivation, reward, prediction, and decision making), and neurological and psychiatric diseases (Leigh & Zee, 2015). Moreover, they can be used for the neurologic localization of motor disorders as a function of the types of saccades that are impaired.

#### 4.4.1.1. Metrics and dynamics of saccades

Typically, humans make approximately two to three saccades per second, and most common ones (more than 85%) are smaller than  $15^0$  in amplitude (Carpenter, 1991). Bigger rotations are often divided into two to three smaller saccades or accompanied by head rotations (Carpenter, 1991).

Saccades are notably stereotyped. The dynamic characteristics of a saccade of a given amplitude are largely independent of its purpose, which kind of stimulus elicits it or its willingness (Bahill & Stark, 1979).

The saccade duration is dependent on its amplitude (Figure 4.7). For example, the duration of saccades measuring few degrees ranges from 10 to 20 ms (milliseconds), while for saccades of  $20^0$  it may exceed 70 ms. Specifically, Yarbus (1967) expressed the relationship between the duration of the saccade and the angle through which the eye turns (amplitude) by the empirical formula:

$$T = 0.021 \alpha_0^{2/5} \quad (4.1)$$

where  $T$  is the duration of the saccade in seconds, and  $\alpha_0$  is the amplitude in degrees. Meanwhile, Carpenter (1988) defined the relationship between saccade duration and amplitude as

$$D = 2.2A + 21 \quad (4.2)$$

where  $D$  is the duration of the saccade in milliseconds and  $A$  is the amplitude in degrees.

After the onset of a saccade, the velocity of the eye movement rises smoothly, reaches a maximum (the peak velocity, up to  $900^0/\text{s}$ ), and falls smoothly to zero (Figure 4.7B) (Bahill, Clark, & Stark, 1975). For saccades smaller than  $15-20^0$ , the increase and decrease of velocity follow a pseudo-sinusoidal rule. However, for saccades bigger than  $20^0$  the acceleration and deceleration periods are asymmetric (Figure 4.7B), i.e. the increase in velocity at the beginning of the saccade is faster than the deceleration at the end, which implies that the velocity profiles become skewed (Collewijn, Erkelens, & Steinman, 1988a; Collins, Semroud, Orriols, & Doré-Mazars, 2008; Yarbus, 1967).

The peak velocity is proportional to the amplitude of the saccade up to approximately  $20$  to  $30^0$ , amplitude value for which peak velocity tends to saturate (Becker, 1991) (Figure 4.8). On average, a  $1^0$  increase in amplitude results in a peak velocity increase of approximately  $20^0/\text{s}$  (Collins et al., 2008). These stereotyped relations between amplitude, duration and peak velocity over a wide range of human saccades are called the *main sequence* (Bahill et al., 1975). It can also be extended to include saccade peak acceleration and deceleration (Bahill, Brockenbrough, & Troost, 1981).

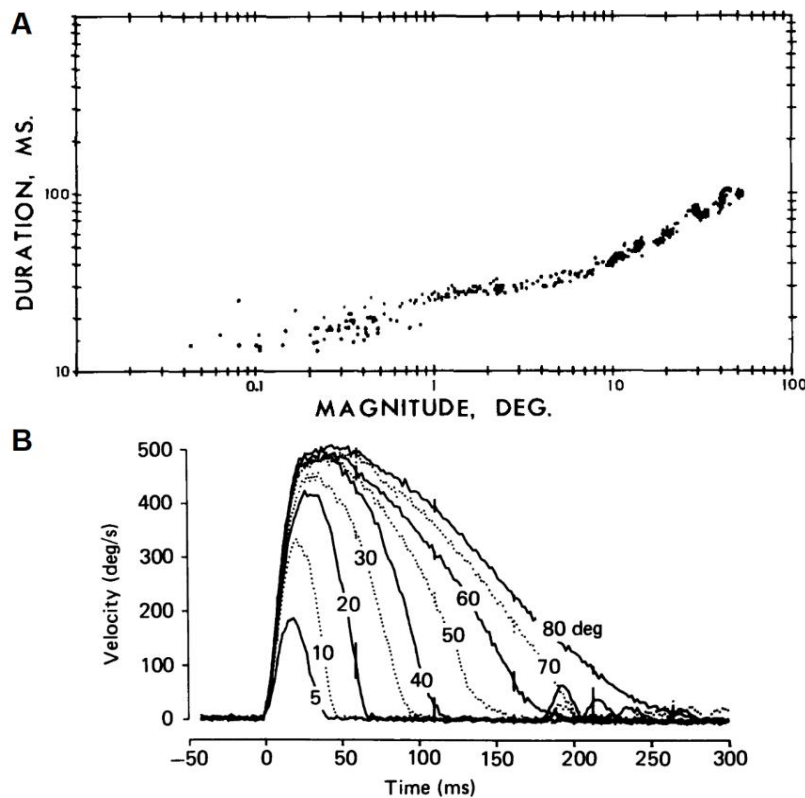


Figure 4.7. (A) Duration versus magnitude (amplitude) of human saccadic eye movements. Source: (Bahill et al., 1975). (B) Typical velocity profiles of horizontal saccades ranging from 5 to 80°. Vertical bars represent  $\pm 1$  standard deviation (SD). The small SD indicates that saccades were very reproducible. Source: (Collewijn et al., 1988a).

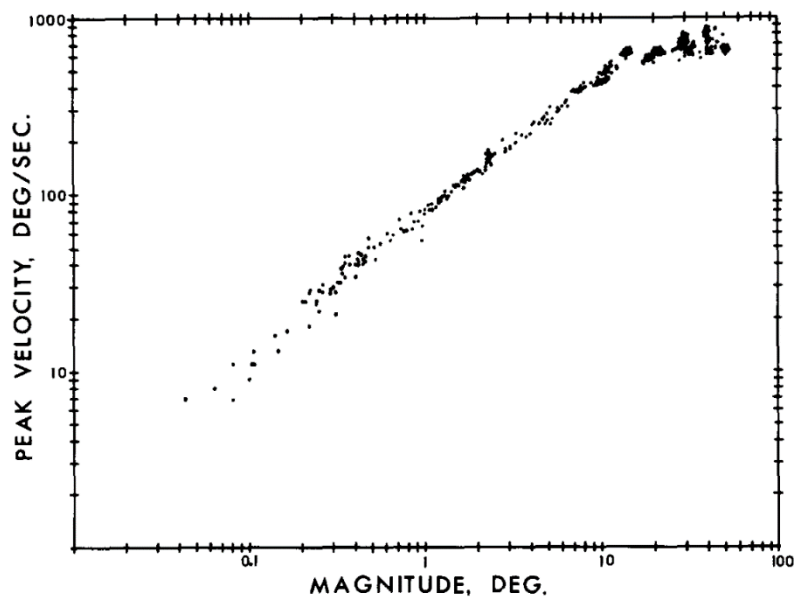


Figure 4.8. Saccadic main sequence. Peak velocity versus magnitude (amplitude) of human saccadic eye movements. Source: (Bahill et al., 1975).

The main sequence is a powerful tool to judge whether a particular saccade is normal or aberrant. The parameters of a normal saccade faithfully follow this relationship. Drugs that reduce alertness (alcohol, barbiturates and diazepam), systemic and neurologic diseases such as Grave's disease, Alzheimer, AIDS or peripheral nerve palsy, or reduced attention and fatigue are factors that may reduce the saccadic peak velocity and, more generally, disturb the kinematics of saccades (Ciuffreda & Tannen, 1995). Moreover, the main sequence plots show that large saccades, microsaccades and the fast phase of optokinetic nystagmus are produced by a common physiological system and they can be used to study the normalcy of eye movements neurophysiological control (Bahill et al., 1975).

Saccade velocity and duration depend to some extent on the direction of the movement and the initial and final orbital position. Temporal saccades are slightly shorter than nasal, with small (between 2 and 4 ms) but significant differences for saccades up to 60° (Collewijn et al., 1988a). Saccades directed toward the center tend to be faster than those directed toward eccentric positions (Collewijn et al., 1988a). Upward saccades made in the upper portion of the ocular motor range are slower than upward saccades made in the lower portion of the ocular motor range. Downward saccades are almost independent of eye position (Collewijn, Erkelens, & Steinman, 1988b).

Oblique saccades are almost indistinguishable from the corresponding characteristics of horizontal or vertical saccades. Thus, any saccade not exceeding 15-20° of the same amplitude can usually be regarded as equal in all respects (Yarbus, 1967).

#### *4.4.1.2. Latency*

The latency, or reaction time, of a saccade has been defined as the period of time between the appearance of the stimulus and the onset of the movement. It is approximately 120 to 350 ms (Carpenter, 1988), although other authors state that it can be up to 1 s (Liversedge, Gilchrist, & Everling, 2011). The distribution of individual saccade latencies is skewed, with a long tail towards longer values (Figure 4.9).

This saccade delay can be thought of as a composite of the time to process the visual stimulus, the accumulation of a decision process and the final motor execution. Over 30 years ago, Carpenter (1981) defined the LATER (Linear Approach to Threshold with Ergodic Rate) model of response times and it has remained popular because of its simplicity (it has only two free parameters) and the ease with which it can be used to model behavior in complex tasks (Noorani & Carpenter, 2016).

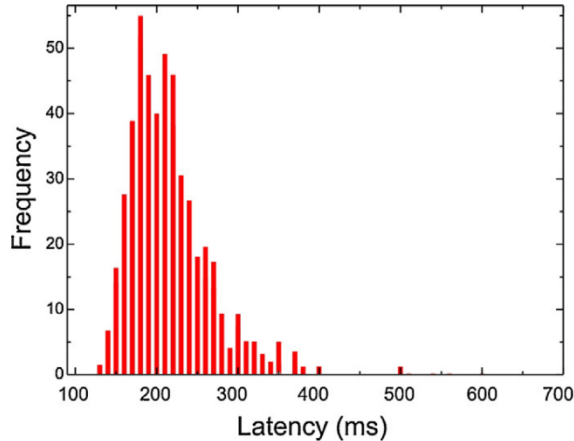


Figure 4.9. Frequency histogram of 486 saccadic latencies. Source: (Noorani & Carpenter, 2016).

One of the key characteristics of saccade latencies is their wide variability, which is significantly larger in children than in adults probably due to poor control over visual fixation (D. P. Munoz, Broughton, Goldring, & Armstrong, 1998; Q. Yang, Bucci, & Kapoula, 2002). Saccade latency is considerably affected by both top-down and bottom-up processes (Leigh & Zee, 2015). Some examples of stimulus characteristics that influence the latency of saccades are: luminance, size, contrast or complexity (Doma & Hallett, 1988; Gerardin, Gaveau, Pélisson, & Prablanc, 2011; Marino & Munoz, 2009); whether the target is visual or auditory (Zambarbieri, 2002); the size of the movement, its direction and the initial eyes position (Bonnet et al., 2013; Fuller, 1996); the predictability of the target (Marino & Munoz, 2009); or the stimulus paradigm (Takagi, Frohman, & Zee, 1995). Latency shortens progressively with age during childhood and increases during adulthood. This may reflect different stages of normal development in children and degeneration in the nervous system in the elderly (D. P. Munoz et al., 1998).

#### *4.4.1.3. Corrective saccades*

Frequently, the amplitude of saccades differs from the angular distance between the points intended for fixation. Then, they are followed by a secondary, or corrective, saccade to reduce the error between the position of the eyes at the end of the primary saccade and the position of the target (Figure 4.10). For target amplitudes greater than  $20^\circ$ , the size of the corrective saccade is typically about 10% of that of the primary component. At target amplitudes of  $5-10^\circ$  the primary saccade tends to be accurate, and below that amplitude overshoot rather than undershoot is generally observed (Carpenter, 1988). Thus, saccades tend to undershoot distant targets but overshoot close ones.

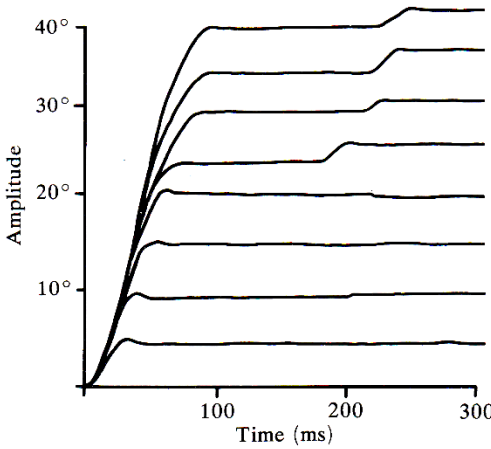


Figure 4.10. Human saccades of different sizes. The beginning of each movement is at time zero. Overshoot for lower amplitude saccades and undershoot for larger amplitude ones can be seen. Source: (Carpenter, 1988).

Corrective saccades are not the result of sensing a visual error at the end of the first saccade. Becker & Fuchs (1969) showed that corrective saccades occurred in total darkness. In the absence of visual feedback, it has been shown that the accuracy of the correction is correlated with the latency of the primary saccades. The longer a subject takes to make the initial saccade, the more accurate the corrective saccade. This implies that the preparation of corrective saccades begins with the preparation of the primary saccades. If visual feedback is available, the prepared correction can be modified to increase the final accuracy (Tian, Ying, & Zee, 2013).

#### *4.4.1.4. Neural control*

In this subsection, a brief overview of the major neural structures involved in the generation and control of saccades is given.

The neural control can be divided into two categories (Ciuffreda & Tannen, 1995). The first reflects higher-level control processes and includes the primary structures involved in target selection, localization, and initial calculation of the desired change in eye position. The second reflects lower-level control processes and includes the primary structures involved in the generation of the pulse-step controller signal to the oculomotor neurons.

The structures of the higher-level control include the frontal eye fields, parietal lobes, superior colliculus, and cerebellum (Figure 4.11). The frontal eye fields are located in the frontal cortex (in Brodmann's area 8) and are involved in the attention and selection of targets for future fixation. Moreover, since they contain a neural map of visual space, they provide the needed information about desired saccade amplitude and direction (Purves et al., 2004). The parietal lobes

are important for shifts of visual attention, which may be accompanied by saccades and are involved in programming saccades to visual targets (Leigh & Zee, 2015). These two structures transmit information to the superior colliculus. The superior colliculus might also contain a motor map, which implies that neurons in a particular region of the superior colliculus are activated by the presentation of visual stimuli in a specific region of visual space. In this region, the information from the frontal eye fields and the parietal lobes is processed, as well as that from other auditory and somatic stimuli, and transmitted to brainstem structures involved in generating the pulse-step signal. The cerebellum controls saccadic accuracy.

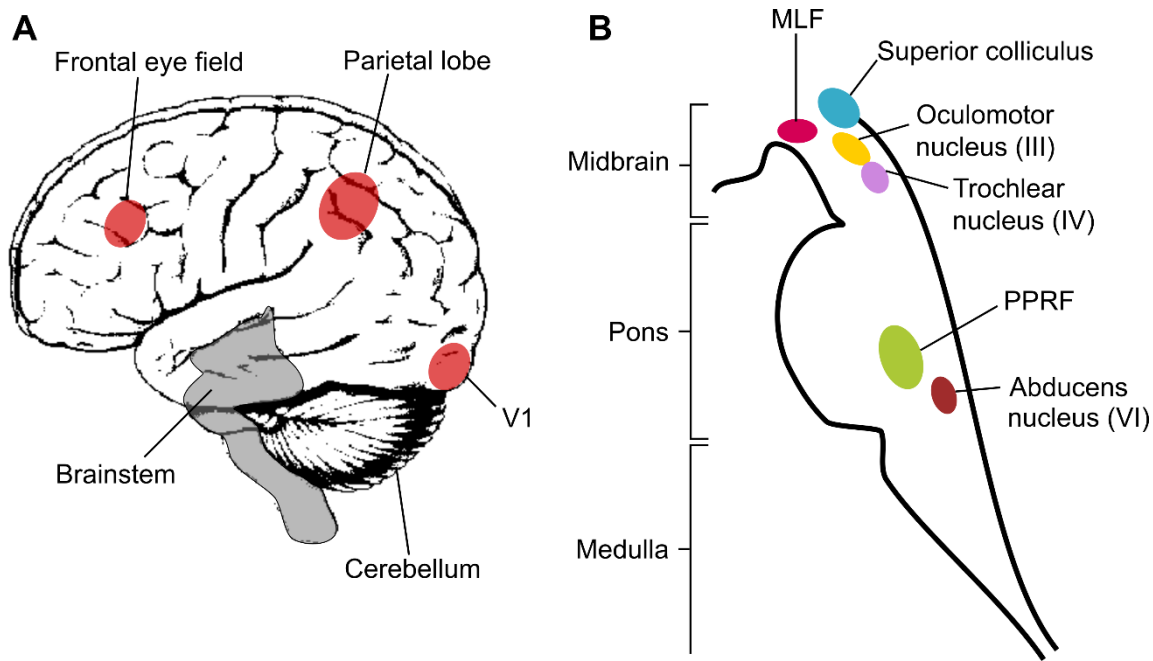


Figure 4.11. (A) The cerebral areas involved in the control of saccades are shaded in red. The brainstem (shaded in gray) is enlarged in panel (B) with a sagittal view. The different brainstem areas that control saccadic movements are represented schematically. V1: primary visual cortex. PPRF: paramedian pontine reticular formation. MLF: medial longitudinal fasciculus.

The direction of saccades is controlled by two different gaze centers in the reticular formation, which receive information from the superior colliculus and the frontal eye field. Horizontal eye movements are generated by a collection of local circuit neurons in the *paramedian pontine reticular formation* (PPRF) or horizontal gaze center. Meanwhile, vertical movements are generated in the *medial longitudinal fasciculus* (MLF) or vertical gaze center (Figure 4.11B). Activation of both centers simultaneously results in oblique movements, whose trajectories are determined by the relative contribution of each center. The pathways for the control and generation of horizontal saccades are illustrated in Figure 4.12. Neurons in the PPRF project to the ipsilateral abducens

nucleus, where there are motor neurons that innervate the ipsilateral lateral rectus, and internuclear neurons that send their axons to the contralateral oculomotor nucleus. The oculomotor nucleus contains motor neurons that innervate the medial rectus. As a result, activation of PPRF neurons on one side of the pons causes a horizontal movement of both eyes towards the same side. In parallel, there is an inhibitory circuit of neurons that project to the contralateral abducens nucleus, where they project on motor neurons to the lateral rectus and internuclear neurons to the contralateral oculomotor nucleus. As a consequence, there is a reduction of activity of the ipsilateral medial rectus and the contralateral lateral rectus (Purves et al., 2004).

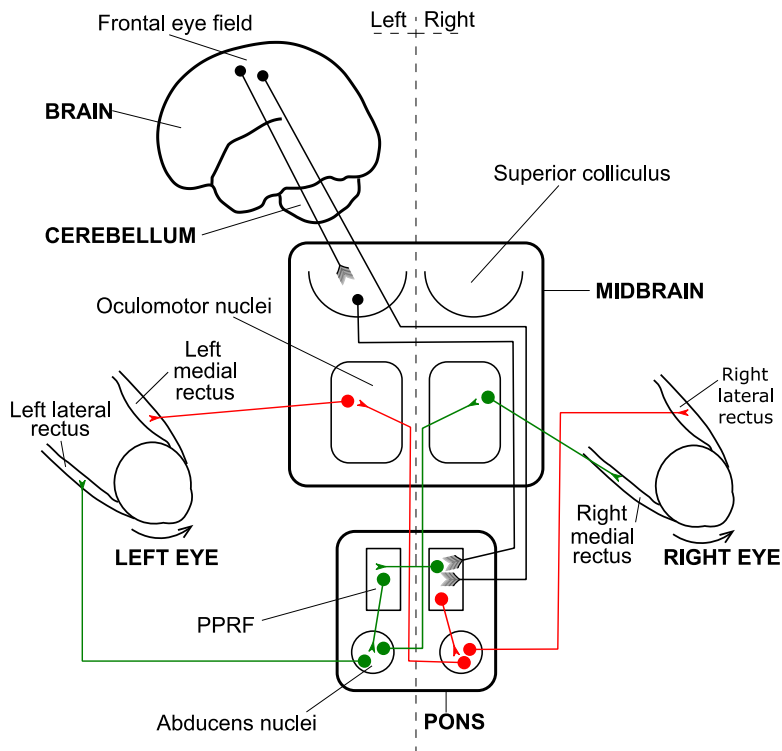


Figure 4.12. Schematic representation of the neural pathways involved in the control of a rightward horizontal saccade. Red: excitatory circuit. Green: Inhibitory circuit. PPRF: Paramedian pontine reticular formation.

The lower-level process involves the generation of the pulse-step neural controller signal (Bahill & Stark, 1979), which is inferred to be the neural signal for the ocular motor neurons to generate saccades. It requires precise synchronization of two basic neural elements: burst and pause neurons (Figure 4.13). The burst neurons for horizontal and vertical saccades are located in the PPRF and the MLF, respectively. They receive information from the superior colliculus and the frontal eye fields and begin high-frequency firing just before and during a saccade. Their pulse of neural activity is correlated with the peak velocity and amplitude of the saccade. The pulse component of the controller signal is responsible for the rapid movement of the eyes. Then, the neural integrator

integrates the pulse, which becomes a step, and the combined pulse-step controller signal is transmitted to the appropriate motor neurons. The step is responsible for maintaining the eyes in the new position (tonic neurons). In contrast, omnipause neurons fire continuously at a constant rate in order to inhibit burst cells except just before and during a saccade. The pulse-step neural controller signal which produces excitation to the agonist muscle is mirrored by a similar inhibitor signal to the antagonist muscle.

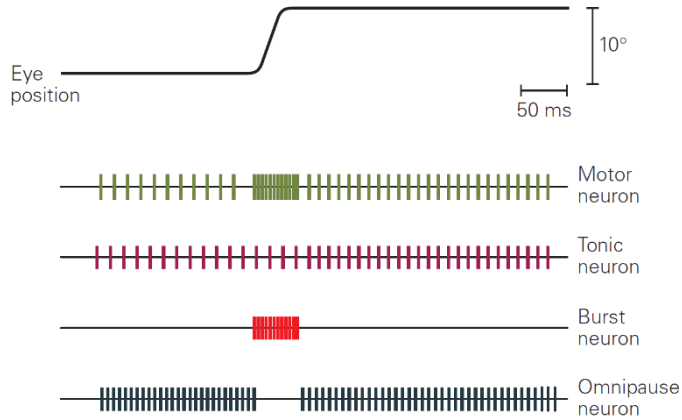


Figure 4.13. Example of the firing rate of different neurons that control saccadic movements. Source: (Kandel, Schwartz, Jessell, Siegelbaum, & Hudspeth, 2013).

#### 4.4.2. Vergence eye movements

Vergence movements are disjunctive movements, which means that the two eyes move in opposite directions. They are used to align the fovea of each eye with targets located at different distances from the observer. For *convergence* movements the angle between both lines of gaze increases in order to have binocular single vision of a nearer object of interest. In contrast, for *divergence* movements this angle decreases as the lines of gaze intersect in a farther target.

##### 4.4.2.1. Stimuli to vergence movements

In 1893, Maddox identified four stimuli that drive vergence movements, which led to classify vergence into four components: disparity vergence, accommodative vergence, proximal vergence, and tonic vergence (Ciuffreda, 1992).

*Disparity or fusional vergence* is driven by binocular retinal disparity as its primary input. Retinal disparity is the angular positional difference at the eyes between an object in the field and the binocular fixation point. Fusional vergence is the response of the motor aspect of binocular vision. Hence, the role of this movement is to reduce the retinal disparity within the limits of Panum's

fusional areas in order to obtain single binocular vision of the object of interest (Ciuffreda & Tannen, 1995). The optimal response of the vergence system is shown with disparity values less than 2 to 4° (Erkelens, 1987; Schor, Robertson, & Wesson, 1986). Therefore, the motor responses are usually initiated by other high-level cues and disparity is mainly used as a feedback to refine the response once the stimulus' disparity is reduced to this range of values.

The disparity vergence system can be characterized according to several aspects. For example, according to its horizontal, vertical, and cyclodisparity retinal components; with respect to the direction of the movement (convergence versus divergence); or with respect to the target spatial location as symmetric or asymmetric disparity vergence. Symmetric disparity vergence is elicited when the targets are aligned along the midline. Then, retinal disparity is symmetrically distributed into the two eyes. Conversely, asymmetric disparity occurs when the target is placed in any other position. An asymmetric vergence response typically consists of a small initial vergence movement followed by a saccade to position the eyes to have fairly symmetric retinal disparity. The response is finished with an approximately symmetric vergence movement (Ciuffreda & Tannen, 1995). The interaction between saccadic and vergence systems is reviewed in section 4.4.2.6.

*Accommodative vergence* is associated with a change in blur-driven accommodation. It is present in both monocular and binocular viewing conditions. While fusional vergence movements aim to reduce the stimulus that produces them (retinal disparity) using negative visual feedback, vergence movements driven by accommodation have no direct effect upon the retinal blur stimulus that evokes them. Thus, they are open-loop responses.

*Proximal vergence* is caused solely by the apparent or perceived nearness of targets in the field. Although it has not been a popular subject of study, some authors concluded that proximal vergence might have a relevant contribution to the overall vergence response (North, Henson, & Smith, 1993; Wick & Bedell, 1989). In open-loop conditions, proximity begins to exert an influence on the vergence system for objects closer than 3 m (Rosenfield, Ciuffreda, & Hung, 1991).

Finally, *tonic vergence* is driven by the baseline midbrain neural stimulation. For this reason, the eyes of a conscious adult subject in the absence of disparity, blur, and proximal stimuli are not in the position of anatomical rest but in a more convergent position at a distance of 120 to 200 cm (Fincham, 1962; Owens & Liebowitz, 1980). It can be regarded as a bias term into the vergence system and is not related with any other oculomotor parameter (Ciuffreda & Tannen, 1995).

#### 4.4.2.2. Interactions between vergence and accommodation

The *near response*, or *near triad*, is comprised of three motor responses that occur when humans shift their gaze from a distant to a near fixation target: convergence, accommodation, and pupil constriction. Under normal viewing conditions, these three actions usually occur in conjunction with saccades and other compensatory eye movements induced by head movements (Mays & Gamlin, 1995b). The interaction between vergence and accommodation systems is of particular interest to understand the whole oculomotor behavior and evaluate binocular vision.

The strength of the association between accommodation (A) and accommodative convergence (AC) is the AC/A ratio, which is typically measured in PD/sphere diopters (D). It can be assessed in the laboratory and clinically by removing the stimulus for disparity vergence. In fact, its assessment is important for the diagnosis of binocular dysfunctions and to determine the appropriate management plan. The expected AC/A ratio in normal subjects is  $4 \pm 2$  PD/D (Scheiman & Wick, 2014). Not only is convergence (C) linked to accommodation but, likewise, accommodation is linked to vergence through convergence-driven accommodation (CA). The CA/C ratio, expressed in D/PD, measures the strength of this relationship and ranges between 0.08 and 0.15 D/PD (Kersten & Legge, 1983; Miles, Judge, & Optican, 1987). The CA/C ratio is not commonly assessed in clinics.

Over the last decades, several authors have proposed different static and dynamic models of the vergence system. The most popular ones are probably those proposed by Clifton M. Schor and George K. Hung. A simplified example of the vergence model proposed by Schor is shown in Figure 4.14. Although the detailed description of these models is out of the scope of this section, a brief overview is given. For a detailed explanation see (Schor, 1992) or (Hung, 1992). Both models are based on negative feedback control and agree in a general organization comprised of a phasic or transient and a tonic or sustained components. The phasic component is responsible for the initial fast response to a stimulus, while the tonic component holds the eyes into the new position. An important feature of the control models is the adaptation of the tonic component to remove progressively the stimulus from the phasic control element. One of the main difference between the models proposed by Schor and Hung is the origin of the cross-links between the accommodative and vergence systems. While Schor supports that cross-links origin before the adaptable tonic component, Hung places them after tonic adaptation. Both models are supported by several observations of the dynamic behavior of accommodation, vergence, and their interactions that fit well with model simulations (Hung, 1992; Schor, 1992). It is important to notice that besides disparity and blur, other cues such as stimulus' proximity, size, or texture also contribute to the overall vergence response (Hung, Ciuffreda, & Rosenfield, 1996; Schor, Alexander, Cormack, & Stevenson, 1992). A parallel field of research

studies how different cues are combined and weighted to give an accurate response (Ernst & Banks, 2002; Girshick & Banks, 2009; Hillis, Watt, Landy, & Banks, 2004).

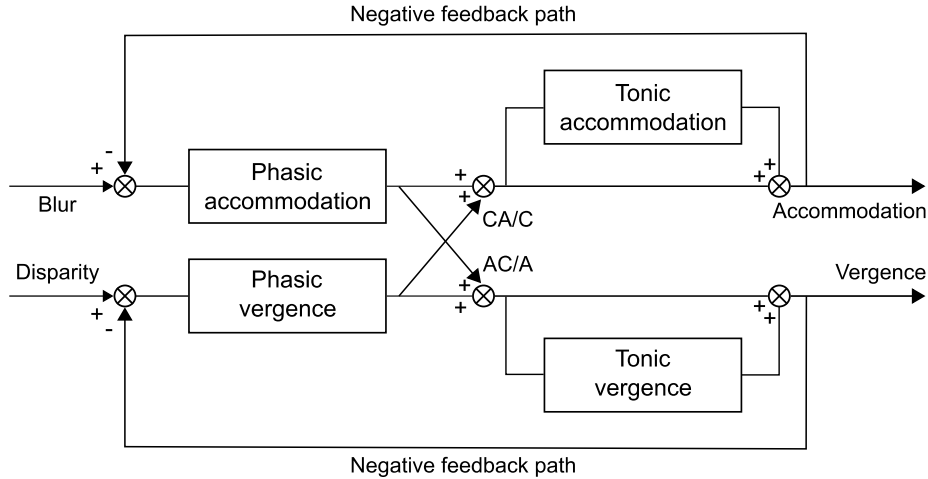


Figure 4.14. Simplified block diagram of a model of accommodation (upper branch) and vergence (lower branch) systems and their interactions proposed by Schor (1992).

#### 4.4.2.3. Dynamics of vergence

Vergence responses to a step change in retinal disparity contain two components: an initial fast open-loop component, which is directly related to the underlying motor neural controller signal and lasts for several hundred milliseconds, followed by a smaller and slower closed-loop component that reduces the residual disparity to within neurosensory tolerances (Panum's fusional area). A phase plane plot (velocity versus position) is useful for analyzing the response dynamics and determining when changes in dynamics occur (Figure 4.15A) (Alvarez, Semmlow, Yuan, & Munoz, 1997). Typically, the difference in vergence amplitude between that found for the fast phase versus the fast-plus-slow phases is less than  $0.5^{\circ}$  (Hung, Ciuffreda, Semmlow, & Horng, 1994).

As discussed for saccades in section 4.4.1.1, there is also a main sequence for vergence movements which relates their peak velocity with their amplitude (Figure 4.15B). Vergence response peak velocity increases in proportion to vergence response amplitude, with a ratio of 4:1 (Hung et al., 1994). Hung et al. (1994) represented main sequences of vergence responses under free viewing condition and using an haploscope. Vergence responses under free viewing condition were elicited by disparity, blur and proximity stimuli, while in the haploscope only disparity vergence was stimulated. They concluded that both types of vergence responses followed the same main sequence (Hung et al., 1994). More recently, Maxwell et al. supported the finding that the main sequence of responses to disparity and blur stimuli was virtually identical to responses to disparity only stimuli

(Maxwell, Tong, & Schor, 2010). In contrast, they found that the velocities of responses to disparity (either only disparity or disparity with blur) were about twice as great as the responses in which blur alone was the cue (Aligned, Monoc Line and Binoc Line in Figure 4.15B). Hung et al. (1994) also tested different conditions that differed on the presence or absence of a target and its periodicity. The fact that the vergence responses in all conditions followed the same main sequence suggested the presence of a *common neural controller* relatively independent of the stimulus conditions.

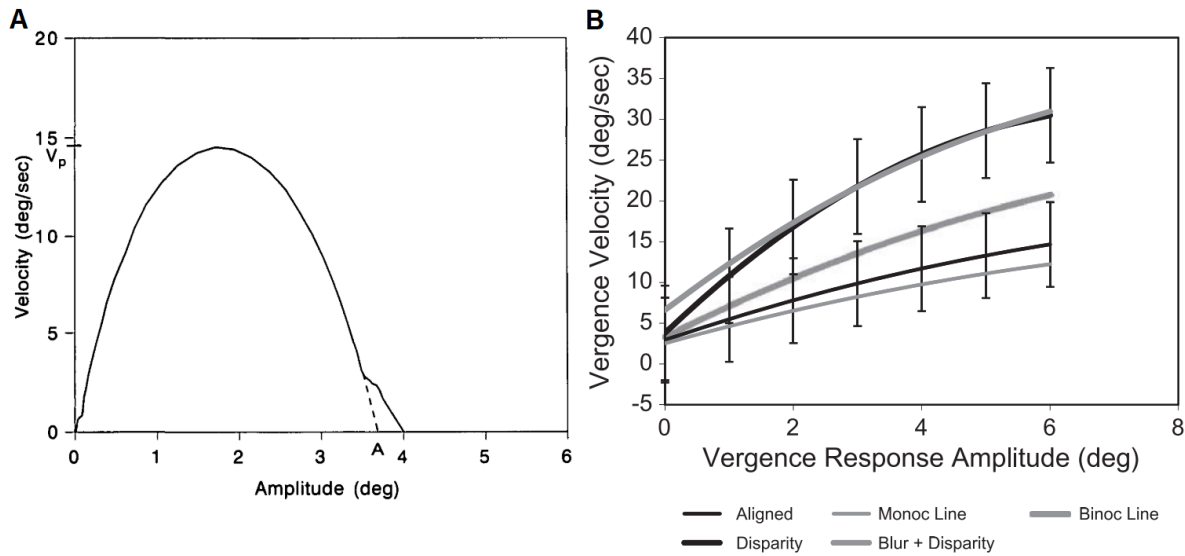


Figure 4.15. (A) Phase plane plot showing peak velocity versus amplitude for a single vergence movement. A: amplitude of the fast component;  $V_p$ : vergence peak velocity. Source: (Hung et al., 1994). (B) Main sequence of accommodative vergence elicited by three different stimuli (Aligned, Monoc Line and Binoc Line), disparity vergence (Disparity), and vergence responses to both disparity and blur cues (Blur + Disparity). The error bars show the SD of the means between subjects for Aligned and Disparity responses. SD for other conditions were similar but not shown for clarity. Source: (Maxwell et al., 2010).

As shown in Figure 4.15, vergence velocities (typically  $<30^\circ/\text{s}$ ) are much slower than saccadic peak velocities. Accordingly, its duration is also much longer. In addition to these fundamental differences between saccades and vergence movements, there are also dissimilarities between convergence and divergence movements. In general, faster dynamics are reported for convergence than divergence movements (Alvarez, Semmlow, Yuan, & Munoz, 2002; Hung, Zhu, & Ciuffreda, 1997; Krishnan, Farazian, & Stark, 1973; Zee, Fitzgibbon, & Optican, 1992). In fact, divergence peak velocity is influenced by the initial position of the stimulus; if the eyes start very converged, then the divergence velocity is faster. However, convergence movements do not show this dependence on starting vergence angle (Alvarez, Semmlow, & Pedrono, 2005). The same research group also showed that divergence dynamics decreased as the visual stimulus moved away for smoothly moving ramp stimuli (Y. Y. Lee, Chen, & Alvarez, 2008).

Vergence dynamics are similar from about 8 years of age until the mid-forties (Qing & Kapoula, 2004). In response to a disparity step stimulus, older subjects generate vergence responses with longer latency and decreased peak velocity and acceleration compared to younger subjects (Rambold, Neumann, Sander, & Helmchen, 2005). However, responses to ramp disparity stimuli are similar in older and younger subjects. Conversely, in response to monocular, mainly accommodative stimuli, older subjects generate similar initial responses to younger subjects, but show a decreased response to ramp disparity stimuli (Rambold et al., 2005). The decrease in steady-state response to accommodative stimuli may be caused by presbyopia. This reduction in accommodative ability may lead to compensatory adaptation in the linkage between convergence and accommodation (Rosenfield & Ciuffreda, 1990; Rosenfield, Ciuffreda, & Chen, 1995).

The occurrence of saccades concurrently with vergence is a common phenomenon and leads to a change in vergence dynamics. This aspect is addressed in the subsection 4.4.2.6.

Another factor that has been found to alter vergence dynamics is the presence of convergence insufficiency. Several studies support that subjects with convergence insufficiency have reduced vergence peak velocities compared to binocularly normal controls (Alvarez et al., 2010; Thiagarajan, Ciuffreda, & Ludlam, 2011; van Leeuwen, Westen, van der Steen, de Faber, & Collewijn, 1999). Alvarez & Kim (2013) showed that the convergence peak velocity was more asymmetric between the two eyes in patients with convergence insufficiency compared to control subjects with normal binocular vision, whose convergence peak velocity was almost identical in the two eyes when they stared at symmetric convergence step stimuli. They also found that the responses of the convergence insufficiency patients became significantly more symmetrical after vergence training. However, in this study they did not take into account the relationship between phoria and phoria adaptation with the convergence and divergence peak velocity, which was previously found by the same group (Kim & Alvarez, 2012a; Kim, Granger-Donetti, Vicci, & Alvarez, 2010). Vergence training has been found to be an effective method to improve vergence temporal characteristics and accuracy also in subjects without binocular dysfunctions (Talasan, Scheiman, Li, & Alvarez, 2016).

#### *4.4.2.4. Latency*

Latency of vergence movements is rather similar to that of saccades, i.e. around 120 to 200 ms, especially in adults. In children, vergence latency tends to be shorter than that of saccades (Bucci, Kapoula, Yang, & Bremond-Gignac, 2006). Latency depends on the prediction degree of the stimulus (Figure 4.16). In response to regular, predictable target jumps of a visual target between far and near locations, most subjects make vergence drifts in anticipation of the target (Kumar, Han, Garbutt, &

Leigh, 2002; Yuan, Semmlow, & Munoz, 2000). For smooth vergence responses to ramp stimuli, latency also decreases when the motion of the target is predictable (Erkelens, van der Steen, Steinman, & Collewijn, 1989). The section 5.4 focuses on the effect of stimulus predictability on vergence movements.

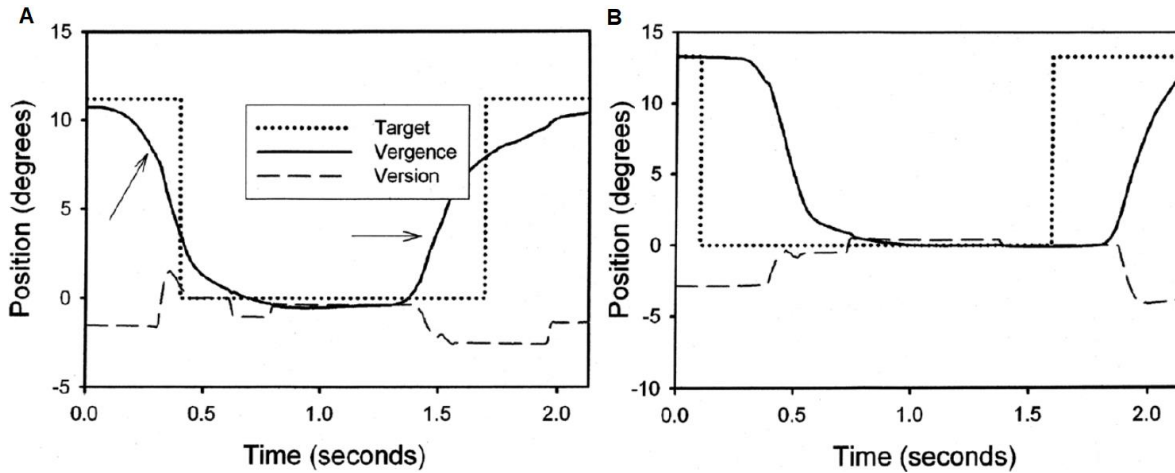


Figure 4.16. (A) Response to a predictable stimulus. Vergence precedes the target jumps (arrows). (B) Response to an unpredictable stimulus. Vergence follows the target jumps. Source: Modified from (Kumar et al., 2002).

Controversy exists regarding the differences in latency between convergence and divergence. Some authors found longer latencies for convergence than divergence (Krishnan et al., 1973; Q. Yang et al., 2002), while others reported the opposite behavior (Alvarez et al., 2002; Hung et al., 1997; Semmlow & Wetzel, 1979). Similarly than for vergence peak velocity, Alvarez et al. (2005) found that divergence latency depends on the starting vergence angle. In contrast, convergence latency seems to be fairly independent of the starting stimulus position.

Considering the disparity and accommodative vergence components separately, latencies for disparity vergence are shorter than for accommodative vergence, both for convergence and divergence movements (Semmlow & Wetzel, 1979). For this reason, under normal binocular viewing conditions, disparity vergence typically precedes any accommodative vergence contribution by approximately 100 ms. This may be functionally beneficial, since it allows the retinal image to approach the fovea first, where the accommodative gain is highest.

#### 4.4.2.5. Neural control

Many neural structures are involved in the control of vergence movements (Figure 4.17). Structures involved in the reception of sensory afferent signals (disparity and blur) and its transmission to motor areas include the primary visual cortex, the medial temporal visual area and the medial superior

temporal visual area, the parietal cortex, the frontal eye fields, the superior colliculus, the nucleus reticularis tegmenti pontis, and some areas of the cerebellum. The posterior interposed nucleus of the cerebellum projects to the supraoculomotor nucleus, which is the area responsible to generate the final controller signal to the oculomotor neurons (Levin et al., 2011).

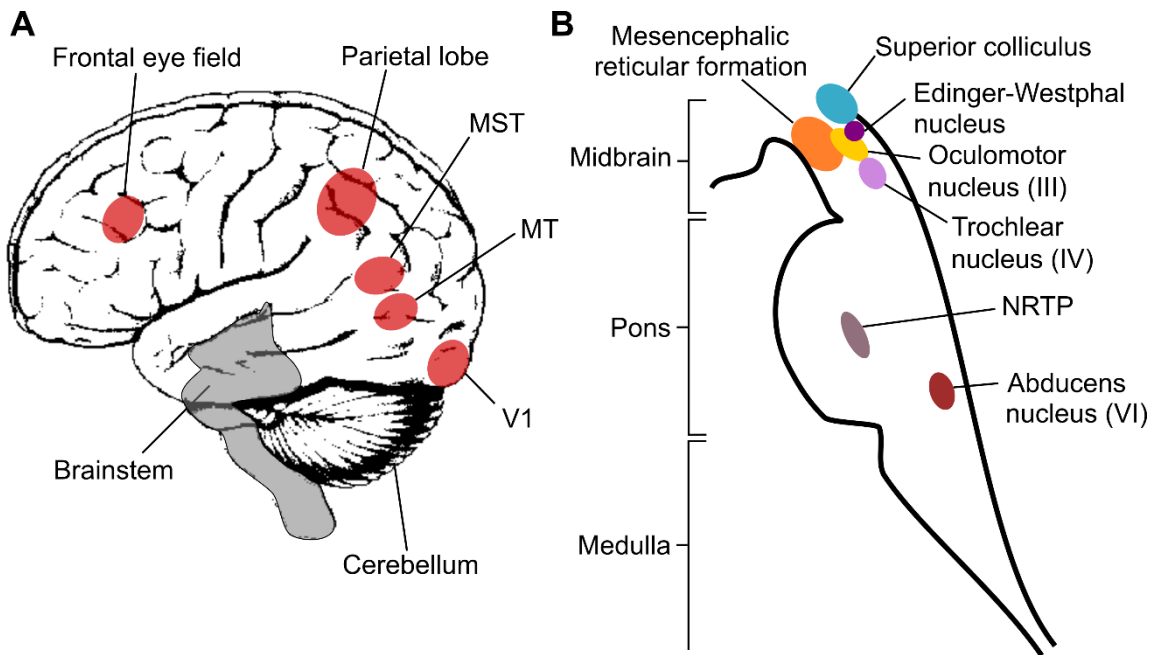


Figure 4.17. (A) The cerebral areas involved in the control of vergence movements are shaded in red. The brainstem (shaded in gray) is enlarged in panel (B) with a sagittal view. The different brainstem areas that control vergence are represented schematically. V1: primary visual cortex. MT: medial temporal visual area. MST: medial superior temporal visual area. NRTP: nucleus reticularis tegmenti pontis.

The final controller signal consists of a small and broad pulse combined with a step having characteristics appropriate for the relatively slow vergence response (Ciuffreda & Tannen, 1995). Three types of midbrain neural cells lying in the mesencephalic reticular formation (Figure 4.17B), near the oculomotor nucleus in a region called the supraoculomotor nucleus, have been found to be responsible for the overall vergence control (Mays, Porter, Gamlin, & Tello, 1986; Zee & Levi, 1989): burst, tonic, and burst-tonic neurons. Vergence burst neurons only fire just before and during the vergence response and have a profile similar to the instantaneous vergence velocity. These cells seem to provide velocity and position signals to the medial rectus motor neurons. There are both convergence and divergence burst neurons, although convergence ones are more abundant (Leigh & Zee, 2015). Vergence tonic neurons change their firing rate 10 ms to 30 ms before the vergence movement, which is proportional to vergence angle. There are more convergence tonic cells than divergence tonic cells (Leigh & Zee, 2015). Vergence burst-tonic neurons combine both vergence

position and velocity information: the burst is related to vergence velocity and the tonic firing rate to vergence angle. Excitatory connections of the supraoculomotor nucleus project to the oculomotor nucleus, which innervates the medial recti muscles. Conversely, inhibitory connections project to the abducens nucleus to inhibit activity of the lateral recti muscles.

Burst neurons in the mesencephalic reticular formation may be part of the substrate for interactions between vergence and accommodation systems as they also provide commands to the Edinger-Westphal nucleus to stimulate accommodation (Mays & Gamlin, 1995b). Stimulation of the Edinger-Westphal nucleus also results in pupillary constriction.

#### *4.4.2.6. Saccade-vergence interactions*

In normal viewing conditions, pure vergence movements rarely occur, as targets should be carefully aligned along the midline to elicit symmetrical movements. Thus, vergence movements typically occur in conjunction with other types of ocular movements.

As shown in the following sections 5.3 and 5.4, even symmetrical vergence elicited by a stimulus carefully aligned along the midline is usually accompanied by involuntary saccades (Collewijn, Erkelens, & Steinman, 1995; Coubard & Kapoula, 2008; Erkelens, Steinman, & Collewijn, 1989; Kenyon, Ciuffreda, & Stark, 1980; Semmlow, Chen, Granger-Donetti, & Alvarez, 2009; Semmlow, Chen, Pedrono, & Alvarez, 2008). Similarly, saccades between isovertgent targets are usually accompanied by characteristic vergence movements (Collewijn et al., 1988a, 1988b; van Leeuwen, Collewijn, & Erkelens, 1998). Some authors reported a higher prevalence of saccades during symmetrical divergence than during symmetrical convergence (Collewijn et al., 1995; Kenyon et al., 1980; Zee et al., 1992).

Saccade-vergence interaction is a valuable tool to investigate the modularity of saccade and vergence systems, which in essence is related to the still unresolved debate between Hering and Helmholtz theories (Coubard, 2013; King, 2011). Hering proposed that the two eyes should be considered as a whole organ, and advocated a binocular control of eye movements by which both eyes receive simultaneously two equal innervations (see section 4.1.4) (Hering, 1977). He defended that vergence and saccadic movements are controlled by two independent systems. Oppositely, Helmholtz supported the hypothesis that eye movements are controlled monocularly by two separate commands for the two eyes instead of for conjugate and vergence movements.

Following Hering's conception, Yarbus (1967) supported the additivity hypothesis by which a combined movement is the result of a linear sum of saccades and vergence movements. However,

Ono & Nakamizo (1978) and Ono et al. (1978) found that saccades were too disconjugate (unequal) in terms of amplitude and velocity between the two eyes to be only explained by the additivity hypothesis. Several authors supported this finding (Enright, 1984; Kenyon et al., 1980), and Enright (1984) concluded that saccades and vergence are not summed in combined movements but they interact. This interaction has been confirmed and formalized with models by other authors (Erkelens, Steinman, et al., 1989; Zee et al., 1992).

As a result of the interaction, the dynamics of combined eye movements are different from those of pure saccade and pure vergence. On the one hand, vergence movements are speeded up by concurrent saccades (Enright, 1984; Erkelens, Steinman, et al., 1989; Kim & Alvarez, 2012b; Maxwell et al., 2010; Semmlow et al., 2008; Zee et al., 1992). Saccades are more likely to occur in vergence responses with reduced peak velocity. Hence, saccades may facilitate the response when the dynamic properties of vergence are modest. An evidence of this fact is the finding that the prevalence of saccades during convergence in patients with convergence insufficiency is significantly higher before vergence training than after it (Alvarez & Kim, 2013). On the other hand, saccades made in conjunction with vergence are slower than pure saccades of a similar amplitude (Collewijn et al., 1995). Interestingly, accommodation is also speeded up when saccades occur concurrently (Schor, Lott, Pope, & Graham, 1999).

The neural mechanisms for vergence-saccade interactions are not fully understood (Leigh & Zee, 2015). One hypothesis is that omnipause neurons not only inhibit saccadic burst neurons, but also provide a weak inhibition of vergence burst neurons (Mays & Gamlin, 1995b). Therefore, the release of omnipause neurons inhibition during a saccade would allow the vergence burst neurons to fire more vigorously, which would result in an increment of vergence velocity. Although electrophysiological results support this hypothesis (Mays & Gamlin, 1995a), there is also some evidence against it (Leigh & Zee, 2015).

#### 4.4.3. Smooth pursuit

Smooth pursuit is the movement of the eyes executed in order to track a small moving target. It is typically accompanied by saccades. It is important to point out the fact that while saccades respond primarily to the position of the retinal image of an object, smooth pursuit responds basically to its motion.

#### 4.4.3.1. Dynamics of smooth pursuit

The usual stimulus for smooth pursuit is movement of an image upon the retina, and its main objective is to match eye velocity to target velocity. Therefore, it maintains retinal image velocity to essentially zero after its initiation. The image of the object does not need to lie on the fovea. Pursuit can occur in any meridian, but it is smoother and more precise in the horizontal direction (Ke, Lam, Pai, & Spering, 2013). The initial acceleration of the eye in response to horizontal target motion is greater for targets moving towards the fovea than for targets moving away from the fovea. For vertical target motions, eye accelerations are greater for stimulus motion in the lower visual field, irrespective of whether the target is moving towards or away from the fovea (Ke et al., 2013).

There are two components to smooth pursuit responses (Carpenter, 1988). In the first 40 ms approximately, the acceleration of the eye is constant and the response is unrelated to any aspect of the stimulus, so it is open-loop. Typical values for this initial eye acceleration range from 40 to  $100^{\circ}/s^2$ , varying from subject to subject (Leigh & Zee, 2015). The later component is in close-loop; thus, influenced more obviously by the nature of the stimulus (its position, velocity and background).

The maximal velocities achieved in humans depend on the kind of target used and ranged from 80 to  $160^{\circ}/s$  (Carpenter, 1988).

During smooth pursuit of a sinusoidal target motion, performance is usually evaluated by measuring gain (peak eye velocity/peak target velocity) and phase, which is a measure of the temporal synchrony between the target and the eye. During ideal pursuit tracking, the gain is close to 1 and phase shift is small (the eye does not lag behind the target). With constant velocity targets (ramps), pursuit gain does not significantly deteriorate until target velocity exceeds about  $100^{\circ}/s$ . Up to this velocity saturation, gain is typically less than 1 but fairly constant (Figure 4.18).

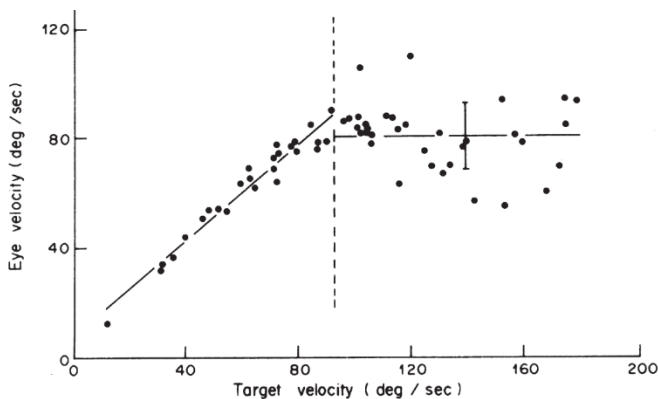


Figure 4.18. Demonstration of pursuit velocity saturation, which becomes evident with target velocities above  $93^{\circ}/s$ . Source: (Meyer, Lasker, & Robinson, 1985).

#### *4.4.3.2. Latency*

The latency of smooth pursuit is very consistent, with a mean of  $100 \pm 5$  ms to targets moving at 5°/s or faster. For lower velocities, latency increases to 125 ms. These values are not only similar among subjects, but they are also very repeatable from day to day for individuals (Carl & Gellman, 1987).

The latency of smooth pursuit depends on several stimuli's characteristics (Leigh & Zee, 2015): bright targets elicit movements with shorter latency than do dim targets, and stationary distractors increase the pursuit latency (Knox & Bekkour, 2004). However, there is no change in the latency of smooth pursuit with age (Morrow & Sharpe, 1993; Straube, Scheuerer, & Eggert, 1997).

#### *4.4.3.3. Effect of prediction*

The study of predictive properties of smooth pursuit has been an active research area (Kowler, Aitkin, Ross, Santos, & Zhao, 2014).

The human pursuit system is capable of learning to improve its response to repetitive stimuli with practice (Westheimer, 1954). In addition, prediction not only occurs when tracking repetitive predictable stimuli, but also when the motion is unpredictable. In this case, anticipatory responses depend on the properties of the motions tracked in the recent past (Santos, Gnang, & Kowler, 2012). Smooth pursuit does not stop when the tracked target is intermittently occluded. Instead, anticipation is involved in matching the motion expected at target reappearance. Anticipatory responses can also be evoked by cues that signal the direction (besides the speed) of future target motion (Kowler et al., 2014).

#### *4.4.3.4. Neural control*

In this section, a brief overview of the neural control of smooth pursuit movements is given (Ciuffreda & Tannen, 1995). For a more detailed explanation, see Leigh & Zee (2015). The main brainstem areas involved in the control of smooth pursuit are represented schematically in Figure 4.19.

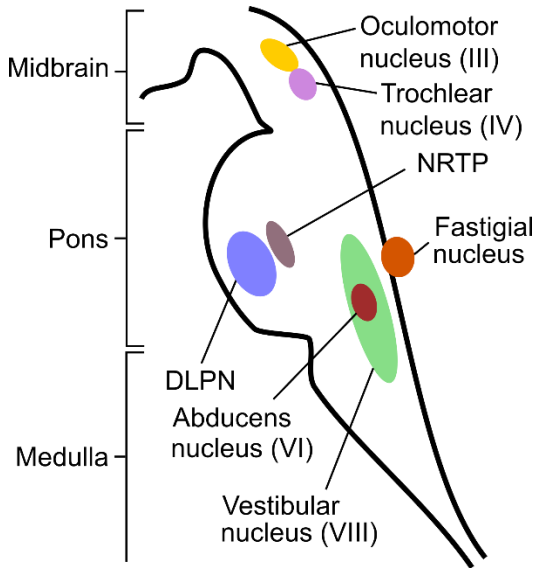


Figure 4.19. Sagittal view of the brainstem with the main areas involved in the control of smooth pursuit. The cerebral areas that project to these regions are represented in Figure 4.20. NRTP: nucleus reticularis segmenti pontis. DLPN: dorsolateral pontine nucleus.

A schematic summary of the neural pathways for smooth pursuit is shown in Figure 4.20. Cells in the primary striate visual cortex (V1) respond to the speed and direction of a moving target, and project to the middle temporal (MT) and medial superior temporal (MST) visual areas. The MT area encodes and processes the direction and velocity of stimulus motion, and the MST area is probably involved in encoding both visual signals related to pursuit and the efference copy of the eye movement command. Then, visual information takes two parallel descending pathways (Leigh & Zee, 2015). In the first pathway (shown in red in Figure 4.20), the MT and MST areas project to the frontal eye fields, which in turn project to the nucleus reticularis segmenti pontis (NRTP), the dorsal vermis in the cerebellum, and the fastigial nucleus. The circuit from the fastigial nucleus to ocular motor neurons has not been defined yet. This pathway is important for smooth pursuit initiation. The second pathway (shown in blue in Figure 4.20) originates from the MT and MST areas, which project to the dorsolateral pontine nucleus (DLPN), the paraflocculus in the cerebellum, and the vestibular nucleus. Neurons in the vestibular nucleus are responsible for integrating the eye velocity signals in eye position signals and project to motor neurons. This second pathway is important for sustaining smooth pursuit. There is an additional pathway (not shown in Figure 4.20) from the MT and MST areas to the nucleus of the optic tract which generates optokinetic nystagmus.

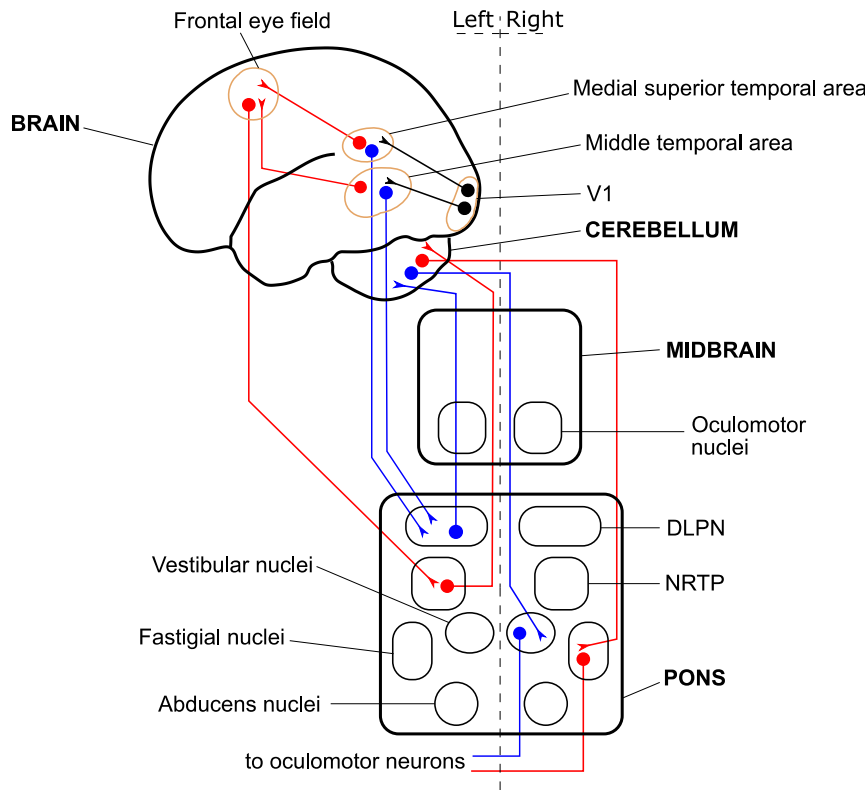


Figure 4.20. Schematic representation of the neural pathways involved in the control of smooth pursuit. Red: pathway involved in smooth pursuit initiation. Blue: pathway involved in sustaining smooth pursuit. DLPN: Dorsolateral pontine nuclei. NRTP: Nucleus reticularis segmenti pontis.

#### 4.4.4. Fixational eye movements

Our visual system is governed by neural adaptation, which means that steady illumination produces weak neural responses, whereas abrupt changes in illumination across space and time generate strong responses (Hartline, 1940). Thus, unchanging features of the scene fade from view. Eye movements during fixation are therefore necessary to overcome the loss of vision due to uniform stimulation of the retinal receptors, even at the potential cost of a decrease in visual acuity in the case of short exposure time to the stimulus (Riggs, Ratliff, Cornsweet, & Cornsweet, 1953). The role of oculomotor fixational mechanisms might not be much retinal stabilization than controlling image motion in an optimal fashion for visual processing (Rucci, Ahissar, & Burr, 2018; Skavenski, Hansen, Steinman, & Winterson, 1979): too much image motion degrades resolution, and too little motion leads to image fading. Even though perfect retinal correspondence is complicated due to the fact that the eyes are never still, we rarely experience diplopia since fixation disparity is maintained within the Panum's fusional areas (Otero-Millan, Macknik, & Martinez-Conde, 2014).

Because of their small amplitude, extensive studies about fixational movements characteristics had to wait for the development of eye tracking techniques exquisitely sensitive to eye movement, but unresponsive to head movement. Moreover, the development of methods to counteract eye movements and thereby cause visual fading led to a large amount of research in the field, especially during the 1950s and 1960s (Ditchburn & Ginsborg, 1952; Riggs & Ratliff, 1952; Yarbus, 1967). It is generally agreed that there are three main types of fixational movements: tremor, drift and microsaccades (Figure 4.21).

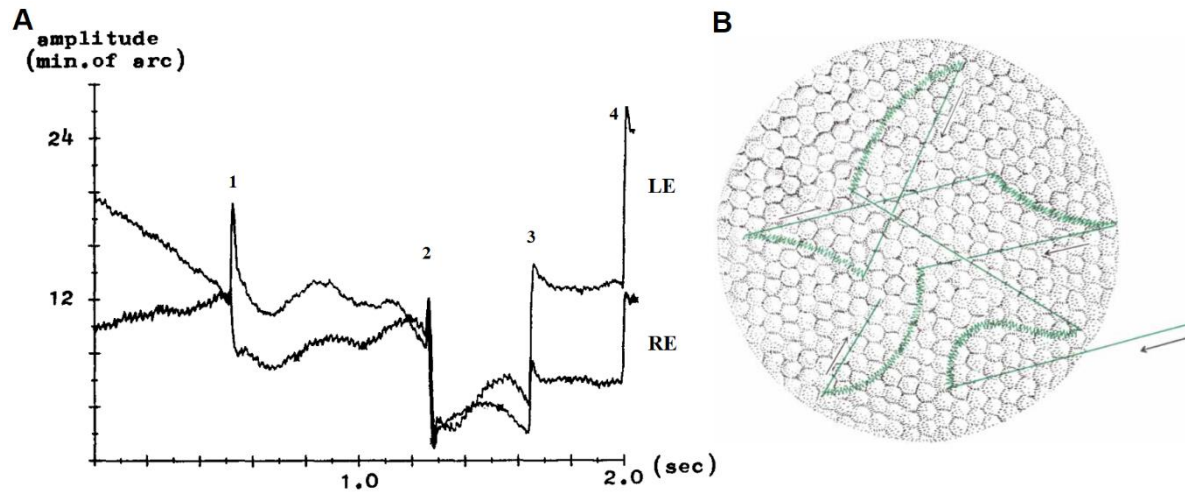


Figure 4.21. (A) Horizontal eyes position of a normal person versus time. The small-amplitude, high-frequency component is tremor; the large and slow excursions are drift; microsaccades are numbered from 1 to 4. LE: left eye. RE: right eye. Source: Modified from (Schulz, 1984). (B) Schematic representation of how fixational eye movements carry the retinal image across the photoreceptors. Tremor is the high-frequency movement superimposed on slow drifts (curved lines). Microsaccades are represented with straight lines. The diameter of the patch of the fovea shown here is 0.05 mm. Source: (Pritchard, 1961).

#### 4.4.4.1. Tremor

Tremor is an aperiodic, wave-like motion of the eyes (Martinez-Conde, Macknik, & Hubel, 2004; Rolfs, 2009). It is the smallest of all eye movements. Only the most accurate eye tracking systems can measure it without falling within the noise level. In fact, some specific devices based on a piezoelectric transduction method have been developed to measure tremor (Bengi & Thomas, 1968; Bolger, Bojanic, Sheahan, Coakley, & Malone, 1999; McCamy, Collins, et al., 2013).

Its amplitude is of the order of the diameter of the smallest cones in the fovea, i.e. around 20 sec arc (Carpenter, 1988; Yarbus, 1967). The frequency of tremor is around 90 Hz (Bolger et al., 1999; Carpenter, 1988). However, reported amplitude and frequency values deviate across various studies depending on the monitoring system used and the performed data analysis. See Table 1 in

Bolger et al. (1999) for a summary of tremor frequency values according to different studies between 1934 and 1999, or Table 1 in Martinez-Conde et al. (2004) for other tremor characteristics according to different authors.

Early binocular examinations found that tremor is independent in the two eyes; there is no binocular correlation (Ditchburn & Ginsborg, 1953). However, Spauschus et al. examined frequency components of ocular tremor and drift and found coherence in the two eyes in both low (up to 25 Hz) and high (60-90 Hz) frequency ranges (Spauschus, Marsden, Halliday, Rosenberg, & Brown, 1999). This finding suggested some level of synchronization that could be due to motor neuron activity.

In general, the main role of fixational eye movements is to preclude visual fading by preventing the eyes from being perfectly still. However, tremor amplitudes rarely exceed the diameter of one photoreceptor. Thus, the importance of this kind of fixational movement in this regard appears to be unclear. Temporal characteristics of tremor – the fact that its frequency is far above the flicker-fusion frequency of the human visual system – have raised further doubts in the significance of this motion for visibility (Yarbus, 1967). Nevertheless, other studies stated that tremor frequencies can be below the flicker fusion limit (Spauschus et al., 1999), and that early visual neurons can follow high-frequency flickering that is over the perceptual threshold for flicker fusion (Martinez-Conde, Macknik, & Hubel, 2002). Therefore, tremor is possibly adequate to maintain activity in the early visual system, which might then lead to visual perception (Martinez-Conde et al., 2004).

Finally, there is no evidence that the amplitude of tremor can be influenced by visual conditions, or by efforts of the will (Carpenter, 1988).

#### *4.4.4.2. Drift*

Drift refers to the irregular, erratic, slow eye movements that occur in between microsaccades during attempted fixation. This motion is random in the sense that a movement is equally likely to be towards or away from the mean direction of the visual axis (Ditchburn & Ginsborg, 1953). Its amplitude is around 2 to 5 min arc and its velocity ranges from 1 to 8 min arc/s, although the mean velocity is 5 min arc/s and the maximum one is 30 min arc/s (Rolfs, 2009; Yarbus, 1967). Therefore, the image of the object being fixated moves across around 15 cones of the central part of the fovea per second. Its frequency is very low, less than 0.5 Hz.

Different studies have obtained discrepant results regarding the binocular coordination of drifts. Some authors concluded that there is no correlation between both eyes (Carpenter, 1991; Krauskopf, Cornsweet, & Riggs, 1960; Yarbus, 1967), while other studies found some level of

synchronization between the two eyes during drifts (Spauschus et al., 1999). Ditchburn & Ginsborg (1953) concluded that the vertical component of drift is conjugate, with the two eyes moving upwards or downwards together, while the horizontal component alternates conjugate movements with periods of convergence and divergence approximately symmetrical for the two eyes.

Cornsweet (1956) concluded that drift is not under direct visual control, it is not error correcting, but it is a result of the instability of the oculomotor system. However, later studies found drifts to correct both fixation position errors (R. M. Steinman, Cunitz, Timberlake, & Herman, 1967) and fixation disparity (St Cyr & Fender, 1969), although only horizontally. More recently, Engbert & Kliegl (2004) showed that on a long timescale (more than 100 ms) both microsaccades and drifts correct fixation position, but only microsaccades correct fixation disparity. Both microsaccades and drift produce random changes in disparity on short timescales (< 20 ms).

#### *4.4.4.3. Microsaccades*

Microsaccades are involuntary small saccades that occur 1-3 times per second during attempted fixation (Otero-Millan, Macknik, et al., 2014). Their amplitude is usually less than 30 min arc, although they can go up to 1° or more (Martinez-Conde, Otero-Millan, & Macknik, 2013; Rolfs, 2009). In fact, most contemporary researchers have adopted the convention of using a 1° upper magnitude threshold. However, microsaccades should not be defined only regarding to their amplitude (Martinez-Conde et al., 2004). Microsaccades duration ranges from 0.2 to 0.3 s, depending on their amplitude (Ditchburn & Ginsborg, 1953; Lord, 1951; Yarbus, 1967).

Microsaccades and saccades share most physical and functional properties. For instance, both saccades and microsaccades are typically binocular and conjugate (Ditchburn & Ginsborg, 1953; Krauskopf et al., 1960; Lord, 1951; Yarbus, 1967). However, Van Horn & Cullen (2012) contradicted this assumption and stated that microsaccades are not strictly conjugate, and other studies reported the presence of monocular microsaccades (Engbert & Kliegl, 2003a; Gautier, Bedell, Siderov, & Waugh, 2016; Hermens & Walker, 2010).

Another feature that shows the link between saccades and microsaccades is the fact that they both follow the main sequence (Otero-Millan, Troncoso, Macknik, Serrano-Pedraza, & Martinez-Conde, 2008; Zuber, Stark, & Cook, 1965) (Figure 4.22). Thus, microsaccades and large saccades (both voluntary and involuntary) might be generated and controlled by the same physiological system (Zuber et al., 1965). Moreover, temporal interactions between saccades and microsaccades further suggest a common triggering mechanism. Rolfs, Laubrock, & Kliegl (2006) found increased latencies for saccades that occur shortly after microsaccades. Later, they showed that this temporal interaction

is strongly dependent on microsaccade amplitude. Microsaccades with larger amplitudes are followed by longer saccadic latencies (Rolfs, Laubrock, & Kliegl, 2008).

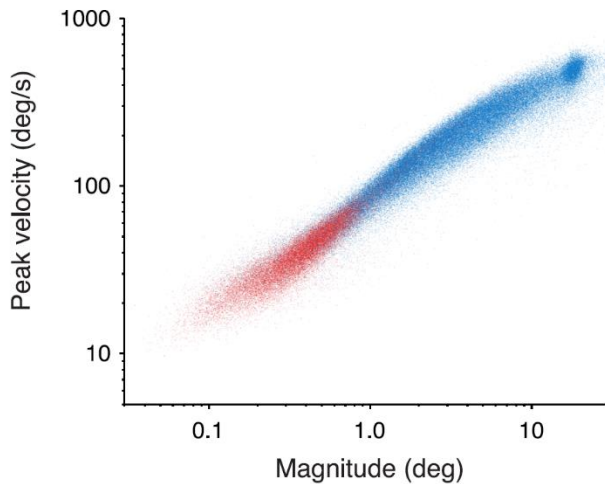


Figure 4.22. Main sequence of saccades in free-viewing conditions (blue) and microsaccades during fixation conditions (red). Source: (Otero-Millan et al., 2008).

The role of microsaccades during visual fixation has been the subject of debate for more than fifty years (see Rolfs (2009) for a review). The first author who tested the initial hypotheses was Cornsweet (1956), who concluded that the role of microsaccades consists in returning the eyes on a fixated target and correct the intersaccadic drift. However, this idea was subsequently challenged. In the early 2000s, Engbert & Kliegl (2004) stated that on a short time scale microsaccades help to counteract retinal adaptation by increasing the persistence of the eyes' random walk (introducing fixation errors), while on a longer time scale they reduce fixation position errors of the eyes, as well as binocular disparity. Although several studies observed lower microsaccade rates during tasks requiring high visual acuity and concluded that microsaccades were detrimental (Bridgeman & Palca, 1980; Winterson & Collewijn, 1976), Ko, Poletti, & Rucci (2010) found that microsaccades precisely relocate the line of sight according to the ongoing demands of the task until they get inhibited at the last moment requiring fine control. Then, their results resolved the apparent contradiction by stating that microsaccades relocate the line of sight until necessary.

More recent studies have shown that microsaccades are the most important eye movement contributor to restoring faded vision during fixation, for both foveal and peripheral targets (McCamy et al., 2012). Moreover, this study showed that multiple microsaccades within a short interval restore faded vision more effectively than single saccades and that microsaccades of all directions are equally effective. One should not confuse the concepts of preventing and reversing visual fading (McCamy,

Macknik, & Martinez-Conde, 2014). In these terms, both drift and microsaccades synergistically prevent fading from occurring (McCamy et al., 2014). To sum up, microsaccades and drift prevent fading, although not perfectly. Then, when vision fades, microsaccades are the fixational movements which restore vision more effectively.

As saccades, microsaccades are often immediately followed by a fast smaller movement in the opposite direction, called a dynamic overshoot. These overshoots are also saccadic in nature, which means that they follow the same main sequence. Dynamic overshoots can be monocular and tend to be more common in the abducting eye (Abadi, Scallan, & Clement, 2000). Due to the oscillation of the lens in the eye, dynamic overshoots may appear larger in recordings performed with video oculography or Dual Purkinje eye tracking systems than in recordings obtained with scleral search coils (Kimmel, Mammo, & Newsome, 2012; Nyström, Hooge, & Holmqvist, 2013).

Regarding the effect of viewing conditions on microsaccades, Krauskopf et al. (1960) found no differences in microsaccades characteristics between far and near viewing. According to their study, microsaccades are larger and less frequent during monocular viewing than during binocular viewing. However, other studies found that microsaccade properties did not differ between monocular and binocular conditions (Schulz, 1984). Microsaccades tend to become larger and less frequent in the dark. This increment in amplitude might be due to the fact that the eyes cannot maintain accurate fixation in complete darkness, and that a visual target is crucial to normal fixation (Cornsweet, 1956). Finally, although microsaccades are generally considered to be involuntary, careful attempts to fixate markedly reduce the rate of microsaccades (R. M. Steinman et al., 1967).

#### **4.4.5. Vestibular-Optokinetic eye movements**

So far different types of eye movements have been described assuming that the head is still. However, this is not the common situation in most everyday activities like during locomotion. This section consists in an overview of the oculomotor systems involved in holding images steady on the retina during movement of the head, i.e. the vestibular system, and the optokinetic system.

The *vestibular system* produces the *vestibulo-ocular reflex* (VOR) to compensate for relatively brief, transient head movements (Leigh & Zee, 2015). It contains two organs that respond, respectively, to angular or rotational components of movements of the head and to linear or translational movements, i.e. three semicircular canals and two otoliths on each side of the head. These two organs are located into the inner ear (Levin et al., 2011). A head rotation in one particular direction leads to the displacement of endolymphatic fluid in the semicircular canals in the opposite direction, which produces a mechanical stimulation of the sensory cells of the system. This signal is

integrated to obtain a head displacement signal and, at the end, results in eye rotations that are approximately equal and in opposite direction to the rotation of the head (Leigh & Zee, 2015). The latency of VOR is as short as 6-15 ms (Maas, Huebner, Seidman, & Leigh, 1989), which is much lower than that of the other types of eye movements mediated by visual stimuli. Only the VOR is fast enough to generate eye movements to compensate for head motions at frequencies from 0.5 to 5 Hz, the predominant frequencies occurring during locomotion (Grossman, Leigh, Abel, Lanska, & Thurston, 1988; Grossman, Leigh, Bruce, Huebner, & Lanska, 1989).

The *optokinetic system* produces the *optokinetic nystagmus* (OKN), a pattern of eye movements that compensates for relatively prolonged, sustained rotational head movements when the response of the vestibular system begins to falter (Leigh & Zee, 2015). While smooth pursuit is concerned with the fixation (alignment of the fovea with the object) of small moving targets, the optokinetic response is evoked when a large part of the visual field moves over the retina (optic flow) (Carpenter, 1988). OKN is a visually guided response consisting in a slow phase in which the eyes follow the moving field interrupted by resetting saccades (fast phase) 1 to 3 times per second. It can be tested by having the patient sit inside a large drum with black and white stripes painted on its inner surface and rotating it at particular velocities (Ciuffreda & Tannen, 1995). The OKN latency is 140 ms (Collewijn, 1989).

When the eyes pursue an object that moves across a stationary background, a conflict between the smooth pursuit and optokinetic systems occurs. The stabilization of the moving target on the fovea by means of pursuit causes optic flow of the stationary background. The same situation may occur between pursuit and the vestibular systems if gaze is controlled with head tracking movements. Consequently, pursuit of a small moving target against a stationary background with eye or head movements requires that OKN and the VOR be ignored or suppressed (Levin et al., 2011). Howard & Marton (1992) found that this is accomplished most effectively when the background and the pursuit target lie at different distances.

#### **4.5. Eye tracking techniques**

An eye-tracker is a device primarily designed to measure eye movements. In general, there are two types of eye movement monitoring techniques: eye tracking itself is the measurement of eye movement, and gaze tracking is the analysis of eye tracking data with respect to the head or visual scene. However, researchers often use the terms eye tracking, gaze tracking or eye-gaze tracking interchangeably.

Nowadays there is a wide variety of eye tracking applications, which can broadly be differentiated as diagnostic or interactive (Duchowski, 2002). In diagnostic applications the eye-tracker provides objective and quantitative evidence of subjects' visual and attentional processes. The stimulus does not change or react to the viewer's gaze. Usually, the data recorded by the eye-tracker is analyzed offline. In its interactive role, the eye-tracker is a powerful input device for visually-mediated applications. Interactive systems respond or interact with the user based on their recorded eye movements. Eye-trackers have applications in several research fields, such as neuroscience, psychology, ophthalmology and optometry, industrial engineering, marketing and advertising or computer science (Duchowski, 2002).

An ideal eye-tracker should be able to measure ocular rotations about all three axes, yet be insensitive to translational movements; linear over a range of more than  $90^\circ$ , yet sensitive enough to record movements of a few seconds of arc; and have a bandwidth extending from zero to up to 1000 Hz. Moreover, the device should not interfere with vision; it should not require the attachment of anything to the eyeball; and should be unaffected by movements of the head (Carpenter, 1988). Although a wide variety of eye tracking techniques have been devised, no system to date meets all these conditions. The best method has to be chosen according to each specific application.

A description of different eye tracking techniques is given in the following subsections. Special emphasis will be placed on video oculography, as it is the most widely used eye tracking technique nowadays.

#### **4.5.1. Electro-oculography**

Electro-oculography (EOG) was the most common technique during the mid-1970s (Young & Sheena, 1975). It is based on measuring the skin's electric potential differences of electrodes placed around the eye. Thus, it is an invasive technique. These potentials are due to a permanent potential difference between the cornea and the fundus of the eye. The recorded values are in the range from 15 to 200  $\mu\text{V}$  (micro volts), with nominal sensitivities of the order of  $20 \mu\text{V}/^\circ$  (Shackel, 1967).

This method can record eye movements in a range up to  $\pm 70^\circ$ . Linearity becomes progressively worse at excursions greater than  $30^\circ$ , especially in the vertical direction. The typical reported accuracy is around  $1.5$  to  $2^\circ$  (Young & Sheena, 1975). It is possible to separate the horizontal and vertical components of eye movements by carefully placing the electrodes on the outer canthi, the bridge of the nose and the upper eyelid. However, EOG measures eye movements relative to head position; thus, it is not suitable for point of gaze measurements unless head position is also tracked.

The main advantages of EOG are its ability to detect eye movements even when the eye is closed and its low cost. However, it has several drawbacks. A fundamental difficulty is the noise produced by muscle artefacts, eyelid interferences, nonlinearities in the technique, and variation in the corneo-retinal potential attributable to light adaptation, diurnal variations and the state of alertness (Young & Sheena, 1975). This noise can lead to not detected eye movements with no corresponding EOG indication or artefacts in potential when the eye is stationary (Carpenter, 1988).

#### 4.5.2. Scleral search coils

The scleral search coil method, first introduced by Robinson (1963), has been considered to be the gold standard technique to measure eye position for research applications for over 40 years. Eye position is determined by placing a silicon annulus on the eye, which contains a coil of thin copper wire. Then, when the subject is placed in an alternating current magnetic field, the position of the eye can be determined from the amplitude of the induction current in the coil. In non-human studies, the coil may be surgically implanted in the sclera of the eye. This eye tracking technique has high spatial (15 seconds of arc) and temporal (1 ms) resolution (Robinson, 1963). For angles up to 20° the deviations from linearity are very small (Collewijn, van der Mark, & Jansen, 1975). The scleral search coil technique is able to measure eye movements in all three degrees of freedom simultaneously, but relative to the head position. Moreover, it is unaffected by translation movements of the head or the eye, so the use of a chinrest or a bite board is not necessary (Meyer et al., 1985).

The main disadvantage of this method is its high degree of intrusiveness. Since the contact lens with the coil has to be tightly attached to the eye, it has to be necessarily large (extending over the cornea and sclera) and fitted with negative pressure, which can result in corneal lesions such as edema and abrasion. Topical anesthesia is needed to lighten the discomfort caused by the contact lens.

Ideally, the contact lens and its associated attached material should not be of a size or mass to interfere with normal eye movements (Young & Sheena, 1975). However, by introducing an object in the eye, the inertia and friction unavoidably change. As a consequence, the force that the eye muscles have to generate to perform a movement also changes. Robinson (1964) showed that a huge increase of the inertia of the eye (by almost a factor 100) resulted in relatively small changes in the shape of saccades, although he did not investigate the kinematic properties of saccades. However, it is known that not only purely mechanical factors may influence them. For instance, the discomfort of wearing scleral search coils itself may change the oculomotor command signals and the behavior of subjects (Frens & van der Geest, 2002).

### 4.5.3. Video oculography

The most widely used commercial eye-trackers nowadays are based on video oculography. In general, most non-intrusive or remote techniques are based on cameras to capture images of the eye. However, they might be somewhat intrusive if they require to be head mounted or head stabilized. Although the accuracy of remote video-based eye-trackers is in general lower than that of intrusive techniques, they are more appropriate to be used during long periods, with children patients, and in a wide variety of environments, not only in specialized laboratory research.

Although Schnipke & Todd (2000) were considerably sceptic about the usability of remote eye tracking techniques in laboratories, video based eye-trackers have increased their efficiency and accuracy, and have had a great impact on many domains of applications (Morimoto & Mimica, 2005).

Video oculography groups different eye movement recording techniques involving the measurement of distinguishable features of the eyes that can be detected and tracked by a camera or other optical or photosensitive devices. The main ones are described in the following subsections.

#### 4.5.3.1. Pupil and limbus detection

The limbus (the boundary between the sclera and the iris) is a feature sometimes used for tracking. Due to the high contrast of the sclera and iris regions, the limbus can be easily tracked horizontally. However, since eyelids cover part of the iris, limbus tracking techniques have lower vertical accuracy.

The pupil is harder to detect and track because of the lower contrast between the pupil and the iris. However, pupil tracking techniques have better accuracy in all directions since most of the time they are not covered by the eyelids. To enhance the contrast between the pupil and the iris, many eye-trackers use an infrared (IR) light source. Since IR is not visible by the users, the light does not influence their eye movements. When the IR light source is placed near the optical axis of the camera, the light reflected from the back of the eye is detected and the pupil is seen bright (Figure 4.23A). However, if it is displaced relative to the optical axis, the pupil is seen dark (Figure 4.23B) (Morimoto & Mimica, 2005). The IR light source also generates a glint on the cornea, which is used as a reference point in the pupil-corneal reflection technique described in section 4.5.3.2.

A variation of the limbus tracking technique with IR lighting was developed by Reulen et al. (1988). It consists in placing IR light emitting diodes and IR light sensitive photo-transistors above and below the eye, which can be mounted on goggles or helmets. Then, the photo-transistors transform the reflected IR light into a voltage. The voltage of the nasally located photo-transistors is compared to the voltage of the temporal located photo-transistors, and the resulting voltage difference

is proportional to the angular deviation of the eye. The main application of this system is in the assessment of horizontal saccades.

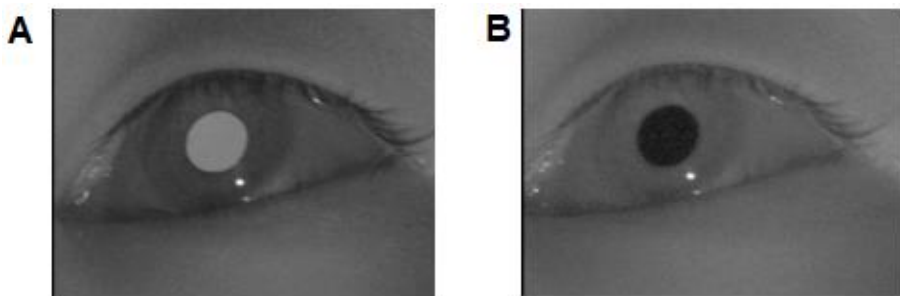


Figure 4.23. Bright (A) and dark (B) pupil images. Source: (Morimoto, Koons, Amir, & Flickner, 2000).

#### *4.5.3.2. Pupil-corneal reflection technique*

The pupil-corneal reflection technique, or Purkinje image eye tracking, is a method based on the estimation of the centers of the pupil and one or more corneal reflections. Corneal reflections were first used for eye tracking purposes by Dodge & Cline (1901). It is the most commonly used technique nowadays due to its simplicity and reasonably good accuracy. The corneal reflections, or glints, correspond to the first Purkinje images of light sources created by the first surface of the cornea, which acts as a convex mirror. Thus, the minimum hardware requirements are a light source, which usually is in the IR domain, and a camera.

The basic principle of most of the current video-based eye-trackers was developed by Merchan, Morrisette, & Porterfield (1974). It uses a camera and a single point light source, and relies on the distance between the corneal reflex of the light source and the center of the pupil (Figure 4.24A). By tracking two elements of the eye that move differently with eye position and head position it is possible to measure net eye movements. As illustrated in Figure 4.24A, assume that the optical axis of the objective of the camera that captures the pupil is coaxial with the illumination system. The corneal reflection appears always in line with the center of curvature of the cornea. Thus, the apparent displacement of the corneal reflection from the center of the pupil is equivalent to the apparent displacement of the center of the corneal curvature from the center of the pupil, which is a function of eye rotation only (Young & Sheena, 1975). Although the separation between the two tracked features is a sine function of the angle of rotation of the eye, the relationship can be regarded as linear within a range of rotation angles of around  $\pm 20^\circ$  (Figure 4.24B).

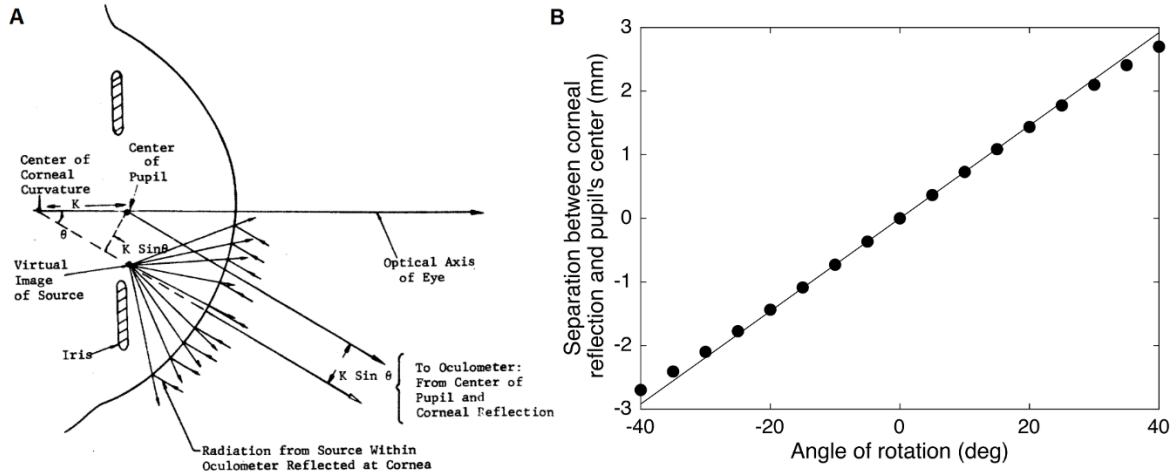


Figure 4.24. (A) Schematic representation of the basic principle of the pupil-corneal reflection technique. K: Linear distance between the center of curvature of the cornea and the center of the pupil.  $\theta$ : angle of rotation of the eye. Source: (Merchan et al., 1974). (B) Estimated separation between the corneal reflection and the center of the pupil as a function of the angle of rotation. Parameters used: radius of curvature of the cornea of 7.7 mm and anterior chamber depth of 3.5 mm.

The eye tracking process can be divided into two stages: the image processing and the gaze estimation parts. The first stage consists in processing the captured images of the eye to locate the pupil's center and the corneal reflection. There are several algorithms to do so, from relatively simple methods such as the Starburst algorithm (D. Li, Winfield, & Parkhurst, 2005), to more complex methods using deformable templates or other edges detectors (Jarjes, Wang, & Mohammed, 2010; Mehrabian & Hashemi-Tari, 2007; Soltany, Zadeh, & Pourreza, 2011; Yuille, Hallinan, & Cohen, 1992).

Once the image has been processed, gaze is deduced as a function of the extracted information. Several methods have been defined to translate the image positions of the pupil and glints into gaze position. In general, they can be divided into two main groups: interpolation and geometrical based methods.

Interpolation based methods describe gaze position as a generic function of the image features. Simple polynomial equations are generally used, whose unknown coefficients are deduced for each user during a calibration procedure. Although Morimoto & Mimica (2005) proposed to increase the order of the polynomial equation in order to improve accuracy in stationary head conditions, other studies using different hardware configurations have shown that increasing the order of the interpolation equation does not reduce significantly the tracking error (Cerrolaza, Villanueva, & Cabeza, 2008; White, Hutchinson, & Carley, 1993). A second order equation is accepted to provide

good accuracy results. One of the main drawbacks of interpolation based methods is the need for head stabilization. Higher robustness against head movements can be achieved by using at least two light sources to produce at least two corneal reflections (Sesma-Sanchez, Villanueva, & Cabeza, 2012) or by tracking the head movements separately. The eye tracking methods proposed in the first study of the thesis rely on interpolation. See section 5.1 for a detailed explanation of its functioning.

Geometrical based methods consider the underlying geometry of the framework as a basis for gaze estimation. They include 3D models of all the elements of the setup, i.e. camera(s), screen, light source(s) and eye, and also their geometrical relationships. Most of these methods require the calibration of all hardware elements, such as the relative position of the screen, camera and light sources, or some intrinsic camera parameters. A wide variety of systems and models with different number of cameras and light sources can be found in the literature (Hansen, Agustin, & Villanueva, 2010; Hansen & Ji, 2010; Kang, Eizenman, Guestrin, & Eizenman, 2008). In general, geometrical based methods require a 1-point calibration procedure to know some subject specific parameters of the model such as the radius of curvature of the cornea, the distance between the center of the pupil and the center of corneal curvature, and the angle between the visual and optical axes (Guestrin & Eizenman, 2006). Other eye-trackers incorporate a population-average value of the conversion factor to convert the separation between the center of the pupil and the corneal reflection into angular units of gaze position, i.e. the Hirschberg ratio (Jagini, Vaidyanath, & Bharadwaj, 2014; Model & Eizenman, 2011; Schaeffel, 2002). An example of a commercial instrument that uses this principle is the PowerRefractor (Plusoptix GmbH, Nuremberg, Germany) (Choi et al., 2000; Schaeffel, 2002).

In general, the complexity of geometrical methods is greater than that of interpolation methods. However, the tolerance to head movements is increased compared to interpolation methods (Cerrolaza, Villanueva, & Cabeza, 2012).

#### *4.5.3.3. Dual Purkinje image eye-tracker*

Dual Purkinje image eye-trackers use not only the first Purkinje image, but also the fourth one (Cornsweet & Crane, 1973). The fourth Purkinje image corresponds to the reflection from the second surface of the lens. The principle of these eye-trackers is based on the fact that if the eye undergoes translation both Purkinje images move through the same distance and direction as the eye; while when the eye rotates the two images move through different distances, so their separation changes. Therefore, the physical separation of these two images is a measure of the angular orientation of the eye independent of translational movements.

The main advantage of this technique is its accuracy of about 1 min of arc, which is much higher than the accuracy of pupil-corneal reflection methods. However, its main drawbacks are the complexity to set up and calibrate the system, its cost, and the post-saccadic oscillations, which are partially due to the wobbling of the lens after saccades and are particularly large (up to five degrees) in data recorded with Dual Purkinje image eye-trackers (Nyström, Andersson, Magnusson, Pansell, & Hooge, 2015; Tabernero & Artal, 2014).

#### **4.5.4. Scanning Laser Ophthalmoscopy**

Scanning Laser Ophthalmoscopy (SLO) is not *per se* an eye tracking technique, but a promising retinal tracking method (Webb & Hughes, 1981). SLO utilizes horizontal and vertical scanning mirrors to scan a specific region of the retina and create raster images. A collimated laser beam passes through a set of optical elements including lenses, beam splitters, concave mirrors and scanning mirrors before entering the eye. The optics of the eye focus the scanned beam on a specific point on the retina. The light reflected back travels along the same optical path and, as in all confocal imaging techniques, it is focused on a pinhole to reject scattered light from outside of the plane of focus. The light that passes through the pinhole reaches the detector and, as a result, an image of the scanned area of the retina by the point of light is obtained (Sheehy et al., 2012).

Tracking Scanning Laser Ophthalmoscopes (TSLO) have been originally used to image the retina of patients with retinal defects and degeneration. Recent TSLO-based instruments allow to image but also track the retina accurately to perform microperimetry and evaluate retinal contrast sensitivity. Their tracking accuracy is in the range of few minutes of arc (Sheehy et al., 2012).

Adaptive Optics Scanning Laser Ophthalmoscopes (AOSLO) have increased lateral resolution by correcting eye's high-order aberrations at the cost of a smaller field of view (Roorda et al., 2002). They have served to determine the spatial distribution of cone cells around the fovea (Chui, Song, & Burns, 2008a) but also their abnormalities with refractive errors (Chui, Song, & Burns, 2008b) or degenerative diseases (Bessho et al., 2008; Duncan et al., 2007).

## **5. Methodology and results**

The four studies carried out in order to achieve the objectives of the thesis are explained in this section. The introduction, methodology, results and discussion of each particular study are described in a different subsection.

### **5.1. Study 1. Robust eye tracking based on multiple corneal reflections for clinical applications**

**NOTE:** The following text in this section corresponds to the published article: **Mestre, C., Gautier, J., & Pujol, J.** (2018). Robust eye tracking based on multiple corneal reflections for clinical applications. *Journal of Biomedical Optics*, 23(3), 035001.

#### **5.1.1. Introduction**

Video oculography (VOG) has become the most popular eye tracking technique in the last few decades due to its performance, versatility, and low intrusiveness. Actually, some video-based systems represent an interesting alternative to the scleral search coil technique (van der Geest & Frens, 2002), which is considered to be the gold standard in oculomotor research (Collewijn, 1998).

Nowadays, most video-based commercial eye-trackers use the pupil-corneal reflection technique. It is based on the assessment of gaze position from the pupil-glint vectors, that is, the relative distance between the centers of the pupil and one or more corneal reflections. In the image, these reflections are called glints. The number of glints depends on the number of infrared (IR) light sources. The eye tracking process can be divided into two stages: the first one consists of processing the eye images in order to locate the center of the pupil and the glint, and the second estimates gaze position from the detected features in the images.

There are several methods for image processing and eye detection (Hansen & Ji, 2010). Some methods rely on the detection of eye features on the images. The pupil is more commonly used as an image feature than the limbus since it has a higher contrast and is less likely to be occluded by the eyelid. Most approaches address pupil detection by thresholding (Goñi, Echeto, Villanueva, & Cabeza, 2004; Javadi, Hakimi, Barati, Walsh, & Tcheang, 2015) or by gradient-based methods, e.g., the Canny edge detector (Fuhl, Santini, Kübler, & Kasneci, 2016; Świrski, Bulling, & Dodgson, 2012). Other approaches consider both methods and decide the one to use depending on the intensity histogram of the images (Fuhl, Kübler, Sippel, Rosenstiel, & Kasneci, 2015).

Once the pupil has been detected, most existing methods refine its position with ellipse fitting. While simple methods such as the direct least squares fitting of ellipses are highly affected by outliers (points which do not correspond to the pupil edge), there exist other approaches that are more robust to points not lying exactly on the pupil edge. On the one hand, voting-based methods, such as the Hough transform, are effective and exhaustive, although computationally expensive and limited to circular shapes, hence, near-frontal images. On the other hand, searching-based methods, such as the random sample consensus (RANSAC) paradigm (Fischler & Bolles, 1981), are based on selecting the best of a set of possible candidate ellipses. The RANSAC method is effective in the presence of a relatively large and unknown amount of outliers. It consists in fitting iteratively an ellipse to a small data subset and finding the one with the most agreement within the complete set of candidate pupil edge points.

The application of RANSAC in eye tracking was first described by Li et al. (2005) when they proposed the well-known Starburst algorithm. First, the corneal reflection is located through an adaptive threshold and removed by radial interpolation. Then, the pupil edge points are detected at the position along a limited number of rays where the gradient is above a fixed threshold. An ellipse is fitted to the edge points using the RANSAC paradigm. Finally, the result of the ellipse fitting is further optimized using a model-based approach. Despite being computationally costly, the pupil tracking based on Starburst algorithm is highly parallelizable and able to achieve up to 530 frames/s with high-resolution images using a general purpose graphics processing unit (Mompean, Aragón, Prieto, & Artal, 2015).

Yuille et al. (1992) proposed a more complex model based on deformable templates, which represents the eyelids with two parabolas and the iris with a circle. This method was extended by Lam & Yan (1996). The combination of both elliptical and complex eye models may quicken the localization and improve the tracking accuracy (Chow & Li, 1993; Deng & Lai, 1997). Other methods, classified as appearance-based (Hansen & Ji, 2010), detect the eyes directly from their appearance in the images, either in the intensity or in a transformed domain. These methods require a large amount of eyes' data of different subjects under different face orientations and illuminations to be trained.

Gaze estimation is the following process, which infers gaze position from the information that has been previously extracted from the images. Gaze estimation methods are typically divided into two main groups: geometry-based and interpolation-based methods. The former methods estimate gaze position based on 3-D models of the eye. The parameters typically used for geometric modeling of the eye include cornea radii, angles between visual and optical axes, index of refraction

of the different ocular media, iris radius, and the distance between the pupil and cornea centers. Most geometrical approaches require camera calibration and a geometric model external to the eye composed of light sources, camera and monitor position, and orientation (Hansen & Ji, 2010). There is a wide variety of possible setups, from one camera and a single light source (Guestrin & Eizenman, 2006; Villanueva & Cabeza, 2007) to multiple cameras and light sources (Beymer & Flickner, 2003; Ohno & Mukawa, 2004), including several other combinations (Hennessey, Noureddin, & Lawrence, 2006; Kang et al., 2008; Villanueva & Cabeza, 2007).

Interpolation-based methods describe the point of gaze as a generic polynomial function of image features (mapping function). As mentioned previously, the pupil and glint centers are commonly used as image features. Subject calibration is required to retrieve the unknown coefficients of the expression. Although the polynomial equation determines not only the accuracy of the system but also the required user calibration process, there are no standards regarding the best mapping function. Several studies analyzed the influence of the order and the number of terms of the polynomial equation on the performance of eye tracking systems (Brolly & Mulligan, 2004; Cerrolaza et al., 2008, 2012; Morimoto & Mimica, 2005; White et al., 1993). Although extensive research has been done to determine the best mapping function, it is not clear whether the conclusions can be generalized to other VOG systems due to the distinct hardware and methodology used in the different studies.

One of the biggest concerns about remote VOG systems is the tolerance to head movements. Although complete head pose invariance is difficult to achieve, the geometry-based methods seem to be more robust to head movements (Cerrolaza et al., 2012). On the other hand, the accuracy of interpolation-based methods decreases as the user moves away from the calibration position, especially with movements in depth (Morimoto & Mimica, 2005). The normalization of the pupil-glint vectors with respect to the distance between two glints in the eye image seems to reduce the effect of head movements (Cerrolaza et al., 2008; Sesma-Sanchez et al., 2012). Other scaling factors of the pupil-glint vectors have also been proposed for systems consisting of four IR light-emitting diodes (LEDs) (Hennessey & Lawrence, 2009). They obtained comparable results to Cerrolaza et al. (2008) and matched the performance of more complex geometrical-based methods that require system calibration (Hennessey & Lawrence, 2009).

A surge toward developing multiple IR light sources eye tracking systems appeared during the last decades. Several approaches used two IR light sources, one placed near the camera optical axis (on-axis) and the other slightly off-axis in order to generate bright and dark pupil images, respectively (Ebisawa & Satoh, 1993; Morimoto et al., 2000; Tomono, Iida, & Kobayashi, 1990).

This strategy allows to detect the pupil on the images relatively easily by differencing the bright and dark pupil images and thresholding. Yoo & Chung (2005) proposed a technique using five IR LEDs and two cameras to estimate gaze position under large head motion. The wide field-of-view camera tracks the face continuously to properly position the other camera, which has a zoom lens to capture magnified images of the eye. One LED is placed on axis to produce bright pupil images and a glint on the cornea. The other four are placed on the corners of the monitor and produce four glints. Gaze position is estimated by computing the cross-ratio of a projective space. Coutinho & Morimoto (2006) extended this method by considering the deviation between the visual and optical axes. Similarly, a method relying on homography normalization and using four IR LEDs was proposed by Hansen et al. (2010). The offset between the optical and visual axes is modeled to a much higher degree than the cross-ratio based methods, hence achieving better accuracy. Although none of the methods are invariant to depth or in-plane head movements, this homography normalization-based method showed better performance (Hansen et al., 2010). These methods represent an alternative to the fully calibrated systems since only the light source's position information is needed.

Hennessey & Lawrence (2009) described the drawbacks of using a single corneal reflection to compute the pupil-glint vector (e.g., distortion or deletion in large eye rotations). They proposed a technique to track a pattern of four corneal reflections and applied a second order interpolation equation to map the pupil-glint vector onto gaze position. In this method, an algorithm that compensates for translation, distortion, addition, and deletion of corneal reflections is applied and the pupil-glint vector is formed from the pupil center to the centroid of the corneal reflections pattern. Thus, the resulting vector is robust to loss, translation, and distortion of the glints. The proposed technique managed to estimate the point of regard in all head positions and eye rotations tested while up to 27% of the time the point of regard would have been lost if only one corneal reflection was used (Hennessey & Lawrence, 2009).

The use of multiple IR light sources has also become common in recent portable commercial eye-trackers. For example, Tobii Pro Glasses 2 (Tobii, Falls Church, Virginia) is a wearable eye tracking system that embeds eight IR LEDs per eye. The Oculus Rift DK2 system (SensoMotoric Instruments, Berlin, Germany) is an eye-tracker embedded in a virtual reality head mounted display, which contains six IR LEDs per eye.

The eye-tracker used in this study consists of a multiple-corneal reflections dark-pupil system, which offers an unprecedented high resolution imaging of the pupil and the cornea ( $640 \times 480$  pixels images with a field-of-view of 16 mm at the pupil plane). It is embedded in the Eye and Vision Analyzer (EVA) system (Davalor Salud, Spain), which is a stereoscopic virtual reality

instrument to perform the optometric tests related to objective and subjective refraction, binocular vision, and accommodation while patients are watching a 3D video game. The vergence-accommodation conflict is avoided by adjusting the accommodative plane with the vergence plane through an electro-optical lens. The EVA system allows to perform both visual diagnosis and visual therapy. The eye-tracker synchronously records both right and left eye movements during all the optometric tests. The intrusiveness of the whole system needs to be restricted to the least possible degree due to its wide clinical application requirements. Hence, the head movements are only restricted with a forehead rest.

This study presents new methods for accurate eye tracking with multiple corneal reflections using interpolation-based techniques. The advantages of a higher number of glints and their optimum arrangement are analyzed to provide new insights for the community. Moreover, a normalization of the pupil-glint vectors method is proposed to increase the eye tracking spatial accuracy.

### 5.1.2. Methods

#### 5.1.2.1. Experimental methodology

The study was approved by the Ethics Committee of Hospital Mutua de Terrassa (Terrassa, Spain). It followed the tenets of the Declaration of Helsinki and all subjects gave informed written consent after receiving a written and verbal explanation of the nature of the study.

Eye images of 20 subjects (mean age  $\pm$  standard deviation (SD) of  $31.9 \pm 9.5$  years) with normal or corrected-to-normal visual acuity were taken with the two cameras embedded in each of the two optical modules comprised in the EVA system (Figure 5.1A and B). Each optical module consists of three subsystems: the autorefractometer, the vision, and the eye-tracker (Figure 5.1C). The refractive error of participants was measured with the autorefractometer subsystem based on a Hartmann–Shack wavefront sensor. The vision subsystem allows the patients to see the liquid crystal on a silicon  $2048 \times 1536$  pixels resolution microdisplay with a field-of-view of  $26^\circ$  horizontally and  $19.8^\circ$  vertically. The spherical and cylindrical refractive errors are corrected with an electro-optical lens and the rotation of two cylindrical lenses, respectively, which are adjusted in order to avoid the need to wear glasses. Spherical refractive errors ranging from  $-18$  diopters (D) to  $+13$  D and cylindrical errors up to  $5$  D can be compensated. Finally, the eye-tracker subsystem consists of a complementary metal-oxide-semiconductor sensor recording  $640 \times 480$  pixels images with a spatial resolution of  $0.0045^\circ$  and a frame rate of  $30$  Hz. The illumination system consists of a ring of  $12$  IR LEDs ( $950$  nm). Participants' heads are partially immobilized with a forehead rest (Figure 5.1D).

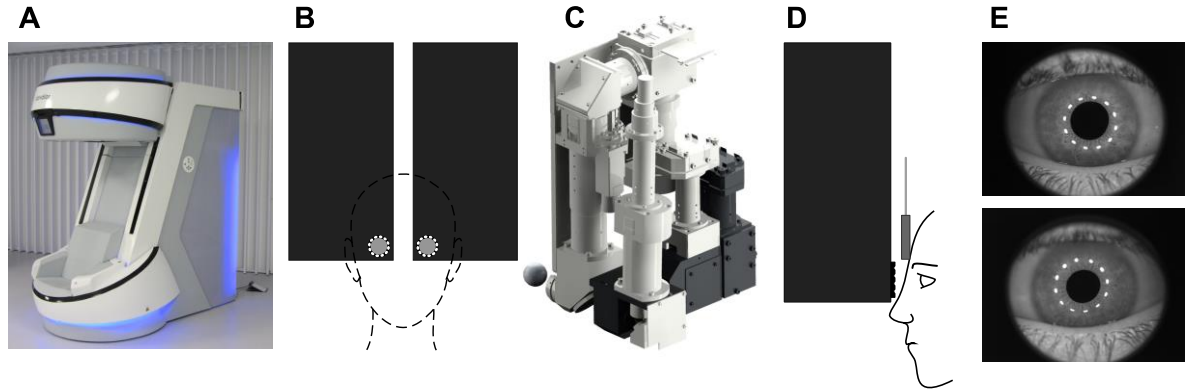


Figure 5.1. Setup. (A) EVA system. Once the patient sits, the head of the machine goes down and adjusts its position according to the patient's height. (B) Frontal view of the optical modules. (C) Schematic representation of the optical module; the eye-tracker is shaded in dark gray while the vision and autorefractometer subsystems are represented in light gray. (D) Lateral view of the system. (E) Right (top) and left (bottom) eye images captured with the system.

Participants were asked to sit down, put their head on a forehead rest, and fixate monocularly a black cross, which subtended an angle of  $0.2^\circ$ , on a mid-gray background. This cross was displayed in a sequence of nine positions of a  $3 \times 3$  grid during both the calibration and validation procedures in the same order. The stimulus was displayed for 1.3 s at each position and eye images were acquired starting 0.3 s after the onset of the stimulus (Figure 5.1E).

#### 5.1.2.2. Image processing

Eye images acquired during the experimental procedure were processed offline with an implementation of the algorithm in Matlab R2015b (MathWorks, Natick, MA, USA). For simplicity, only data from the right eye were analyzed. The Starburst algorithm was extended in order to fit the characteristics of illumination sources, resolution of our eye images, and improve the accuracy of the original algorithm.

The location of the corneal reflections process was adapted to the content of the images used in this study, which have up to 12 glints. Then, an ellipse was fitted to the centroid of each glint using a direct least squares fitting method (Fitzgibbon, Pilu, & Fisher, 1999). Instead of removing the glints by radial interpolation as in original Starburst, they were simply masked in order to avoid their interference in the pupil contour detection. Although the iterative process to detect the edge pupil points was essentially maintained from the original Starburst, the feature points were redefined as the positions along each ray where the gradient is maximum. That way, the feature points are located more precisely on the pupil edge, which otherwise would tend to underestimate the pupil border and its size.

One of the main challenges of pupil tracking is the detection of the pupil when it is partially occluded by dropped eyelids or downward eyelashes. In order to overcome this issue, our second proposal is an eyelid detector based on the visibility of the upper glints. When the complete ring of 12 glints was visible, the rays were traced from the estimated center along 360°, as was done originally. However, when some glint was missing, no rays were traced in that direction. Thus, pupil edge points were not located erroneously on the eyelid or eyelashes.

Once the edge pupil points were detected, the RANSAC method was applied to find the best fitted ellipse. A subset of six points instead of five, as originally suggested (Fischler & Bolles, 1981), was chosen randomly but ensuring that they were equally distributed around all the regions of the pupil. Although these contributions produce a low improvement on accuracy, its main benefit is in terms of computing efficiency (Figure 5.2). In addition, geometrical constraints on the maximum and minimum radius and eccentricity of the fitted ellipse were added based on anatomical parameters of the pupil (Atchison & Smith, 2000).

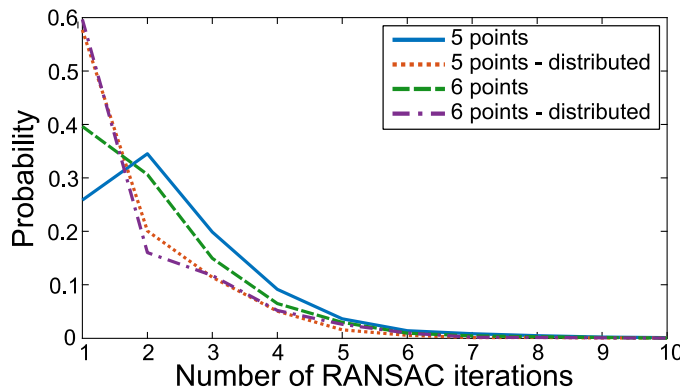


Figure 5.2. Histogram of the number of RANSAC iterations with the original algorithm (5 points, solid), choosing 5 points and distributing them spatially (5 points - distributed, dotted), considering a subset of 6 points without constraints about distribution (6 points, dashed) and considering 6 points and distributing them spatially (6 points – distributed, dotted-dashed).

Since images were processed offline, computation time was not critical. The prototype version of this implementation written in Matlab and run by a processor Intel i5-4200M CPU at 2.50 Hz with 8 GB of RAM operates at  $\sim$ 1.11 frames/s. Around 70% of the algorithm's runtime is needed for the localization and masking of the 12 corneal reflections while the other 30% is needed for the pupil edge detection and ellipse fitting on the pupil. The results presented in this paper were obtained with this implementation. However, we have worked on a faster implementation of the algorithm using Nvidia compute unified device architecture (CUDA) parallelism in order to reduce the computation time and run the algorithm in real time. The hardware used to test this implementation

consisted of a GPU Nvidia Quadro K5200 with 2304 CUDA cores and 8 GB of memory. The computation time could be reduced to around 2 ms/image.

The first objective of this study was to analyze the performance of the eye-tracker with different configurations of light sources. The tested configurations (Figure 5.3) were chosen to study the optimal number of glints, the putative benefits of higher number of glints, and their optimum arrangement considering the possible interference of the eyelids. In a preliminary study, the different configurations were tested switching off the corresponding LEDs. After confirming by visual inspection that similar levels of image luminance could be obtained by retaining only two light sources and increasing their illumination power, we decided to acquire all eye images with the 12 LEDs switched on in order to simplify the experimental procedure. Then, the corresponding glints were removed from the eye images using radial interpolation assuming that their intensity profile follows a symmetric bivariate Gaussian distribution.

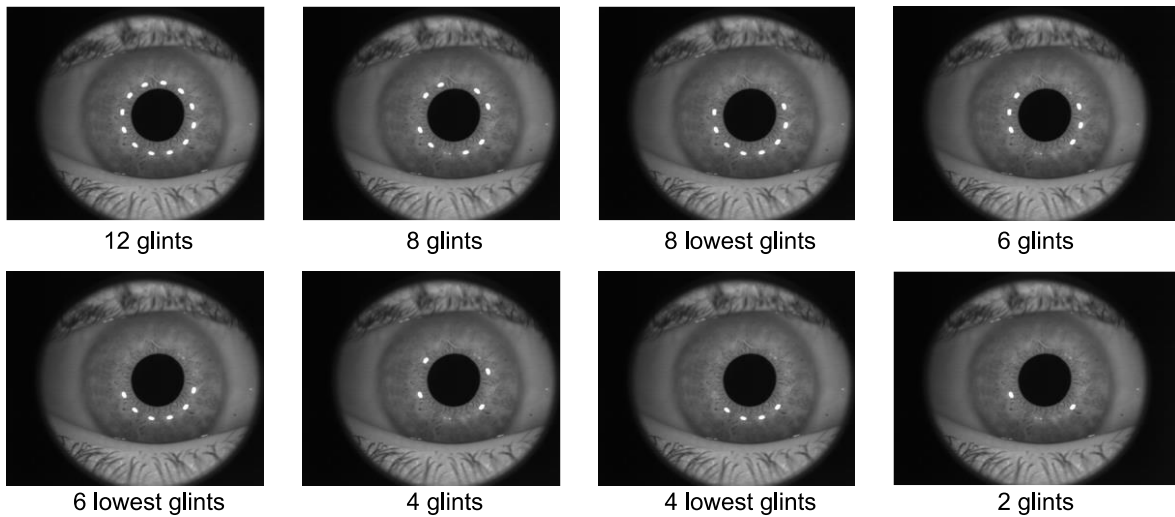


Figure 5.3. Eye images with the tested light sources configurations.

#### *5.1.2.3. Gaze estimation*

Before estimating the gaze position with an interpolation-based method, the data obtained from the eye images were filtered using a trimmed mean to select the 50% of the 30 images available at each point. The trimmed or truncated mean reduces the effects of outliers on the calculated average by removing a certain percentage of the largest and smallest values before computing it.

A second order polynomial Eq. (5.1) was used to map the tracked image features onto gaze position:

$$\begin{pmatrix} PoR_x \\ PoR_y \end{pmatrix} = C \cdot \begin{pmatrix} 1 \\ \vartheta_x \\ \vartheta_y \\ \vartheta_x^2 \\ \vartheta_y^2 \\ \vartheta_x \vartheta_y \end{pmatrix} \quad (5.1)$$

where  $PoR_x$  and  $PoR_y$  are the horizontal and vertical coordinates, respectively, of the point of regard;  $C$  is the coefficient matrix determined during calibration; and  $\vartheta_x$  and  $\vartheta_y$  are the horizontal and vertical components, respectively, of the pupil-glint vector.

During the calibration procedure, Eq. (5.1) was used to calculate the polynomial coefficients in the matrix  $C$  assuming that  $PoR_x$  and  $PoR_y$  are the horizontal and vertical coordinates, respectively, of the stimulus, and computing the pupil-glint vector of the images captured during this procedure. During the validation procedure, the coordinates of the point of regard could be computed from the pupil-glint vector of the validation images and the known  $C$  matrix.

As mentioned previously, robustness against head movements is one of the main challenges of current video-based eye-trackers. The system used in this study exceeded the minimum hardware required (i.e., two light sources) to normalize the pupil-glint vectors, which was shown to improve overall spatial accuracy in interpolation-based eye tracking methods (Cerrolaza et al., 2008; Hennessey & Lawrence, 2009). The normalization proposed by Sesma-Sánchez et al. (2012) based on the interglint distance was adapted to the content of the images of each tested configuration.

When normalization was not applied, the components of the pupil-glint vector of the eye images captured during both calibration and validation procedures were computed as follows:

$$\vartheta_x = p_x - g_x, \quad \vartheta_y = p_y - g_y \quad (5.2)$$

where  $p_x$  and  $p_y$  are the image coordinates of the pupil center. In the configurations with 12 and 8 glints,  $g_x$  and  $g_y$  are the image coordinates of the center of the ellipse fitted on the glints centroids, whereas in the configurations with 6, 4, and 2 glints,  $g_x$  and  $g_y$  are the image coordinates of the mean glints position. This difference among configurations is due to the fact that at least five points are required to fit an ellipse.

In the configurations with 12 and 8 glints, when normalization was applied, the horizontal and vertical components of the pupil-glint vector of the eye images captured during both calibration and validation procedures were defined as follows:

$$\vartheta_x = \frac{p_x - g_x}{r}, \quad \vartheta_y = \frac{(1-k) - g_y}{r} \quad (5.3)$$

where  $r$  is the major radius of the glints ellipse and  $k$  is a vertical weighting factor to attribute a higher weight to the glints in order to compensate for the higher uncertainty in the pupil detection, especially vertically. The same value of  $k$  was used for both calibration and validation procedures. Its optimum value for each configuration of light sources was determined empirically as the one that optimizes the accuracy of the eye-tracker averaged for all participants.

In the configurations with 6 or less glints, the normalized pupil-glint vectors of the eye images captured during both calibration and validation procedures were computed as follows:

$$\vartheta_x = \frac{p_x - g_x}{D}, \quad \vartheta_y = \frac{(1-k) - g_y}{D} \quad (5.4)$$

where  $g_x$  and  $g_y$  become the image coordinates of the mean glints position and  $D$  is the mean Euclidean distance between opposite glints.

Two normalization methods were proposed for the different configurations due to the limitation of the minimum number of points required to fit an ellipse. Although an ellipse could be fitted on 6 glints, preliminary results showed no robust results even when the normalization was not applied in those configurations. Therefore, in the configurations *6 glints* and *6 lowest glints*, the pupil-glint vectors were computed as in the configurations *4 glints*, *4 lowest glints*, and *2 glints*, considering the mean glints position and the Euclidean distance between them. As a result, a unique normalization method was applied on each light source configuration.

The gaze estimation algorithm was also written in Matlab. Approximately 30 ms were needed to compute the coefficients of the second order polynomial equation using the pupil-glint vectors extracted from the eye images captured during the calibration procedure, and 10 ms were needed to interpolate and compute the point of regard during the validation procedure.

#### 5.1.2.4. Evaluation

The eye-tracker performance was evaluated by analyzing the horizontal and vertical accuracies. They were defined as the horizontal and vertical angular distances between the interpolated points of regard on the image plane using the eye images registered during the validation procedure and the real target positions that subjects were fixating on. The data reported in this paper correspond to the average horizontal and vertical accuracies obtained by averaging all the horizontal and vertical distances, respectively, over the  $3 \times 3$  grid.

The determination of the optimum value of the factor  $k$  of Eqs. (5.3) and (5.4) requires to evaluate the eye-tracker's accuracy. Hence, it was determined from images obtained during the validation procedure.

#### 5.1.2.5. Statistical analysis

Statistical analysis was performed using SPSS Statistics 23 (IBM Corp., Armonk, NY, USA). Nonparametric statistics were used after checking that most variables did not follow a normal distribution by applying the Shapiro–Wilk test and comparing the skewness and kurtosis statistics to the standard error.

Friedman tests were performed along both horizontal and vertical directions to compare the accuracy of the eight configurations. Significance was set at  $p < 0.05$ . When significance was obtained, post-hoc comparisons of configurations were made by Wilcoxon signed-rank tests with a Bonferroni adjustment given by the number of possible pairwise configuration comparisons, with significance  $p < 0.05/28$ . The same tests were also used to compare the accuracy of the eight configurations when the pupil-glint vectors were normalized. Spearman's correlations were applied to identify associations between the differences in accuracy for certain pairs of configurations and other features of each configuration, such as the percentage of images in which the eye was detected or the percentage of images in which some glints were occluded. Finally, the Wilcoxon signed-rank test was performed to compare the horizontal and vertical accuracies for each configuration without applying the normalization of the pupil-glint vectors and normalizing them.

### 5.1.3. Results

Before analyzing the differences in terms of accuracy for the different tested configurations, the intrinsic repeatability of the algorithm is described. It is defined as the within-subject standard deviation of the accuracy in both horizontal and vertical directions. It might be thought as a descriptor of the random component of measurement error and is due to randomness in the selection of the initial subset of points for the RANSAC ellipse fitting. For the original *12 glints* configuration, the within-subject standard deviation horizontally was  $0.027^\circ$  (95% confidence interval (CI),  $0.026^\circ$  to  $0.027^\circ$ ), whereas vertically, it was  $0.034^\circ$  (95% CI,  $0.033^\circ$  to  $0.035^\circ$ ).

Table 5.1 gives the descriptive statistics of horizontal and vertical accuracies for each configuration.

Table 5.1. Median (interquartile range; IQR) of the horizontal and vertical accuracies in degrees for different configurations.

<b>Configuration</b>	<b>Horizontal accuracy (°)</b>	<b>Vertical accuracy (°)</b>
<i>12 glints</i>	0.41 (0.19 to 0.49)	0.47 (0.40 to 0.70)
<i>8 glints</i>	0.42 (0.23 to 0.53)	0.53 (0.40 to 0.70)
<i>8 lowest glints</i>	0.38 (0.17 to 0.52)	0.54 (0.31 to 0.70)
<i>6 glints</i>	0.48 (0.24 to 0.55)	0.74 (0.47 to 0.84)
<i>6 lowest glints</i>	0.43 (0.18 to 0.55)	0.60 (0.48 to 0.87)
<i>4 glints</i>	0.51 (0.26 to 0.58)	0.69 (0.46 to 0.87)
<i>4 lowest glints</i>	0.39 (0.21 to 0.61)	0.57 (0.48 to 0.81)
<i>2 glints</i>	0.44 (0.21 to 0.57)	0.65 (0.45 to 0.87)

The Friedman test showed significant differences in both horizontal ( $\chi^2(7)=18.27, p=0.011$ ) and vertical ( $\chi^2(7)=20.50, p=0.005$ ) accuracies for the different configurations. The post-hoc test performed along each direction showed statistically significant differences horizontally between the configurations *8 lowest glints* and *4 glints* ( $p=0.001$ ). Any pairwise comparison vertically showed significant differences.

Although they were not statistically significant, the differences in accuracy between the configurations with the same number of light sources (i.e., *8 glints* and *8 lowest glints*, *6 glints* and *6 lowest glints*, and *4 glints* and *4 lowest glints*) are especially remarkable and might be justified by the fact that in some cases, the upper glints were occluded by the eyelid (Figure 5.4). There was a moderate, positive, and significant correlation between the difference in vertical accuracy between the configurations *8 glints* and *8 lowest glints* and the percentage of images in which the glints 8, 9, and 11, and only these, were occluded ( $r_s=0.46, p=0.042$ ). There was no significant correlation horizontally.

In the four configurations with 6 and 4 glints, all the considered glints had to be visible, otherwise the eye could not be detected on that frame. Hence, the improvement in accuracy when the lowest glints were considered cannot be justified directly by the occlusion of some upper glints. Alternatively, it can be explained by the improvement in robustness defined as the percentage of images in which the eye is detected. There was a moderate, positive, and significant correlation between the difference in vertical accuracy between the configurations *6 glints* and *6 lowest glints* and the difference in robustness between both configurations ( $r_s=0.65, p=0.003$ ). For the configurations *4 glints* and *4 lowest glints*, there was also a moderate, positive, and significant

correlation ( $r_s=0.50$ ,  $p=0.029$ ). There was no correlation horizontally for the configurations *6 glints* and *6 lowest glints* nor for *4 glints* and *4 lowest glints*.

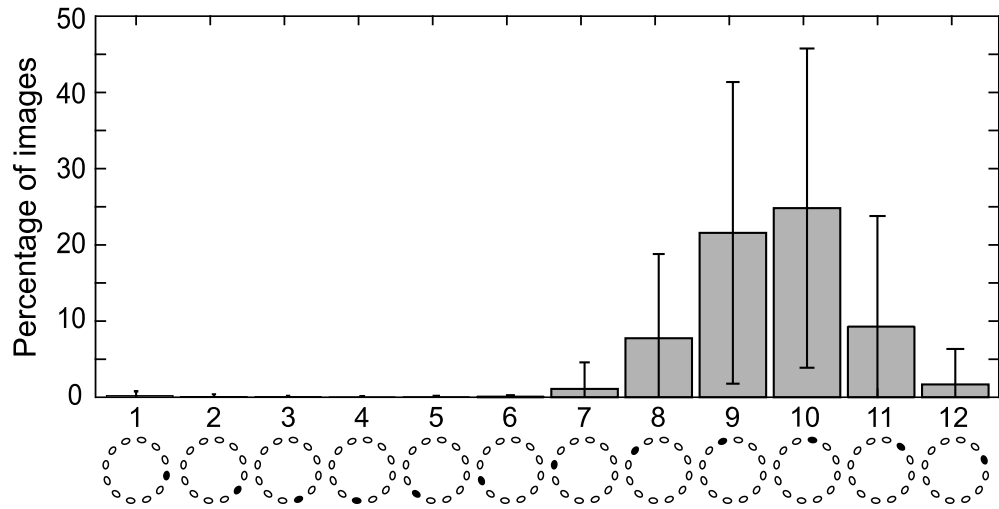


Figure 5.4. Percentage of images averaged for all participants in which each glint is occluded. The corresponding occluded glints are represented in black in the schemes below the bars. Error bars show  $\pm 1$  SD.

Table 5.2 shows the descriptive statistics of horizontal and vertical accuracies for each configuration when the normalization of the pupil-glint vectors was applied according to Eqs. (5.3) and (5.4).

Table 5.2. Median (IQR) of the horizontal and vertical accuracies in degrees for different configurations when the pupil-glint vectors were normalized.

Configuration	Horizontal accuracy (°)	Vertical accuracy (°)
12 glints	0.44 (0.19 to 0.51)	0.39 (0.22 to 0.66)
8 glints	0.41 (0.20 to 0.52)	0.38 (0.29 to 0.73)
8 lowest glints	0.39 (0.16 to 0.54)	0.46 (0.32 to 0.64)
6 glints	0.46 (0.24 to 0.55)	0.42 (0.25 to 0.89)
6 lowest glints	0.45 (0.18 to 0.54)	0.39 (0.24 to 0.69)
4 glints	0.47 (0.24 to 0.60)	0.41 (0.28 to 0.93)
4 lowest glints	0.45 (0.22 to 0.63)	0.44 (0.27 to 0.72)
2 glints	0.43 (0.22 to 0.57)	0.37 (0.26 to 0.74)

The Friedman test showed significant differences in horizontal accuracy for the different configurations ( $\chi^2(7)=16.75$ ,  $p=0.019$ ). The post-hoc test showed statistically significant differences

between the configurations *8 lowest glints* and *4 glints* ( $p=0.001$ ). There were no significant differences in vertical accuracy for the different configurations ( $\chi^2(7)=6.04$ ,  $p=0.535$ ).

There were no statistically significant differences (Wilcoxon signed-rank test) in any configuration between the horizontal accuracy when the pupil-glint vectors were not normalized and when the normalization was applied. Moreover, in most configurations, the differences were lower than the horizontal within-subject standard deviation. However, the normalization significantly improved the vertical accuracy and the differences were above the vertical within-subject standard deviation in all configurations. The relative improvement of the median vertical accuracy due to the normalization of the pupil-glint vectors ranged from 43.2% for *6 glints* to 14.8% for *8 lowest glints* (Figure 5.5).

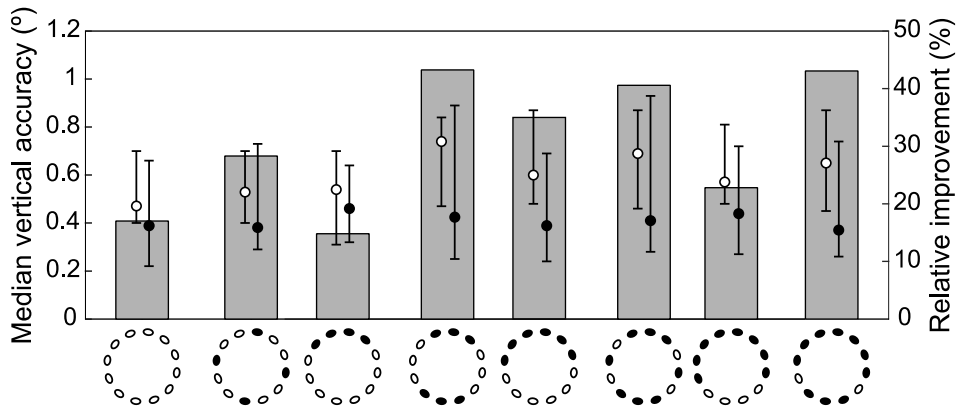


Figure 5.5. Median vertical accuracy in degrees without normalizing the pupil-glint vectors (empty circles) and applying the normalization (solid circles). Each configuration of light sources is represented in the schemes below the bars, where active and inactive LEDs are represented in white and black, respectively. Error bars show the IQR. Bars correspond to the relative improvement of vertical accuracy due to the normalization.

#### 5.1.4. Discussion

##### 5.1.4.1. Light sources configurations

The median horizontal accuracy of the eye-tracker used in this study is systematically better than the median vertical accuracy in all configurations. A similar tendency was found by Cerrolaza et al. (2012) in their study of polynomial mapping functions to optimize the calibration process of interpolation-based systems. Since there is no clearly preferred direction in the dispersion of gaze in tasks of sustained fixation (Cherici, Kuang, Poletti, & Rucci, 2012), it is hypothesized that this difference is due to the interference of the eyelid and eyelashes in the detection of the upper pupil

region. The higher uncertainty in this region also implies a poorer repeatability of the algorithm vertically than horizontally.

Although there are no statistically significant differences of vertical accuracy with the distinct tested configurations, there is a tendency for increasing accuracy with the number of glints, especially in the vertical direction. There is a significant negative correlation between the number of glints and the median vertical accuracy (Table 5.1) of the best configurations (i.e., *12 glints*, *8 lowest glints*, *6 lowest glints*, *4 lowest glints*, *2 glints*;  $r_s=-0.90$ ,  $p=0.037$ ). The correlation is weaker and not significant in the horizontal direction ( $r_s=-0.50$ ,  $p=0.391$ ). The between-subjects variability of the accuracies is rather similar in all configurations and along both directions.

The arrangement of the light sources seems to have a stronger effect than the number of glints itself. To our knowledge, this is the first study that addresses the question of the best positioning of the IR LEDs to optimize the accuracy of a VOG system. Figure 5.4 confirms the intuitive thought that the upper glints are the most likely to be occluded by the eyelid. The fact that the lower eyelid hardly ever interferes with the glints justifies our choice of considering the lowest corneal reflections in the configurations *8 lowest glints*, *6 lowest glints*, and *4 lowest glints*. However, one should bear in mind the specific eye-tracker setup used in this study with the cameras placed in front of the eyes. The results regarding the optimum arrangement of light sources might not be applicable to other systems in which the cameras are located in other positions.

In the configurations in which an ellipse is fitted on the glints (*12 glints*, *8 glints*, and *8 lowest glints*), the total number of active glints was not always visible. As can be seen in Figure 5.6, there was a considerable percentage of images in which some glints were occluded, especially in the *12 glints* configuration (Figure 5.6A). However, since a dataset of at least five points is required to fit an ellipse, at least five corneal reflections needed to be visible so as to track the eye in each frame. The main difference between the configurations *8 glints* and *8 lowest glints* was the number of glints available to fit the ellipse, which was not always 8 due to eyelid occlusion. The mean  $\pm$  SD percentage of images in which all eight corneal reflections were visible with the *8 glints* configuration was 76.9%  $\pm$  19.7% (Figure 5.6B), whereas with the *8 lowest glints* configuration, they were all visible in 95.6%  $\pm$  5.5% of the images ( $p=0.001$ ) (Figure 5.6C). Therefore, the improvement in accuracy when the lowest glints were considered might be explained by a more robust ellipse fitting with a larger dataset of points.

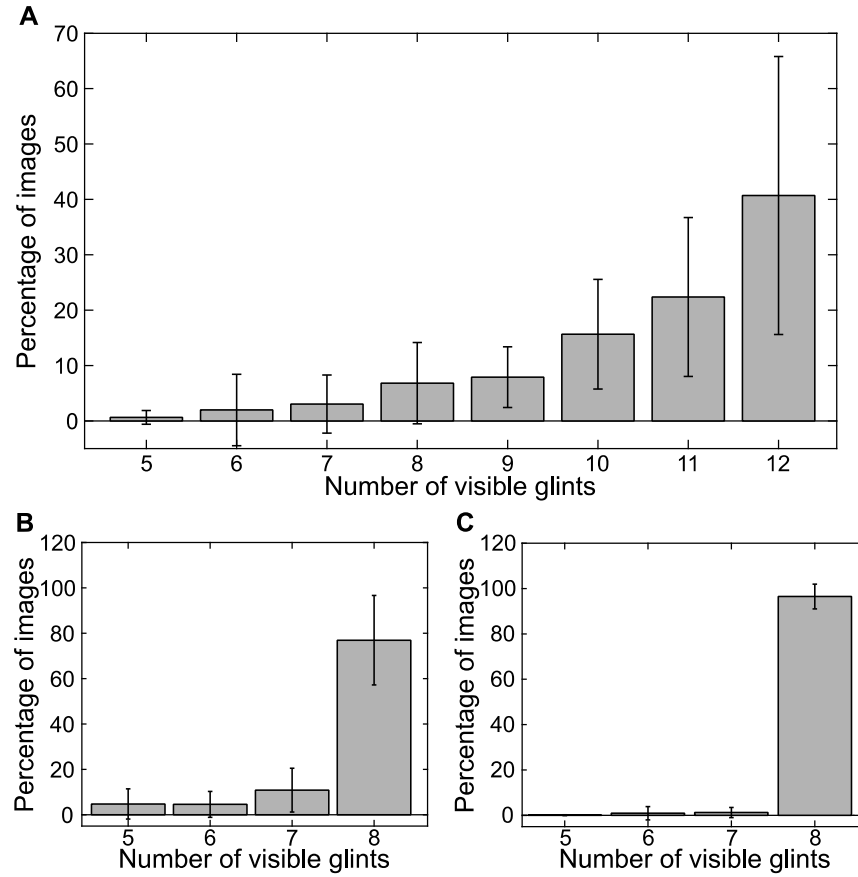


Figure 5.6. Percentage of images averaged for all participants in which there were five or more visible glints for the configurations (A) 12 glints, (B) 8 glints, and (C) 8 lowest glints. Error bars show  $\pm 1$  SD.

In the configurations with six or less corneal reflections, the average glints position was used to compute the pupil-glint vectors. In these configurations, the number of glints must be the same in all frames. Otherwise, the components of the pupil-glint vectors would be modified regardless of eye movements, which in turn would lead to an incorrect measurement of eye position. Hence, the advantage of the configuration *6 lowest glints* over the *6 glints* is reflected in the robustness of the system (i.e., the percentage of frames in which the eye is detected). The mean  $\pm$  SD robustness of *6 glints* configuration was  $89.9\% \pm 11.4\%$ , whereas with the *6 lowest glints* configuration, it was  $96.6\% \pm 3.4\%$  ( $p=0.001$ ). Similarly, the mean  $\pm$  SD robustness of *4 glints* configuration was  $89.9\% \pm 11.5\%$ , whereas with the *4 lowest glints* configuration, it was  $96.9\% \pm 2.6\%$  ( $p=0.001$ ).

The improvement of accuracy in the configurations in which more data is available (higher robustness) suggests that an increase in sampling frequency might lead to a better performance of the eye-tracker not only regarding temporal measurements but also in terms of spatial accuracy.

#### 5.1.4.2. Normalization of the pupil-glint vectors

Our results suggest that the normalization of the pupil-glint vectors is an effective method to improve the accuracy of VOG systems.

Previous studies working with eye-trackers with two or more IR light sources tested the tolerance to head movements in depth applying different types of normalization (Cerrolaza et al., 2012; Hennessey & Lawrence, 2009; Sesma-Sánchez et al., 2012). The head movements in other directions (parallel to the display) were not tested since they were shown to be considerably less problematic in VOG systems (Morimoto & Mimica, 2005). To do so, they acquired eye images locating the subjects' head in three different positions separated by 5 cm. The experimental procedure of our study did not include testing in different locations of the head due to the shallow depth of field of the eye-tracker's cameras. Nevertheless, the head of the patients was not fully immobilized.

On the one hand, it is hypothesized that the improvement in accuracy shown in all configurations when the pupil-glint vectors were normalized might be partially due to the compensation of small, although not quantified, head movements allowed by the forehead rest, since previous works obtained satisfactory results applying similar normalization methods with this purpose (Cerrolaza et al., 2012; Sesma-Sánchez et al., 2012). On the other hand, as seen in Figure 5.5, the relative improvement in accuracy due to normalization was different for each configuration. This implies that the normalization of pupil-glint vectors might have further effects besides the compensation of head movements and might be due to the  $k$  factor, whose optimum value varies among configurations.

The main improvement when the pupil-glint vectors were normalized was in terms of vertical accuracy. Actually, the differences in horizontal direction were neither statistically significant nor relevant, since in most configurations they were below the within-subject standard deviation, which means that they might be simply due to the intrinsic variability of the algorithm. The stronger effect of normalization vertically than horizontally might be justified by the fact that most of the coefficients of the mapping function have a higher value in the polynomial equation for determining the  $PoR_y$  than in the equation for the  $PoR_x$ . Thus, when the normalization of the pupil-glint vectors was applied, the change in the computed gaze positions was more prominent in the vertical direction than horizontally.

As discussed previously, horizontal accuracy was below  $0.5^\circ$  and already better horizontally than vertically when the pupil-glint vectors were not normalized. This suggests that the weaker effect of normalization horizontally might be also explained by the fact that horizontal accuracy might be

limited by lack of exactitude in stages prior to gaze estimation, such as the image acquisition and processing or the dispersion of gaze itself due to fixational eye movements. The pronounced improvement vertically contributed to reduce the difference in performance between both directions and equalize the horizontal and vertical accuracies.

Since normalization had a small effect in the horizontal direction, the between-subjects variability of horizontal accuracy was similar than when the normalization was not applied. However, the interquartile range of vertical accuracy was considerably wider with normalization, except for the configurations *8 lowest glints*, *6 lowest glints*, and *2 glints* in which it was rather similar. As shown by the error bars in Figure 5.5, the distribution of vertical accuracy tends to become more asymmetric when normalization was applied. This means that in most participants, normalization improved vertical accuracy although in some subjects with poorer accuracy, the effect was weaker.

Several eye tracking methods published previously were evaluated using the Euclidean distance between the estimated point of gaze and the true eye position instead of considering separately the horizontal and vertical directions. The accuracy of the eye-tracker used in this study was also computed as the Euclidean distance for the purpose of comparing it with existing methods. Its median value was  $0.6^\circ$  for the *12 glints* configuration and normalizing the pupil-glint vectors, which is better than the average accuracy of  $1^\circ$  of visual angle shown by the original Starburst algorithm (D. Li et al., 2005). Other interpolation-based methods using one glint obtained an accuracy around  $0.8^\circ$  (Blignaut, 2014; Brolly & Mulligan, 2004). Cerrolaza et al. (2012) obtained a considerably better accuracy with two IR LEDs, a second order interpolation equation, the interglint distance to normalize the pupil-glint vectors, and with the patients' head stabilized using a chin rest ( $0.2^\circ$  horizontally and  $0.3^\circ$  vertically).

Comparable values of accuracy were obtained with geometry-based and head pose invariant models (Beymer & Flickner, 2003). Several systems consisting of more than two IR LEDs rely on the cross ratio (Coutinho & Morimoto, 2006; Huang, Cai, Liu, Ahuja, & Zhang, 2014; Zhang & Cai, 2014) of a projective space or homography normalization (Hansen et al., 2010). Although these methods allow head movement, their optimum accuracy values, which are below  $0.5^\circ$ , were shown with the head stabilized with a chin rest (Hansen et al., 2010; Huang et al., 2014).

To conclude, different lighting configurations for on-axis eye tracking have been proposed and studied. In particular, the interference of the corneal reflections with the upper eyelid has been emphasized. One should take into account that the high variability in the anatomical shape of eyelids leads to high variability of the results. Then, the configuration with the best performance might be

different depending on factors such as the ethnicity or the age of the eye-tracker's users. The proposed normalization of the pupil-glint vectors seems to be an effective method to improve the accuracy of VOG systems. It also counteracts the tendency for increasing accuracy with the number of glints. Therefore, if they are properly positioned, our normalization proposal allows to be independent from the need for higher number of light sources.



## 5.2. Study 2. An automated and objective cover test to measure heterophoria

**NOTE:** The following text in this section corresponds to the published article: Mestre, C., Otero, C., Díaz-Doutón, F., Gautier, J., & Pujol, J. (2018). An automated and objective cover test to measure heterophoria. PLoS ONE, 13(11), e0206674.

### 5.2.1. Introduction

A normal functioning of binocular vision, including both sensory and motor components, guarantees proper alignment of the eyes. While the sensory fusion component unifies the perception of the images of the two eyes, the motor fusion component is responsible to align the eyes in such a manner that sensory fusion can be maintained. If one eye is artificially excluded from participating in vision (i.e., the sensory and motor fusion components of binocular vision are suspended), a relative deviation of the visual axes may appear in most subjects, which is called heterophoria, or phoria (Von Noorden & Campos, 2002). When the fusion mechanism does not function properly, a manifest deviation of one eye is present. This deviation is called heterotropia, tropia or strabismus. While tropia is a manifest deviation, phoria is latent and becomes evident only when the normal fusion mechanisms are disrupted. This deviation may be horizontal, if the visual axis of one eye converges or diverges more than the other; vertical, if one visual axis is higher than the other; or cyclorotary, if there is a misalignment of the eyes due to a clockwise or counterclockwise rotation of one eye.

Since an abnormal value of phoria may lead to symptoms like visual fatigue, headache or double vision (Scheiman & Wick, 2014), it is routinely assessed in clinical optometric practice. There are several methods to measure phoria such as the cover test or the modified Thorington test.

There are different variants of the cover test. The unilateral cover test consists in covering one eye and observing the movements of the other eye. If the non-occluded eye moves to take up fixation, the patient exhibits tropia. If contrarily there is no movement of the fellow eye, that eye is then covered and the other eye is observed. Once it has been established that the fellow eye does not move when either eye is covered, a cover-uncover test is typically performed to determine whether the patient has a phoria. The cover-uncover test is equivalent to the unilateral cover test but now the examiner observes the movements of the occluded eye when the cover is removed. If phoria is present, the covered eye moves to its heterophoric position and when uncovered, the eye makes a movement in the opposite direction to recover fixation. The alternate cover test brings out the maximal ocular deviation regardless of whether it is a phoria or tropia. In this case, the occluder is quickly switched

from one eye to the other avoiding any period of binocular fixation between occlusions. In the three variants of the cover test, the deviation can be measured with a prism bar as the amount of prism diopters (PD) needed to cancel out the recovery (or re-fixation) movement (prism cover test). A prism is defined as having 1 PD when it causes a deflection of a light ray of 1 cm measured at a distance of 1 m. Thus, the degrees of eye rotation can be transformed into PD as 100 times the tangent of the rotation angle. The cover test is considered an objective method since the result does not depend on the answers of the patients, although it depends on the criteria and ability of the examiner (H. A. Anderson, Manny, Cotter, Mitchell, & Irani, 2010; Hryncak, Herriot, & Irving, 2010; Johns, Manny, Fern, & Hu, 2004).

The modified Thorington test is a subjective method that uses the Bernell Muscle Imbalance Measure (MIM) card (Bernell Corp., Mishawaka, IN, USA) to measure phoria. It has a row and a column of numbers that are separated by 1 PD at 40 cm. A penlight is shown to the patients through a hole in the center of the card while they hold a Maddox rod before the right eye. Patients are asked through which number the line created by the Maddox rod passes and on which side of the penlight's light.

Several studies concluded that the different tests to measure phoria are not interchangeable due to their low level of agreement (Antona et al., 2011; Sanker et al., 2012). There is controversy about the most repeatable test, but it is typically agreed that the cover test and the modified Thorington test offer the best results in terms of repeatability (Antona et al., 2011; Cebrian et al., 2014; Rainey et al., 1998).

The use of the cover test to measure phoria in clinical practice is extremely common. However, it suffers from several limitations such as its non-objectivity. Although the result does not depend on the answer of the patients, it depends on the examiner. Several authors have found no clinically relevant mean differences between experienced and novice examiners, although the 95% limits of agreement were rather wide (H. A. Anderson et al., 2010; Hryncak et al., 2010). Another source of interexaminer variability might be the use of a different criterion for the neutralization point (Johns et al., 2004). The endpoint of the movement that should be recorded as the result of the test is still unclear. One possible endpoint is the first amount of prism with which no movement is seen (first neutral). Other possibilities are any point in the range of prism after the first neutral in which no additional movement of the eye is seen, or the prism that causes an opposite movement of the eye (reversal point) (Johns et al., 2004). It is generally accepted that some execution aspects such as the time of occlusion have a direct influence on the measured phoria (H. A. Anderson et al., 2010; Barnard & Thomson, 1995). The poor resolution is also a limitation of the cover test. Several authors

showed that under ideal conditions, the smallest eye movement that a person (the examiner) can detect with unaided eye is 2 PD (Fogt, Baughman, & Good, 2000; Ludvigh, 1949). As a consequence, the threshold commonly used to decide whether differences are clinically significant is 2 PD. This value has not been established on the grounds of diagnostic significance but based on a limitation of the measurement test. Finally, the fact that basically the covered eye cannot be observed represents an impediment to analyze how the eye reaches its heterophoric position (Pickwell, 1989).

It is generally accepted that the modified Thorington test is simple and easy for patients to understand. However, its principal drawback is its subjectivity, as the results solely rely on the answer of the patients. A specific emphasis needs to be placed on asking the patients to keep the grid and numbers of the MIM card focused. The dissociation system used, which creates rivalry between the eyes and unusual viewing conditions, does not favor a proper control of accommodation.

These limitations could be overcome by using eye tracking systems. The calculation of phoria from the eye-tracker's recordings relies solely on patient actual eye deviation, and not his subjectivity nor the one of the examiner. Moreover, if the proper occluder is used, it becomes possible to register the movements of the covered eye and automate the whole process in order that the test is always executed equally. The first studies using objective eye tracking systems during the cover test described the dynamics of eye movements during both the cover and recovery phases (Barnard & Thomson, 1995; Peli & McCormack, 1983). More recently, several works used different eye tracking techniques to measure phoria and compared the results with clinical methods. Han, Guo, Granger-Donetti, Vicci, & Alvarez (2010) used a limbus eye tracking system and an haploscope to quantify objectively phoria. They obtained a precision from 0.7 PD to 1.1 PD, similar to the Maddox rod method and the alternate cover test, but a resolution of 0.17 PD, which is noticeably better. Moreover, a strong and significant correlation between the phoria measured with the limbus eye tracking system and the Maddox rod method ( $r = 0.85$ ,  $p = 0.008$ ) was observed. In the version of the Maddox rod method that Han et al. performed, subjects viewed a penlight in primary position. Their right eye was occluded for 15 s and then it was uncovered and covered rapidly to assess the position of the red line on a calibrated grid. This was repeated until the subjects could report on which number the red line appeared. Babinsky, Sreenivasan, & Candy (2015) used the MCS PowerRefractor (Multi Channel Systems, Reutlingen, Germany) to assess simultaneously accommodation and ocular alignment data in children.

Other studies used eye tracking systems to obtain objective measurements of other binocular vision parameters, such as fixation disparity (Jaschinski, 2016, 2017; Jaschinski, Jainta, & Kloke, 2010; Schroth, Joos, & Jaschinski, 2015; Švede, Treija, Jaschinski, & Krūmiņa, 2015). Fixation

disparity is a small vergence error common even among subjects with normal binocular vision. It can be measured subjectively with psychophysical methods or objectively using eye-trackers. These studies found significant correlation between the objective fixation disparity and phoria. Additionally, Švede et al. (2015) showed that objective fixation disparity is different depending on whether the calibration is performed in monocular or binocular vision and found no correlation between fixation disparity and phoria when the eye-tracker is calibrated binocularly.

In the current study, the eye-tracker EyeLink 1000 Plus (SR Research Ltd., Ontario, Canada) was used to record eye movements during the performance of the cover test at near distance. Two different methods, detailed in subsequent sections, were used to measure phoria from the eye-tracker's recordings. In the first method, the deviation of only the occluded eye from its previous binocular position was considered in order to measure phoria, as it is done when the conventional cover test is performed in clinics. However, there is evidence that the fixating eye might occasionally move in the same direction as the covered eye instead of remaining still as it is generally assumed (Griffin, 1982). Since by definition phoria is a relative deviation between the two eyes, the deviation measured with the prism bar might be in fact greater than the true phoria. Thus, in the second proposed method the deviations of both the occluded and fixating eyes from their previous binocular positions were considered to compute it. The main objective of this study was to determine the differences between these two methods of phoria computation and validate them with the cover-uncover test and the modified Thorington test.

Pickwell (1973) stated that the fixating eye often moves, particularly during the recovery phase (i.e. when the occluder is removed) and observed that the amplitude of this movement is greater when the dominant eye is covered. Peli & McCormack (1983) also noted similar movements of the fixating eye during the recovery phase and obtained significantly different responses between the two eyes, especially for those subjects with clear ocular dominance. The symmetry of phoria between the two eyes and the effect of motor ocular dominance was analyzed in the current study. It is hypothesized that the greater amplitude of the fixating eye's movement when the dominant one is occluded might be justified by a greater deviation of the dominant eye (greater magnitude of phoria).

### **5.2.2. Methods**

#### *5.2.2.1. Subjects*

Thirty non-presbyopic adults (15 females and 15 males) participated in the study. Their mean age  $\pm$  standard deviation (SD) was  $27.9 \pm 4.6$  years and ranged from 21 to 38 years. All had 20/25 or better visual acuity in each eye at far and near distance with their habitual correction and no manifest

deviation (strabismus) as measured with the unilateral cover test. The horizontal phoria at near assessed with the cover-uncover test and measured with a prism bar ranged from +14 PD (esophoria) to -14 PD (exophoria).

All subjects were informed about the nature of the study before starting the experimental procedure and signed informed consent. The study followed the tenets of the Declaration of Helsinki and was approved by the Ethics Committee of Hospital Mutua de Terrassa (Terrassa, Spain).

#### *5.2.2.2. Materials and instrumentation*

Phoria was measured with three different methods: the cover-uncover test with a prism bar, the modified Thorington test and the automated and objective cover test using an eye-tracker.

During the cover-uncover test patients were asked to hold a visual acuity card at 40 cm and fixate a 20/30 visual acuity letter. The examiner covered the patients' eyes with an opaque occluder and a prism bar with powers of 1, 2, 4 to 20 PD in 2 PD steps and powers of 25 to 45 PD in 5 PD steps (Gulden Ophthalmics, Elkin Park, PA, USA) was used to measure horizontal phoria.

The horizontal phoria was also measured with the modified Thorington test using a Maddox rod and the MIM card. It has a measurement range from 28 PD esophoria to 28 PD exophoria with a resolution of 1 PD.

Finally, phoria was assessed objectively with an infrared video-based eye-tracker. Binocular eye data were registered with an EyeLink 1000 Plus at a sampling rate of 250 Hz (Figure 5.7A). The visual stimulus was printed on a white card which covered a visual field of  $40.5^\circ \times 42.9^\circ$  and placed at 40 cm of the patient. The fixation stimulus consisted of an empty black circle of  $1.6^\circ$ . The inner white region subtended an angle of  $0.9^\circ$  with a 20/50 (0.21°) Snellen E letter at the center to favor fine fixation and proper stimulation of accommodation (Figure 5.7B). The fixation stimulus was placed  $16^\circ$  downwards from primary position in order to optimize eye-tracker's data quality. Primary position refers to the position assumed by the eye when one is looking straight ahead with body and head erect. All eye movements were within the gaze tracking range reported by the manufacturer of  $32^\circ$  horizontally and  $25^\circ$  vertically. While patients fixated the Snellen E they also viewed peripherally the other eight identical stimuli at an eccentricity of  $16^\circ$  horizontally and  $9^\circ$  vertically used to calibrate the eye-tracker. The subjects' head was restrained using a chin rest.

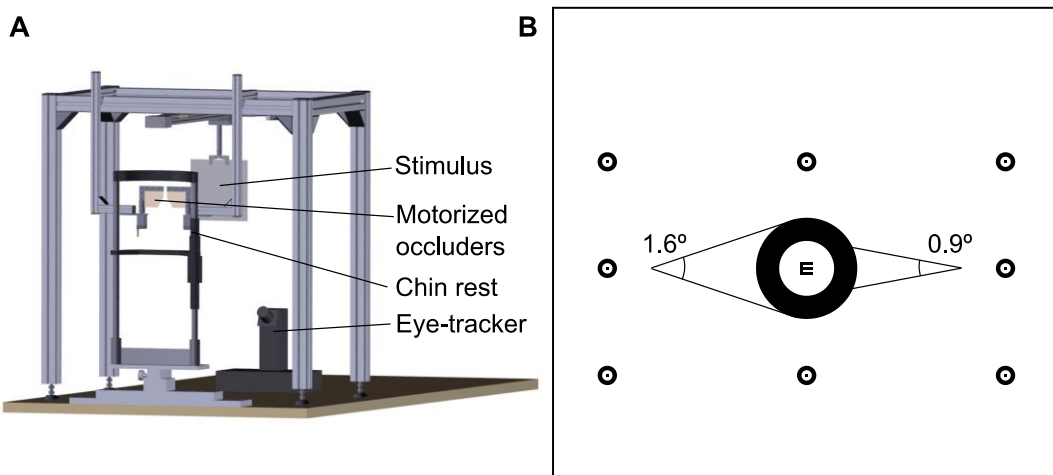


Figure 5.7. (A) Schematic representation of the experimental setup. (B) Visual stimulus. The central target has been enlarged for the sake of visibility. The other eight stimuli were identical and used to calibrate the eye-tracker.

In order to disrupt fusional vergence, each eye was occluded in turn similarly to the cover-uncover test. The occluders consisted of two crossed polarizers which blocked visible light but transmitted infrared wavelengths, hence allowing to register eye movements continuously even when the eyes were occluded. In order to check that the two pairs of crossed polarizers completely occlude the fixation target, their transmittance was measured with the spectrometer SPECTRO 320 (Instrument Systems, GmbH, Germany). Their mean transmittance in the visible range (from 380 nm to 780 nm) was 0.63%. It was also verified by visual inspection that observers could not have a residual view of the target through the occluders. They were driven by two stepper motors and controlled with a custom software coded in Matlab R2017a (MathWorks, Natick, MA, USA). It took approximately 0.27 seconds to occlude completely the visual field.

#### *5.2.2.3. Experimental procedure*

The experimental procedure was divided into two different sessions separated by a rest of 40 minutes approximately. The first session lasted 30 minutes approximately while the second was 15 minutes long. Participants wore their habitual refractive correction (either glasses or soft contact lenses) during all measurements.

The first session started by checking that the patient met the inclusion criteria of normal visual acuity and absence of strabismus. Then, the cover-uncover test was performed at 40 cm and the phoria was measured with a prism bar. While the patient fixated the stimulus, special emphasis was put on the importance of maintaining sharp vision in order to stimulate properly accommodation (Schroeder,

Rainey, Goss, & Grosvenor, 1996). The examiner covered each patients' eye in turn for approximately 5 seconds and increased the prism power to neutralize the recovery movement until its direction was reversed. Then, the considered value of phoria was the midpoint of all the range of prism powers with which no movement was perceived. A single measurement of phoria was obtained by placing the prism bar in front of either the right or the left eye.

After the cover-uncover test, the modified Thorington test was performed at 40 cm. As the MIM card is calibrated for the right eye, the Maddox rod was held before the right eye. The patient was asked to fixate the penlight that the examiner held in the center of the card and report through which number the vertical red line seen by the right eye crossed the horizontal axis. The measured phoria corresponded to the number reported by the patient.

Finally, the patient was positioned on a chin rest to perform the automated and objective cover test with the eye-tracker. Before starting the test, the eye-tracker was calibrated in binocular vision. Following the built-in calibration procedure of EyeLink, the patient was asked to fixate sequentially each E of the  $3 \times 3$  grid (Figure 5.7B) in a non-random order. Then, the patient was asked to fixate again the same targets in order to validate the fitted model and ensure acceptable spatial accuracy. The test began immediately after the eye-tracker's calibration. The test consisted in 3 cycles each composed of binocular fixation, left eye occlusion, binocular fixation and right eye occlusion. Each binocular or monocular fixation period lasted 5 seconds (Figure 5.8). Thus, the complete cover test lasted 60 seconds. The oculomotor responses during this procedure were saved for offline analysis.

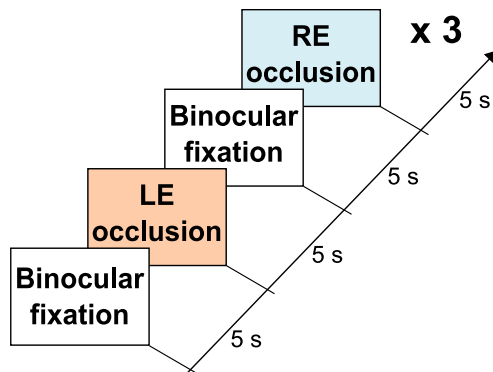


Figure 5.8. Test sequence.

This order of the tests was kept constant across all patients in order to prevent the examiner from being influenced by the response of the patient during the modified Thorington test or the

movement of the eyes seen on the display of the eye-tracker's computer during the automated and objective cover test.

The second session consisted in repeating the measurement of this automated and objective cover test for test-retest repeatability analysis. Patients were positioned in the setup and the eye-tracker was calibrated again before starting the test.

Motor ocular dominance was assessed with the Hole-in-the-Card test (J. Li et al., 2010). The test was repeated three times throughout both sessions: at the beginning and at the end of the first session and at the end of the second one. It is common to repeat the Hole-in-the-Card test several times in order to confirm motor ocular dominance (Johansson, Seimyr, & Pansell, 2015; J. Li et al., 2010; Rice, Leske, Smestad, & Holmes, 2008; Zhou et al., 2017). The three answers were collapsed to two categories: "right" if the right eye was dominant the majority of times and "left" if it was the left eye.

Hereafter, we will use the initials CT, TH and ET to refer to the cover-uncover test, the modified Thorington test and the automated and objective cover test with an eye-tracker, respectively.

#### 5.2.2.4. Eye-tracker data processing

Binocular eye data registered with the eye-tracker were processed offline using Matlab. Periods of 100 ms before and after each blink identified by the EyeLink software were removed in order to avoid artifacts associated with the onset and offset of blinks. These empty periods were replaced by linear interpolation after confirming by visual inspection that this did not bias the traces. Additional tests were performed in preliminary analyses with a time window of 200 ms and without interpolating blink periods and results did not differ remarkably.

The eye position at each monocular or binocular period was defined as the median of the last 0.5 seconds. The displacement of the occluded eye from its previous binocular position needed to be larger than the displacement of the fixating eye in the same period in order to measure a phoria during that occlusion. When this condition was not fulfilled, no phoria was measured.

Phoria was computed using two different methods. Firstly, the phoria computed with the *1-eye* method in left eye (LE) and right eye (RE) occlusion periods, respectively, was defined as

$$Het\ LE_{1\text{-}eye} = (L_{occ} - L_{bin}) \quad (5.5)$$

$$Het\ RE_{1\text{-}eye} = -(R_{occ} - R_{bin}) \quad (5.6)$$

where  $L_{occ}$  is the position of the LE during the LE occlusion period,  $L_{bin}$  is the LE position during the binocular fixation period prior the occlusion,  $R_{occ}$  is the position of the RE during the RE occlusion period, and  $R_{bin}$  is the RE position during the binocular fixation period prior the occlusion. This method mimics the measurement conditions of the cover test, in which only the movement of the occluded eye is considered. Secondly, the phoria computed with the *2-eyes* method in a LE and RE occlusion periods, respectively, was defined as

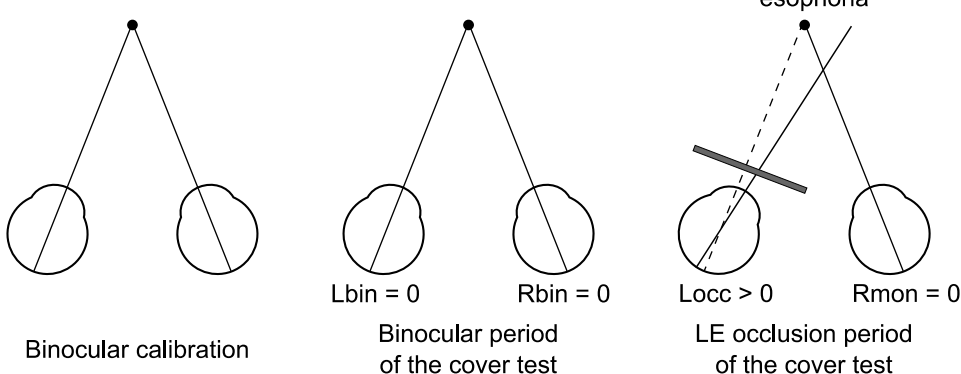
$$\text{Het } LE_{2\text{-eyes}} = (L_{occ} - L_{bin}) + (R_{mon} - R_{bin}) \quad (5.7)$$

$$\text{Het } RE_{2\text{-eyes}} = -(R_{occ} - R_{bin}) - (L_{mon} - L_{bin}) \quad (5.8)$$

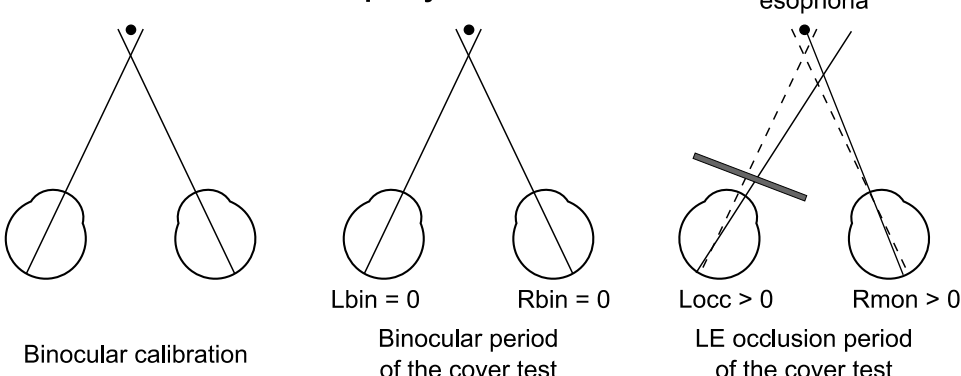
where  $R_{mon}$  is the position of the RE during the LE occlusion period, and  $L_{mon}$  is the position of the LE during the RE occlusion period. The deviation between the occluded *and* fixating eyes from their respective positions in the previous binocular fixation period are considered in this method. Thus, it strictly adheres to the definition which refers to phoria as a relative deviation between the eyes.

In Eqs. (5.5)–(5.8), theoretically,  $R_{bin}$  and  $L_{bin}$  are expected to be 0, as the eye-tracker's calibration was performed binocularly. The terms  $(R_{mon} - R_{bin})$  and  $-(L_{mon} - L_{bin})$  in Eqs. (5.7) and (5.8) correspond to the RE and LE components of fixation disparity, respectively, and are added to the measured phoria if they are in the same direction, whereas they are subtracted from the phoria if the uncovered eye moves in the opposite direction of the occluded eye. Following the sign convention typically used, exophorias are negative and esophorias are positive. In both methods the final phoria was computed as the median of the measurements obtained across the six occlusions. Figure 5.9 shows examples of the movements of the occluded and fixating eyes during the cover test in subjects with and without fixation disparity.

**A. Case with no fixation disparity**



**B. Case with eso fixation disparity**



**C. Case with exo fixation disparity**

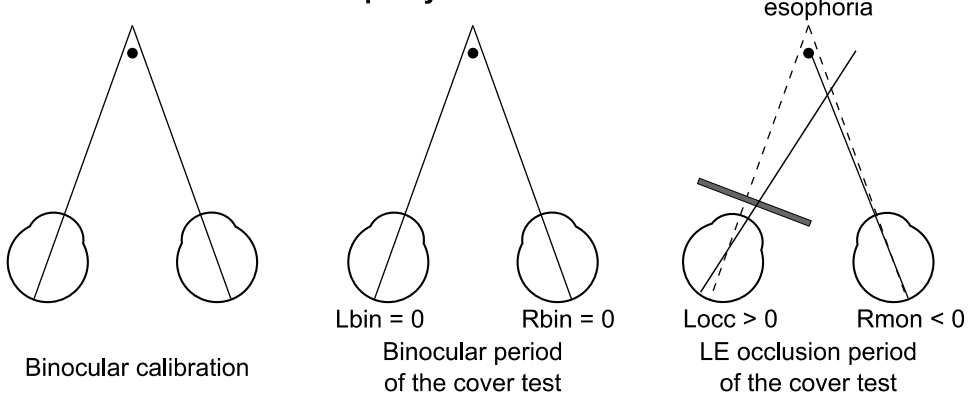


Figure 5.9. Examples of the movements of both eyes during the performance of the cover test. (A) Example of a subject with no fixation disparity. During the binocular calibration and the binocular period of the cover test both visual axes cross exactly at the target. As the subject has an esophoria, the LE turns right when it is occluded. Note that this scheme might not represent the most typical condition in which zero fixation disparity generally is accompanied by a small phoria. (B) Example of a subject with eso fixation disparity. In binocular viewing conditions the visual axes cross in front of the target. When the LE is occluded, it turns right to its heterophoric position and the RE refixates the target. This scheme illustrates the most physiologically plausible condition, in which esophoria occurs with eso fixation disparity. (C) Example of a subject with exo fixation disparity. In binocular viewing conditions the visual axes cross behind the target. When the LE is occluded, it turns right to its heterophoric position and the RE makes a leftward movement to refixate the target. Like (A), this scheme does not represent the most typical condition, as an exo fixation disparity generally is associated with an exophoria.

### 5.2.2.5. Statistical analysis

Statistical analyses were performed using SPSS Statistics 24 (IBM Corp., Armonk, NY, USA). The significance level was set at 0.05. The Shapiro-Wilk test was used to verify that each variable was normally distributed.

According to the sign convention typically used, exophorias were represented with a negative sign and esophorias with a positive sign. Comparing the signed phoria values we can know whether one condition is biased towards more esophoric or exophoric values compared to another. However, differences towards eso- and exo- direction cancel out. In order to know whether there is an over- or under-estimation of the magnitude of phoria in one condition compared to another regardless of its direction, the absolute values of phoria were also compared.

Paired t-tests were performed to determine whether the phoria measured with the *1-eye* and *2-eyes* methods differed significantly, to assess the intersession repeatability of the ET, and to analyze the differences in phoria between the eyes. A repeated measures ANOVA was used to determine the agreement between the signed phoria results obtained with the different methods. As our data violated the assumption of sphericity according to the Mauchly test, a Greenhouse-Geisser correction was applied. The agreement between the absolute phoria results of the different tests was determined with the non-parametric Friedman test since the data was not normally distributed. Post-hoc analysis with Wilcoxon signed-rank tests with Bonferroni correction was conducted. In this case, the Bonferroni correction set the significance level at  $p < 0.017$  ( $0.05/3 = 0.017$ ). The repeatability and agreement between CT, TH and ET were also assessed with Bland and Altman analysis (Bland & Altman, 1986). Pearson's correlation coefficients were obtained to determine the strength of association between: (1) the mean magnitude of phoria computed with the *1-eye* and *2-eyes* methods and the difference between them, (2) the results of phoria measured in the first and second sessions and (3) the difference between the phoria measured with the three different tests and its mean magnitude (three pairs). The Chi-square test of association (or Pearson's Chi-square test) was used to analyze the relationship between the direction of phoria measured with the different methods. Finally, the Welch test was performed to determine a potential effect of motor ocular dominance on the symmetry of phoria between the eyes after verifying that homogeneity of variances could not be assumed according to the Levene's test.

### 5.2.3. Results

#### 5.2.3.1. Differences between 1-eye and 2-eyes methods

Eye movements were registered with the EyeLink 1000 Plus during the performance of the ET. Figure 5.10 shows an example of the ocular traces from a representative participant. It can be clearly seen how both eyes point to the fixation target during the binocular periods (their horizontal position is around 0°) and how one eye deviates to reach its heterophoric position when it is occluded. The accuracy of the eye-tracker reported by the calibration step performed immediately before the test was  $0.27^\circ \pm 0.11^\circ$  for both RE and LE averaged across patients and sessions.

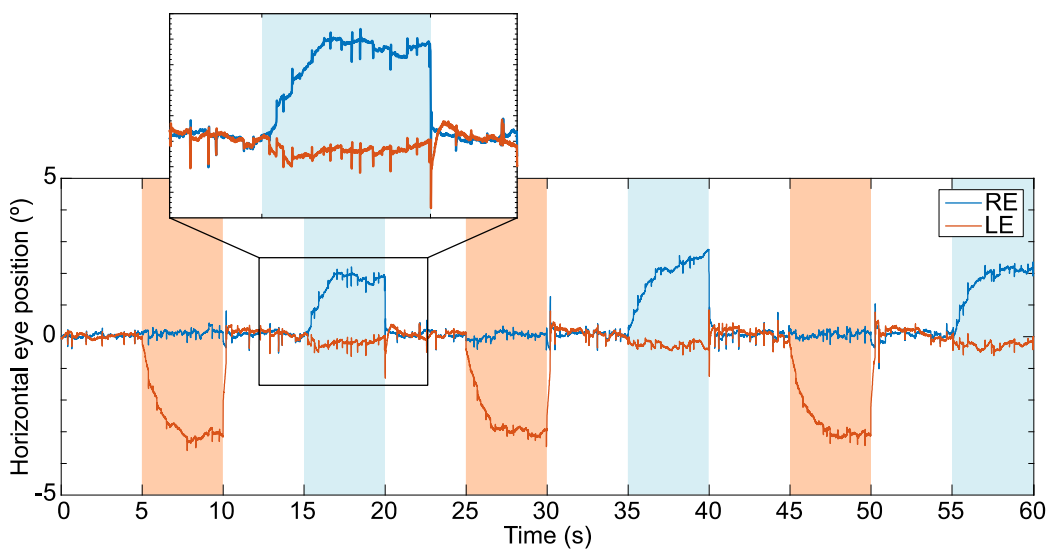


Figure 5.10. Ocular traces from a representative observer during the performance of the cover test. Horizontal RE and LE positions are represented with blue and orange lines, respectively. Periods of LE occlusion are shaded in orange and periods of RE occlusion are shaded in blue. The non-shaded areas correspond to binocular fixation periods. The inset panel zooms in on the eye traces during a RE occlusion period and shows how the RE stabilizes on its heterophoric position.

The mean  $\pm$  SD phoria averaged across participants and sessions was  $-1.24 \pm 3.53$  PD measured with the *1-eye* method, and  $-1.10 \pm 3.47$  PD measured with the *2-eyes* method (Figure 5.11A). The *1-eye* method results were significantly biased towards more negative, exophoric values than those produced by the *2-eyes* method [ $t(29)=-2.79, p=0.009$ ].

The mean  $\pm$  SD phoria in absolute value (i.e. the magnitude of the deviation independent of whether subjects exhibited exo- or esophorias) was  $2.90 \pm 2.32$  PD measured with the *1-eye* method, and  $2.80 \pm 2.28$  PD measured with the *2-eyes* method (Figure 5.11B). There were no significant

differences between the magnitude of phoria measured with the *1-eye* and *2-eyes* methods [ $t(29)=1.88, p=0.071$ ].

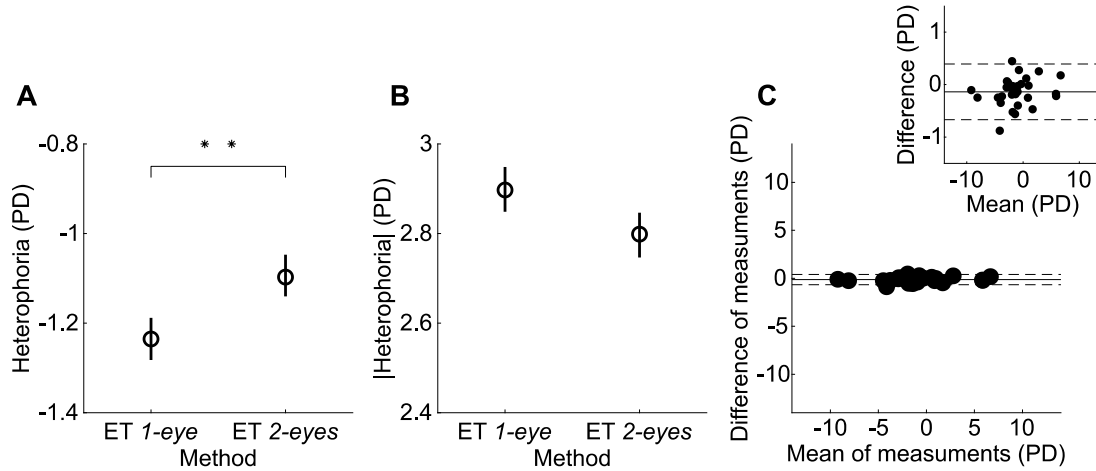


Figure 5.11. Agreement between ET phoria measurements obtained with the *1-eye* and *2-eyes* methods. (A) Phoria measurements obtained with the *1-eye* and *2-eyes* methods, averaged across sessions and participants. \*\* $p<0.01$ . (B) Magnitude (absolute value) of phoria measurements obtained with the *1-eye* and *2-eyes* methods, averaged across sessions and participants. In (A,B) circles are means and error bars represent 95% within-subject bootstrapped confidence intervals of the mean. (C) Bland and Altman plot showing the differences between *1-eye* and *2-eyes* ET phoria measurements as a function of the mean of both methods. The solid line represents the mean difference between methods. The dashed lines show the 95% limits of agreement. The inset in (C) shows the same plot, rescaled along the y-axis.

In spite of the statistically significant differences between ET phoria measurements computed with the *1-eye* and *2-eyes* methods, we nevertheless observed a good level of agreement between the two methods. The Bland-Altman plot in Figure 5.11C shows how the range of observed differences between *1-eye* and *2-eyes* ET phoria measurements is a small fraction of the range of observed measurements averaged across the two methods. The inset in Figure 5.11C shows that there was not a significant correlation between the mean of the two measures and the difference between them ( $r=0.21, p=0.258$ ).

Hereafter, the reported results of ET will correspond to the phoria values computed with the *2-eyes* method since it keeps strictly to the theoretical definition of this latent deviation of the visual axes.

#### 5.2.3.2. Repeatability of ET method

The repeatability of the ET phoria was determined within and between sessions. Intrasession repeatability was assessed considering the six measurements done consecutively at each occlusion. In the first session, the direction of the deviation was consistent across all occlusions except for four

subjects whose magnitude of phoria did not exceed 1 PD. The within-subjects standard deviation of the six phoria measurements was 1.11 PD. Considering the ET data obtained in the second session, the within-subjects standard deviation of the six partial measurements was 0.95 PD. In this case the direction of the deviation also agreed across all occlusions except for four subjects.

Intersession repeatability compares the results of the ET phoria of the two different sessions. The direction of the deviation was the same between sessions in all subjects. On average, the level of phoria measured with the ET method in the first session was  $-0.98 \pm 3.75$  PD. It did not differ significantly from the mean  $\pm$  SD phoria measured in the second session, that was  $-1.22 \pm 3.25$  PD [ $t(29)=-1.32$ ,  $p=0.197$ ] (Figure 5.12A). This implies that there was no bias towards more exo- or esophoric values between the two sessions. The two measurements were highly correlated ( $r=0.97$ ,  $p<0.001$ ). The within-subjects standard deviation of the two sessions was 0.71 PD.

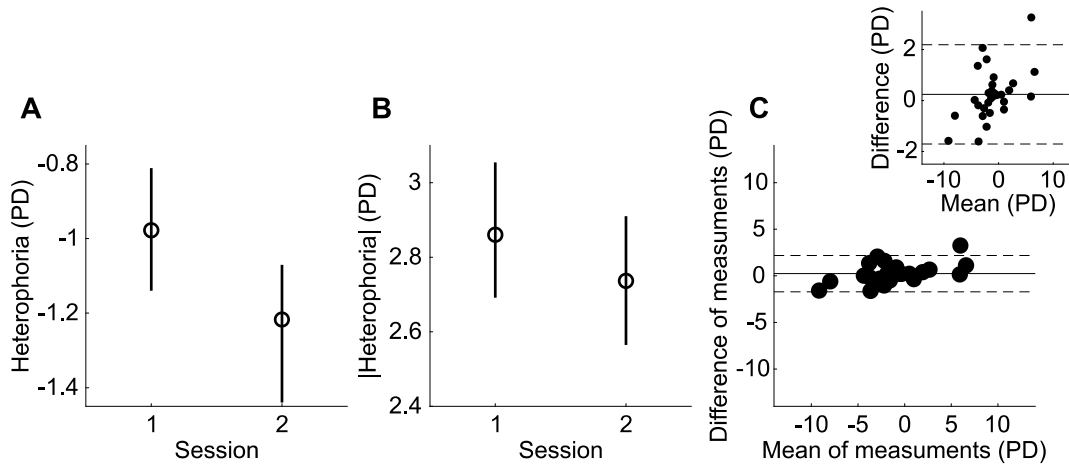


Figure 5.12. Repeatability of the ET method. (A) Phoria measurements obtained with the ET 2-eyes method in the first and second sessions, averaged across participants. (B) Magnitude (absolute value) of ET 2-eyes phoria measurements obtained in the first and second sessions, averaged across participants. In (A,B) circles are means and error bars represent 95% within-subject bootstrapped confidence intervals of the mean. (C) Bland and Altman plot showing the differences between the two sessions as a function of the mean of them. The solid line represents the mean difference between methods. The dashed lines show the 95% limits of agreement. The inset in (C) shows the same plot rescaled along the y-axis.

Considering the absolute values, the mean  $\pm$  SD phoria measured with the ET method was  $2.86 \pm 2.57$  PD in the first session and  $2.74 \pm 2.08$  PD (Figure 5.12B). There was no tendency towards an increment or a decrease of the magnitude of phoria measured with the ET method between the two sessions [ $t(29)=0.67$ ,  $p=0.508$ ].

The Bland-Altman plot in Figure 5.12C shows the high intersession repeatability results, with a small mean difference and 95% limits of agreement of  $\pm 1.95$  PD. In most participants the difference

of phoria between the two sessions was smaller than what it is typically considered as clinically different.

### 5.2.3.3. Agreement between CT, TH and ET methods

The agreement between the three tests used to measure horizontal phoria was also assessed. Individually, the mean  $\pm$  SD signed phoria was  $-1.00 \pm 6.35$  PD with CT,  $-0.72 \pm 5.12$  PD with TH and  $-1.10 \pm 3.47$  PD with ET (Figure 5.13A). The phoria results of the ET method reported here were first averaged across sessions. A repeated measures ANOVA with a Greenhouse-Geisser correction showed no statistically significant differences between the mean phoria measured with the three different methods [ $F(1.582,45.874)=0.31$ ,  $p=0.683$ ]. This implies that none of the methods were significantly biased towards more exo- or esophoric values.

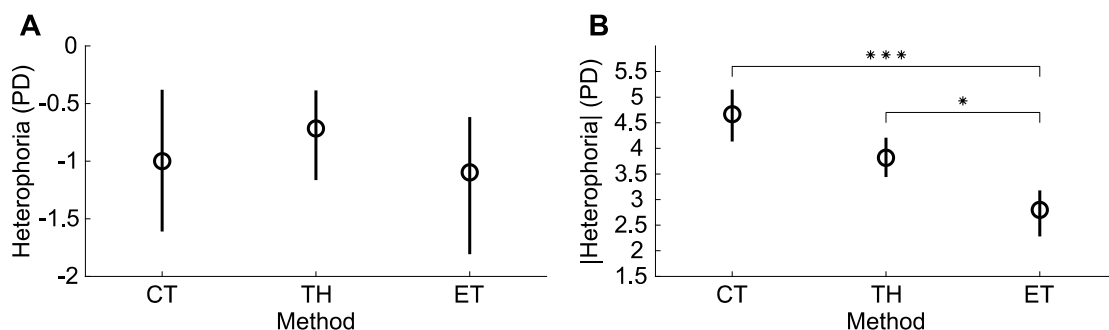


Figure 5.13. Agreement between CT, TH, and ET methods. (A) Phoria measurements obtained with the CT, TH and ET methods. CT and TH results are averaged across participants and ET results are averaged across sessions and participants. (B) Magnitude (absolute value) of phoria measurements obtained with the CT, TH and ET methods, averaged across participants for the CT and TH, and across sessions and participants for the ET. Circles are means and error bars represent 95% within-subject bootstrapped confidence intervals of the mean. \*  $p<0.05$ ; \*\*\*  $p<0.001$ .

Non-parametric statistical tests were used to analyze the agreement of the absolute magnitude of phoria measured with the three different methods. The median (interquartile range) phoria in absolute value was 4 PD (1.75 to 6 PD) with CT, 3.5 PD (1 to 5 PD) with TH and 2.05 PD (0.99 to 3.73 PD) with ET (Figure 5.13B). The Friedman test showed statistically significant differences between the magnitude of phoria measured with the three methods [ $\chi^2(2)=14.81$ ,  $p=0.001$ ]. Post-hoc analysis with Wilcoxon signed-rank test was conducted with a Bonferroni correction, resulting in a significance level set at  $p<0.017$ . There were no significant differences between the magnitude of phoria measured with the two conventional clinical methods [ $Z=2.217$ ,  $p=0.027$ ]. However, the results of the ET method were significantly smaller than those obtained with the CT [ $Z=3.569$ ,

$p<0.001$ ] and with the TH [ $Z=2.499, p=0.012$ ] independently of whether subjects exhibited exo- or esophoria.

The Bland-Altman plots in Figure 5.14 show a mean difference between methods close to 0 PD in the three pairs although wide 95% limits of agreement. The ET method showed narrower 95% limits of agreement with the TH than with the CT. Additionally, the plots in Figure 5.14 show a tendency towards poorer agreement for larger magnitudes of phoria, either exophoria or esophoria. The Pearson's correlation coefficient between the differences of the two measures and the average of them was 0.51 ( $p=0.004$ ) for the CT–TH pair, 0.87 ( $p<0.001$ ) for the CT–ET pair and 0.74 ( $p<0.001$ ) for the TH–ET pair.

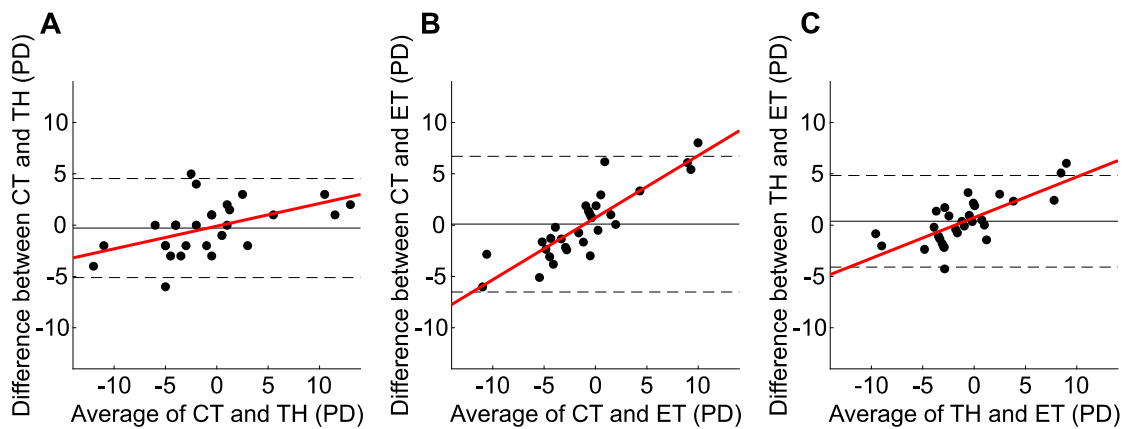


Figure 5.14. Agreement between the three pairs of methods. Bland and Altman plots comparing the CT with the TH (A), the CT with the ET (B), and the TH with the ET (C). The solid lines represent the mean difference between methods. The dashed lines show the 95% limits of agreement. The best fitting regression line through each pair of data is shown in red.

In order to analyze the agreement in the direction of the deviation assessed with the three different methods, all deviations smaller than 1 PD have been classified as orthophoria. This consideration is especially relevant for the ET method, in which very small deviations could be measured. There was agreement in terms of the direction of the phoria in 66.7% of the cases between the CT and the TH methods, in 70% of the cases between the CT and the ET methods and in 70% of the cases between the TH and the ET methods. The association between the percentage of exophoric ( $\geq 1$  PD of exophoria), esophoric ( $\geq 1$  PD of esophoria) and orthophoric (less than 1 PD of horizontal deviation) patients measured across the different methods was tested with the Chi-square test of association. It showed a statistically significant association between all pairwise comparisons:  $\chi^2(4)=18.23, p=0.001$  for the CT–TH pair;  $\chi^2(4)=19.77, p=0.001$  for the CT–ET pair; and  $\chi^2(4)=17.55, p=0.002$  for the TH–ET pair.

#### 5.2.3.4. Effect of motor ocular dominance on phoria

ET phoria was also computed separately for each eye. Then, RE and LE phorias were calculated as the median of the three values of phoria obtained when the RE and LE were occluded, respectively.

The direction of the deviation agreed between the eyes in 27 (90%) subjects. The three subjects who showed esophoria in the RE and exophoria in the LE or vice versa were excluded from this analysis. From the other 27 subjects, 23 gave consistent answers across the three repetitions of the Hole-in-the-Card test. As a result, 63% were RE dominant and 37% were LE dominant.

On average, the magnitude of RE phoria was  $2.66 \pm 2.35$  PD (mean  $\pm$  SD). The mean  $\pm$  SD LE phoria was  $3.47 \pm 2.43$  PD (Figure 5.15A). The magnitude of phoria in the RE was significantly smaller than in the LE [ $t(26)=-2.97$ ,  $p=0.006$ ]. There was no significant effect of motor ocular dominance on the differences of the magnitude of phoria between the eyes as shown by the Welch test [ $t(23.901)=-0.10$ ,  $p=0.922$ ] after checking that homogeneity of variances could not be assumed according to the Levene's test ( $p=0.03$ ). On average, the inter-eye difference was  $-0.83 \pm 1.71$  PD for the 17 subjects with RE dominance and  $-0.78 \pm 0.77$  PD for the 10 subjects with LE dominance (Figure 5.15B).

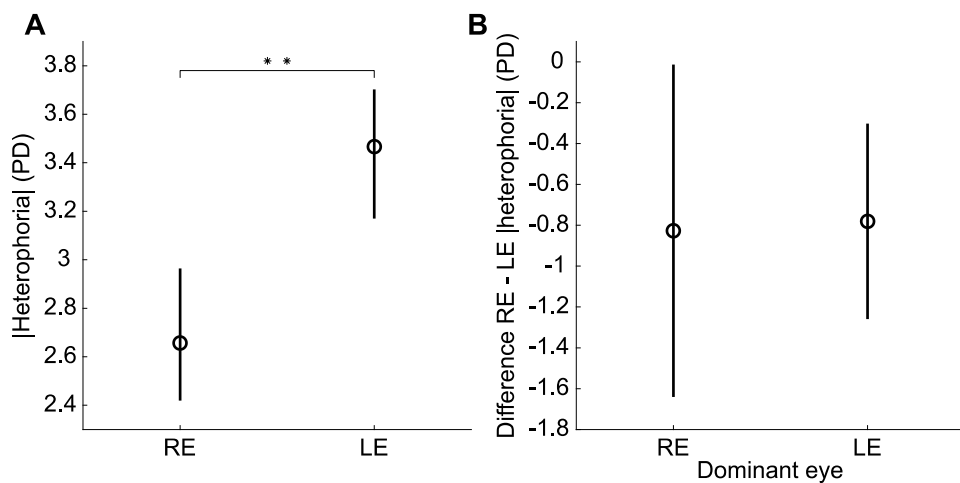


Figure 5.15. Difference between the phoria measured in the right and left eyes as a function of motor ocular dominance. (A) Magnitude (absolute value) of phoria measured separately in the right and left eyes with the ET 2-eyes method, averaged across sessions and participants. Circles are means and error bars represent 95% within-subject bootstrapped confidence intervals of the mean. \*\*  $p<0.01$ . (B) Difference between the magnitudes of phoria measured in the RE and in the LE as a function of motor ocular dominance. Circles are means and error bars represent 95% confidence intervals of the mean.

### 5.2.4. Discussion

#### 5.2.4.1. Differences between *1-eye* and *2-eyes* methods

According to the static position of the eyes before and after occlusion, the movements during the cover test are considered to be asymmetric vergence movements in which the fixating eye does not move when the other eye is covered. Considering the actual trajectory of the eyes, the movements are a combination of vergence and saccades in both the occluded and fixating eyes (Peli & McCormack, 1983). Thus, Griffin (1982) reported an occasional flick of the fixating eye in the same direction as the movement of the covered eye. This movement might imply an overestimation of the magnitude of phoria measured with the prism cover test.

Our eye tracking recordings revealed that the fixating eye drifted slowly during the cover phase instead of maintaining steady fixation, especially in cases with large phoria. This drift is hypothesized to be an expression of the Hering's law of equal innervation, which states that corresponding muscles of each eye receive equal innervations to contract or relax and perform an eye movement. For example, when a neural impulse for the performance of a rightward movement is sent out, the right lateral rectus and left medial rectus muscles receive equal innervation to contract. Another source of movement of the uncovered eye is fixation disparity. During the binocular fixation periods, the right and left lines of sight may cross behind or in front of the fixation target depending on the fixation disparity of the observer. However, when one eye is covered, the fixating eye moves to achieve precise foveal fixation and eliminate a monocular component of fixation disparity. The present discussion will be confined to phoria since it is generally agreed that the best practice in fixation disparity studies is to apply monocular calibrations with targets that optimize the eye tracking accuracy (Švede et al., 2015).

The impact of the movement of the fixating eye on the measurement of phoria might not be clinically relevant. The mean difference between the magnitudes of phoria measured with the *1-eye* and *2-eyes* methods, which is not artificially minimized by the positive and negative values according to the direction of the deviation, did not exceed 1.0 PD.

Objective and automated measurement systems as the one used in this study need to be robust to non-desirable situations in which patients do not cooperate properly. The measurement of the relative deviation between both eyes, i.e. the *2-eyes* method, is useful to distinguish a heterophoric deviation from a conjugate movement of both eyes, e.g. a saccade. Otherwise, a saccadic movement could be measured as a tropia (Figure 5.16). In relation to that, a limitation of the method is its inability to detect and/or measure properly paralytic tropias, since in these conditions the secondary

deviation (the deviation when the paretic eye is fixating) is always greater than the primary deviation (when the non-paretic eye is fixating) (Von Noorden & Campos, 2002).

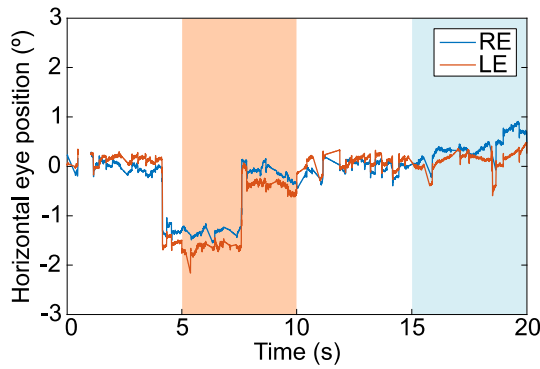


Figure 5.16. Ocular traces of a non-cooperative patient during two occlusion periods. Horizontal RE and LE positions are represented with blue and orange lines, respectively. The LE occlusion period is shaded in orange and the RE occlusion period is shaded in blue. The non-shaded areas correspond to binocular fixation periods. In the LE occlusion, a 1.80 PD esotropia of the RE would have been measured with the *1-eye* method although the displacement of the RE is due to a leftward saccadic movement of both eyes.

#### 5.2.4.2. Repeatability of ET method

The obtained intersession repeatability for the ET method is considerably better than the ones previously reported for the cover test and the modified Thorington test in terms of both signed and absolute mean difference (Figure 5.17). The articles reviewed in Figure 5.17 analyzed the intersession repeatability of either the cover test, the modified Thorington test, or a method to quantify phoria from eye tracking traces at near distance, and reported the signed and/or absolute mean difference  $\pm$  SD between sessions. There are some methodological differences between studies, e.g. the sample size, the age of participants, the range of measured phorias or the experimental procedure, which might explain certain variability of the results.

Neither the signed nor the absolute mean difference between sessions is greater than 2 PD except for the modified Thorington test in the study from Antona et al. (2011). This is why in general the cover test and the modified Thorington test are considered repeatable methods to measure phoria (Antona et al., 2011; Hirsch & Bing, 1948; Johns et al., 2004; Morris, 1960) according to the threshold of differences greater than 2 PD for clinical significance (Fogt et al., 2000; Ludvigh, 1949). Nevertheless, the ET method proposed in the current study has the lowest mean difference between sessions and is one of the only two methods whose 95% limits of agreement (1.96 times the SD of the differences) did not exceed  $\pm 2$  PD.

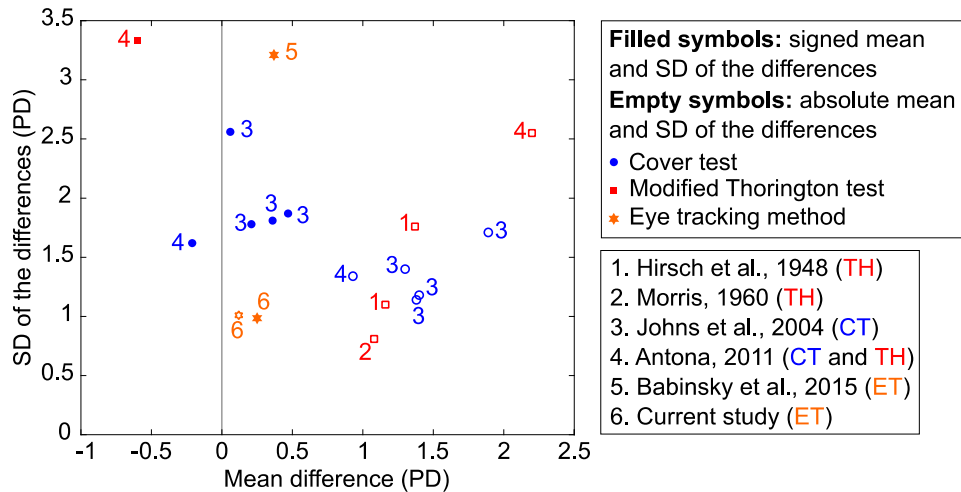


Figure 5.17. Comparison of published intersession repeatability results of different methods. Repeatability results of cover test, modified Thorington test, and eye tracking methods are represented with blue circles, red squares, and orange stars, respectively. Mean differences are plotted against the SD of the differences. Filled symbols correspond to signed mean and SD of the differences and empty symbols correspond to absolute mean and SD of the differences. Data extracted from (Antona et al., 2011; Babinsky et al., 2015; Hirsch & Bing, 1948; Johns et al., 2004; Morris, 1960).

Intrasession repeatability computed as the within-subjects standard deviation of the six individual measures is an estimate of the precision of the final value of ET phoria. It is not commonly assessed for the other clinical methods since none of them is objective. Thus, consecutive measurements would be influenced by the previous responses of the patients or biased due to non-masked examiners. Alternatively, interexaminer repeatability is typically assessed. The signed mean differences between examiners ranged between 0.05 PD and 0.74 PD with SD between 1.6 PD and 2.24 PD for the cover test (Johns et al., 2004; Rainey et al., 1998) and depends on the experience of the examiner (H. A. Anderson et al., 2010; Hryncak et al., 2010). Similar interexaminer repeatability results were obtained for the modified Thorington test (Rainey et al., 1998; E. P. F. Wong, Fricke, & Dinardo, 2002).

The high intrasession and intersession repeatability results obtained with the ET method might be justified by the fact that the sources of variability are minimized. The results were not biased by the patient nor the examiner, the test was always executed equally and the experimental conditions were maintained. Thus, the found variability is likely due to physiologic variations of vergence system only.

#### 5.2.4.3. Agreement between CT, TH, and ET methods

The signed mean differences between the phoria measured with the three tested methods were considerably close to 0 PD, which means that on average none of the methods were clearly biased towards more esophoric or exophoric values. To our knowledge, this is the first study that analyzes the agreement of the modified Thorington test with an eye tracking method to measure near phoria.

The agreement obtained in the current study between the cover test and the modified Thorington test ( $-0.28 \pm 2.46$  PD) is comparable to previous reports. Antona et al. (2011) found a bias of the modified Thorington test towards more exophoric values with respect to the cover test with a mean difference of -0.59 PD, and 95% limits of agreement of  $\pm 5.82$  PD. Sanker et al. (2012) obtained a mean difference between both tests of -0.88 PD and 95% limits of agreement of  $\pm 3.64$  PD.

Tests with similar dissociation methods and accommodative control are expected to show better agreement. Therefore, the ET method should show better agreement with the CT than with the TH. Although the mean difference between the CT–ET pair was slightly lower than between the TH–ET pair (0.10 PD and 0.38 PD, respectively), the former showed wider 95% limits of agreement ( $\pm 6.62$  PD and  $\pm 4.46$  PD, respectively). Three methodological differences between both cover tests could justify the lack of agreement. First, it has been shown that the magnitude of phoria increases with the dissociation time (H. A. Anderson et al., 2010; Barnard & Thomson, 1995) since it takes at least 5 seconds (and sometimes longer) for the occluded eye to reach its heterophoric position. Although the examiner attempted to cover each eye for approximately 5 seconds and left some periods of binocular fixation between occlusions in order to mimic the occlusion sequence of the ET, the number of occlusions and hence the total dissociation time was not controlled in the CT.

Besides fusional vergence, the vergence system has three more components (Ciuffreda, 1992). Accommodative vergence is driven by blur, and is the consequence of the relationship between the accommodative and vergence systems (Von Noorden & Campos, 2002). Proximal vergence is driven by the perception of apparent nearness of an object. The perception of a near object stimulates both the accommodative and the vergence systems (Ciuffreda, 1992). Finally, the tonic vergence is driven by the baseline neural innervation. Phoria depends on tonic, accommodative and proximal vergence response (Schroeder et al., 1996). In particular, North et al. (1993) showed that proximal cues have a significant effect on phoria. The second methodological difference that could justify the lack of agreement between the CT and the ET is related to proximal vergence. While tonic and accommodative vergence were stimulated similarly in the CT and the ET, the stimulation of the proximal component differed due to some particularities of the experimental setup. In both methods

the test was placed at 40 cm from the patient, but in the ET a structure to support the occluders and the two motors were positioned around the patients' face during the test. As a result, we could expect an increment in proximal vergence stimulation. One would expect in turn an increase in esophoria and/or a decrease in exophoria due to proximal effects. However, our results showed a decrease in the magnitude of phoria (either esophoria or exophoria) with the ET method.

Third, different criteria about the endpoint of the cover test might result in different values of phoria (Johns et al., 2004). The endpoint criteria used in the prism cover test was the midpoint from reversal, while the heterophoric position registered with the eye-tracker possibly corresponds to the first neutral endpoint. Johns et al. (2004) concluded that the differences between the first neutral and the midpoint from reversal endpoints were not clinically significant. However, it is relevant to note that there was a tendency of increased differences between the two endpoints with the magnitude of phoria according to the reported Bland and Altman plots. Therefore, the poorer agreement showed in the cases of large phoria might be partially due to the different endpoints used in each method together with the greater movement of the fixating eye not considered in the CT as reported above.

Another aspect that might partially justify the poor agreement between methods relies on whether a single phoria measurement was obtained for one eye (as in the CT and TH methods) or if it was computed as the median of the measures obtained for left and right eyes (as in the ET method). This might play a significant role in this study due to the asymmetry of phoria between the eyes found with the ET method. Nevertheless, the effect of the different dissociation methods between the TH and the ET might be more prominent since a similar level of agreement was obtained between the TH results and the ET phoria computed separately for the RE (mean difference  $\pm$  SD of  $0.10 \pm 2.50$  PD). The same analysis cannot be done with the CT-ET pair since in the CT the phoria was measured either on the right or the left eye without distinction.

Hryncak et al. (2010) analyzed the agreement of the phoria measured with a prism bar during the alternate cover test and with a head mounted eye-tracker. They obtained considerably better results, especially at the 95% limits of agreement. They considered only the deviation of the occluded eye to measure phoria from the eye tracking traces and did not find an effect of the deviation magnitude on the cover tests agreement. The 95% limits of agreement obtained in the current study were comparable with the ones obtained by Babinsky et al. (2015) on a sample of young children. Recently, Troyer, Sreenivasan, Peper, & Candy (2017) obtained slightly better agreement than Babinsky yet still comparable values between cover test and objective measurements in both children and adults.

#### *5.2.4.4. Effect of motor ocular dominance on phoria*

Regarding the symmetry between the eyes, on average phoria was significantly greater in the LE than in the RE. Previously, these asymmetries were attributed to the occlusion sequence and explained by the different time courses of relaxation of the fast and slow components of fusional vergence (Barnard & Thomson, 1995). However, the results of the current study showed greater phoria in the first occluded eye. Similar results were obtained by Van Rijn, Ten Tusscher, De Jong, & Hendrikse (1998), who could not show an effect of the occlusion order on the asymmetry of phoria.

There was no significant effect of motor ocular dominance on the asymmetry of phoria between the eyes. The mean difference in phoria between the eyes is essentially the same in RE and LE dominant subjects. Although there is evidence for an effect of ocular dominance on the dynamics of the recovery movements (Peli & McCormack, 1983), the amplitude of the movement during the cover phase might be independent of motor ocular dominance.

The reason for the horizontal phoria asymmetries found in the current study is not known. Further analyses are needed to evaluate possible causes for these differences. Particular attention was paid to center the optical axis of the camera relatively to patients' heads and obtain symmetrically positioned elements. Asymmetries could be partially explained by differences in the accommodative state between both eyes (Van Rijn et al., 1998). All patients wore their habitual refractive correction during the measurements, but a monocular uncorrected refractive error might lead to a different contribution of the accommodative vergence on the magnitude of phoria between the eyes.

To conclude, the use of eye-trackers to measure phoria overcomes several limitations of the conventional clinical methods and offers various advantages: movements of the occluded eye can be recorded; better resolution, accuracy, and intrasession and intersession repeatability are obtained; the measure is objective; and it provides new insights into the movements of both the fixating and occluded eyes during the cover test. The possibility to have binocular and monocular recordings of the viewing and covered eye offers the opportunity to do a more complete analysis. Further studies could be done to include the measurement of objective fixation disparity and analyze its relationship with phoria if the eye-tracker is calibrated monocularly and with high accuracy.

None of the existing methods to measure phoria are interchangeable. However, as eye-trackers become common tools in clinical settings, their use should be the new gold standard for the automated and objective measurement of phoria.



### 5.3. Study 3. Characteristics of saccades during the near point of convergence test

**NOTE:** The following text in this section corresponds to the submitted article: **Mestre, C.**, Gautier, J., Bedell, H. E., Díaz-Doutón, F., & Pujol, J. Characteristics of saccades during the near point of convergence test. [in review]

#### 5.3.1. Introduction

The near point of convergence (NPC) is the nearest point on which the eyes can converge (Scheiman & Wick, 2014). Its assessment is widely used in clinical practice, as a remote NPC value is the sign most frequently used by optometrists for the diagnosis of convergence insufficiency (Rouse, Hyman, et al., 1997). The NPC is determined by asking the patient to maintain fixation on an object placed in the midline while it is moved toward the patient's eyes. In the objective version of the test, the examiner observes the eyes of the patient to detect when one of them loses fixation. Alternatively, in the subjective version the patient is asked to report diplopia. The distance at which one eye turns out or the patient perceives double vision is the break point of convergence. The recovery point is the distance at which the eyes realign to the target or where the patient reports single vision again. The result of the NPC test typically is reported as the values of both the break and recovery points. The expected values in a young adult population are less than 5 cm for the break and less than 7 cm for the recovery (Scheiman et al., 2003).

Different fixation targets have been suggested for the assessment of the NPC including an accommodative target, a penlight, or a penlight with a red filter in front of one eye. Scheiman et al. (2003) found statistically significant differences between the results obtained with these three different targets in adult subjects with normal binocular vision, although the differences were clinically irrelevant (< 0.5 cm). However, Scheiman et al. (2003) found statistically significant and clinically meaningful differences between the break and recovery points obtained with an accommodative target and a penlight with red/green glasses in subjects diagnosed with convergence insufficiency. Nearer break and recovery values were obtained with the accommodative target. It is generally accepted that an accommodative target is preferable because it maximizes the accommodative demand and stimulates accommodative convergence (Adler, Clegg, Viollier, & Woodhouse, 2007; Scheiman et al., 2003). However, if convergence insufficiency is suspected, the NPC test should be repeated with a penlight and a red filter (Capobianco, 1952; Pang, Gabriel, Frantz, & Saeed, 2010; Scheiman et al., 2003).

Provided the fixation target is precisely positioned along the subjects' midline sagittal plane, the assessment of the NPC is a pure symmetrical vergence task. However, even when the target requires pure vergence movements and there is no demand for version, involuntary saccades occur (Collewijn et al., 1995; Coubard & Kapoula, 2008; Erkelens, Collewijn, & Steinman, 1989; Erkelens, Steinman, et al., 1989; Kenyon et al., 1980; Zee et al., 1992). Similarly, transient vergence movements have been found during saccades between isovergence targets (Collewijn et al., 1988a, 1988b). The presence of concurrent saccades and vergence eye movements led to the possibility to study the interaction between these two eye-movement systems (Coubard, 2013; Coubard & Kapoula, 2008; Kenyon et al., 1980; Ono et al., 1978; Zee et al., 1992).

Although some authors found a higher prevalence of saccades during symmetrical divergence than during symmetrical convergence (Collewijn et al., 1995; Kenyon et al., 1980; Zee et al., 1992), it is generally agreed that the frequency and dynamic characteristics of these versional movements is idiosyncratic (Coubard & Kapoula, 2008; Erkelens, Steinman, et al., 1989; Zee et al., 1992). Saccades during vergence have been found to be of unequal amplitude in the two eyes (i.e., not perfectly conjugate). Erkelens et al. (1989b) concluded that the disjunctive component of the saccades contributed to the "effectiveness" of the vergence movement, suggesting that saccades are not a mere "intrusion" into the vergence response but have a functional purpose. As concurrent saccades have been shown to speed up vergence movements (Erkelens, Steinman, et al., 1989), they might contribute to a strategy to bring one eye, perhaps the dominant eye, closer to the target in a shorter amount of time. As a result, the other eye would be moved transiently away from the target (Collewijn et al., 1995; Zee et al., 1992). Kenyon et al. (1980) concluded that despite the disconjugacy in amplitude, the saccades during vergence have normal dynamics, as they follow the saccadic main sequence.

Few studies have analyzed the characteristics of involuntary saccades during symmetrical vergence movements or during binocular fixation at different viewing distances, and none of them used ramp vergence stimuli. Krauskopf et al. (1960) found no consistent differences between saccades' features during binocular fixation at far (infinity) and near (55 cm) distances. However, the tested distances are not within the operational range of the NPC test and are far from the normal limits of convergence (Scheiman et al., 2003). Two pieces of evidence lead to the plausible expectation that the characteristics of concurrent saccades during vergence may change as a function of the vergence demand at different viewing distances (Otero-Millan, Macknik, et al., 2014): (1) greater saccadic frequency has been found during slower vergence movements compared to faster vergence movements in response to symmetrical vergence stimuli velocity (Kim & Alvarez, 2012b); and (2)

convergence peak velocity has been found to be reduced in subjects with convergence insufficiency (Alvarez et al., 2010; Thiagarajan et al., 2011; Yuan & Semmlow, 2000).

The main purpose of this study was to analyze the characteristics of small saccades that occur during NPC testing as a function of vergence demand. Specifically, we wondered whether some saccadic features can be used as objective markers to predict NPC break and/or recovery points.

### 5.3.2. Methods

#### 5.3.2.1. Subjects

Eleven non-presbyopic adults participated in the study (mean age  $\pm$  standard deviation (SD) of  $25.4 \pm 2.2$  years). All subjects had 20/20 visual acuity or better in both eyes at distance and near with their habitual refractive correction. Spherical refractive errors ranged from -6.50 D to +0.50 D with astigmatism up to -0.75 D. During the experiment, four subjects wore spectacles and 2 subjects wore contact lenses. All but 2 of the participants had a NPC break point (assessed with a pen tip and averaged across 3 replications) equal to or closer than 5 cm and a recovery point closer than 7 cm. All except 1 of the participants had stereoacuity of 20 arc sec or better measured with the graded circle test of the Random Dot 2 Stereo Acuity Test with Lea SYMBOLS (Vision Assessment Corp., Elk Grove Village, IL, USA). One subject had a break point of 5.3 cm and two had a recovery point of 8.3 cm. One participant had a stereoacuity of 23 arc sec. The two subjects with slightly receded NPCs had normal stereopsis.

The study was approved by the Ethics Committee of Hospital Mutua de Terrassa (Terrassa, Spain) and followed the tenets of the Declaration of Helsinki. All subjects gave informed written consent prior to participation in the study.

#### 5.3.2.2. Instrument and visual stimulus

The fixation target was a crosshair consisting of a  $2 \times 2$  mm cross surrounded by a 7 mm diameter circle. On the upper and bottom part of the circle there were two vertical lines with a length of 28 mm vertically aligned with the central cross. As a result, the cross subtended an angle of  $0.29^\circ$  and the whole stimulus subtended angles of  $1.00^\circ$  (width) and  $5.01^\circ$  (height) at 40 cm. The fixation target was black printed on white paper.

The visual stimulus was mounted on a track along which it could be moved forward and backward by a stepper motor. The motor was controlled by custom software coded in Matlab R2017a (MathWorks, Natick, MA, USA). Binocular eye movements were registered with an EyeLink 1000

Plus (SR Research Ltd., Ontario, Canada) at a sampling rate of 500 Hz. The EyeLink was positioned at its normal operating distance (around 50 cm) under the track and the target.

### *5.3.2.3. Experimental procedure*

Participants were positioned on a chinrest and aligned so that the central fixation cross and subjects' eyes lay on the same horizontal plane and the target moved along the midline to elicit symmetrical convergence and divergence movements.

First, the built-in 9-point EyeLink calibration was performed for each eye separately by asking the subjects to fixate on each of the 9 circles that subtended an angle of 0.86°. Instead of using a monitor to display the calibration targets, they were printed on white paper and mounted on the track at a viewing distance of 40 cm. The eye-tracker was able to locate the pupil and detect the first Purkinje image for the whole range of convergence angles required during the NPC test. However, this span of angles is considerably wider than the linear tracking range of the eye-tracker according to manufacturer's specifications (32° horizontally). For that reason, a further custom dynamic calibration procedure was carried out.

During the dynamic calibration, participants fixated separately with each eye on the same stimulus used later for the NPC testing while it moved from 40 cm to 2.8 cm along the midline at a constant velocity of 2 cm/s and back to 40 cm again. Participants were advised beforehand that they would perceive the target blurred at the closest distances. They were asked to maintain fixation on the center of the cross as precisely as possible. The complete calibration sequence was as follows: 9-point EyeLink calibration of the right eye and left eye, dynamic calibration of the right eye, and dynamic calibration of the left eye.

The NPC test started immediately after the calibration procedures were completed. Subjects were asked to fixate binocularly on the central part of the cross of the crosshair, which was placed initially at 40 cm. After a random time between 1 and 3 seconds, it started moving toward the subject at a constant velocity of 2 cm/s until it reached a viewing distance of 2.8 cm. Participants were asked to press a key on the keyboard when they perceived double vision. Regardless of the moment they reported diplopia, the target always reached the shortest distance. It remained at that position and after 1 second it moved backward to 40 cm at the same velocity. Participants were asked to press again a key when they recovered single binocular vision. The total vergence demand during the test varied from about 8.6° at 40 cm to 93.9° at 2.8 cm. The exact angles were slightly different across subjects depending on their interpupillary distance. This procedure was repeated three times

consecutively, during which the EyeLink recorded the positions of both eyes at a sampling rate of 500 Hz.

#### 5.3.2.4. Eye movement data analysis

Eye position data were processed offline using Matlab R2018a. Periods of 200 ms of the signal before and after each blink identified by the EyeLink software were removed to avoid artifacts associated with the onset and offset of blinks.

The EyeLink's HREF coordinate system was used to register eye position data following the recommendation of the manufacturer's support team (personal communication, September 18, 2017). Then, horizontal and vertical data were converted from HREF coordinates to degrees as

$$eyeX = \left( \frac{HREF_x}{f} + \tan^{-1} \frac{IPD}{2 \cdot calDist} \right) \cdot \frac{180}{\pi} \quad (5.9)$$

$$eyeY = -\frac{HREF_y}{f} \cdot \frac{180}{\pi} \quad (5.10)$$

where  $eyeX$  and  $eyeY$  are the horizontal and vertical eye positions in degrees, respectively;  $HREF_x$  and  $HREF_y$  are the raw horizontal and vertical HREF coordinates, respectively;  $IPD$  is the interpupillary distance;  $calDist$  is the calibration distance (40 cm); and  $f$  is a constant with a value of 15000. The EyeLink's intrinsic heuristic filter was switched off during the registration of eye position. Then, the data were filtered offline with a third order Savitzky-Golay filter of length 11 samples (22 ms) (Savitzky & Golay, 1964).

A fourth order polynomial equation was adjusted by least-squares fitting to the curve defined by the actual target position and the horizontal eye position during the convergence and divergence periods of the dynamic calibration computed with Eq. (5.9). The coefficients of the fitted polynomial were then applied to the horizontal data registered during NPC testing to compensate for the potential non-linearity of the eye-tracker at large convergence angles. The signals from each eye were calibrated separately with the dynamic calibration coefficients of the corresponding eye.

Although the target did not move vertically, some subjects exhibited variations in their vertical eye position with the target distance. In some cases, this resulted in changes in vertical vergence which were thought to be due to system noise (Bedell & Stevenson, 2013) or a vertical misalignment between the two eyes and the fixation target. Even a small linear difference in vertical position resulted in a considerable angular error, which increased at shorter fixation distances. The vertical eye-position traces computed with Eq. (5.10) were corrected to overcome this error (see section 5.3.5.1 in Appendix A for details).

Saccades were detected with an unsupervised clustering method (Otero-Millan, Castro, Macknik, & Martinez-Conde, 2014). A few changes were incorporated to adapt the online version of the algorithm to our data. This included removing the constraint of ignoring a 1-second period at the beginning of each trial, and correcting an apparent error in the implementation of the algorithm in which the direction of the right eye during binocular saccades was computed using the horizontal position of the left eye. The velocity-threshold-based algorithm proposed by Engbert & Kliegl (2003b) and modified subsequently by Engbert & Mergenthaler (2006) with  $\lambda = 6$  and a minimum duration of 6 ms also was used to identify saccades. The Engbert-Kliegl algorithm relies on the fact that the mean horizontal and vertical velocities during fixation are zero (Engbert & Kliegl, 2003b). Thus, the algorithm was modified to fit our data, in which the mean eye velocity is not zero due to the movement of the fixation target (see section 5.3.5.2 in Appendix A). Two detected saccades separated by less than 20 ms were fused into a single movement. A minimum intersaccadic interval of 20 ms also was imposed by the Otero-Millan algorithm. The performance of both the Otero-Millan and Engbert-Kliegl algorithms was checked by visual inspection of the traces. The Results section, below, reports the results from the unsupervised clustering method while the results obtained with the velocity-threshold-based algorithm are shown in Appendix B (section 5.3.6).

#### *5.3.2.5. Statistical analysis*

Statistical analysis was performed using SPSS Statistics 24 (IBM Corp., Armonk, NY, USA). The significance level was set at 0.05. Parametric tests were used with normally distributed variables while non-parametric tests were used when the variables were not distributed normally according to the Shapiro-Wilk test.

Saccades detected during the periods when the target was fixed at 40 cm or 2.8 cm were not included in the analysis, except to compute the evolution of saccade rate over time. Spearman's rank-order correlation was used to determine the strength of the associations between the saccade amplitude and peak velocity (main sequence) and vergence demand. The Mann-Whitney test was used to analyze whether the distributions of saccade amplitude and directional differences between the two eyes differed as a function of the direction of the concurrent vergence movement (convergence vs divergence). The Kruskal-Wallis test was used to assess the effect of the saccades' direction (horizontal vs vertical vs oblique) on the differences in the direction of the two eyes. The paired t-test was used to assess the differences in mean saccade rate as a function of the direction of the vergence movement, and between the number of corrective and uncorrective saccades.

RStudio (Boston, MA, USA) and R's Circular Package (Agostinelli & Lund, 2017) were used to apply circular statistical tests in order to analyze the saccade direction data. Watson's test was used to determine whether the directions of saccades were uniformly distributed. Fisher's nonparametric test was used to analyze the differences in saccade direction as a function of the direction of the vergence movement.

### 5.3.3. Results

Participants' break and recovery points based on their reports of diplopia and fusion are shown in Table 5.3. Two subjects did not report diplopia during the test. All subjects exhibited saccades during the vergence movements.

Table 5.3. Subjective break and recovery points averaged across the three repetitions of the NPC test  $\pm$  SD for all subjects, and total number of saccades exhibited during the three convergence and divergence periods.

<b>Subject</b>	<b>Break point (cm)</b>	<b>Recovery point (cm)</b>	<b>Number of saccades</b>
1	$3.9 \pm 0.4$	$5.2 \pm 0.2$	29
2	$5.9 \pm 0.9$	$7.2 \pm 0.2$	160
3	$3.4 \pm 0.5$	$5.0 \pm 0.4$	135
4	$3.9 \pm 0.3$	$4.9 \pm 0.3$	126
5	$3.5 \pm 0.7$	$5.6 \pm 0.2$	165
6	$4.8 \pm 0.1$	$7.3 \pm 0.8$	146
7	$3.0 \pm 0$	$6.9 \pm 1.1$	102
8	-	-	186
9	$3.0 \pm 0$	$4.3 \pm 0.7$	113
10	$3.0 \pm 0$	$6.7 \pm 2.1$	308
11	-	-	84

A total of 1554 saccades with a median amplitude of  $0.48^\circ$  (range from  $0.12$  to  $12.26^\circ$ ) were detected in the periods when the fixation target moved forward and backward. Most of the saccades (83.6%) had an amplitude smaller than  $1^\circ$ . Saccades during convergence and divergence followed the main sequence ( $r_s=0.95$ ,  $p<0.001$ ) as shown in Figure 5.18A.

Saccade amplitude increased significantly with vergence demand ( $r_s=0.60$ ,  $p<0.001$ ) (Figure 5.18B). All individual subjects showed a significant positive correlation with coefficients ranging from 0.55 to 0.85 (all values of  $p\leq 0.001$ ). There was no significant effect of the direction of the

vergence movement on the amplitude of saccades according to the Mann-Whitney test ( $p=0.224$ ) (Figure 5.18C).

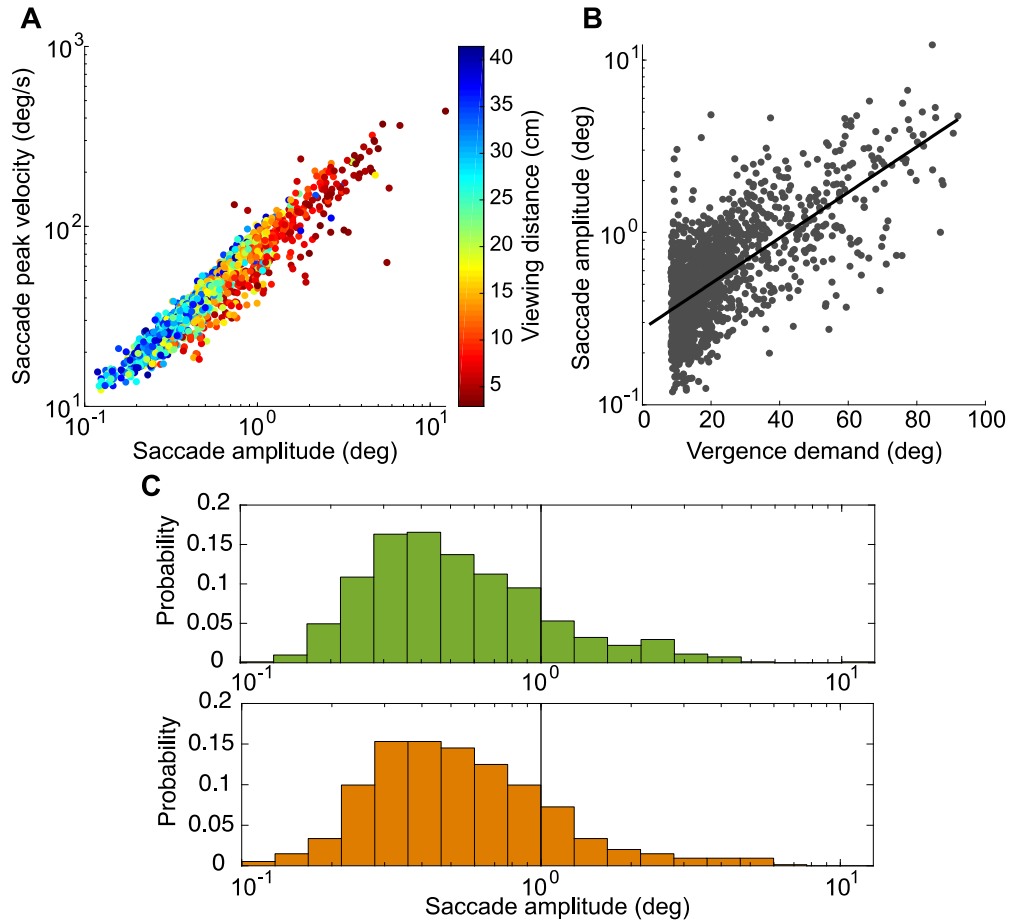


Figure 5.18. (A) Main sequence on a log-log scale as a function of the viewing distance. The color code exposes the tendency for greater saccade amplitudes and peak velocities at shorter viewing distances. (B) Saccade amplitude as a function of vergence demand. The black line corresponds to the least-squares regression fit, which is shown only for illustrative purposes ( $R^2=0.48$ ). (C) Amplitude distribution of saccades detected during convergence (top) and divergence (bottom) periods. The black vertical lines at amplitude =  $10^{0\circ}$  show that most saccades had an amplitude smaller than  $1^\circ$  and can therefore be presumably considered to be equivalent to fixational microsaccades in terms of size, even though the fixation target in our experiment was not stationary.

The distribution of saccade directions is shown in Figure 5.19. The directions of saccades differed significantly from a uniform distribution as shown by Watson's test for circular uniformity ( $p<0.01$ ). A higher prevalence of horizontal than vertical saccades was found, with more upwards than downwards vertical components. According to Fisher's nonparametric test for common median directions, the median direction of saccades during convergence ( $70.80^\circ$ ) and divergence ( $63.28^\circ$ ) did not differ significantly ( $p=0.542$ ).

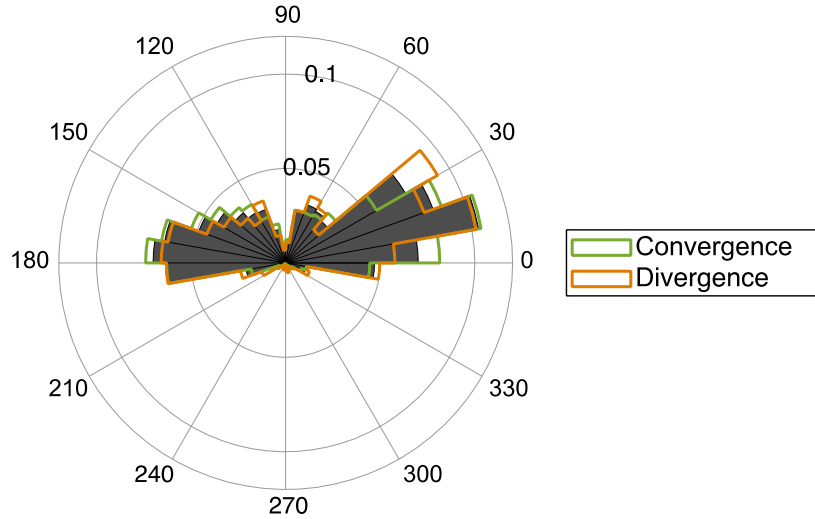


Figure 5.19. Polar histogram of the saccade directions (gray sectors). The directions of saccades during convergence and divergence periods are shown with green and orange lines, respectively. Zero and 90 degrees indicate rightward and upward saccades, respectively.

Both horizontal (directions of  $\pm 22.5^\circ$  from horizontal) and vertical (directions of  $\pm 22.5^\circ$  from vertical) saccades exhibited the same trend as all saccades to increase in amplitude with vergence demand (horizontal:  $r_s=0.62$ ,  $p<0.001$ ; vertical:  $r_s=0.56$ ,  $p<0.001$ ). All individual subjects except one showed a significant positive correlation between the amplitude of horizontal saccades and vergence demand with correlation coefficients ranging from 0.54 to 0.86 (all values of  $p\leq 0.008$ ). Higher inter-subject variability was found for vertical saccades. Only the three participants who made more than a total of 25 vertical saccades showed a significant correlation.

The difference in saccade direction between the two eyes is shown in Figure 5.20A. In 193 saccades (12.4%) the direction of the two eyes was found to differ more than  $\pm 45^\circ$ , and in 109 (7.0%) the difference was greater than  $\pm 90^\circ$ . Overall, the occurrence of directionally non-conjugate saccades was similar during the periods of convergence and divergence. However, the distribution of the directional differences was significantly different as a function of the direction of vergence according to the Mann-Whitney test ( $p<0.001$ ) (Figure 5.20B). The long tails towards positive angular differences during convergence and toward negative differences during divergence indicate that the right-eye direction tended to be more leftward than the direction of the left eye during convergence and more rightward during divergence. This behavior is illustrated further in Figure 5.21, in which the directions of the right and left eyes during the directionally non-conjugate saccades are represented as a function of the direction of the concurrent vergence movement.

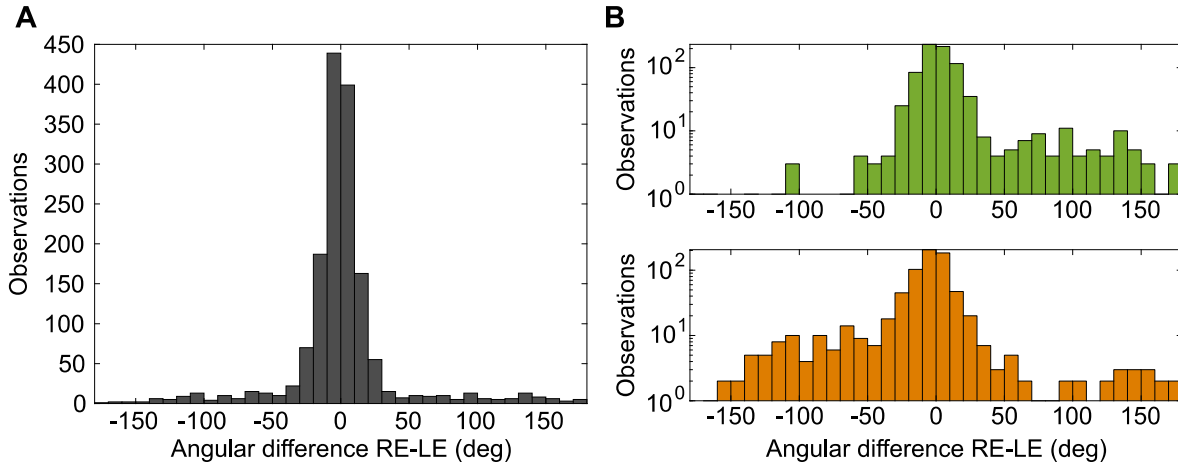


Figure 5.20. (A) Histogram of the difference in saccade direction between the two eyes (direction of the right eye minus direction of the left eye) in degrees. An angular difference of 0° means that the two eyes moved in the same direction, whereas  $\pm 180^\circ$  means that the saccade had opposite directions in the two eyes. (B) Histograms of the between-eye differences in saccade direction during convergence (top) and divergence (bottom). Note that the vertical axes are scaled logarithmically in panel (B) to emphasize the numbers of saccades that differed in direction in the two eyes.

The medians (IQR) of the directional differences were similar for horizontal, vertical and oblique saccades: 0.28° (12.74°) for horizontal saccades, -6.72° (31.24°) for vertical saccades, and -2.07° (24.67°) for oblique saccades. Nevertheless, the distributions of the directional differences between the eyes differed significantly as a function of the direction of the saccades as shown by the Kruskal-Wallis test ( $p < 0.001$ ). Specifically, the distribution of the directional differences between the eyes of horizontal saccades differed significantly from that of vertical and oblique saccades ( $p < 0.001$ ). No significant differences were found between vertical and oblique saccades ( $p = 0.316$ ).

The saccade rate averaged across subjects and the three repetitions was  $1.34 \pm 0.66$  Hz. Overall, the mean saccade rate during convergence ( $1.39 \pm 0.68$  Hz) and divergence ( $1.28 \pm 0.67$  Hz) did not differ significantly [ $t(10)=1.53$ ,  $p=0.158$ ] (Figure 5.22). The evolution of saccade rate over time was computed by using a moving time window of 1 s. On average, saccade rate decreased to around 0.5 Hz at the closest target distance (Figure 5.23A). However, the prevalence of saccades during vergence movements was idiosyncratic. While five participants showed a decreased saccade rate with higher vergence demand (Figure 5.23B), two subjects showed the opposite behavior and made more saccades at the closest target distance (Figure 5.23C). The other four subjects showed no clear trend to change saccade rate with vergence demand.

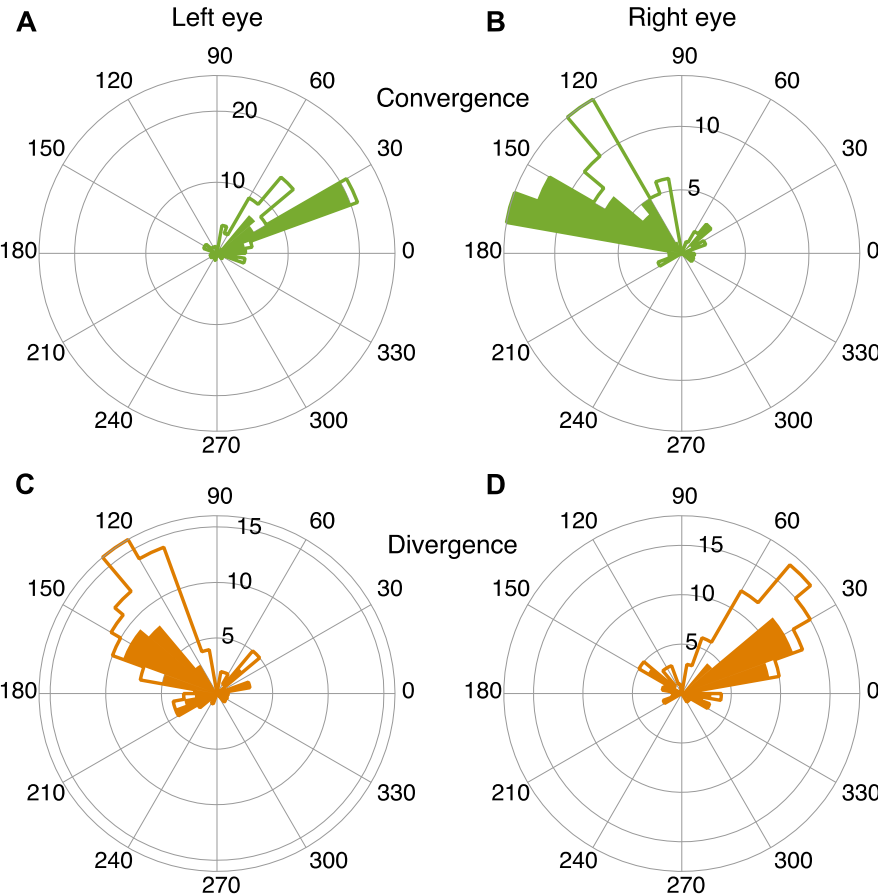


Figure 5.21. Distribution of the right (panels (B) and (D)) and left (panels (A) and (C)) eyes directions for the directionally non-conjugate saccades as a function of the direction of the concurrent vergence movement (convergence: panels (A) and (B); divergence: panels (C) and (D)). The unfilled distributions limited by the solid lines are the directions of saccades which differed in the two eyes by more than  $\pm 45^\circ$ , while the areas shaded in color represent the directions of saccades which differed in the two eyes by more than  $\pm 90^\circ$ .

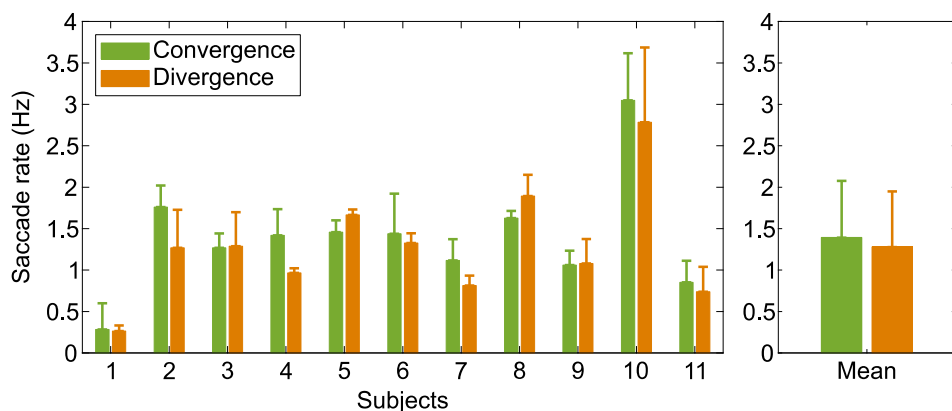


Figure 5.22. Saccade rate of each subject averaged across the three repetitions as a function of the direction of the concurrent vergence movement. The bars in the right subplot represent the mean saccade rate of all subjects. Error bars correspond to  $\pm 1$  SD.

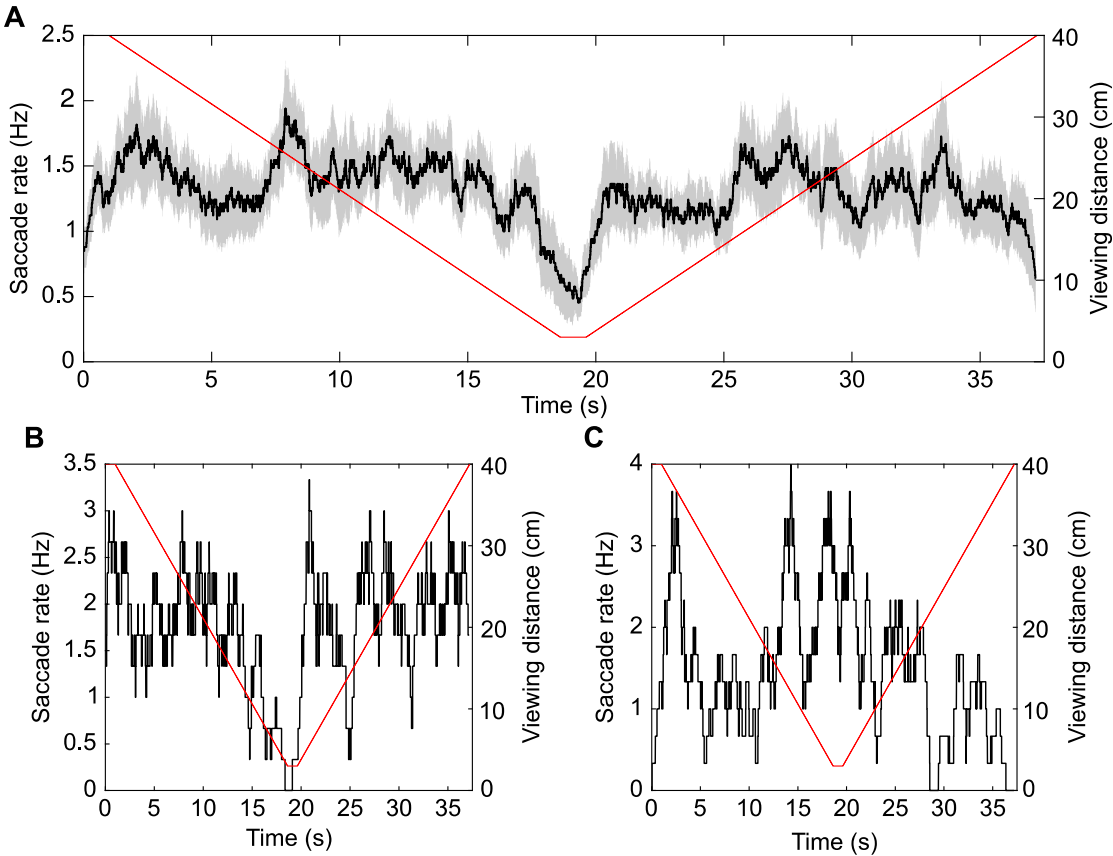


Figure 5.23. (A) Saccade rate over time averaged across subjects and the three repetitions (black line). The shaded area corresponds to  $\pm 1$  standard error of the mean (SEM). The right axis and the red line represent the target distance. (B) Saccade rate over time averaged across the three repetitions for a representative subject (Subject 8) who showed a decreased saccade rate at the closest target distance (black line). The right axis and the red line represent the target distance. This participant did not report diplopia during any of the three repetitions of the test. (C) Saccade rate over time averaged across the three repetitions for a representative subject (Subject 2) who showed an increased saccade rate at the closest target distance (black line). The right axis and the red line represent the target distance.

Overall, the number of saccades that corrected a horizontal vergence error (disparity) exceeded significantly the number of error-producing saccades [ $t(10)=2.81$ ,  $p=0.018$ ]. The convergent and divergent components of saccades are illustrated in Figure 5.20 and emphasized in Figure 5.21 for directionally non-conjugate saccades. All subjects except two (Subjects 4 and 11) made more disparity-correcting saccades than disparity-inducing saccades (Table 5.4). Considering the horizontal fixation position error of each eye separately, for most subjects saccades tended either to move one eye closer to the target and the other eye either farther from the target or produced no change. The number of saccades of each subject in which the right and left eyes moved closer to the target is shown in Table 5.4. For all subjects except Subject 1, the eye with more corrective saccades corresponded to the dominant eye (see the numbers in bold in Table 5.4). The eye dominance was

determined by visually inspecting the ocular traces as the eye that either maintained fixation or deviated less after fusion loss, or the eye that made the initial recovery movement in the correct direction. The dominant eye of subjects 8 and 11 could not be determined as these participants did not lose fusion during the NPC test.

Table 5.4. Number of saccades that corrected or produced a horizontal disparity error; number of saccades that brought the right eye (RE) or the left eye (LE) closer to the target; and the dominant eye of each subject.

<b>Subject</b>	<b>Disparity correcting saccades</b>	<b>Disparity inducing saccades</b>	<b>Saccades correcting RE fixation position</b>	<b>Saccades correcting LE fixation position</b>	<b>Dominant eye</b>
1	16	13	13	17	RE
2	86	74	81	<b>94</b>	LE (1 <sup>st</sup> and 2 <sup>nd</sup> rep); RE (3 <sup>rd</sup> rep)
3	100	35	46	<b>103</b>	LE
4	57	69	<b>70</b>	35	RE
5	107	58	59	<b>65</b>	LE
6	106	40	<b>89</b>	58	RE
7	55	47	<b>58</b>	48	RE
8	129	57	80	107	-
9	57	56	43	<b>54</b>	LE
10	176	132	<b>170</b>	135	RE
11	38	46	28	52	-

Rep: repetition.

### 5.3.4. Discussion

All participants made a considerable number of saccades while they fixated on a target moving in depth to test the NPC. Their saccades followed the main sequence with a similar slope to that reported for visually-guided saccades (Coubard & Kapoula, 2008) and slightly lower but still comparable to that for fixational microsaccades (Galfano, Betta, & Turatto, 2004).

Saccade amplitude increased and, on average, rate decreased with vergence demand. One might hypothesize that these effects could be explained by the increased effort of the vergence system to maintain fusion at short viewing distances. If that would be the case, saccade amplitude and

frequency could be used as objective markers to predict the break point of the NPC test. However, the evolution of saccade rate over time was idiosyncratic. The observations that one of the subjects who did not lose fusion during the test clearly exhibited fewer saccades at shorter viewing distances (Figure 5.23B), and that a minority of subjects showed the opposite trend (Figure 5.23C) lead to the conclusion that these parameters cannot be used as an accurate indicator of fusion loss. A higher number of saccades around the break point of the NPC was not expected because binocular disparity is not a stimulus for microsaccades (Krauskopf et al., 1960; St Cyr & Fender, 1969).

Alternatively, the changes in amplitude and saccadic rate might be explained by the more rapid change of vergence demand and the greater angular size of the fixation target at near than at far (McCamy, Najafian Jazi, Otero-Millan, Macknik, & Martinez-Conde, 2013; R. M. Steinman, 1965). While the central fixation cross subtended an angle of 0.29° at 40 cm, its angular size increased nonlinearly up to 4.1° at 2.8 cm. The accommodation limit and the blurred perception of the fixation target at close distance might also lead to greater saccade amplitudes (Ghasia & Shaikh, 2015). Further research with subjects with a receded NPC and/or using targets with constant angular size might be useful to disentangle the effect of target characteristics such as blur and size from the effect strictly related to the effort of the vergence system.

In agreement with the reported distributions of fixational microsaccades, saccades detected during vergence movements show a preference for horizontal directions (Abadi & Gowen, 2004; Engbert, 2006; Nyström, Andersson, Niehorster, & Hooge, 2017). However, vertical and oblique saccades were not observed as exceptionally as previously reported. When saccades exhibited a vertical component, it was generally upwards (Figure 5.19). Downwards saccades were rarely observed. This bias in the vertical direction cannot be explained by a potential movement of the target in the vertical plane because the saccade direction did not reverse between convergence and divergence periods (Figure 5.19). Instead, the high prevalence of upward saccades might reflect the tendency of some normal subjects to exhibit an *upbeating vertical nystagmus* (Figure 5.24). Six participants showed this behavior during the experiment. Stevenson, Sheehy, & Roorda (2016) previously reported this pattern of eye movement in the fixation of some normal observers, as registered using a binocular Scanning Laser Ophthalmoscope. The amplitude of vertical nystagmus also increased significantly with vergence demand as shown by the significant positive correlation between the amplitude of vertical saccades and vergence demand.

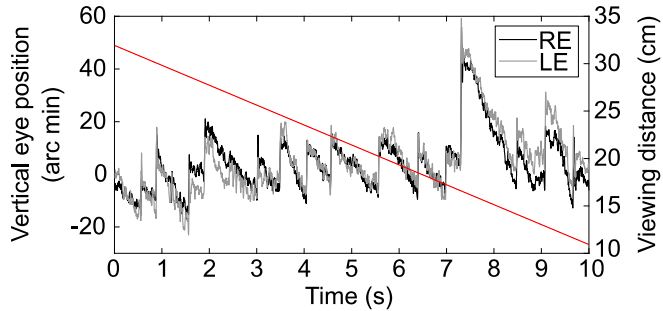


Figure 5.24. Vertical traces of a representative observer (Subject 5) who exhibited an upbeat vertical nystagmus (slow downward drift interrupted by upward saccades). Positive and negative values mean upward and downward movements, respectively. The right axis and the red line represent the target distance.

Saccades performed during vergence movements are not perfectly conjugated (Erkelens, Steinman, et al., 1989; Kenyon et al., 1980). In the current study special emphasis was placed on directional disconjugacy. The percentage of saccades in which the direction of both eyes differed more than 45 degrees agreed with other studies of fixational microsaccades (Møller, Laursen, Tygesen, & Sjølie, 2002; Nyström et al., 2017). Previously, Krauskopf et al. (1960) found a higher degree of conjugacy between the directions of the saccades made by the two eyes. The occurrence of directionally non-conjugate saccades and its prevalence in convergence or divergence periods were idiosyncratic among subjects, in agreement with Erkelens, Steinman, et al. (1989). In general, horizontal saccades (directions  $\pm 22.5^\circ$  from horizontal) were more conjugated than vertical and oblique saccades. The directionally non-conjugate saccades were mostly oblique or vertical to a lesser extent. According to the polar plots in Figure 5.21, the direction of the vertical saccadic component of these non-conjugate saccades appeared to be similar in the two eyes and the main source of disconjugacy was horizontal, as convergent and divergent components were found. This association of vertical version and horizontal vergence movements was also found in the version-vergence nystagmus exhibited in response to optical flow on the ground plane (D. Yang, Zhu, Kim, & Hertle, 2007; Zhu, Hertle, & Yang, 2008). The occurrence of directionally non-conjugate saccades with convergent and divergent components supports other observations that vergence eye movements are not always slow (Leigh & Zee, 2015). The disjunctive component of directionally non-conjugate saccades was mostly in the correct direction to reduce vergence error as shown in Figure 5.20 and Figure 5.21.

The potential role of fixational eye movements in maintaining accurate binocular fixation has been a matter of study for several decades (Otero-Millan, Macknik, et al., 2014). Our results suggest that 59.7% of all the saccades performed during the NPC test reduced horizontal vergence errors (Table 5.4). However, two observers made more error-inducing than correcting saccades. Overall, the

median horizontal vergence error compensated by saccades during the convergence and divergence periods was 0.78 min arc and 3.12 min arc, respectively. Involuntary microsaccades during fixation of a stationary target have been also found to correct similar amounts of binocular disparity (Engbert & Kliegl, 2004). However, these authors also found a considerable percentage of error producing microsaccades.

Our results reveal a preference of subjects to reduce the fixation position error of one eye at the expense of inducing (or at least not correcting) the fixation error of the other eye. Most subjects chose the dominant eye to reduce its fixation position error, as previously suggested by Zee et al. (1992). In 4 participants, the median error induced in the non-dominant eye was smaller than the median error corrected by the dominant one. Two participants showed the opposite behavior. In 2 other subjects, saccades induced a small fixation error in both eyes, although it was smaller in the dominant eye. The dominant eye of the 3 other subjects either could not be assessed or did not coincide with the eye in which saccades were more corrective.

In summary, all observers made involuntary small saccades during the NPC test. Both the average saccade amplitude and rate changed with vergence demand. However, the increment in amplitude and decrease in rate might be explained by the greater angular size of the fixation target at near than at far, rather than by the interactions between the saccadic and vergence systems. In general, the direction of the vergence movement had no significant effect on saccade characteristics. A small percentage of saccades was not conjugated as they contained convergent or divergent components. Most non-conjugate saccades tended to correct binocular disparity errors. Finally, in most participants the majority of saccades tended to correct the fixation position error of the dominant eye.

### 5.3.5. Appendix A

#### 5.3.5.1. Correction of vertical eye-position traces

If the two eyes of the observer were not exactly at the same height in the head, vertical vergence would be required to maintain binocular fixation at close fixation distances. The change in vertical eye position would be expected to be explained by the inverse tangent of the vertical misalignment between the eye and target heights divided by the viewing distance.

Figure 5.25A shows an example of the change in vertical eye position during the dynamic calibration with viewing distance. The vertical traces of 8 participants showed a similar behavior during the NPC test. The function

$$\text{vertical position} = \tan^{-1} \left( \frac{a}{\text{distance}} \right) + b \quad (5.11)$$

was fitted to the dynamic calibration data, where  $a$  is the parameter indicative of the vertical misalignment, *distance* is the distance of the fixation target from the observer, and  $b$  is a constant vertical position error. The estimated vertical misalignment ( $a$ ) ranged between 0.01 mm to 0.44 cm.

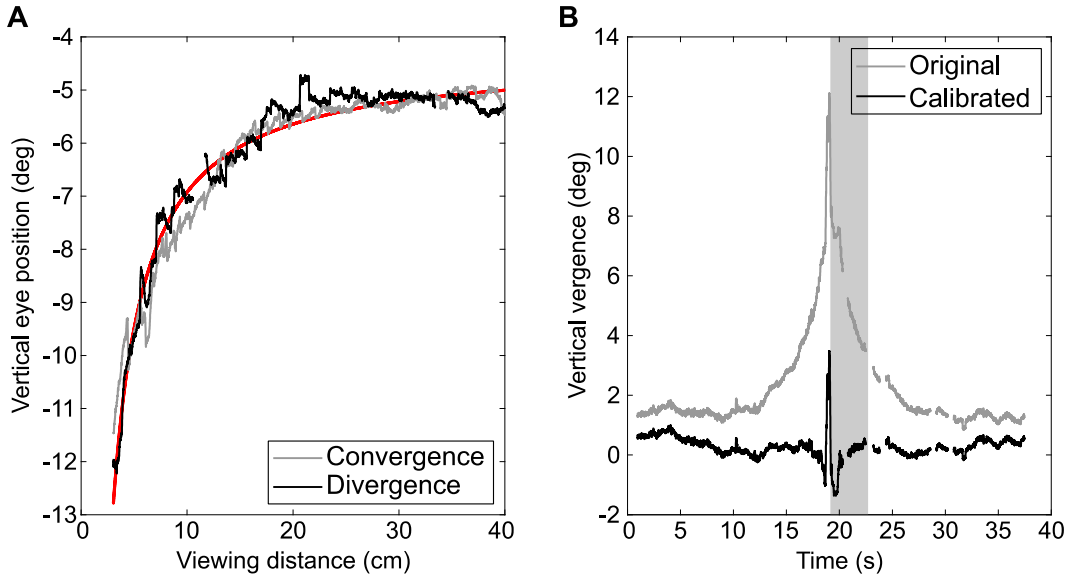


Figure 5.25. (A) Vertical right eye position of Subject 10 during convergence (gray line) and divergence (black line) periods of dynamic calibration as a function of the viewing distance. The red line corresponds to the fitted function according to Eq. (5.11) ( $a=-0.44$  cm,  $b=-4.4^\circ$ ,  $R^2=0.96$ ). (B) Vertical vergence exhibited by the same subject during the first repetition of the NPC test before (gray line) and after (black line) correction of the vertical traces. The shaded area corresponds to the period when the subject reported diplopia. The large spike in the two vertical vergence traces before time = 20 s might be an artifact associated with the loss of fusion.

The vertical position of each eye during the NPC test was corrected separately by subtracting the model fitted to the dynamic calibration data in Eq. (5.11) from the raw measured position. As a result, the abnormal increase in vertical vergence shown at close distance due to relative misalignment in the height of the two eyes and the target was reduced substantially (Figure 5.25B).

### 5.3.5.2. Modification of the Engbert-Kliegl (E-K) algorithm

Engbert & Kliegl (2003b) proposed a saccade detection algorithm based on a velocity threshold adapted to the level of noise in the data. Specifically, the algorithm uses a multiple of the standard deviation of the velocity distribution as the saccade-detection threshold. This threshold is computed separately for horizontal and vertical eye-movement components. Saccades are identified as “outliers” in velocity space, i.e., samples with a velocity that lies outside an ellipse whose horizontal and vertical radii are the velocity thresholds. Because the mean eye velocity during fixation is assumed to be effectively zero, the ellipse is centered at zero horizontal and vertical velocity.

However, the mean horizontal velocity during the NPC test cannot be assumed to be zero, as the fixation target moved forward and backward at a constant linear velocity. The horizontal angular velocity of the eyes actually increased at close target distances. Therefore, two sliding time windows of 5 s and 48 ms were used to divide the time series and apply the detection algorithm. The velocity threshold was computed during each 5-second period similarly than in the original E-K algorithm. The center of the ellipses used to identify the saccades in velocity space was computed as the median eye velocity over the shorter (48-ms) time window (Figure 5.26). The lengths of the sliding time windows were determined as the ones which detected saccades that clustered optimally around the main sequence.

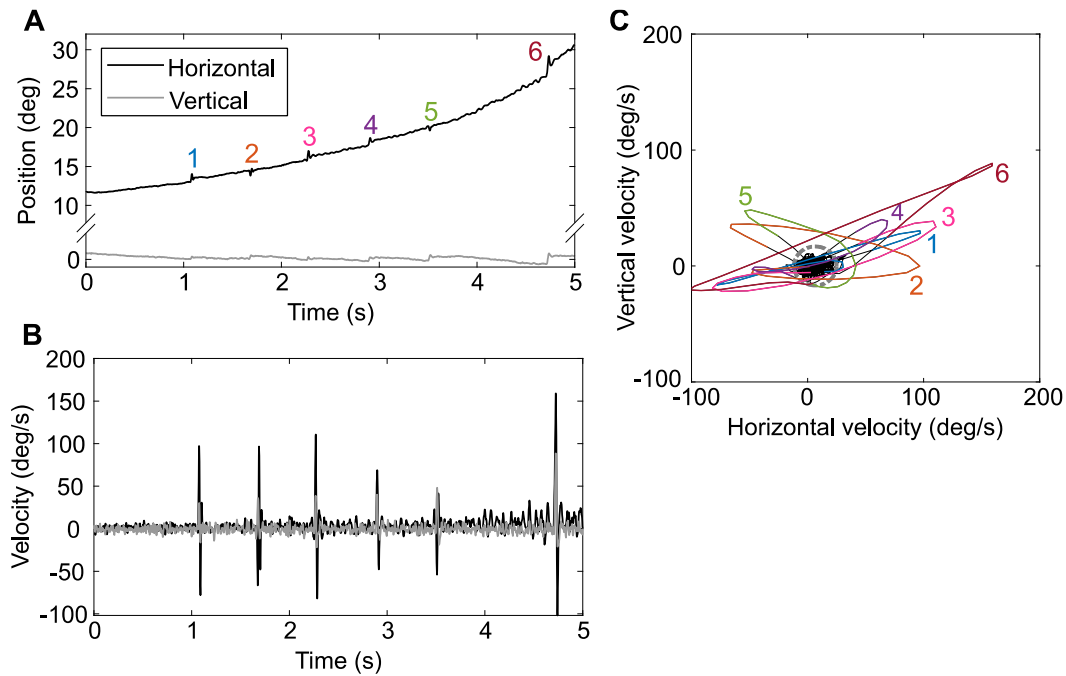


Figure 5.26. (A) Horizontal (black) and vertical (gray) eye position of Subject 5 during a 5-second period of the NPC test. During this period the observer exhibited six saccades, which are identified with numbers. (B) Horizontal (black) and vertical (gray) components of eye velocity during the same period of the NPC test. (C) Plot of the trajectory in velocity space. The ellipse used as the criterion to identify saccades is represented in gray. Its horizontal and vertical center is at 6.60 and 0 %/s, respectively. The six saccades showed considerably higher velocities than the median velocity during the 5-second period.

### 5.3.6. Appendix B

In this section, the results with the modified E-K algorithm are shown.

A total of 1639 saccades were detected by the modified version of the velocity-threshold-based algorithm. The number of saccades exhibited by each subject is shown in Table 5.5. For all

observers except two, more saccades were detected with the E-K algorithm than with the clustering method (see Table 5.3).

Table 5.5. Number of saccades exhibited during convergence and divergence movements by each subject.

<b>Subject</b>	<b>Number of saccades</b>
1	34
2	172
3	141
4	120
5	176
6	151
7	118
8	196
9	128
10	320
11	83

The median saccade amplitude was  $0.42^\circ$  (range from  $0.04^\circ$  to  $8.90^\circ$ ). Saccades during convergence and divergence followed the main sequence ( $r_s=0.97$ ,  $p<0.001$ ) as shown in Figure 5.27A. Most of the saccades (86%) had an amplitude smaller than  $1^\circ$ . The amplitude distribution of saccades differed significantly between the two detection algorithms according to the Mann-Whitney test ( $p<0.001$ ) (Figure 5.27C).

A significant positive correlation between saccade amplitude and vergence demand was found ( $r_s=0.55$ ,  $p<0.001$ ) (Figure 5.27B). This association was showed by all individual subjects, with correlation coefficients ranging from 0.32 to 0.86 (all values of  $p\leq 0.001$ ). Similarly as with the clustering method, there was no significant influence of the direction of the vergence movement on the amplitude of saccades, according to the Mann-Whitney test ( $p=0.212$ ).

The distribution of saccade directions is shown in Figure 5.28. The directions of saccades differed significantly from a uniform distribution as shown by Watson's test for circular uniformity ( $p<0.01$ ). Similar to the saccades detected by the clustering algorithm, a higher prevalence of horizontal than vertical saccades was found, with more upwards than downwards vertical components. The median direction of saccades during convergence ( $78.50^\circ$ ) and divergence ( $72.54^\circ$ ) did not differ significantly ( $p=0.387$ ).

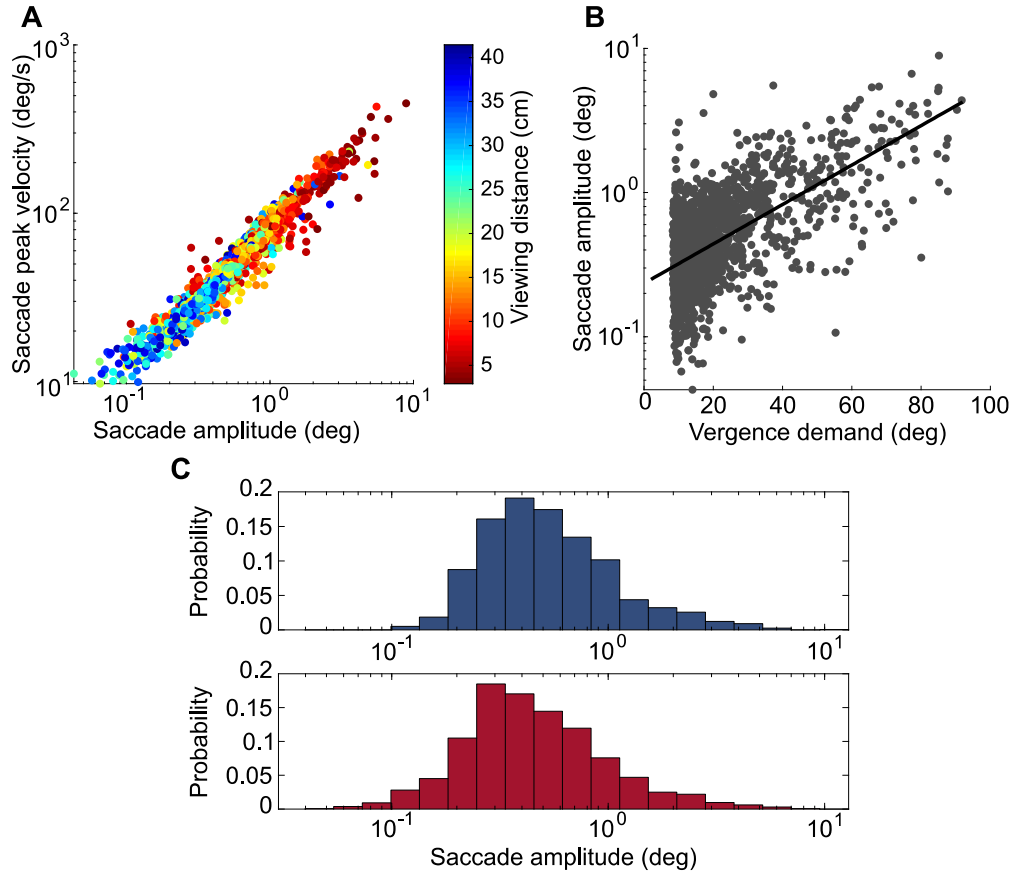


Figure 5.27. (A) Main sequence on log-log scale as a function of the viewing distance. The color code exposes the tendency for greater saccade amplitude and peak velocity at shorter viewing distances. (B) Saccade amplitude as a function of vergence demand. The black line corresponds to the least-squares regression fit, which is shown only for illustrative purposes ( $R^2=0.40$ ). (C) Amplitude distribution of saccades detected with the clustering method (top) and with the modified version of the E-K algorithm (bottom).

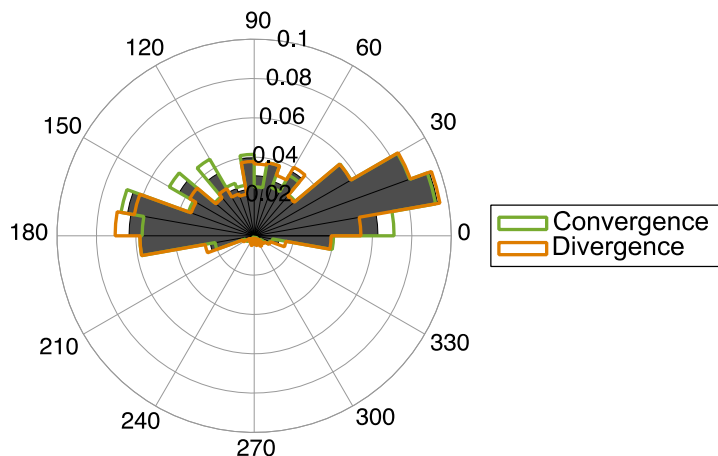


Figure 5.28. Polar histogram of the saccade directions (gray sectors). The direction of saccades during convergence and divergence periods is shown with green and orange lines, respectively. Zero and 90 degrees indicate rightward and upward saccades, respectively.

Both horizontal (directions of  $\pm 22.5^\circ$  from horizontal) and vertical (directions of  $\pm 22.5^\circ$  from vertical) saccades exhibited the same trend to increase in amplitude with vergence demand (horizontal:  $r_s=0.59, p<0.001$ ; vertical:  $r_s=0.49, p<0.001$ ). All individual subjects except one showed a significant positive correlation between the amplitude of horizontal saccades and vergence demand with correlation coefficients ranging from 0.42 to 0.86 (all values of  $p\leq 0.04$ ). Higher inter-subject variability was found for vertical saccades. All participants except four showed a significant correlation between vertical saccade amplitude and vergence demand, with correlation coefficients ranging from 0.53 to 0.91 ( $p\leq 0.03$ ).

The difference in saccade direction between the two eyes is shown in Figure 5.29A. In general, the number of directionally non-conjugate saccades is similar to that detected by the clustering algorithm. In 230 saccades (14.0%), the direction of the two eyes was found to differ more than  $\pm 45^\circ$ , and in 124 (7.6%) the difference was higher than  $\pm 90^\circ$ . Overall, the occurrence of directionally non-conjugate saccades was similar during the periods of convergence and divergence. However, the distribution of the directional differences was significantly different as a function of the direction of vergence according to the Mann-Whitney test ( $p<0.001$ ) (Figure 5.29B). The directions of the right and left eyes during the directionally non-conjugate saccades are represented as a function of the direction of the concurrent vergence movement in Figure 5.30.

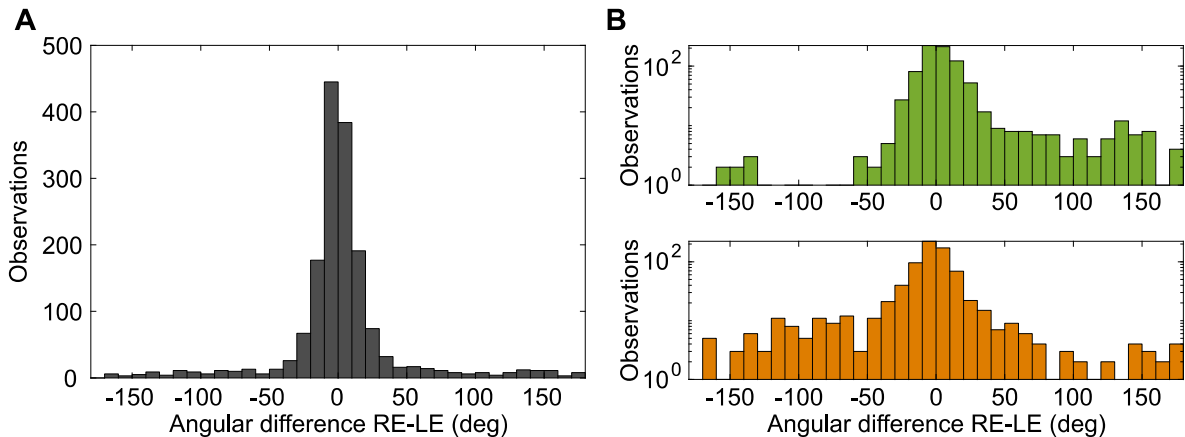


Figure 5.29. (A) Histogram of the difference in saccade direction between the two eyes (direction of the right eye minus direction of the left eye) in degrees. An angular difference of  $0^\circ$  means that the two eyes moved in the same direction, whereas  $\pm 180^\circ$  means that the saccade had opposite directions in the two eyes. (B) Histograms of the between-eye differences in saccade direction during convergence (top) and divergence (bottom). Note that the vertical axes are scaled logarithmically in panel (B) to emphasize the numbers of saccades that differed in direction in the two eyes.

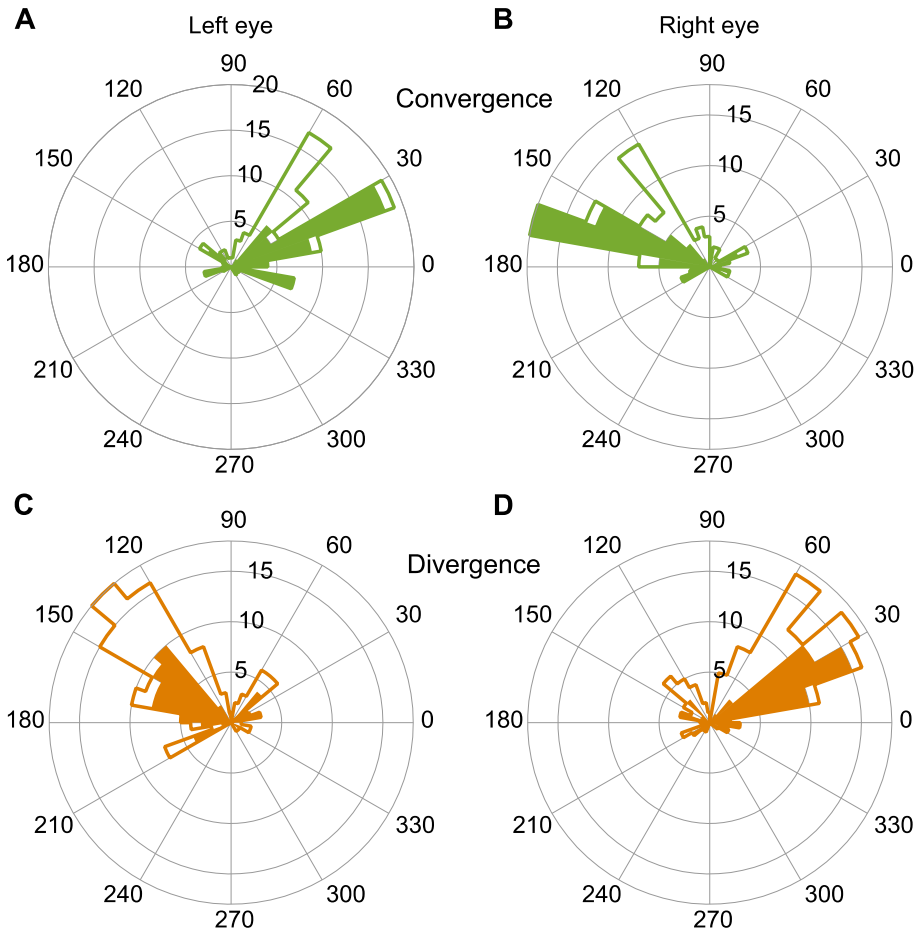


Figure 5.30. Distribution of the right (panels (B) and (D)) and left (panels (A) and (C)) eyes directions for the directionally non-conjugate saccades as a function of the direction of the concurrent vergence movement (convergence: panels (A) and (B); divergence: panels (C) and (D)). The unfilled distributions limited by the solid lines are the directions of saccades which differed in the two eyes by more than  $\pm 45^\circ$ , while the areas shaded in color represent the directions of saccades which differed in the two eyes by more than  $\pm 90^\circ$ .

The median (IQR) of the directional differences between saccades was similar for horizontal, vertical and oblique saccades:  $0.82^\circ$  ( $13.07^\circ$ ) for horizontal saccades,  $-3.96^\circ$  ( $92.48^\circ$ ) for vertical saccades, and  $-1.07^\circ$  ( $23.34^\circ$ ) for oblique saccades. However, the distribution of the directional differences between the eyes differed significantly as a function of the direction of the saccades as shown by the Kruskal-Wallis test ( $p=0.006$ ). Specifically, the distribution of the directional differences between the eyes of horizontal saccades differed significantly from that of oblique saccades ( $p=0.015$ ). The difference between the distributions of horizontal and vertical saccades also approached significance ( $p=0.056$ ). No significant differences were found between vertical and oblique saccades ( $p=1.000$ ).

The saccade rate averaged across subjects and the three repetitions was  $1.41 \pm 0.69$  Hz. Overall, the mean saccade rate during convergence ( $1.45 \pm 0.66$  Hz) and divergence ( $1.37 \pm 0.74$  Hz) did not differ significantly [ $t(10)=1.13 p=0.287$ ] (Figure 5.31). The evolution of saccade rate over time was computed by using a moving time window of 1 s. As stated in section 5.3.3, variations in the saccade rate as a function of the vergence demand were rather idiosyncratic. On average, the variation of saccade rate followed a similar behavior to the saccades detected with the clustering algorithm. Averaged across all subjects, the saccade rate decreased to around 0.5 Hz at the closest target distance (Figure 5.32).

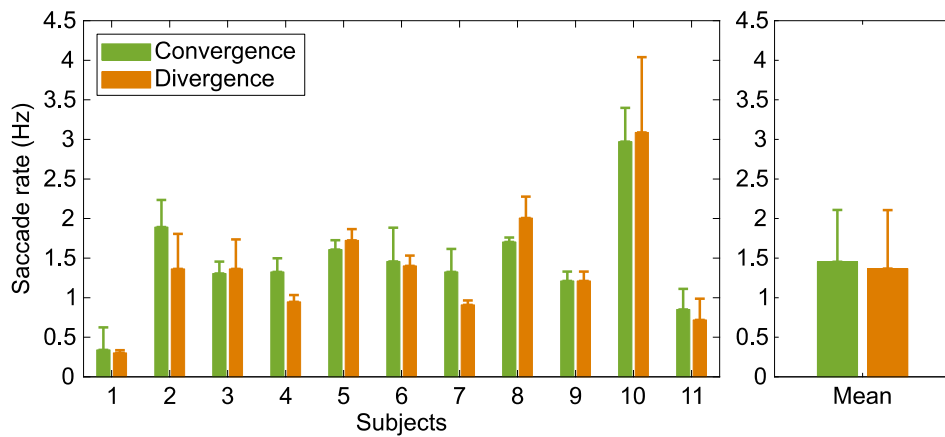


Figure 5.31. Saccade rate of each subject averaged across the three repetitions as a function of the direction of the concurrent vergence movement. The bars in the right subplot represent the mean saccade rate of all subjects. Error bars correspond to  $\pm 1$  SD.

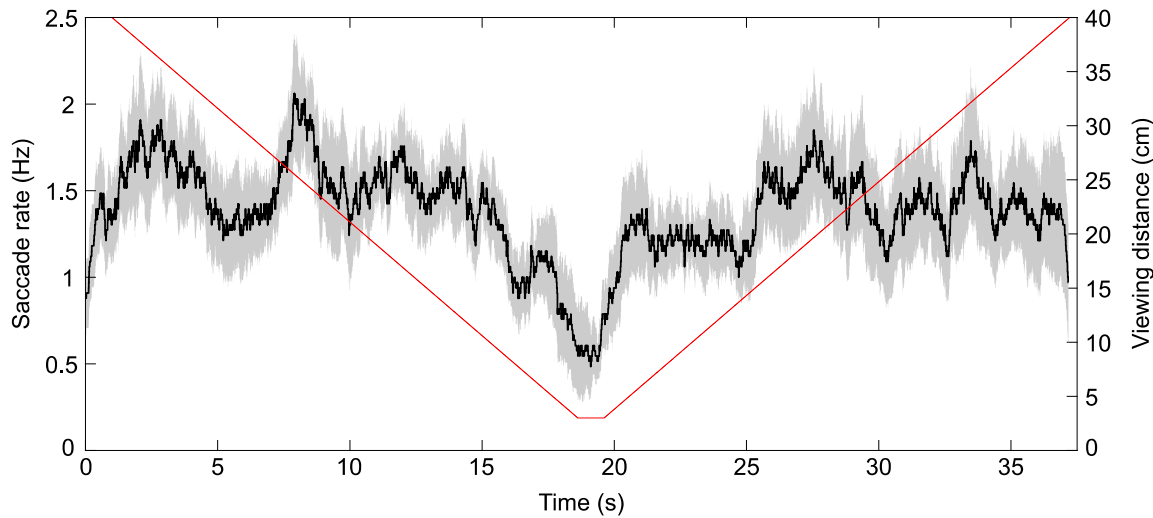


Figure 5.32. Saccade rate over time averaged across subjects and the three repetitions (black line). The shaded area corresponds to  $\pm 1$  standard error of the mean (SEM). The right axis and the red line represent the target distance.

Overall, the number of saccades that corrected a horizontal vergence error (disparity) exceeded the number of error-producing saccades. However, this difference was at the limit of significance [ $t(10)=2.19, p=0.053$ ]. All subjects except three made more disparity-correcting saccades than disparity-inducing saccades (Table 5.6). Considering the horizontal fixation position error of each eye separately, for most subjects saccades either tended to move one eye closer to the target and the other eye either farther from the target, or produced no vergence change. The number of saccades for each subject in which the right and left eyes moved closer to the target is shown in Table 5.6. For all subjects except Subject 1 and the two subjects for whom eye dominance could not be established (Subjects 8 and 11), the eye with more corrective saccades corresponded to the dominant eye (see the numbers in bold in Table 5.6).

Table 5.6. Number of saccades that corrected or produced a horizontal disparity error; number of saccades that brought the right eye (RE) or the left eye (LE) closer to the target; and the dominant eye of each subject.

Subject	Disparity correcting saccades	Disparity inducing saccades	Saccades correcting fixation position	Saccades correcting fixation position	Dominant eye
1	19	15	14	19	RE
2	86	86	83	<b>87</b>	LE (1 <sup>st</sup> and 2 <sup>nd</sup> rep); RE (3 <sup>rd</sup> rep)
3	85	56	47	<b>103</b>	LE
4	53	67	<b>58</b>	31	RE
5	116	60	60	<b>68</b>	LE
6	108	43	<b>97</b>	60	RE
7	68	50	<b>65</b>	55	RE
8	85	111	79	107	-
9	80	48	59	<b>62</b>	LE
10	185	135	<b>180</b>	134	RE
11	42	41	32	52	-

Rep: repetition.

## 5.4. Study 4. Effects of stimulus' predictability on the vergence facility test: a preliminary study

**NOTE:** The following text in this section corresponds to the article in preparation for submission to *Investigative Ophthalmology & Visual Science*: Mestre, C., Gautier, J., & Pujol, J. Effects of stimulus' predictability on the vergence facility test: a preliminary study. [to be submitted]

### 5.4.1. Introduction

The assessment of fusional, or disparity, vergence is fundamental to evaluate binocular vision. Besides the amplitude of convergence and divergence movements, it is also important to measure vergence facility, especially in symptomatic subjects with compensated phoria and normal fusional vergence amplitude (Gall & Wick, 2003). The vergence facility test assesses the ability to make rapid repetitive vergence changes over an extended period of time (Scheiman & Wick, 2014). The test is generally performed by alternating flipper or loose prisms with powers of 3 prism diopters (PD) base-in (BI) and 12 PD base-out (BO) (Gall et al., 1998). BI prisms elicit divergence movements while BO prisms stimulate convergence movements. Subjects are asked to look at a close or distant fixation target and try to fuse it as fast as possible. They are required to report when they perceive single vision, and only then the prism is flipped from BI to BO state or vice versa. The vergence facility is typically measured as the number of cycles per minute (cpm) that the target can be fused while alternating BI and BO prisms (Scheiman & Wick, 2014). The expected value at near vision is 15 cpm (Gall et al., 1998).

Hence, the vergence facility test consists in a predictable vergence step task, as the same convergence and divergence demands are alternated over a relatively extended period of time, generally 1 minute. After few cycles, subjects can predict when the examiner will flip the prisms. To perform the task, subjects need to rapidly alternate their vergence state from 1.7° of divergence ( $1PD = 100 \tan \text{angle}$ ) to 6.8° of convergence from a baseline convergence of 8.6° if the test is performed at 40 cm (for 3 PD BI and 12 PD BO prisms, and an interpupillary distance of 6 cm). The baseline convergence is 0.6° if it is performed at 6 m. The required vergence movements are asymmetric.

Prediction is a property of the oculomotor system not only demonstrated for vergence movements (Rashbass & Westheimer, 1961), but also for saccades and smooth pursuit (Kowler et al., 2014; Kowler & Steinman, 1979). Rashbass & Westheimer (1961) were the first to demonstrate anticipated vergence movements, but only in response to predictable sinusoidal stimulus. Later,

Krishnan et al. (1973) found a reduced vergence latency in response to predictable vergence step stimulus. Several authors have analyzed the effects of predictable symmetrical vergence steps on the vergence system and concluded that: (1) most subjects showed anticipatory slow vergence drifts before the fast transient in response to predictable vergence steps (Alvarez et al., 2002; Kumar et al., 2002; Yuan et al., 2000); (2) vergence latency was shorter for stimulus predictable either in time, direction or magnitude (Alvarez et al., 2002; Krishnan et al., 1973; Kumar et al., 2002; Yuan et al., 2000); and (3) vergence movements in response to predictable stimulus had faster dynamics (Alvarez et al., 2002). In contrast, Yuan et al. (2000), in a model-based analysis, found that predictable vergence movements had lower peak velocity than movements in response to unpredictable vergence steps, and concluded that high-level processes might be involved in the vergence prediction.

Most of the previous studies analyzing the effect of stimulus' prediction on the properties of vergence movements elicited small magnitude vergence steps, e.g.  $4^\circ$  is a common step magnitude (Alvarez et al., 2002; Yuan et al., 2000); and did not analyze separately the effects of timing, step magnitude and direction randomizations on the same participants. Relatively small sample sizes are typically used in these studies, where subjects are composed of both expert and naïve observers.

The main goal of the present study is to analyze the effects of stimulus' predictability in magnitude, time, and those combined factors on the temporal characteristics of the vergence system. In the proposed setup, the magnitude of the elicited steps is comparable to the vergence demands used in the clinical vergence facility test. The subjects' previous experience with the test and their direction of phoria have been added to the analysis in order to understand the potential effects of these factors on the result of the clinical vergence facility test.

### **5.4.2. Methods**

#### *5.4.2.1. Subjects*

A total of 37 non-presbyopic subjects participated in the study (mean age  $\pm$  standard deviation (SD) of  $26.9 \pm 5.8$  years). All participants had 20/25 visual acuity or better in both eyes with their habitual refractive correction. During the experiment, 16 subjects wore spectacles and 5 subjects wore soft contact lenses. Spherical refractive errors ranged from  $-6.50$  D to  $+2.25$  D with astigmatism up to  $-2.75$  D. Participants' horizontal phoria ranged from 6 PD of esophoria to 11 PD of exophoria measured with a Maddox rod and the Bernell Muscle Imbalance Measure (MIM) card (Bernell Corp., Mishawaka, IN, USA). Eleven subjects were esophores and 26 were exophores. All participants had stereoacuity of 50 arc sec or better measured with the graded circle test of the Random Dot 2 Stereo Acuity Test with Lea SYMBOLS (Vision Assessment Corp., Elk Grove Village, IL, USA).

Participants were able to complete at least 13 cpm with 3 PD BI and 12 PD BO when testing the vergence facility at 40 cm.

The sample was divided into two separate groups according to the subjects' expertise in the vergence facility test. Seventeen subjects were naïve to this test and had never performed it before, while another group of 20 participants were familiar with the vergence facility test. The latter group consisted of optometrists and optometry students. All subjects of both groups were unaware of the purpose of the study. A summary of each subject's characteristics is shown in Table 5.7.

The study was approved by the Ethics Committee of Hospital Mutua de Terrassa (Terrassa, Spain) and followed the tenets of the Declaration of Helsinki. All subjects gave informed written consent prior to participation in the study.

Table 5.7. Age, expertise, refractive error of right eye (RE) and left eye (LE), phoria at 40 cm, vergence facility (VF) performed clinically at 40 cm, and stereopsis of the 37 participants. N: naïve; E: expert; negative values of phoria correspond to exophoria and positive values correspond to esophoria.

<b>Subject</b>	<b>Age</b> <b>(years)</b>	<b>Expertise</b>	<b>Refraction RE</b> <b>(D)</b>	<b>Refraction LE</b> <b>(D)</b>	<b>Phoria</b> <b>(PD)</b>	<b>VF</b> <b>(cpm)</b>	<b>Stereopsis</b> <b>(arc sec)</b>
1	25	N	-2.75 -0.75 5°	-2.50 -0.25 159°	-10	20	12.5
2	32	E	-3.00 -0.50 180°	-2.75 -0.75 180°	-7	17	16
3	33	N	-4.25 -0.25 144°	-4.25 -0.25 66°	-8	23	23
4	38	E	+0.50	+0.50	+1	18	50
5	24	N	-2.50	-3.25	-1	18	12.5
6	22	E	+1.00 -0.50 5°	+0.75 -0.50 157°	-1	13	23
7	25	E	+1.25 -0.75 109°	+1.75	-1	18	16
8	21	E	-1.75 -2.75 12°	+0.25 -2.25 169°	+3	16	20
9	26	N	+1.75 -1.25 3°	+2.25 -0.75 13°	-4	16	20
10	21	E	-2.00 -1.25 176°	-0.75 -2.75 180°	-7	21	12.5
11	22	E	-0.50	0	-1	14	20
12	37	N	+0.75 -0.50 20°	+0.50 -0.50 171°	-9	25	12.5
13	22	N	+0.75 -0.50 78°	+1.25 -0.75 60°	+2	22	23
14	28	N	-0.50 -1.00 103°	-0.75 -0.25 120°	+3	22	16
15	38	N	+1.25 -1.25 1°	+0.50 -1.00 138°	-4	25	12.5
16	28	E	-0.75	-0.50	-1	18	20
17	28	E	-0.50	0	+6	19	16
18	26	N	-4.25 -2.25 5°	-3.25 -2.25 6°	-4	19	16

Table 5.7. (continued).

<b>Subject</b>	<b>Age</b>	<b>Expertise</b>	<b>Refraction RE</b>	<b>Refraction LE</b>	<b>Phoria</b>	<b>VF</b>	<b>Stereopsis</b>
	(years)		(D)	(D)	(PD)	(cpm)	(arc sec)
19	28	N	-0.75 -1.00 65°	-1.00 -0.50 64°	-2	14	40
20	28	N	-1.50 -0.50 75°	-1.75 -0.50 77°	-2	23	12.5
21	39	N	-4.75 -0.75 20°	-3.75 -0.50 100°	-7	19	32
22	28	E	0 -0.75 180°	+0.25 -0.75 6°	-2	18	40
23	26	E	+0.50 -0.75 100°	+0.50 -0.25 85°	+2	24	12.5
24	25	E	-2.00 -1.25 110°	-2.50	+2	30	12.5
25	21	E	-3.50 -0.75 83°	-2.75	+4	20	20
26	22	E	-1.25 -2.25 22°	-2.50 -1.50 169°	-1	20	20
27	21	E	+0.25 -0.25 116°	+0.50 -0.25 72°	+1	18	23
28	20	E	-1.25 -0.50 140°	-1.75 -0.25 35°	-4	14	20
29	27	N	-6.00	-6.00	-1	19	12.5
30	21	N	+0.50 -0.25 112°	+0.50 -0.25 62°	+1	19	12.5
31	36	N	0	+0.25 -0.25 56°	-1	18	23
32	20	E	-6.50	-6.50	-11	25	20
33	27	E	-3.00	-2.75	-6	20	16
34	38	N	+1.50 -1.50 7°	+1.25 -1.75 169°	-3	19	12.5
35	22	E	-2.5 -1.50 100°	-1.75 -1.25 71°	-4	17	16
36	30	N	-1.25	-0.50	+4	23	12.5
37	21	E	-0.25	-0.25 -0.25 1°	-2	20	12.5

#### 5.4.2.2. Instrumentation and visual stimulus

The experimental setup consisted in an haploscope composed of two identical computer screens and two cold mirrors. These elements were arranged so that the optical distance between the screens and the patients' eyes was 40 cm. The accommodation plane was held constant at 2.50 D while symmetrical disparity vergence stimuli could be generated.

Eye movements were registered with an EyeLink 1000 Plus (SR Research Ltd., Ontario, Canada) at a sampling rate of 500 Hz. The EyeLink was positioned at a distance of 60 cm approximately from the chinrest. Eye movements could be registered through the cold mirrors thanks to their high transmittance at IR wavelengths.

A custom Matlab R2015a (MathWorks, Natick, MA, USA) program using the Psychophysics Toolbox extensions (Brainard, 1997; Kleiner et al., 2007; Pelli, 1997) controlled the stimuli presentation and data collection from the eye-tracker. The letter-column stimulus of the rotating near-point card NC-1 (Topcon Corp., Japan) was reproduced digitally and presented at each screen. The digitized stimulus consisted in a column of black letters with 20/50 visual acuity, approximately, on a white background of  $18 \times 17$  cm. The rest of the screen was set at plain mid-gray. The disparity vergence demand was stimulated by eliciting a change in the object rendered disparity along the horizontal axis. The program changed the stimuli position at each screen in a synchronous step-like fashion. The total vergence demand was divided symmetrically into the two eyes, e.g. a vergence demand of 6 PD was stimulated in each eye for a total demand of 12 PD. The experiment was performed in a dark room so that participants could only fixate and fuse on the stimuli presented on each screen.

#### *5.4.2.3. Experimental procedure*

Subjects were instructed to fuse the stimuli presented on each screen as fast as possible and press a key on the keyboard when they perceive them singly. They were informed that to achieve single vision they might need to cross their eyes. After positioning the participants on the chinrest, the position of the stimulus at each screen was adjusted with a real target located along the subjects' midline at a distance of 40 cm. After that, the built-in 9-point EyeLink calibration was performed for each eye separately. Subjects were asked to fixate on each of the 9 circles of  $1.86^\circ$  that appeared at different positions. The experimental procedure started immediately after the calibration process was completed.

Four experimental conditions were presented to each subject in strictly random order (Table 5.8). In condition 1, the stimulus sequence was completely predictable as the disparity vergence demand alternated with steps from 3 PD BI to 12 PD BO and vice versa every 2 seconds. In condition 2, the disparity vergence demand was identical as in condition 1 but the stimuli remained at the same position for a random duration of 2, 3 or 4 s. In condition 3, the vergence demand was randomly selected among seven possible disparities: 8 PD BI, 5 PD BI, 3 PD BI, 3 PD BO, 6 PD BO, 12 PD BO, 20 PD BO. The exposure time at each demand was fixed to 2 seconds. In condition 4, the sequence of both vergence demand and exposure time was random among the possibilities detailed in Table 5.8. The sequence of vergence demand in conditions 3 and 4 was actually pseudo-random, as a minimum of 3 transitions between 3 PD BI and 12 PD BO and vice versa were forced in order to have sufficient data in each condition for the analysis. Participants pressed a key on the keyboard to initiate each condition when they felt ready. Participants were instructed that they could stop the

experiment at any time if they felt uncomfortable or tired. Each experimental condition lasted 1 minute.

Table 5.8. Summary of the characteristics of the four experimental conditions.

<b>Condition</b>	<b>Randomness character</b>	<b>Vergence</b>	<b>Exposure</b>
		<b>demands (PD)</b>	<b>times (s)</b>
1	Not random	3 BI, 12 BO	2
2	Random exposure time; non-random vergence demand	3 BI, 12 BO	2, 3, 4
3	Random vergence demand; non-random exposure time	8 BI, 5 BI, 3 BI, 3 BO, 6 BO, 12 BO, 20 BO	2
4	Random exposure time; random vergence demand	8 BI, 5 BI, 3 BI, 3 BO, 6 BO, 12 BO, 20 BO	2, 3, 4

After each condition, participants were asked to give a score on a 5-point scale based on their own subjective perception of predictability. A level of 1 meant that the sequence of the stimuli was completely predictable, while a level of 5 meant that it was totally unpredictable or random. These subjective responses were recorded by the examiner.

The same procedure was repeated in a second session after a short break.

#### 5.4.2.4. Data analysis

Data were processed and analyzed offline using a custom Matlab R2018a program.

Periods of 200 ms before and after each blink were removed from the signal to avoid artifacts associated with the onset and offset of blinks. Since the EyeLink's intrinsic heuristic filter was switched off during the registration of eye position, the data were filtered offline with a third order Savitzky-Golay filter of length 11 samples (22 ms) (Savitzky & Golay, 1964) as in Nyström et al. (2017).

The vergence response was computed by subtracting the left and right eyes data, while version consisted of the average of both eyes. The vergence signal was filtered with a fourth order Butterworth low-pass filter with a cutoff frequency of 50 Hz as in Talasan et al. (2016). The vergence velocity was then calculated over a time window of 20 ms (10 samples).

At each vergence transition (change of stimulus' position), three variables were computed: latency, time to peak velocity, and response time (Figure 5.33). *Latency* was defined as the time between the onset of the stimulus at a specific vergence demand and the start of the vergence movement. This was determined as the time when the vergence velocity exceeded 5 °/s. This criterion is standard and commonly used by other authors (Coubard & Kapoula, 2008; Kapoula et al., 2016; Q. Yang et al., 2002). The *time to peak velocity* was defined as the time between the onset of the stimulus at a specific vergence demand and the vergence peak velocity. This timing metric was also used in previous studies as it is an easily identifiable point in time less ambiguous than the onset of the vergence movement (Alvarez et al., 2002; Yuan et al., 2000). The *response time* was calculated as the time between the onset of the stimulus at a specific vergence demand and the moment when the participants pressed a key on the keyboard to report single vision.

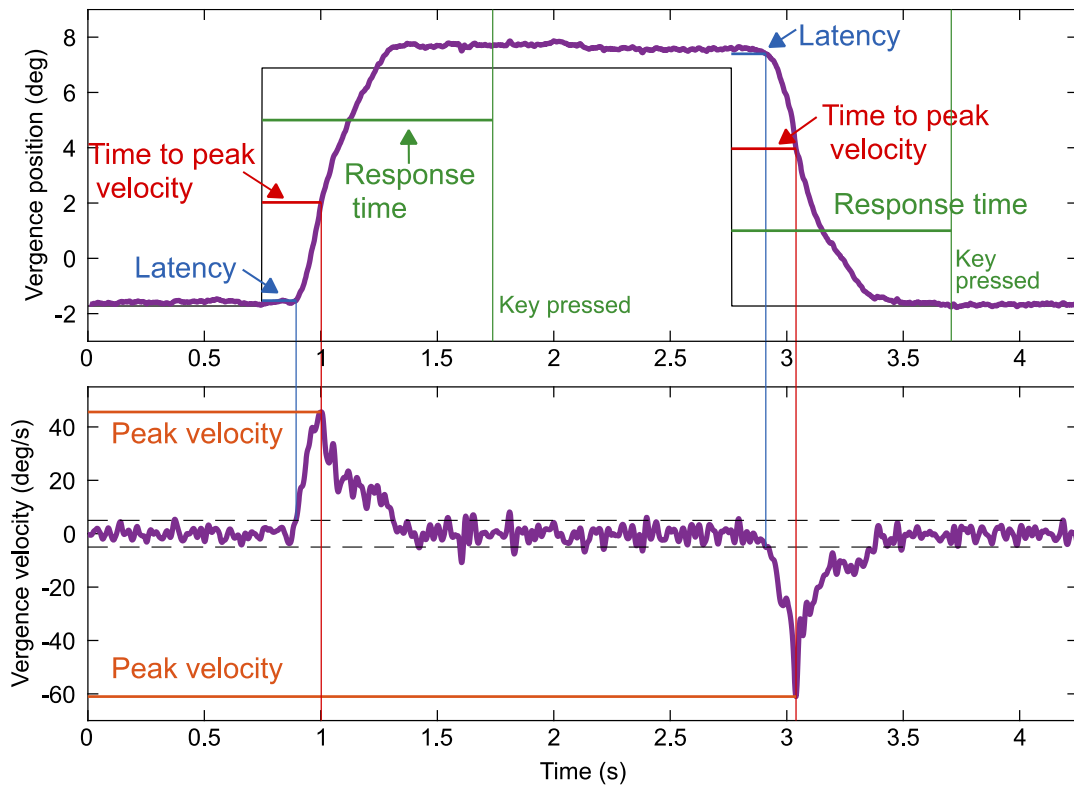


Figure 5.33. Example of the data analysis in a convergent and a divergent transition. The black square wave function in the upper plot represents the vergence demand. The two vertical green lines represent the moments when the patient pressed the key to report single vision. The two horizontal dashed lines in the lower plot represent the velocity thresholds used to determine the onset of convergence and divergence movements, respectively. Positive vergence positions and velocity correspond to convergence and negative vergence positions and velocity correspond to divergence.

All data and the placement of the time markers by the algorithm were verified visually. Responses in which a blink occurred during the transient portion of the movement were omitted from the analysis. In agreement with previous studies, almost all vergence responses were accompanied by saccades (Collewijn et al., 1995; Kumar et al., 2002). During visual inspection, the versional component of the responses was also analyzed. The transitions were manually classified based on the presence or absence of saccadic movements and the moment when they occurred: before the onset of the vergence movement, between the onset of vergence and the vergence peak velocity, at the same moment as vergence peak velocity ( $\pm 2$  ms), or after vergence peak velocity. The most prevalent condition found in our data consisted in saccades occurring when vergence velocity was maximum. Vergence transitions accompanied by “intrusive” saccadic movements at the initial portion of the response before the vergence peak velocity were omitted from the analysis.

Since the dynamics and temporal characteristics of vergence movements are affected by the magnitude and the initial vergence demand (Alvarez, Semmlow, et al., 2005; Maxwell et al., 2010), only transitions from 3 PD BI to 12 PD BO and from 12 PD BO to 3 PD BI were included in the analysis. These particular transitions were chosen because they are typically used in the vergence facility test performed in clinics (Gall et al., 1998). Data from the two sessions were pooled together and used to compute the mean latency, time to peak velocity, and response time in each experimental condition.

Statistical analysis was performed using SPSS Statistics 24 (IBM Corp., Armonk, NY, USA). The significance level was set at 0.05.

The three outcome variables were analyzed using a mixed ANOVA with two within-subjects' factors and two between-subjects' factors. The two within-subjects' factors were: randomness condition {1, 2, 3 or 4} (see Table 5.8), and vergence direction {convergence or divergence}. The two between-subjects' factors were: expertise {naïve or expert}, and phoria direction measured clinically beforehand {esophoria or exophoria}.

The scores of the perceived predictability attributed by participants to each condition were first averaged across sessions. Then, they were analyzed using the Friedman test. The Wilcoxon signed-rank test was used to determine which pairwise comparisons were statistically significant. The significance level for the post-hoc test was set at 0.008 ( $0.05/6=0.008$ ) according to the Bonferroni correction.

### 5.4.3. Results

The naïve and expert groups did not differ in refractive error (spherical equivalent), magnitude of phoria, stereopsis, nor clinically measured vergence facility, as shown by the independent t test ( $p>0.05$ ). However, expert subjects ( $24.5 \pm 4.7$  years) were significantly younger than naïve participants ( $29.8 \pm 5.9$  years) ( $p=0.005$ ).

The results of the mixed ANOVA for the vergence latency, the time to peak velocity and the response time are summarized in Table 5.9.

Table 5.9.  $p$ -values obtained with the mixed ANOVA with two within-subjects' factors (Randomness condition and Vergence direction) and two between-subjects' factors (Expertise and Phoria direction). \*Statistically significant.

Factor	Latency	Time to peak velocity	Response time
<b>Randomness condition</b>	<b>0.003*</b>	<b>0.010*</b>	<b>0.011*</b>
<b>Vergence direction</b>	0.973	0.837	<0.001*
<b>Expertise</b>	0.487	<b>0.020*</b>	0.117
<b>Phoria direction</b>	0.672	<b>0.013*</b>	0.929
Randomness condition*Vergence direction	0.391	0.243	0.127
Randomness condition*Expertise	0.364	0.732	0.832
Randomness condition*Phoria direction	0.961	0.731	0.105
Randomness condition*Expertise*Phoria direction	0.535	0.537	0.654
Vergence direction*Expertise	0.549	0.459	0.717
<b>Vergence direction*Phoria direction</b>	<b>0.003*</b>	0.398	0.098
Vergence direction*Expertise*Phoria direction	0.515	0.656	0.409
Randomness condition*Vergence direction*Expertise	0.560	0.684	0.283
Randomness condition*Vergence direction*Phoria direction	0.815	0.920	0.709
Randomness condition*Vergence direction*Expert*Phoria direction	0.343	0.357	0.785

Vergence latency was affected by the stimulus predictability (Figure 5.34A). The Bonferroni post-hoc test showed significant differences in vergence latency between fixed or time-randomized stimuli presentation alternating 3 PD BI and 12 PD BO vergence demands (conditions 1 and 2) ( $p=0.002$ ), with a mean difference  $\pm$  SD of  $-9 \pm 15$  ms. Moreover, the interaction term *Vergence*

*direction\*Phoria direction* also showed statistically significant differences (Figure 5.34E). The Bonferroni post-hoc test showed that in exophores, the latency of convergent transitions ( $151 \pm 11$  ms) was significantly longer than in divergent transitions ( $142 \pm 17$  ms) ( $p=0.004$ ). Oppositely, in esophores, the latency of divergent transitions ( $150 \pm 9$  ms) was longer than in convergent transitions ( $138 \pm 12$  ms). However, the differences were at the limit of statistical significance ( $p=0.067$ ). In convergent transitions, the latency exhibited by exophores was significantly longer than that exhibited by esophores ( $p=0.003$ ). In divergent transitions, esophores exhibited longer latencies than exophores, although the differences were not statistically significant ( $p=0.187$ ). The main effects of the other factors shown in Figure 5.34 (panels from B to D) nor their interactions were not significant.

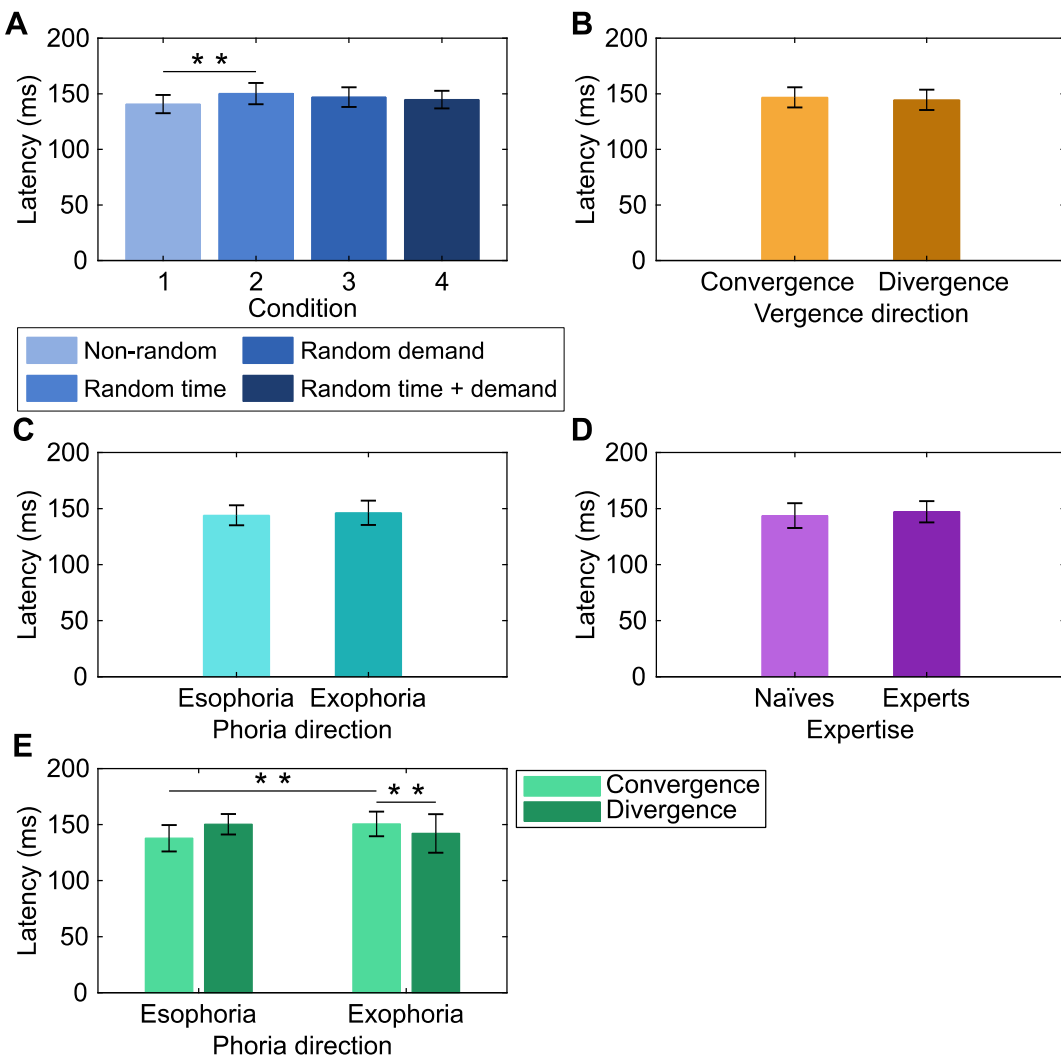


Figure 5.34. (A) Mean vergence latency at each experimental condition. (B) Mean vergence latency as a function of the vergence direction. (C) Mean vergence latency as a function of the direction of phoria. (D) Mean vergence latency as a function of the subjects' expertise. (E) Mean latency exhibited by esophoric and exophoric participants as a function of the direction of the vergence transitions. Error bars in panels (A) and (B) show  $\pm 1$  within-subjects' SD. Error bars in panels (C), (D) and (E) show  $\pm 1$  SD. \*\* Statistically significant ( $p<0.01$ ).

The time to peak velocity was also significantly different between the four experimental conditions (Figure 5.35A). The Bonferroni post-hoc test showed statistically significant differences in time to peak velocity between the non-random and time-randomized conditions (conditions 1 and 2) ( $p=0.045$ ), but also between the non-random and random in vergence demand conditions (conditions 1 and 3) ( $p=0.027$ ). The mean difference in time to peak velocity  $\pm$  SD between conditions 1 and 2 was  $-15 \pm 23$  ms, and  $-13 \pm 21$  ms between conditions 1 and 3. The time to peak velocity was also affected by the two between-subjects' factors of the model. Esophoric participants showed a significantly shorter time to peak velocity ( $274 \pm 21$  ms) than exophoric participants ( $295 \pm 27$  ms) ( $p=0.013$ ) (Figure 5.35C). The mean time to peak velocity exhibited by naïve subjects regardless of their phoria ( $279 \pm 27$  ms) was significantly shorter than that exhibited by experienced subjects ( $298 \pm 25$  ms) ( $p=0.020$ ) (Figure 5.35D). So far, while the latency was influenced by randomness and *Vergence direction\*Phoria direction* interaction, the time to peak velocity appeared to be more sensitive to be affected by phoria direction and subjects' expertise.

Response time differed significantly across the four experimental randomness conditions (Figure 5.36A). Similarly than for the time to peak velocity, the Bonferroni post-hoc test showed that the response time in the non-random condition (condition 1) was significantly shorter than in the random in time condition (condition 2) ( $p=0.014$ ) and in the random in vergence demand condition (condition 3) ( $p=0.029$ ). The mean difference  $\pm$  SD between conditions 1 and 2 was  $-44 \pm 109$  ms, and  $-47 \pm 105$  ms between conditions 1 and 3. Unlike latency and time to peak velocity, response time is the unique variable affected by vergence direction. The mean response time of convergent transitions ( $887 \pm 158$  ms) was significantly shorter than that of divergent transitions ( $1017 \pm 173$  ms) ( $p<0.001$ ) (Figure 5.36B). The mean response time of naïve subjects ( $916 \pm 134$  ms) followed the same trend as the time to peak velocity, and was shorter than that of expert subjects ( $981 \pm 135$  ms). However, the difference in response time was not significant (Figure 5.36D). Finally, the interaction *Vergence direction\*Phoria direction* for response time was near statistical significance. The response time in convergent transitions was significantly shorter than in divergent transitions both in esophores ( $p=0.002$ ) and exophores ( $p=0.039$ ) (Figure 5.36E). The differences were higher among esophores ( $854 \pm 190$  ms for convergence and  $1054 \pm 171$  ms for divergence) than among exophores ( $901 \pm 145$  ms for convergence and  $1001 \pm 175$  ms for divergence). In both convergent and divergent transitions, the response time exhibited by esophoric and exophoric participants did not differ significantly ( $p=0.372$  for convergence and  $p=0.314$  for divergence).

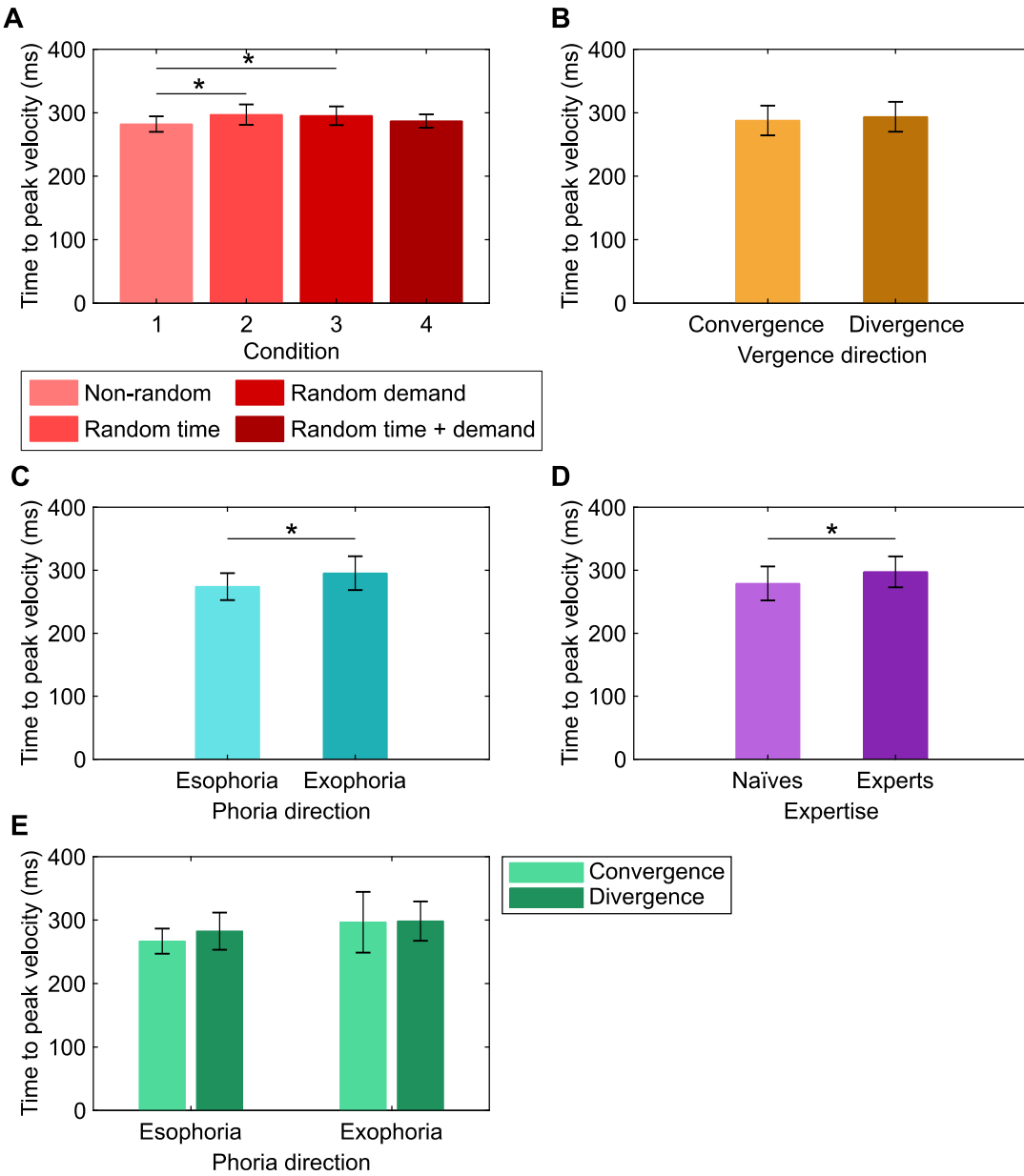


Figure 5.35. (A) Mean time to peak velocity at each experimental condition. (B) Mean time to peak velocity as a function of the vergence direction. (C) Mean time to peak velocity as a function of the direction of phoria. (D) Mean time to peak velocity as a function of the subjects' expertise. (E) Mean time to peak velocity exhibited by esophoric and exophoric participants as a function of the direction of the vergence transitions. Error bars in panels (A) and (B) show  $\pm 1$  within-subjects' SD. Error bars in panels (C), (D) and (E) show  $\pm 1$  SD. \* Statistically significant ( $p < 0.05$ ).

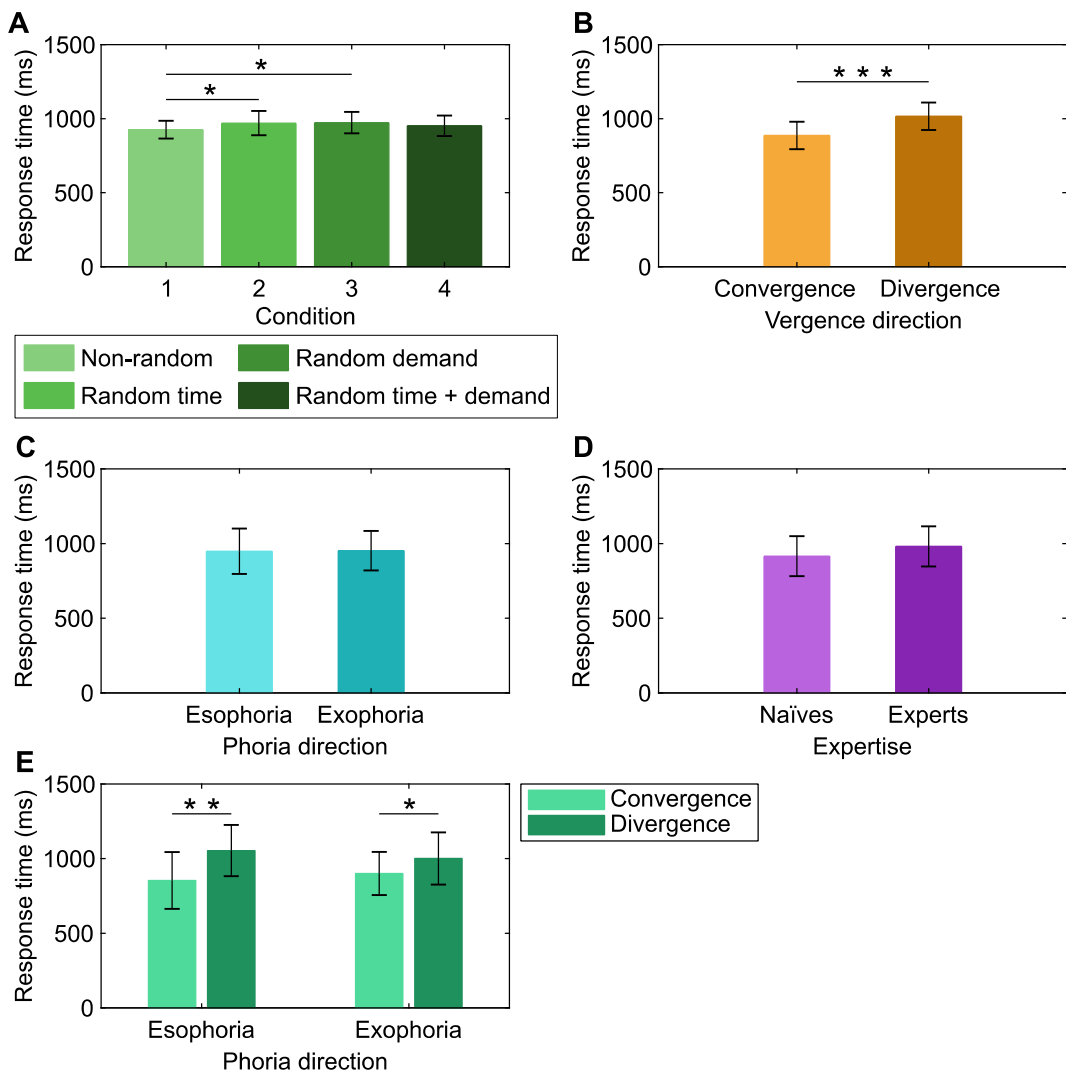


Figure 5.36. (A) Mean response time at each experimental condition. (B) Mean response time as a function of the vergence direction. (C) Mean response time as a function of the direction of phoria. (D) Mean response time as a function of the subjects' expertise. (E) Mean response time exhibited by esophoric and exophoric participants as a function of the direction of the vergence transitions. Error bars in panels (A) and (B) show  $\pm 1$  within-subjects' SD. Error bars in panels (C), (D) and (E) show  $\pm 1$  SD. \* Statistically significant ( $p<0.05$ ). \*\* ( $p<0.01$ ). \*\*\* ( $p<0.001$ ).

Regarding the subjective reports of predictability, the differences in the predictability scores given to each condition were statistically significant ( $\chi^2=60.12, p<0.001$ ). The Wilcoxon post-hoc test with Bonferroni correction showed statistically significant differences between the scores of all pairs of conditions (all  $p$ -values  $\leq 0.006$ ) except between conditions 3 and 4 ( $p=0.824$ ). Descriptive statistics of the predictability scores attributed to each randomness condition are shown in Figure 5.37.

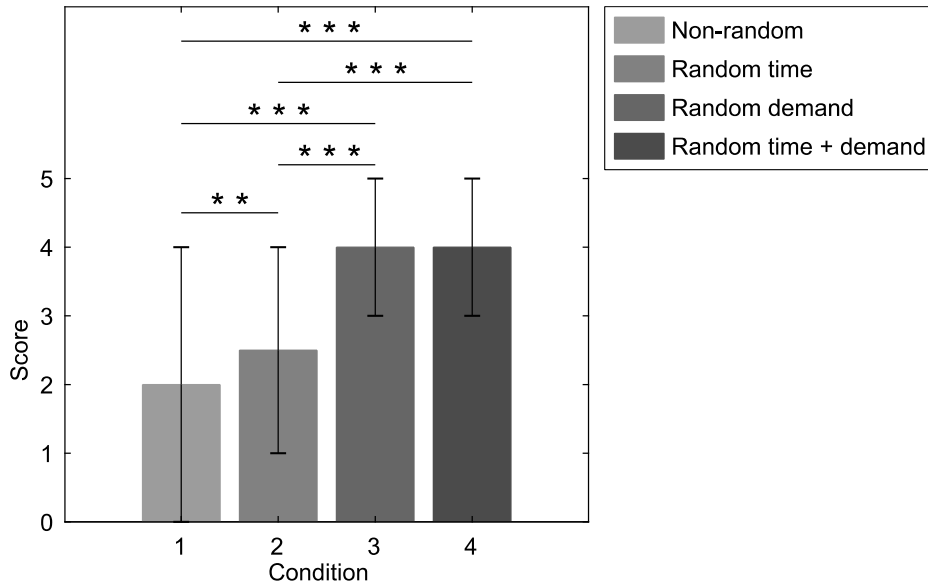


Figure 5.37. Median perceptual predictability scores given to each experimental condition. A score of 1 means a totally predictable condition while 5 means totally random. Error bars show  $\pm 1$  interquartile range. \*\* Statistically significant ( $p<0.01$ ). \*\*\* ( $p<0.001$ ).

Although in general participants were able to correctly report whether the stimulus was predictable, the mean latency, time to peak velocity and response time in each condition were not associated to the scores given by subjects (Figure 5.38). The time to peak velocity in condition 3 (random in vergence demand) showed the highest Pearson's correlation coefficient with the perceptual predictability score ( $r=-0.362$ ,  $p=0.028$ ). In fact, this variable and condition was the only one to show a significant correlation, which was unexpectedly negative.

#### 5.4.4. Discussion

Our results showed that the randomness of the vergence stimulus affects the vergence latency, time to peak velocity and the response time. As expected, the shorter latency, time to peak velocity and response time were observed for the totally predictable stimulus (condition 1) (Alvarez, Bhavsar, Semmlow, Bergen, & Pedrono, 2005; Kumar et al., 2002; Semmlow & Yuan, 2002). Some of these studies used other non-temporal metrics such as the increment in vergence peak velocity or magnitude of peak acceleration to highlight the effect of a predictable vergence step stimulus on the dynamics of vergence movements (Alvarez et al., 2002; Kumar et al., 2002). Two other effects associated with a change in vergence peak velocity due to repetitive step stimulus are fatigue and training. Vergence peak velocity has been found to decrease with visual fatigue (Yuan & Semmlow, 2000), and increase after vergence training (P. Munoz, Semmlow, Yuan, & Alvarez, 1999).

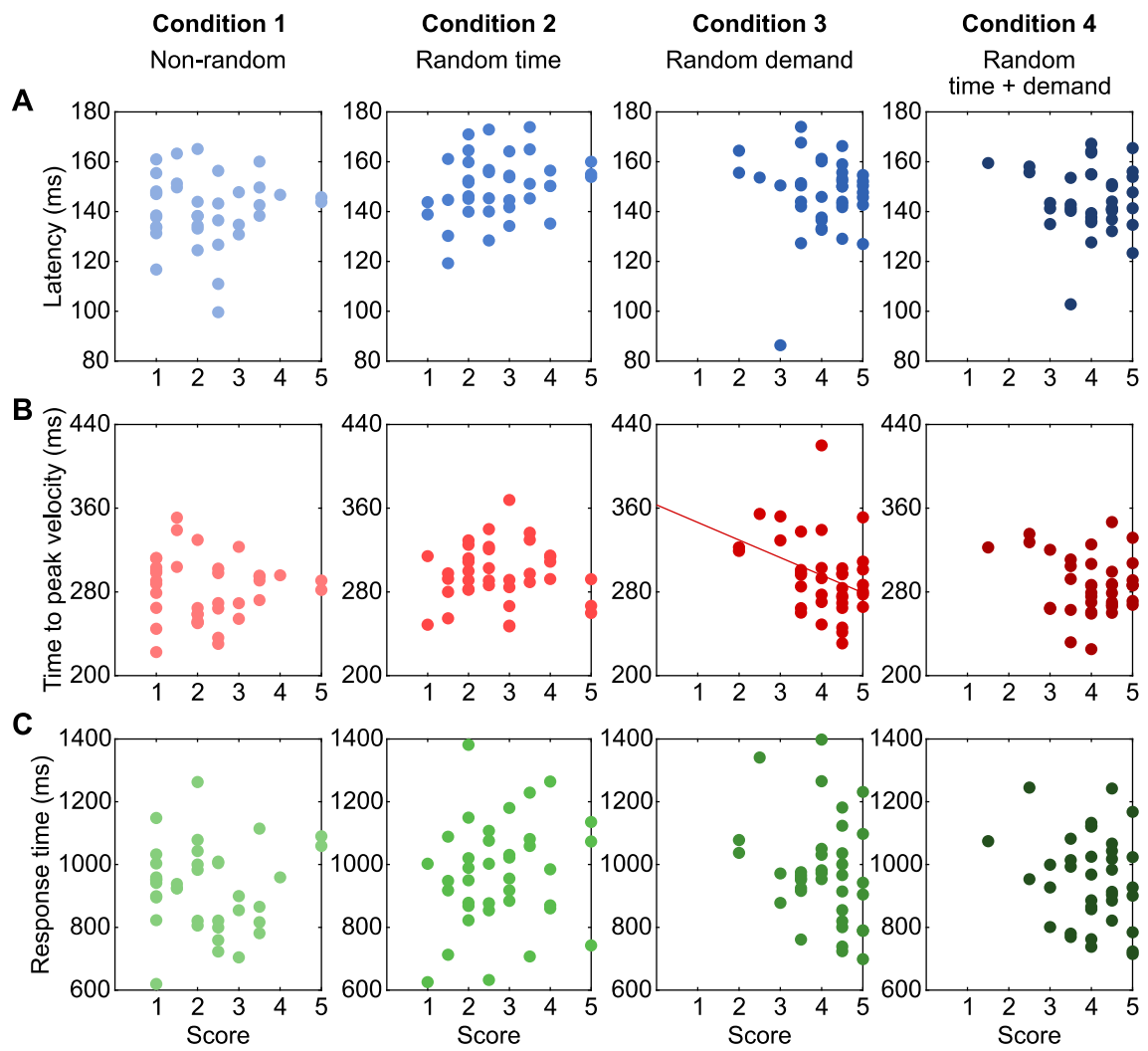


Figure 5.38. Latency (A), time to peak velocity (B), and response time (C) as a function of the perceptual predictability score attributed to each randomness condition. The only significant correlation was shown by the time to peak velocity in condition 3.

In general, subjects were able to distinguish the predictability of all conditions, except between conditions 3 and 4, which were perceived as the most random ones by most participants. However, the highest and significant differences were found between the non-random and time randomized conditions (conditions 1 and 2), and the non-random and random in vergence demand conditions (conditions 1 and 3) for the time to peak velocity and response time. Two possible explanations not mutually exclusive may justify this result. The first possibility is that randomizing the stimulus sequence in terms of time or magnitude of the vergence step may have the same impact on the vergence latency, time to peak velocity and response time. The second possibility is related to a methodological aspect. All transitions in conditions 1 and 2 were included in the analysis as all of

them were from 3 PD BI to 12 PD BO or vice versa. In contrast, vergence demand was randomized in conditions 3 and 4, and only those standard transitions between the same vergence demands as in conditions 1 and 2 were included in the analysis. The effect of randomizing the vergence sequence might not be reflected in the analyzed responses if the forced transitions between 3 PD BI and 12 PD BO appeared at the beginning of the condition.

In relation to the perceived predictability score, it is interesting to notice that no significant correlation was found between the observers' subjective report and the objective temporal metrics that described vergence responses in almost any condition (Figure 5.38).

Our initial hypothesis was that experienced participants would perform better (shorter latency, time to peak velocity and response time) than naïve subjects. However, naïve participants showed shorter latency, time to peak velocity and response time than expert participants. The differences between the two groups were significant only for the time to peak velocity variable. Besides the disparity, accommodation, and other sensory cues that drive vergence, non-sensory factors such as voluntary effort (Erkelens, Steinman, et al., 1989) or attention (Francis, Jiang, Owens, & Tyrrell, 2003) also control vergence responses. Horwood & Riddell (2010) concluded that these latter factors may enhance the vergence responses of experienced or expert subjects to a greater extent than in naïve subjects. However, our results on 37 subjects suggested the opposite behavior.

On the one hand, the instructions given to the participants before starting the experiment were the same for all subjects and equal emphasis was put on the fact that they needed to fuse the stimuli “as fast as possible” and on the “necessity to cross their eyes” to perform the task. However, it is not possible to assess to what extent observers made an effort to comply strictly with the instructions. In this regard, there is the possibility that naïve participants felt more pressure or urgency to follow exactly the instructions and do their utmost to perform the task.

On the other hand, recall that some of the analyzed vergence responses were accompanied by saccades that occurred at the same moment as the vergence peak velocity. It has been shown that saccades enhance vergence movements by increasing the vergence peak velocity and shortening the movement (Alvarez & Kim, 2013; Collewijn et al., 1995; Kim & Alvarez, 2012b; Ono et al., 1978; Saida & Ono, 1984). Our results showed a significant association between the prevalence of saccades during the vergence peak velocity and the subjects' experience according to the Chi-square test of association ( $\chi^2(1)=6.141, p=0.013$ ). A total of 73.6% of the transitions performed by naïve observers were accompanied by saccades, while saccades occurred in 69.8% of the transitions made by experts. The highest prevalence of saccades during the vergence peak velocity among naïve participants might

have contributed to the reduction of the time to peak velocity in this group of observers. The median (IQR) time to peak velocity of all vergence responses accompanied by a saccade during the vergence peak velocity (278 (56) ms) was significantly shorter than that from transitions free of saccades (284 (59) ms) ( $p=0.001$ ). The differences in the median response time of transitions with and without saccades during the vergence peak velocity were also significant ( $p<0.001$ ) but in opposite direction. The median (IQR) response time of vergence responses accompanied by saccades during the vergence peak velocity was 932 (318) ms, while that of responses without concurrent saccades was 858 (319) ms. The occurrence of saccades during the vergence peak velocity did not affect the latency of the response ( $p=0.956$ ).

Although best practice would be to have two age-matched groups, the significant difference in time to peak velocity between expert and naïve observers is probably better attributable to their usage of saccades during these large vergence movements rather than to their age.

An especially relevant result is the statistically significant interaction term of *Vergence direction\*Phoria direction* for vergence latency (Figure 5.34E). Several authors have analyzed the controversial differences in latency between convergence and divergence movements (Alvarez, Semmlow, et al., 2005; Alvarez et al., 2002; Hung et al., 1997; Krishnan et al., 1973; Q. Yang et al., 2002). However, to our best knowledge, there is no study identifying phoria direction as a potential factor influencing vergence latency. The longer latency in divergent transitions than in convergent transitions among esophoric subjects and the opposite behavior among exophoric subjects might be explained by the tendency towards poorer negative fusional vergence of esophores and poorer positive fusional vergence of exophores (Scheiman & Wick, 2014). Actually, examples of clinical signs used to diagnose binocular dysfunctions associated with abnormally high values of exophoria or esophoria include the reduced vergence facility with BO prism and the reduced vergence facility with BI prism, respectively (Scheiman & Wick, 2014). Our results suggest that these trends are manifested in the latency of vergence movements even among subjects with normal binocular function. Interestingly, Kim et al. (2010) did analyze the relationship between phoria and the ratio of convergence peak velocity to divergence peak velocity and found that esophores tend to have higher convergence peak velocity than divergence peak velocity. The opposite tendency was shown by exophores. Therefore, our results broaden their conclusion that phoria is a factor in the asymmetry between peak velocity of convergence and divergence (Kim et al., 2010), as phoria is also a factor in the asymmetry between convergence and divergence latency.

For the time to peak velocity, this effect may be hidden by the prevalence of saccades during the vergence peak velocity. The mean time to peak velocity of convergent and divergent transitions

are very similar (Figure 5.35B). However, the prevalence of saccades is significantly higher when diverging than converging ( $\chi^2(1)=713.07, p<0.001$ ). A 92.3% of the divergent transitions were accompanied by saccades during the vergence peak velocity, while saccades occurred in 51.3% of the convergent transitions. These percentages are similar if esophoric and exophoric subjects are considered separately. Previous studies also reported a higher prevalence of saccades during divergence than during convergence (Collewijn et al., 1995; Kenyon et al., 1980; Zee et al., 1992), although others found an idiosyncratic behavior (Erkelens, Steinman, et al., 1989; Zee et al., 1992).

Response time was significantly longer in divergent transitions than in convergent transitions (Figure 5.36B). This might be explained by the fact that divergence movements have been found to have slower dynamics than convergence (Alvarez, Semmlow, et al., 2005; Alvarez et al., 2002; Hung et al., 1997; Krishnan et al., 1973). Then, subjects may perform more saccades in an attempt to enhance the concurrent divergence movements, especially those who are naïve. A 97.1% of the divergent transitions performed by naïve participants were accompanied by saccades during the vergence peak velocity, while the prevalence of saccades in divergent transitions of expert participants was 88.4%. The prevalence of saccades in convergent transitions was 50.8% and 51.7% for naïve and expert observers, respectively.

To sum up, vergence movements to predictable stimulus have shorter latency, time to peak velocity and response time than when the stimulus is random either in time or vergence demand. The subjects' previous experience with this task seems to be a relevant factor modifying the vergence temporal characteristics. However, other aspects not strictly related with subjects' experience, such as the degree of attention or voluntary effort, may also play a role and mask some expected tendencies. The convergence and divergence latencies are influenced by the direction of the phoria. Finally, saccades that occurred frequently during the vergence step responses modify the time to peak velocity and response time.

The results of this study might have several implications for the clinical vergence facility test. The fact that the stimulus sequence of this test is absolutely predictable for the patient might overestimate the real ability to make fast vergence changes between targets placed at different distances in a real world. Moreover, the results of the clinical vergence facility test might be influenced by other factors such as the subjects' previous experience with the test, the degree of effort and attention, or their willingness to perform the required task. Finally, subjects could counteract a deficiency in the vergence system with intrusive saccades and pass apparently satisfactorily the vergence facility test. Further research is needed to quantify the impact of all these factors on the results of the clinical test.

## **6. Conclusions and future work**

By carrying out the four studies reported in the last four chapters the goals of the thesis have been achieved. The first study led to the development of methods to improve the spatial accuracy of an eye tracking system based on multiple corneal reflections. In the other three studies, new methodologies to evaluate objectively and automatically binocular vision have been proposed, and relevant features of eye movements in clinically interesting situations have been described. Specifically, the main conclusions of each study are outlined next.

**Study 1. Robust eye tracking based on multiple corneal reflections for clinical applications:**

1. Eye tracking accuracy with multiple corneal reflections was poorer vertically than horizontally. This might be explained by the difficulty in detecting the upper pupil region due to the interference of the eyelid and eyelashes.
2. Vertical accuracy was slightly better with a higher number of corneal reflections. However, the arrangement of the light sources appeared to be more relevant. Those configurations with the reflections in the lower region of the cornea showed higher accuracy in an on-axis camera system.
3. The normalization of the pupil-glint vectors led to the improvement of vertical accuracy. It also counteracted the tendency for increasing accuracy with the number of glints. Therefore, the proposed normalization method allowed to be independent from the need for more than two light sources provided that they are properly positioned.

**Study 2. An automated and objective cover test to measure heterophoria:**

1. The proposed automated and objective method to measure phoria was significantly more repeatable than the conventional clinical methods probably due to the minimization of the sources of variability. The remained variability might be explained by individual variations of subjects' vergence system.
2. The results of the prism cover test, the modified Thorington test, and the objective cover test with an eye-tracker are not interchangeable. The objective cover test showed significantly smaller phoria values than the two clinical methods. There was a tendency towards poorer agreement for larger phoria values in all three pairwise comparisons.
3. There was no significant effect of motor ocular dominance on the asymmetry of phoria between the two eyes. The found asymmetries might be partially explained by differences in

the accommodative state between the eyes due to potential monocular uncorrected refractive errors.

4. When eye-trackers become common tools in clinical settings, their use should be the new gold standard for the measurement of phoria, as it has been shown to overcome several limitations of the conventional clinical methods. Moreover, the possibility to register movements of the occluded eye provides new insights into the oculomotor dynamics during the cover test.

**Study 3. Characteristics of saccades during the near point of convergence test:**

1. A dynamic calibration procedure based on monocular fixation of an in-depth moving target was proposed to estimate eye position in 3D over a horizontal tracking range from 4.3° to 47.0°. An additional method to correct the vertical eye position error due to differences in the vertical position of the eyes in the head was proposed based on a geometric extrapolation function.
2. The characteristics of saccades occurring during the near point of convergence test changed as a function of vergence demand. The greater amplitude and lower saccadic rate at close distances might be explained by the more rapid change of vergence demand and the greater angular size of the fixation target at near than at far.
3. The high prevalence of upward saccades might reflect the tendency of some normal subjects to exhibit an upbeat vertical nystagmus whose amplitude also increased significantly with vergence demand.
4. A small percentage of saccades was not conjugated as they contained convergent or divergent components. In most cases, the disjunctive horizontal component was in the correct direction to reduce vergence errors. In most subjects, saccades also reduced the fixation position error of the dominant eye.

**Study 4. Effects of stimulus' predictability on the vergence facility test: a preliminary study:**

1. Vergence movements to predictable stimulus exhibited shorter latency, time to peak velocity and response time than when the stimulus was random either in time or vergence demand.

2. Convergence and divergence latencies have been found to be influenced by the direction of the phoria. Esophoric subjects exhibited longer vergence latencies in divergent transitions than in convergent movements. Exophoric subjects exhibited the opposite behavior.
3. Vergence responses that occurred concurrently with saccades exhibited shorter time to peak velocity but longer response time.
4. Other high-level factors such as attention or voluntary effort might affect the temporal characteristics of vergence responses.

While each of the four studies led to the achievement of their associated objectives, they also raised other questions to be addressed in future works.

A future work could be done as a continuation of the first study in the implementation of the corneal reflection and pupil tracking algorithms to measure eye position in real time and at higher frame rates up to 500 Hz. The current frequency of 30 Hz does not allow to measure rapid eye movements such as saccades. A prototype algorithm to track the pupil at 500 Hz implemented in CUDA (Nvidia) has demonstrated its potential for pupil tracking. Other algorithms could be also explored to further increase spatial tracking accuracy.

The second study could be replicated but by calibrating the eye-tracker monocularly for each observer. This way, objective fixation disparity could be probably assessed simultaneously with the measurement of phoria. The repeatability of the automated and objective cover test to measure vertical deviations and its agreement with clinical methods need also to be addressed in the future.

Regarding the third study, it would be interesting to include in the analysis subjects with a receded near point of convergence and compare the characteristics of their saccades with the ones obtained in this thesis for normal observers. Could some saccadic characteristics be a sign for the diagnosis of convergence insufficiency? It would be useful to repeat the measurements using targets with constant angular size to disentangle the effect of target's increasing size from the effect related to the effort of the vergence system. This could be done using an haploscopic setup combined with varifocal lenses to avoid the vergence-accommodation conflict. Finally, if a large dataset of ocular traces during the near point of convergence test is collected, machine learning techniques could potentially be applied to identify patterns of eye movements to predict the break and recovery points.

Future works will analyze the implications of the results of the fourth study for the clinical vergence facility test. This analysis should lead us to answer whether the vergence facility test

provides a valid assessment of the real ability to make fast vergence changes between targets placed at different distances in a real world.

More globally, other research lines related to this thesis are the analysis of ocular movements to diagnose or grade the severity of other visual dysfunctions such as amblyopia, or monitor objectively the effectiveness of visual training to treat binocular dysfunctions.

## **7. Dissemination of results**

A list of publications in which the results of this thesis have been disseminated is included in this section.

### **7.1. Journal publications**

**Mestre, C.**, Gautier, J., & Pujol, J. (2018). Robust eye tracking based on multiple corneal reflections for clinical applications. *Journal of Biomedical Optics*, 23(3), 035001.

**Mestre, C.**, Otero, C., Díaz-Doutón, F., Gautier, J., & Pujol, J. (2018). An automated and objective cover test to measure heterophoria. *PLoS ONE*, 13(11), e0206674.

### **7.2. Papers in submission**

**Mestre, C.**, Gautier, J., Bedell, H. E., Díaz-Doutón, F., & Pujol, J. Characteristics of saccades during the near point of convergence test. [submitted]

### **7.3. Oral presentations in conferences**

**Mestre, C.**, Otero, C., Gautier, J., Salvador, M., Pujol, J. Cover test might overestimate the phoria values. EAEO 2017. Barcelona, Spain.

**Mestre, C.**, Otero, C., Díaz-Doutón, F., Gautier, J., Pujol, J. Repeatability and agreement of an automated and objective cover test. ARVO 2018. Honolulu, USA.

**Mestre, C.**, Otero, C., Díaz-Doutón, F., Gautier, J., Pujol, J. An automated and objective cover test to measure phoria. EAEO 2018. Pula, Croatia.

**Mestre, C.**, Otero, C., Díaz-Doutón, F., Gautier, J., Pujol, J. Phoria measurement with an automated and objective cover test. RNO 2018. Castellón, Spain.

### **7.4. Poster presentations in conferences**

**Mestre, C.**, Gautier, J., Pujol, J. New methods for an eye-tracker based on multiple corneal reflections. ECVP 2016. Barcelona, Spain.

**Mestre, C.**, Otero, C., Gautier, J., Pujol, J. Does cover test overestimate systematically the phoria values? ARVO 2017. Baltimore, USA.

**Mestre, C.**, Gautier, J., Bedell, H. E., Díaz-Doutón, F., & Pujol, J. Characteristics of saccades when testing the near point of convergence. Accepted to be presented in ARVO 2019. Vancouver, Canada.

## 8. References

- Abadi, R. V., & Gowen, E. (2004). Characteristics of saccadic intrusions. *Vision Research*, 44(23), 2675–2690.
- Abadi, R. V., Scallan, C. J., & Clement, R. A. (2000). The characteristics of dynamic overshoots in square-wave jerks and in congenital and manifest latent nystagmus. *Vision Research*, 40(20), 2813–2829.
- Adler, P. M., Clegg, M., Viollier, A. J., & Woodhouse, J. M. (2007). Influence of target type and RAF rule on the measurement of near point of convergence. *Ophthalmic and Physiological Optics*, 27, 22–30.
- Agostinelli, C., & Lund, U. (2017). R package “circular”: Circular Statistics (version 0.4-93). Retrieved from <https://r-forge.r-project.org/projects/circular/>
- Alvarez, T. L., Bhavsar, M., Semmlow, J. L., Bergen, M. T., & Pedrono, C. (2005). Short-term predictive changes in the dynamics of disparity vergence eye movements. *Journal of Vision*, 5(7), 640–649.
- Alvarez, T. L., & Kim, E. H. (2013). Analysis of saccades and peak velocity to symmetrical convergence stimuli: binocularly normal controls compared to convergence insufficiency patients. *Investigative Ophthalmology & Visual Science*, 54(6), 4122–4135.
- Alvarez, T. L., Semmlow, J. L., & Pedrono, C. (2005). Divergence eye movements are dependent on initial stimulus position. *Vision Research*, 45(14), 1847–1855.
- Alvarez, T. L., Semmlow, J. L., Yuan, W., & Munoz, P. (1997). Dynamic analysis of disparity vergence eye movements: Beyond the main sequence. In *19th International Conference IEEE Engineering in Medicine and Biology Society* (pp. 2755–2759).
- Alvarez, T. L., Semmlow, J. L., Yuan, W., & Munoz, P. (2002). Comparison of disparity vergence system responses to predictable and non-predictable stimulations. *Current Psychology of Cognition*, 21(2–3), 243–261.
- Alvarez, T. L., Vicci, V. R., Alkan, Y., Kim, E. H., Gohel, S., Barrett, A. M., ... Biswal, B. B. (2010). Vision therapy in adults with convergence insufficiency: Clinical and functional magnetic resonance imaging measures. *Optometry and Vision Science*, 87(12), E985-1002.
- Anderson, H. A., Manny, R. E., Cotter, S. A., Mitchell, G. L., & Irani, J. A. (2010). Effect of examiner

- experience and technique on the alternate cover test. *Optometry and Vision Science*, 87(3), 168–175.
- Anderson, T. J., & MacAskill, M. R. (2013). Eye movements in patients with neurodegenerative disorders. *Nature Reviews. Neurology*, 9(2), 74–85.
- Antona, B., Barrio, A., Barra, F., Gonzalez, E., & Sanchez, I. (2008). Repeatability and agreement in the measurement of horizontal fusional vergences. *Ophthalmic & Physiological Optics*, 28(5), 475–491.
- Antona, B., Gonzalez, E., Barrio, A., Barra, F., Sanchez, I., & Cebrian, J. L. (2011). Strabometry precision: intra-examiner repeatability and agreement in measuring the magnitude of the angle of latent binocular ocular deviations (heterophorias or latent strabismus). *Binocular Vision and Strabology Quarterly, Simms-Romano*, 26(2), 91–104.
- Atchison, D., & Smith, G. (2000). The pupil. In *Optics of the Human Eye* (1st ed., pp. 21–29). Edinburgh: Butterworth-Heinemann.
- Bababekova, Y., Rosenfield, M., Hue, J. E., & Huang, R. R. (2011). Font size and viewing distance of handheld smart phones. *Optometry and Vision Science*, 88(7), 795–797.
- Babinsky, E., Sreenivasan, V., & Candy, T. R. (2015). Near heterophoria in early childhood. *Investigative Ophthalmology and Visual Science*, 56(2), 1406–1415.
- Bahill, A. T., Brockenbrough, A., & Troost, B. T. (1981). Variability and development of a normative data base for saccadic eye movements. *Investigative Ophthalmology & Visual Science*, 21(1), 116–125.
- Bahill, A. T., Clark, M. R., & Stark, L. (1975). The main sequence, a tool for studying human eye movements. *Mathematical Biosciences*, 24(3–4), 191–204.
- Bahill, A. T., & Stark, L. (1979). The trajectories of saccadic eye movements. *Scientific American*, 240(1), 108–117.
- Barnard, N. A. S., & Thomson, D. (1995). A quantitative analysis of eye movements characteristics during the cover test - a preliminary report. *Ophthalmic & Physiological Optics*, 15(5), 413–419.
- Becker, W. (1991). Saccades. In R. H. S. Carpenter (Ed.), *Vision and Visual Dysfunction, vol 8, Eye Movements* (pp. 95–137). Boca Raton: CRC Press.

- Becker, W., & Fuchs, A. F. (1969). Further properties of the human saccadic system: eye movements and correction saccades with and without visual fixation points. *Vision Research*, 9(10), 1247–1258.
- Bedell, H. E., & Stevenson, S. B. (2013). Eye movement testing in clinical examination. *Vision Research*, 90, 32–37.
- Bengi, H., & Thomas, J. G. (1968). Three electronic methods for recording ocular tremor. *Journal of Medical and Biological Engineering*, 6(2), 171–179.
- Bessho, K., Fujikado, T., Mihashi, T., Yamaguchi, T., Nakazawa, N., & Tano, Y. (2008). Photoreceptor images of normal eyes and of eyes with macular dystrophy obtained in vivo with an adaptive optics fundus camera. *Japanese Journal of Ophthalmology*, 52(5), 380–385.
- Beymer, D., & Flickner, M. (2003). Eye gaze tracking using an active stereo head. In *2003 IEEE Computer Society Conference on Computer Vision and Pattern Recognition* (Vol. 2, pp. 451–458).
- Blake, R., & Logothetis, N. K. (2002). Visual competition. *Nature Reviews Neuroscience*, 3, 13–21.
- Bland, J. M., & Altman, D. G. (1986). Statistical Methods for Assessing Agreement Between Two Methods of Clinical Measurement. *The Lancet*, 1(8476), 307–310.
- Blignaut, P. (2014). Mapping the Pupil-Glint Vector to Gaze Coordinates in a Simple Video-Based Eye Tracker. *Journal of Eye Movement Research*, 7(1), 1–11.
- Bolger, C., Bojanic, S., Sheahan, N. F., Coakley, D., & Malone, J. F. (1999). Dominant frequency content of ocular microtremor from normal subjects. *Vision Research*, 39(11), 1911–1915.
- Bonnet, C., Hanuška, J., Rusz, J., Rivaud-Péchoux, S., Sieger, T., Majerová, V., ... Růžička, E. (2013). Horizontal and vertical eye movement metrics: What is important? *Clinical Neurophysiology*, 124(11), 2216–2229.
- Borsting, E., Rouse, M., Shin, S., Dold, E., & McClallen, A. (2007). Repeatability of the Visagraph II in the analysis of children's eye movements during reading. *Optometry and Vision Development*, 38(2), 67–73.
- Brainard, D. H. (1997). The Psychophysics Toolbox. *Spatial Vision*, 10(4), 433–436.
- Bridgeman, B., & Palca, J. (1980). The role of microsaccades in high acuity observational tasks. *Vision Research*, 20(9), 813–817.

- Brolly, X. L. C., & Mulligan, J. B. (2004). Implicit Calibration of a Remote Gaze Tracker. In *Conference on Computer Vision and Pattern Recognition Workshop* (p. 134).
- Bucci, M. P., Kapoula, Z., Yang, Q., & Bremond-Gignac, D. (2006). Latency of saccades, vergence, and combined movements in children with early onset convergent or divergent strabismus. *Vision Research*, 46(8–9), 1384–1392.
- Cacho-Martínez, P., García-Muñoz, Á., & Ruiz-Cantero, M. T. (2010). Do we really know the prevalence of accommodative and nonstrabismic binocular dysfunctions? *Journal of Optometry*, 3(4), 185–197.
- Capobianco, N. M. (1952). The subjective measurement of the near point of convergence and its significance in the diagnosis of convergence insufficiency. *American Orthoptic Journal*, 2(1), 40–42.
- Carl, J. R., & Gellman, R. S. (1987). Human smooth pursuit: stimulus-dependent responses. *Journal of Neurophysiology*, 57(5), 1446–1463.
- Carpenter, R. H. S. (1981). Oculomotor procrastination. In D. F. Fisher, R. A. Monty, & J. W. Senders (Eds.), *Eye Movements: Cognition and Visual Perception* (pp. 237–246). Hillsdale: Lawrence Erlbaum.
- Carpenter, R. H. S. (1988). *Movements of the eyes*. London: Pion.
- Carpenter, R. H. S. (1991). *Eye Movements*. Boca Raton: CRC Press.
- Cebrian, J. L., Antona, B., Barrio, A., Gonzalez, E., Gutierrez, A., & Sanchez, I. (2014). Repeatability of the Modified Thorington Card Used to Measure Far Heterophoria. *Optometry and Vision Science*, 91(7), 786–792.
- Cerrolaza, J. J., Villanueva, A., & Cabeza, R. (2008). Taxonomic study of polynomial regressions applied to the calibration of video-oculographic systems. In *Proceedings of the 2008 Symposium on Eye Tracking Research & Applications* (pp. 259–266).
- Cerrolaza, J. J., Villanueva, A., & Cabeza, R. (2012). Study of Polynomial Mapping Functions in Video-Oculography Eye Trackers. *ACM Transactions on Computer-Human Interaction*, 19(2), 1–25.
- Cherici, C., Kuang, X., Poletti, M., & Rucci, M. (2012). Precision of sustained fixation in trained and untrained observers. *Journal of Vision*, 12(6), 1–16.

- Choi, M., Weiss, S., Schaeffel, F., Seidemann, A., Howland, H. C., Wilhelm, B., & Wilhelm, H. (2000). Laboratory, clinical, and kindergarten test of a new eccentric infrared photorefractor (PowerRefractor). *Optometry and Vision Science*, 77(10), 537–548.
- Chow, G., & Li, X. (1993). Towards a system for automatic facial feature detection. *Pattern Recognition*, 26(12), 1739–1755.
- Chui, T. Y., Song, H., & Burns, S. A. (2008a). Adaptive-optics imaging of human cone photoreceptor distribution. *Journal of the Optical Society of America A*, 25(12), 3021–3029.
- Chui, T. Y., Song, H., & Burns, S. A. (2008b). Individual variations in human cone photoreceptor packing density: variations with refractive error. *Investigative Ophthalmology and Visual Science*, 49(10), 4679–4687.
- Ciuffreda, K. J. (1992). Components of clinical near vergence testing. *Journal of Behavioral Optometry*, 3(1), 3–13.
- Ciuffreda, K. J., & Tannen, B. (1995). *Eye Movement Basics for the Clinician*. St. Louis: Mosby.
- Colby, D., Laukkanen, H. R., & Yolton, R. L. (1998). Use of the Taylor Visagraph II system to evaluate eye movements made during reading. *Journal of the American Optometric Association*, 69(1), 22–32.
- Collewijn, H. (1989). The optokinetic contribution. In R. H. S. Carpenter (Ed.), *Vision and Visual Dysfunction, vol 8, Eye Movements* (pp. 45–70). Boca Raton: CRC Press.
- Collewijn, H. (1998). Eye movement recording. In R. H. S. Carpenter & J. G. Robson (Eds.), *Vision Research: a Practical Guide to Laboratory Methods* (pp. 245–285). New York: Oxford University Press.
- Collewijn, H., Erkelens, C. J., & Steinman, R. M. (1988a). Binocular co-ordination of human horizontal saccadic eye movements. *Journal of Physiology*, 404(1), 157–182.
- Collewijn, H., Erkelens, C. J., & Steinman, R. M. (1988b). Binocular co-ordination of human vertical saccadic eye movements. *Journal of Physiology*, 404(1), 183–197.
- Collewijn, H., Erkelens, C. J., & Steinman, R. M. (1995). Voluntary binocular gaze-shifts in the plane of regard: Dynamics of version and vergence. *Vision Research*, 35(23/24), 3335–3358.
- Collewijn, H., van der Mark, F., & Jansen, T. C. (1975). Precise recording of human eye movements. *Vision Research*, 15(3), 447–450.

## References

---

- Collins, T., Semroud, A., Orriols, E., & Doré-Mazars, K. (2008). Saccade dynamics before, during, and after saccadic adaptation in humans. *Investigative Ophthalmology and Visual Science*, 49(2), 604–612.
- Cornsweet, T. N. (1956). Determination of the stimuli for involuntary drifts and saccadic eye movements. *Journal of the Optical Society of America*, 46(11), 987–988.
- Cornsweet, T. N., & Crane, H. D. (1973). Accurate two-dimensional eye tracker using first and fourth Purkinje images. *Journal of the Optical Society of America*, 63(8), 921–928.
- Coubard, O. A. (2013). Saccade and vergence eye movements: A review of motor and premotor commands. *European Journal of Neuroscience*, 38, 3384–3397.
- Coubard, O. A., & Kapoula, Z. (2008). Saccades during symmetrical vergence. *Graefe's Archive for Clinical and Experimental Ophthalmology*, 246(4), 521–536.
- Coutinho, F., & Morimoto, C. (2006). Free head motion eye gaze tracking using a single camera and multiple light sources. In *19th Brazilian Symposium on Computer Graphics and Image Processing* (pp. 171–178). Manaus.
- Deng, J.-Y., & Lai, F. (1997). Region-based template deformation and masking for eye-feature extraction and description. *Pattern Recognition*, 30(3), 403–419.
- Diner, D. B., & Fender, D. H. (1988). Dependence of Panum's fusional area on local retinal stimulation. *Journal of the Optical Society of America A*, 5(7), 1163–1169.
- Ditchburn, R. W., & Ginsborg, B. L. (1952). Vision with a stabilized retinal image. *Nature*, 170, 36–37.
- Ditchburn, R. W., & Ginsborg, B. L. (1953). Involuntary eye movements during fixation. *The Journal of Physiology*, 119, 1–17.
- Dodge, R., & Cline, T. S. (1901). The angle velocity of eye movements. *Psychological Review*, 8(2), 145–157.
- Doma, H., & Hallett, P. E. (1988). Dependence of saccadic eye-movements on stimulus luminance, and an effect of task. *Vision Research*, 28(8), 915–924.
- Duchowski, A. T. (2002). A breadth-first survey of eye-tracking applications. *Behavior Research Methods, Instruments, and Computers*, 34(4), 455–470.
- Duchowski, A. T. (2017). *Eye Tracking Methodology. Theory and Practice* (3rd ed.). London:

- Springer International Publishing.
- Duncan, J. L., Zhang, Y., Gandhi, J., Nakanishi, C., Othman, M., Branham, K. E. H., ... Roorda, A. (2007). High-resolution imaging with adaptive optics in patients with inherited retinal degeneration. *Investigative Ophthalmology and Visual Science*, 48(7), 3283–3291.
- Duwaer, A. L., & Van Den Brink, G. (1981). What is the diplopia threshold? *Perception & Psychophysics*, 29(4), 295–309.
- Ebisawa, Y., & Satoh, S. -i. (1993). Effectiveness of pupil area detection technique using two light sources and image difference method. In *Proceedings of the 15th Annual International Conference of the IEEE Engineering in Medicine and Biology Society* (pp. 1268–1269). San Diego.
- Engbert, R. (2006). Microsaccades: a microcosm for research on oculomotor control, attention, and visual perception. *Progress in Brain Research*, 154, 177–192.
- Engbert, R., & Kliegl, R. (2003a). Binocular coordination in microsaccades. In J. Hyönä, R. Radach, & H. Deubel (Eds.), *The Mind's Eye: Cognitive and Applied Aspects of Eye Movement Research* (pp. 103–117). Amsterdam: Elsevier Science.
- Engbert, R., & Kliegl, R. (2003b). Microsaccades uncover the orientation of covert attention. *Vision Research*, 43(9), 1035–1045.
- Engbert, R., & Kliegl, R. (2004). Microsaccades keep the eyes' balance during fixation. *Psychological Science*, 15(6), 431–436.
- Engbert, R., & Mergenthaler, K. (2006). Microsaccades are triggered by low retinal image slip. *Proceedings of the National Academy of Sciences*, 103(18), 7192–7197.
- Enright, J. T. (1984). Changes in vergence mediated by saccades. *Journal of Physiology*, 350, 9–31.
- Erkelens, C. J. (1987). Adaptation of ocular vergence to stimulation with large disparities. *Experimental Brain Research*, 66(3), 507–516.
- Erkelens, C. J., Collewijn, H., & Steinman, R. M. (1989). Asymmetrical adaptation of human saccades to anisotropic spectacles. *Investigative Ophthalmology and Visual Science*, 30(6), 1132–1145.
- Erkelens, C. J., Steinman, R. M., & Collewijn, H. (1989). Ocular vergence under natural conditions. II. Gaze shifts between real targets differing in distance and direction. *Proceedings of the Royal*

- Society of London. Series B: Biological Sciences*, 236(1285), 441–465.
- Erkelens, C. J., van der Steen, S. J., Steinman, R. M., & Collewijn, H. (1989). Ocular vergence under natural conditions. I. Continuous changes of target distance along the median plane. *Proceedings of the Royal Society of London. Series B: Biological Sciences*, 236(1285), 417–440.
- Ernst, M. O., & Banks, M. S. (2002). Humans integrate visual and haptic information in a statistically optimal fashion. *Nature*, 415(6870), 429–433.
- Evans, B. J. (2007). *Pickwell's Binocular Vision Anomalies* (5th ed.). Edinburgh: Elsevier Butterworth Heinemann.
- Fender, D., & Julesz, B. (1967). Extension of Panum's fusional area in binocularly stabilized vision. *Journal of the Optical Society of America*, 57(6), 819–830.
- Fincham, E. F. (1962). Accommodation and convergence in the absence of retinal images. *Vision Research*, 1(5–6), 425–432.
- Fischler, M. A., & Bolles, R. C. (1981). Random Sample Consensus: A Paradigm for Model Fitting with Applications to Image Analysis and Automated Cartography. *Communications of the ACM*, 24(6), 381–395.
- Fitzgibbon, A., Pilu, M., & Fisher, R. B. (1999). Direct least square fitting of ellipses. *IEEE Transactions on Pattern Analysis and Machine Intelligence*, 21(5), 476–480.
- Fogt, N., Baughman, B. J., & Good, G. (2000). The effect of experience on the detection of small eye movements. *Optometry and Vision Science*, 77(12), 670–674.
- Francis, E. L., Jiang, B., Owens, D. A., & Tyrrell, R. A. (2003). Accommodation and vergence require effort-to-see. *Optometry and Vision Science*, 80(6), 467–473.
- Frens, M. A., & van der Geest, J. N. (2002). Scleral search coils influence saccade dynamics. *Journal of Neurophysiology*, 88(2), 692–698.
- Friedman, D. S., Repka, M. X., Katz, J., Giordano, L., Ibironke, J., Hawse, P., & Tielsch, J. M. (2009). Prevalence of amblyopia and strabismus in White and African American children aged 6 through 71 months: The Baltimore Pediatric Eye Disease Study. *Ophthalmology*, 116(11), 2128–2134.
- Fuhl, W., Kübler, T., Sippel, K., Rosenstiel, W., & Kasneci, E. (2015). ExCuSe: Robust Pupil

- Detection in Real-World Scenarios. In G. Azzopardi & N. Petkov (Eds.), *Computer Analysis of Images and Patterns* (pp. 39–51). New York: Springer.
- Fuhl, W., Santini, T. C., Kübler, T., & Kasneci, E. (2016). Else: Ellipse selection for robust pupil detection in real-world environments. In *Proceedings of the 9th Biennial ACM Symposium on Eye Tracking Research & Applications - ETRA '16* (pp. 123–130). Charlseton.
- Fuller, J. H. (1996). Eye position and target amplitude effects on human visual saccadic latencies. *Experimental Brain Research*, 109(3), 457–466.
- Galfano, G., Betta, E., & Turatto, M. (2004). Inhibition of return in microsaccades. *Experimental Brain Research*, 159(3), 400–404.
- Gall, R., & Wick, B. (2003). The symptomatic patient with normal phorias at distance and near: what tests detect a binocular vision problem? *Optometry*, 74(5), 309–322.
- Gall, R., Wick, B., & Bedell, H. E. (1998). Vergence facility: Establishing clinical utility. *Optometry and Vision Science*, 75(10), 731–742.
- Gautier, J., Bedell, H. E., Siderov, J., & Waugh, S. J. (2016). Monocular microsaccades are visual-task related. *Journal of Vision*, 16(3), 1–16.
- Gerardin, P., Gaveau, V., Périsson, D., & Prablanc, C. (2011). Integration of visual information for saccade production. *Human Movement Science*, 30(6), 1009–1021.
- Ghasia, F. F., & Shaikh, A. G. (2015). Uncorrected myopic refractive error increases microsaccade amplitude. *Investigative Ophthalmology & Visual Science*, 56(4), 2531.
- Girshick, A. R., & Banks, M. S. (2009). Probabilistic combination of slant information: Weighted averaging and robustness as optimal percepts. *Journal of Vision*, 9(9), 1–20.
- Goñi, S., Echeto, J., Villanueva, A., & Cabeza, R. (2004). Robust algorithm for pupil-glint vector detection in a video-oculography eyetracking system. In *Proceedings of the 17th International Conference on Pattern Recognition* (Vol. 4, pp. 941–944). IEEE.
- Griffin, J. R. (1982). *Binocular anomalies: Procedures for vision therapy* (2nd ed). New York: Professional Press Books.
- Grossman, G. E., Leigh, R. J., Abel, L. A., Lanska, D. J., & Thurston, S. E. (1988). Frequency and velocity of rotational head perturbations during locomotion. *Experimental Brain Research*, 70(3), 470–476.

- Grossman, G. E., Leigh, R. J., Bruce, E. N., Huebner, W. P., & Lanska, D. J. (1989). Performance of the human vestibuloocular reflex during locomotion. *Journal of Neurophysiology*, 62(1), 264–272.
- Guestrin, E. D., & Eizenman, M. (2006). General theory of remote gaze estimation using the pupil center and corneal reflections. *IEEE Transactions on Biomedical Engineering*, 53(6), 1124–1133.
- Han, S. J., Guo, Y., Granger-Donetti, B., Vicci, V. R., & Alvarez, T. L. (2010). Quantification of heterophoria and phoria adaptation using an automated objective system compared to clinical methods. *Ophthalmic and Physiological Optics*, 30(1), 95–107.
- Hansen, D. W., Agustin, J. S., & Villanueva, A. (2010). Homography normalization for robust gaze estimation in uncalibrated setups. In *Proceedings of the 2010 Symposium on Eye-Tracking Research & Applications - ETRA '10* (pp. 13–20). Austin: ACM Press.
- Hansen, D. W., & Ji, Q. (2010). In the eye of the beholder: a survey of models for eyes and gaze. *IEEE Transactions on Pattern Analysis and Machine Intelligence*, 32(3), 478–500.
- Hartline, H. K. (1940). The nerve messages in the fibers of the visual pathway. *Journal of Optical Society of America*, 30(6), 239–247.
- Hennessey, C. A., & Lawrence, P. D. (2009). Improving the accuracy and reliability of remote system-calibration-free eye-gaze tracking. *IEEE Transactions on Biomedical Engineering*, 56(7), 1891–1900.
- Hennessey, C. A., Noureddin, B., & Lawrence, P. (2006). A single camera eye-gaze tracking system with free head motion. In *Proceedings of the 2006 symposium on Eye tracking research & applications - ETRA '06* (pp. 87–94). San Diego: ACM Press.
- Hering, E. (1977). *The theory of binocular vision*. New York: Plenum Press.
- Hermens, F., & Walker, R. (2010). What determines the direction of microsaccades? *Journal of Eye Movement Research*, 3(4), 1–20.
- Hillis, J. M., Watt, S. J., Landy, M. S., & Banks, M. S. (2004). Slant from texture and disparity cues: Optimal cue combination. *Journal of Vision*, 4(12), 967–992.
- Hirsch, M. J., & Bing, L. B. (1948). The effect of testing method on values obtained for phoria at forty centimeters. *American Journal of Optometry and Archives of American Academy of Optometry*, 31(1), 1–10.

- Optometry*, 25(9), 407–416.
- Holmqvist, K., & Nyström, M. (2011). *Eye Tracking. A comprehensive guide to methods and measures* (1st ed.). Oxford: Oxford University Press.
- Horwood, A. M., & Riddell, P. M. (2010). Differences between naïve and expert observers' vergence and accommodative responses to a range of targets. *Ophthalmic and Physiological Optics*, 30(2), 152–159.
- Howard, I. P., & Marton, C. (1992). Visual pursuit over textured backgrounds in different depth planes. *Experimental Brain Research*, 90(3), 625–629.
- Hryncak, P. K., Herriot, C., & Irving, E. L. (2010). Comparison of alternate cover test reliability at near in non-strabismus between experienced and novice examiners. *Ophthalmic and Physiological Optics*, 30(3), 304–309.
- Huang, J.-B., Cai, Q., Liu, Z., Ahuja, N., & Zhang, Z. (2014). Towards accurate and robust cross-ratio based gaze trackers through learning from simulation. In *Proceedings of the Eye Tracking Research and Applications Symposium* (pp. 75–82). ACM.
- Hung, G. K. (1992). Adaptation model of accommodation and vergence. *Ophthalmic and Physiological Optics*, 12(3), 319–326.
- Hung, G. K., Ciuffreda, K. J., & Rosenfield, M. (1996). Proximal contribution to a linear static model of accommodation and vergence. *Ophthalmic and Physiological Optics*, 16(1), 31–41.
- Hung, G. K., Ciuffreda, K. J., Semmlow, J. L., & Horng, J. L. (1994). Vergence eye movements under natural viewing conditions. *Investigative Ophthalmology and Visual Science*, 35(9), 3486–3492.
- Hung, G. K., Zhu, H., & Ciuffreda, K. J. (1997). Convergence and divergence exhibit different response characteristics to symmetric stimuli. *Vision Research*, 37(9), 1197–1205.
- Jagini, K. K., Vaidyanath, H., & Bharadwaj, S. R. (2014). Utility of theoretical Hirschberg ratio for gaze position calibration. *Optometry and Vision Science*, 91(7), 778–785.
- Jarjes, A. A., Wang, K., & Mohammed, G. J. (2010). GVF snake-based method for accurate pupil contour detection. *Information Technology Journal*, 9(8), 1653–1658.
- Jaschinski, W. (2016). Pupil size affects measures of eye position in video eye tracking: implications for recording vergence accuracy. *Journal of Eye Movement Research*, 9(4), 1–14.
- Jaschinski, W. (2017). Individual objective and subjective fixation disparity in near vision. *PLoS*

- ONE, 12(1), e0170190.
- Jaschinski, W., Jainta, S., & Kloke, W. B. (2010). Objective vs subjective measures of fixation disparity for short and long fixation periods. *Ophthalmic & Physiological Optics*, 30(4), 379–390.
- Javadi, A.-H., Hakimi, Z., Barati, M., Walsh, V., & Tcheang, L. (2015). SET: a pupil detection method using sinusoidal approximation. *Frontiers in Neuroengineering*, 8(4), 1–10.
- Johansson, J., Seimyr, G. Ö., & Pansell, T. (2015). Eye dominance in binocular viewing conditions. *Journal of Vision*, 15(9), 1–17.
- Johns, H. A., Manny, R. E., Fern, K., & Hu, Y.-S. (2004). The intraexaminer and interexaminer repeatability of the alternate cover test using different prism neutralization endpoints. *Optometry and Vision Science*, 81(12), 939–946.
- Jordan, D. R., Mawn, L., & Anderson, R. L. (2012). *Surgical anatomy of the ocular adnexa. A clinical approach* (2nd ed., Vol. 9). New York: Oxford University Press.
- Julesz, B. (1971). *Foundations of cyclopean perception*. Chicago: The University of Chicago Press.
- Kandel, E. R., Schwartz, J. H., Jessell, T. M., Siegelbaum, S. A., & Hudspeth, A. J. (2013). *Principles of neural science* (5th ed.). New York: McGraw-Hill. pp. 905.
- Kang, J. J., Eizenman, M., Guestrin, E. D., & Eizenman, E. (2008). Investigation of the Cross-Ratios Method for Point-of-Gaze Estimation. *IEEE Transactions on Biomedical Engineering*, 55(9), 2293–2302.
- Kapoula, Z., Morize, A., Daniel, F., Jonqua, F., Orssaud, C., & Brémont-Gignac, D. (2016). Objective evaluation of vergence disorders and a research-based novel method for vergence rehabilitation. *Translational Vision Science & Technology*, 5(2), 1–24.
- Ke, S. R., Lam, J., Pai, D. K., & Spering, M. (2013). Directional asymmetries in human smooth pursuit eye movements. *Investigative Ophthalmology & Visual Science*, 54(6), 4409–4421.
- Kenyon, R. V., Ciuffreda, K. J., & Stark, L. (1980). Unequal saccades during vergence. *American Journal of Optometry and Physiological Optics*, 57(9), 586–594.
- Kersten, D., & Legge, G. E. (1983). Convergence accommodation. *Journal of the Optical Society of America*, 73(3), 332–338.
- Kertesz, A. E. (1981). Effect of stimulus size on fusion and vergence. *Journal of the Optical Society of America*

- of America*, 71(3), 289–293.
- Kim, E. H., & Alvarez, T. L. (2012a). The Changes in Phoria and Convergence to Divergence Peak Velocity Ratio Are Correlated. *Current Eye Research*, 37(11), 1054–1065.
- Kim, E. H., & Alvarez, T. L. (2012b). The frequency of horizontal saccades in near and far symmetrical disparity vergence. *Vision Research*, 63, 9–19.
- Kim, E. H., Granger-Donetti, B., Vicci, V. R., & Alvarez, T. L. (2010). The relationship between phoria and the ratio of convergence peak velocity to divergence peak velocity. *Investigative Ophthalmology & Visual Science*, 51(8), 4017–4027.
- Kimmel, D. L., Mammo, D., & Newsome, W. T. (2012). Tracking the eye non-invasively: simultaneous comparison of the scleral search coil and optical tracking techniques in the macaque monkey. *Frontiers in Behavioral Neuroscience*, 6(49), 1–17.
- King, W. M. (2011). Binocular coordination of eye movements - Hering's Law of equal innervation or uniocular control? *European Journal of Neuroscience*, 33(11), 2139–2146.
- Kleiner, M., Brainard, D. H., Pelli, D. G., Ingling, A., Murray, R., & Broussard, C. (2007). What's new in Psychtoolbox-3? *Perception*, 36(14), 1–16.
- Knox, P. C., & Bekkour, T. (2004). Spatial mapping of the remote distractor effect on smooth pursuit initiation. *Experimental Brain Research*, 154(4), 494–503.
- Ko, H., Poletti, M., & Rucci, M. (2010). Microsaccades precisely relocate gaze in a high visual acuity task. *Nature Neuroscience*, 13(12), 1549–1553.
- Kowler, E., Aitkin, C. D., Ross, N. M., Santos, E. M., & Zhao, M. (2014). Davida Teller Award Lecture 2013: The importance of prediction and anticipation in the control of smooth pursuit eye movements. *Journal of Vision*, 14(5), 1–16.
- Kowler, E., & Steinman, R. M. (1979). The effect of expectations on slow oculomotor control—I. Periodic target steps. *Vision Research*, 19(6), 619–632.
- Krauskopf, J., Cornsweet, T. N., & Riggs, L. A. (1960). Analysis of eye movements during monocular and binocular fixation. *Journal of the Optical Society of America*, 50(6), 572–578.
- Krishnan, V. V., Farazian, F., & Stark, L. (1973). An analysis of the latencies and prediction in the fusional vergence system. *American Journal of Optometry and Archives of American Academy of Optometry*, 50(12), 933–939.

## References

---

- Kumar, A. N., Han, Y., Garbutt, S., & Leigh, R. J. (2002). Properties of anticipatory vergence responses. *Investigative Ophthalmology & Visual Science*, 43(8), 2626–2632.
- Lam, K. M., & Yan, H. (1996). Locating and extracting the eye in human face images. *Pattern Recognition*, 29(5), 771–779.
- Lee, Y. C. (2007). Active eye-tracking improves LASIK results. *Journal of Refractive Surgery*, 23(6), 581–585.
- Lee, Y. Y., Chen, T., & Alvarez, T. L. (2008). Quantitative assessment of divergence eye movements. *Journal of Vision*, 8(12), 1–13.
- Leigh, R. J., & Zee, D. S. (2015). *The Neurology of Eye Movements* (5th ed.). New York: Oxford University Press.
- Levin, L. A., Nilsson, S. F., Ver Hoeve, J., Wu, S. M., Alm, A., & Kaufman, P. L. (2011). *Adler's physiology of the eye* (11th ed.). Philadelphia: Elsevier.
- Li, D., Winfield, D., & Parkhurst, D. J. (2005). Starburst: A hybrid algorithm for video-based eye tracking combining feature-based and model-based approaches. In *Proceedings of the IEEE Computer Society Conference on Computer Vision and Pattern Recognition*. San Diego: IEEE.
- Li, J., Lam, C. S. Y., Yu, M., Hess, R. F., Chan, L. Y. L., Maehara, G., ... Thompson, B. (2010). Quantifying sensory eye dominance in the normal visual system: A new technique and insights into variation across traditional tests. *Investigative Ophthalmology and Visual Science*, 51(12), 6875–6881.
- Liversedge, S. P., Gilchrist, I. D., & Everling, S. (2011). *The Oxford Handbook of Eye Movements*. New York: Oxford University Press.
- Lord, M. P. (1951). Measurement of binocular eye movements of subjects in the sitting position. *British Journal of Ophthalmology*, 35(1), 21–30.
- Ludvigh, E. (1949). Amount of eye movement objectively perceptible to the unaided eye. *American Journal of Ophthalmology*, 32(5), 649–650.
- Maas, E. F., Huebner, W. P., Seidman, S. H., & Leigh, R. J. (1989). Behavior of human horizontal vestibulo-ocular reflex in response to high-acceleration stimuli. *Brain Research*, 499(1), 153–156.
- Marino, R. A., & Munoz, D. P. (2009). The effects of bottom-up target luminance and top-down

- spatial target predictability on saccadic reaction times. *Experimental Brain Research*, 197(4), 321–335.
- Martinez-Conde, S. (2006). Fixational eye movements in normal and pathological vision. *Progress in Brain Research*, 154, 151–176.
- Martinez-Conde, S., Macknik, S. L., & Hubel, D. H. (2002). The function of bursts of spikes during visual fixation in the awake primate lateral geniculate nucleus and primary visual cortex. *Proceedings of the National Academy of Sciences of the United States of America*, 99, 13920–13925.
- Martinez-Conde, S., Macknik, S. L., & Hubel, D. H. (2004). The role of fixational eye movements in visual perception. *Nature Reviews Neuroscience*, 5, 229–240.
- Martinez-Conde, S., Otero-Millan, J., & Macknik, S. L. (2013). The impact of microsaccades on vision: towards a unified theory of saccadic function. *Nature Reviews Neuroscience*, 14, 83–96.
- Maxwell, J., Tong, J., & Schor, C. M. (2010). The first and second order dynamics of accommodative convergence and disparity convergence. *Vision Research*, 50(17), 1728–1739.
- Mays, L. E., & Gamlin, P. D. R. (1995a). A neural mechanism subserving saccade-vergence interactions. In J. M. Findlay, R. Walker, & R. W. Kentridge (Eds.), *Eye Movement Research: Mechanisms, Processes and Applications* (pp. 215–223). Amsterdam: Elsevier.
- Mays, L. E., & Gamlin, P. D. R. (1995b). Neuronal circuitry controlling the near response. *Current Opinion in Neurobiology*, 5(6), 763–768.
- Mays, L. E., Porter, J. D., Gamlin, P. D. R., & Tello, C. A. (1986). Neural control of vergence eye movements: neurons encoding vergence velocity. *Journal of Neurophysiology*, 56(4), 1007–1021.
- McCamy, M. B., Collins, N., Otero-Millan, J., Al-Kalbani, M., Macknik, S. L., Coakley, D., ... Martinez-Conde, S. (2013). Simultaneous recordings of ocular microtremor and fixational microsaccades with a piezoelectric sensor and a commercial video tracking system. *PeerJ*, 1, e14.
- McCamy, M. B., Macknik, S. L., & Martinez-Conde, S. (2014). Different fixational eye movements mediate the prevention and the reversal of visual fading. *Journal of Physiology*, 592(19), 4381–4394.

## References

---

- McCamy, M. B., Najafian Jazi, A., Otero-Millan, J., Macknik, S. L., & Martinez-Conde, S. (2013). The effects of fixation target size and luminance on microsaccades and square-wave jerks. *PeerJ*, 1, e9.
- McCamy, M. B., Otero-Millan, J., Macknik, S. L., Yang, Y., Troncoso, X. G., Baer, S. M., ... Martinez-Conde, S. (2012). Microsaccadic efficacy and contribution to foveal and peripheral vision. *The Journal of Neuroscience*, 32(27), 9194–9204.
- Mehrabian, H., & Hashemi-Tari, P. (2007). Pupil boundary detection for iris recognition using graph cuts. In *Proceedings of the International Conference on Image and Vision Computing New Zealand (IVCNZ)* (pp. 77–82).
- Merchan, J., Morrisette, R., & Porterfield, J. L. (1974). Remote measurement of eye direction allowing subject motion over one cubic foot of space. *IEEE Transactions in Biomedical Engineering*, 21(4), 309–317.
- Meyer, C. H., Lasker, A. G., & Robinson, D. A. (1985). The upper limit of human smooth pursuit velocity. *Vision Research*, 25(4), 561–563.
- Miles, F. A., Judge, S. J., & Optican, L. M. (1987). Optically induced changes in the couplings between vergence and accommodation. *The Journal of Neuroscience*, 7(8), 2576–2589.
- Model, D., & Eizenman, M. (2011). An automated Hirschberg test for infants. *IEEE Transactions on Biomedical Engineering*, 58(1), 103–109.
- Møller, F., Laursen, M. L., Tygesen, J., & Sjølie, A. K. (2002). Binocular quantification and characterization of microsaccades. *Graefe's Archive for Clinical and Experimental Ophthalmology*, 240(9), 765–770.
- Mompean, J., Aragón, J. L., Prieto, P., & Artal, P. (2015). GPU-accelerated High-speed Eye Pupil Tracking System. In *27th International Symposium on Computer Architecture and High Performance Computing (SBAC-PAD)* (pp. 17–24). Florianópolis.
- Morimoto, C. H., Koons, D., Amir, A., & Flickner, M. (2000). Pupil detection and tracking using multiple light sources. *Image and Vision Computing*, 18(4), 331–335.
- Morimoto, C. H., & Mimica, M. R. M. (2005). Eye gaze tracking techniques for interactive applications. *Computer Vision and Image Understanding*, 98(1), 4–24.
- Morris, F. M. (1960). The influence of kinesthesia upon near heterophoria measurements. *American*

- Journal of Optometry and Archives of American Academy of Optometry*, 37(7), 327–351.
- Morrow, M. J., & Sharpe, J. A. (1993). Smooth pursuit initiation in young and elderly subjects. *Vision Research*, 33(2), 203–210.
- Munoz, D. P., Broughton, J. R., Goldring, J. E., & Armstrong, I. T. (1998). Age-related performance of human subjects on saccadic eye movement tasks. *Experimental Brain Research*, 121(4), 391–400.
- Munoz, P., Semmlow, J. L., Yuan, W., & Alvarez, T. L. (1999). Short term modification of disparity vergence eye movements. *Vision Research*, 39(9), 1695–1705.
- Myers, K. J. (1975). Some considerations of ocular rotations. *American Journal of Optometry and Physiological Optics*, 52, 106–122.
- Noorani, I., & Carpenter, R. H. S. (2016). The LATER model of reaction time and decision. *Neuroscience and Biobehavioral Reviews*, 64, 229–251.
- North, R. V., Henson, D. B., & Smith, T. J. (1993). Influence of proximal, accommodative and disparity stimuli upon the vergence system. *Ophthalmic and Physiological Optics*, 13(3), 239–243.
- Nyström, M., Andersson, R., Magnusson, M., Pansell, T., & Hooge, I. (2015). The influence of crystalline lens accommodation on post-saccadic oscillations in pupil-based eye trackers. *Vision Research*, 107, 1–14.
- Nyström, M., Andersson, R., Niehorster, D. C., & Hooge, I. (2017). Searching for monocular microsaccades – A red Hering of modern eye trackers? *Vision Research*, 140, 44–54.
- Nyström, M., Hooge, I., & Holmqvist, K. (2013). Post-saccadic oscillations in eye movement data recorded with pupil-based eye trackers reflect motion of the pupil inside the iris. *Vision Research*, 92, 59–66.
- Ohno, T., & Mukawa, N. (2004). A free-head, simple calibration, gaze tracking system that enables gaze-based interaction. In *Proceedings of the Eye tracking research & applications symposium on Eye tracking research & applications* (pp. 115–122). San Antonio: ACM Press.
- Ono, H., & Nakamizo, S. (1978). Changing fixation in the transverse plane at eye level and Hering's law of equal innervation. *Vision Research*, 18(5), 511–519.
- Ono, H., Nakamizo, S., & Steinbach, M. J. (1978). Nonadditivity of vergence and saccadic eye

- movement. *Vision Research*, 18(6), 735–739.
- Otero-Millan, J., Castro, J. L. A., Macknik, S. L., & Martinez-Conde, S. (2014). Unsupervised clustering method to detect microsaccades. *Journal of Vision*, 14(2), 1–17.
- Otero-Millan, J., Macknik, S. L., & Martinez-Conde, S. (2014). Fixational eye movements and binocular vision. *Frontiers in Integrative Neuroscience*, 8(52), 1–10.
- Otero-Millan, J., Troncoso, X. G., Macknik, S. L., Serrano-Pedraza, I., & Martinez-Conde, S. (2008). Saccades and microsaccades during visual fixation, exploration, and search: Foundations for a common saccadic generator. *Journal of Vision*, 8(14), 1–18.
- Owens, D. A., & Liebowitz, H. W. (1980). Accommodation, convergence, and distance perception in low illumination. *American Journal of Optometry and Physiological Optics*, 57(9), 540–550.
- Pang, Y., Gabriel, H., Frantz, K. A., & Saeed, F. (2010). A prospective study of different test targets for the near point of convergence. *Ophthalmic and Physiological Optics*, 30(3), 298–303.
- Park, R. S., & Park, G. E. (1933). The center of ocular rotation in the horizontal plane. *American Journal of Physiology*, 104(3), 545–552.
- Peli, E., & McCormack, G. (1983). Dynamics of cover test eye movements. *American Journal of Optometry and Physiological Optics*, 60(8), 712–724.
- Pelli, D. G. (1997). The VideoToolbox software for visual psychophysics: transforming numbers into movies. *Spatial Vision*, 10(4), 437–442.
- Pickwell, L. D. (1973). Eye movements during the cover test. *British Journal of Physiological Optics*, 28(1), 23–25.
- Pickwell, L. D. (1989). *Binocular Vision Anomalies: Investigation and Treatment*. Oxford: Butterworth-Heinemann. pp. 15-21.
- Pritchard, R. M. (1961). Stabilized images on the retina. *Scientific American*, 204(6), 72–78.
- Purves, D., Augustine, G. J., Fitzpatrick, D., Hall, W. C., LaMantia, A., McNamara, J. O., & Williams, S. M. (2004). *Neuroscience* (3th ed.). Sunderland: Sinauer Associates, Inc.
- Qing, Y., & Kapoula, Z. (2004). Saccade-vergence dynamics and interaction in children and in adults. *Experimental Brain Research*, 156(2), 212–223.
- Rainey, B. B., Schroeder, T. L., Goss, D. A., & Grosvenor, T. P. (1998). Inter-examiner repeatability

- of heterophoria tests. *Optometry and Vision Science*, 75(10), 719–726.
- Rambold, H., Neumann, G., Sander, T., & Helmchen, C. (2005). Age-related changes of vergence under natural viewing conditions. *Neurobiology of Aging*, 27(1), 163–172.
- Rashbass, C., & Westheimer, G. (1961). Disjunctive eye movements. *Journal of Physiology*, 159(2), 339–360.
- Reulen, J. P. H., Marcus, J. T., Koops, D., de Vries, F. R., Tiesinga, G., Boshuizen, K., & Bos, J. E. (1988). Precise recording of eye movement: the IRIS technique Part 1. *Medical and Biological Engineering and Computing*, 26(1), 20–26.
- Rice, M. L., Leske, D. A., Smestad, C. E., & Holmes, J. M. (2008). Results of ocular dominance testing depend on assessment method. *Journal of American Association for Pediatric Ophthalmology and Strabismus*, 12(4), 365–369.
- Riggs, L. A., & Ratliff, F. (1952). The effects of counteracting the normal movements of the eye. *Journal of the Optical Society of America*, 42, 872–873.
- Riggs, L. A., Ratliff, F., Cornsweet, J. C., & Cornsweet, T. N. (1953). The disappearance of steadily fixated visual test objects. *Journal of the Optical Society of America*, 43(6), 495–501.
- Robinson, D. A. (1963). A method of measuring eye movement using a scleral search coil in a magnetic field. *IEEE Transactions in Biomedical Engineering*, 10(4), 137–145.
- Robinson, D. A. (1964). The mechanics of human saccadic eye movements. *Journal of Physiology*, 174(2), 245–264.
- Rolfs, M. (2009). Microsaccades: small steps on a long way. *Vision Research*, 49(20), 2415–2441.
- Rolfs, M., Laubrock, J., & Kliegl, R. (2006). Shortening and prolongation of saccade latencies following microsaccades. *Experimental Brain Research*, 169(3), 369–376.
- Rolfs, M., Laubrock, J., & Kliegl, R. (2008). Microsaccade-induced prolongation of saccadic latencies depends on microsaccade amplitude. *Journal of Eye Movement Research*, 1(3), 1–8.
- Roorda, A., Romero-Borja, F., Donnelly III, W. J., Queener, H., Hebert, T. J., & Campbell, M. C. W. (2002). Adaptive optics scanning laser ophthalmoscopy. *Optics Express*, 10(9), 405–412.
- Rosenfield, M. (2011). Computer vision syndrome: a review of ocular causes and potential treatments. *Ophthalmic and Physiological Optics*, 31(5), 502–515.

- Rosenfield, M., & Ciuffreda, K. J. (1990). Accommodative convergence and age. *Ophthalmic & Physiological Optics, 10*(4), 403–404.
- Rosenfield, M., Ciuffreda, K. J., & Chen, H. W. (1995). Effect of age on the interaction between the AC/A and CA/C ratios. *Ophthalmic & Physiological Optics, 15*(5), 451–455.
- Rosenfield, M., Ciuffreda, K. J., & Hung, G. K. (1991). The linearity of proximally induced accommodation and vergence. *Investigative Ophthalmology & Visual Science, 32*(11), 2985–2991.
- Rouse, M., Borsting, E., Hyman, L., Hussein, M., Cotter, S., & Flynn, M. (1999). Frequency of convergence insufficiency among fifth and sixth graders. *Optometry and Vision Science, 76*(9), 643–649.
- Rouse, M., Hyman, L., CIRS Study Group. (1997). How do you make the diagnosis of convergence insufficiency? Survey results. *Journal of Optometric Vision Development, 28*, 91–97.
- Rouse, M., Hyman, L., Hussein, M., Solan, H., CIRS Study Group. (1998). Frequency of convergence insufficiency in optometry clinic settings. *Optometry and Vision Science, 75*(2), 88–96.
- Rucci, M., Ahissar, E., & Burr, D. (2018). Temporal coding of visual space. *Trends in Cognitive Sciences, 22*(10), 883–895.
- Saida, S., & Ono, H. (1984). Interaction between saccade and tracking vergence. *Vision Research, 24*(10), 1289–1294.
- Sanker, N., Prabhu, A., & Ray, A. (2012). A comparison of near-dissociated heterophoria tests in free space. *Clinical and Experimental Optometry, 95*(6), 638–642.
- Santos, E. M., Gnang, E. K., & Kowler, E. (2012). Anticipatory smooth eye movements with random-dot kinematograms. *Journal of Vision, 12*(11), 1–20.
- Savitzky, A., & Golay, M. J. E. (1964). Smoothing and differentiation of data by simplified least-squares procedures. *Analytical Chemistry, 36*(8), 1627–1639.
- Schaeffel, F. (2002). Kappa and Hirschberg ratio measured with an automated video gaze tracker. *Optometry and Vision Science, 79*(5), 329–334.
- Scheiman, M., Gallaway, M., Coulter, R., Reinstein, F., Ciner, E., Herzberg, C., & Parisi, M. (1996). Prevalence of vision and ocular disease conditions in a clinical pediatric population. *Journal of the American Optometric Association, 67*(4), 193–202.

- Scheiman, M., Gallaway, M., Frantz, K. A., Peter, R. J., Hatch, S., Cuff, M., & Mitchell, L. (2003). Nearpoint of convergence: Test procedure, target selection, and normative data. *Optometry and Vision Science, 80*(3), 214–225.
- Scheiman, M., & Wick, B. (2014). *Clinical management of Binocular Vision. Heterophoric, Accommodative, and Eye Movement Disorders* (4th ed.). Philadelphia: Lippincott Williams & Wilkins.
- Schnipke, S. K., & Todd, M. W. (2000). Trials and tribulations of using an eye-tracking system. In *Human Factors in Computing Systems Conference* (pp. 273–274). ACM.
- Schor, C. M. (1992). A dynamic model of cross-coupling between accommodation and convergence: simulations of step and frequency responses. *Optometry and Vision Science, 69*(4), 258–269.
- Schor, C. M., Alexander, J., Cormack, L., & Stevenson, S. (1992). Negative feedback control model of proximal convergence and accommodation. *Ophthalmic and Physiological Optics, 12*(3), 307–318.
- Schor, C. M., Lott, L. A., Pope, D., & Graham, A. D. (1999). Saccades reduce latency and increase velocity of ocular accommodation. *Vision Research, 39*(22), 3769–3795.
- Schor, C. M., Robertson, K. M., & Wesson, M. (1986). Disparity vergence dynamics and fixation disparity. *American Journal of Optometry and Physiological Optics, 63*(8), 611–618.
- Schor, C. M., & Tyler, C. W. (1981). Spatio-temporal properties of Panum's fusional area. *Vision Research, 21*(5), 683–692.
- Schroeder, T. L., Rainey, B. B., Goss, D. A., & Grosvenor, T. P. (1996). Reliability of and comparisons among methods of measuring dissociated phoria. *Optometry and Vision Science, 73*(6), 389–397.
- Schroth, V., Joos, R., & Jaschinski, W. (2015). Effects of Prism Eyeglasses on Objective and Subjective Fixation Disparity. *PLoS One, 10*(10), e0138871.
- Schulz, E. (1984). Binocular micromovements in normal persons. *Graefe's Archive for Clinical and Experimental Ophthalmology, 222*(2), 95–100.
- Schwartz, S. (2009). *Visual Perception: A Clinical Orientation* (4th ed.). New York: McGraw-Hill Medical.
- Semmlow, J. L., Chen, Y.-F., Granger-Donetti, B., & Alvarez, T. L. (2009). Correction of saccade-

- induced midline errors in responses to pure disparity vergence stimuli. *Journal of Eye Movement Research*, 2(5), 1–13.
- Semmlow, J. L., Chen, Y.-F., Pedrono, C., & Alvarez, T. L. (2008). Saccadic behavior during the response to pure disparity vergence stimuli I: General properties. *Journal of Eye Movement Research*, 1(2), 1–11.
- Semmlow, J. L., & Wetzel, P. (1979). Dynamic contributions of the components of binocular vergence. *Journal of the Optical Society of America*, 69(5), 639–645.
- Semmlow, J. L., & Yuan, W. (2002). Components of disparity vergence eye movements: application of independent component analysis. *IEEE Transactions on Biomedical Engineering*, 49(8), 805–811.
- Sesma-Sánchez, L., Villanueva, A., & Cabeza, R. (2012). Gaze estimation interpolation methods based on binocular data. *IEEE Transactions on Biomedical Engineering*, 59(8), 2235–2243.
- Shackel, B. (1967). Eye movement recording by electro-oculography. In P. H. Venables & I. Martin (Eds.), *Manual of Psychophysical Methods* (pp. 229–334). Amsterdam: Elsevier Science.
- Sheedy, J. E. (1980). Fixation disparity analysis of oculomotor imbalance. *American Journal of Optometry and Physiological Optics*, 57(9), 632–639.
- Sheedy, J. E., & Saladin, J. J. (1977). Phoria, vergence, and fixation disparity in oculomotor problems. *American Journal of Optometry and Physiological Optics*, 54(7), 474–478.
- Sheedy, J. E., & Saladin, J. J. (1978). Association of symptoms with measures of oculomotor deficiencies. *American Journal of Optometry and Physiological Optics*, 55(10), 670–676.
- Sheehy, C. K., Yang, Q., Arathorn, D. W., Tiruveedhula, P., de Boer, J. F., & Roorda, A. (2012). High-speed, image-based eye tracking with a scanning laser ophthalmoscope. *Biomedical Optics Express*, 3(10), 2611–2622.
- Skavenski, A. A., Hansen, R. M., Steinman, R. M., & Winterson, B. J. (1979). Quality of retinal image stabilization during small natural and artificial body rotations in man. *Vision Research*, 19(6), 675–683.
- Soltany, M., Zadeh, S. T., & Pourreza, H. R. (2011). Fast and accurate pupil positioning algorithm using circular Hough transform and gray projection. In *Proceedings of the International Conference on Computer Communication and Management* (Vol. 5, pp. 556–561). Sydney.

- Spauschus, A., Marsden, J., Halliday, D. M., Rosenberg, J. R., & Brown, P. (1999). The origin of ocular microtremor in man. *Experimental Brain Research*, 126(4), 556–562.
- St Cyr, G. J., & Fender, D. H. (1969). The interplay of drifts and flicks in binocular fixation. *Vision Research*, 9(2), 245–265.
- Steinman, R. M. (1965). Effect of target size, luminance, and color on monocular fixation. *Journal of Optical Society of America*, 55(9), 1158–1165.
- Steinman, R. M., Cunitz, R. J., Timberlake, G. T., & Herman, M. (1967). Voluntary control of microsaccades during maintained monocular fixation. *Science*, 155(3769), 1577–1579.
- Steinman, S. B., Steinman, B. A., & Garzia, R. P. (2000). *Foundations of Binocular Vision: A Clinical Perspective*. Maidenhead: McGraw-Hill.
- Stevenson, S. B., Sheehy, C. K., & Roorda, A. (2016). Binocular eye tracking with the Tracking Scanning Laser Ophthalmoscope. *Vision Research*, 118, 98–104.
- Straube, A., Scheuerer, W., & Eggert, T. (1997). Target velocity and age influence the initial smooth pursuit response in humans. *Neuro-Ophthalmology*, 18(4), 191–198.
- Švede, A., Treija, E., Jaschinski, W., & Krūmiņa, G. (2015). Monocular versus binocular calibrations in evaluating fixation disparity with a video-based eye-tracker. *Perception*, 44(8–9), 1110–1128.
- Świrski, L., Bulling, A., & Dodgson, N. (2012). Robust real-time pupil tracking in highly off-axis images. In *Proceedings of the Symposium on Eye Tracking Research and Applications* (pp. 173–176). Santa Barbara: ACM Press.
- Tabernero, J., & Artal, P. (2014). Lens oscillations in the human eye. Implications for post-saccadic suppression of vision. *PLoS ONE*, 9(4), e95764.
- Takagi, M., Frohman, E. M., & Zee, D. S. (1995). Gap-overlap effects on latencies of saccades, vergence and combined vergence-saccades in humans. *Vision Research*, 35(23–24), 3373–3388.
- Talasan, H., Scheiman, M., Li, X., & Alvarez, T. L. (2016). Disparity vergence responses before versus after repetitive vergence therapy in binocularly normal controls. *Journal of Vision*, 16(1), 1–19.
- Thiagarajan, P., Ciuffreda, K. J., & Ludlam, D. P. (2011). Vergence dysfunction in mild traumatic brain injury (mTBI): a review. *Ophthalmic and Physiological Optics*, 31(5), 456–468.

- Tian, J., Ying, H. S., & Zee, D. S. (2013). Revisiting corrective saccades: Role of visual feedback. *Vision Research*, 89, 54–64.
- Tomono, A., Iida, M., & Kobayashi, Y. (1990). A TV camera system which extracts feature points for non-contact eye movement detection. In *Optics, Illumination, and Image Sensing for Machine Vision* (pp. 2–12). Philadelphia: SPIE.
- Troyer, M. E., Sreenivasan, V., Peper, T. J., & Candy, T. R. (2017). The heterophoria of 3–5 year old children as a function of viewing distance and target type. *Ophthalmic and Physiological Optics*, 37(1), 7–15.
- van der Geest, J. N., & Frens, M. A. (2002). Recording eye movements with video-oculography and scleral search coils: A direct comparison of two methods. *Journal of Neuroscience Methods*, 114(2), 185–195.
- Van Horn, M. R., & Cullen, K. E. (2012). Coding of microsaccades in three-dimensional space by premotor saccadic neurons. *Journal of Neuroscience*, 32(6), 1974–1980.
- van Leeuwen, A. F., Collewijn, H., & Erkelens, C. J. (1998). Dynamics of horizontal vergence movements: interaction with horizontal and vertical saccades and relation with monocular preferences. *Vision Research*, 38(24), 3943–3954.
- van Leeuwen, A. F., Westen, M. J., van der Steen, S. J., de Faber, J. T., & Collewijn, H. (1999). Gaze-shift dynamics in subjects with and without symptoms of convergence insufficiency: influence of monocular preference and the effect of training. *Vision Research*, 39(18), 3095–3107.
- Van Rijn, L. J., Ten Tusscher, M. P. M., De Jong, I., & Hendrikse, F. (1998). Asymmetrical vertical phorias indicating dissociated vertical deviation in subjects with normal binocular vision. *Vision Research*, 38(19), 2973–2978.
- Villanueva, A., & Cabeza, R. (2007). Models for gaze tracking systems. *Journal on Image and Video Processing*, 2007(3), 023570.
- Von Noorden, G. K., & Campos, E. C. (2002). *Binocular Vision and Ocular Motility: Theory and management of strabismus* (6th ed.). St. Louis: Mosby.
- Webb, R. H., & Hughes, G. W. (1981). Scanning Laser Ophthalmoscope. *IEEE Transactions on Biomedical Engineering*, 28(7), 488–492.
- Westheimer, G. (1954). Eye movement responses to a horizontally moving visual stimulus. *Archives*

- of *Ophthalmology*, 52(6), 932–941.
- White, K. P., Hutchinson, T. E., & Carley, J. M. (1993). Spatially dynamic calibration of an eye-tracking system. *IEEE Transactions on Systems, Man, and Cybernetics*, 23(4), 1162–1168.
- Wick, B., & Bedell, H. E. (1989). Magnitude and velocity of proximal vergence. *Investigative Ophthalmology and Visual Science*, 30(4), 755–760.
- Winterson, B. J., & Collewijn, H. (1976). Microsaccades during finely guided visuomotor tasks. *Vision Research*, 16(12), 1387–1390.
- Wong, A. M. F. (2004). Listing's law: Clinical significance and implications for neural control. *Survey of Ophthalmology*, 49(6), 563–575.
- Wong, E. P. F., Fricke, T. R., & Dinardo, C. (2002). Interexaminer repeatability of a new, modified Prentice card compared with established phoria tests. *Optometry and Vision Science*, 79(6), 370–375.
- Woo, G. C. S. (1974). Temporal tolerance of the foveal size of Panum's area. *Vision Research*, 14(8), 633–635.
- Yang, D., Zhu, M., Kim, C. H., & Hertle, R. W. (2007). Vergence nystagmus induced by motion in the ground plane: Normal response characteristics. *Vision Research*, 47(9), 1145–1152.
- Yang, Q., Bucci, M. P., & Kapoula, Z. (2002). The latency of saccades, vergence, and combined eye movements in children and in adults. *Investigative Ophthalmology and Visual Science*, 43(9), 2939–2949.
- Yarbus, A. L. (1967). *Eye movements and vision*. New York: Plenum Press.
- Yoo, D. H., & Chung, M. J. (2005). A novel non-intrusive eye gaze estimation using cross-ratio under large head motion. *Computer Vision and Image Understanding*, 98(1), 25–51.
- Young, L. R., & Sheena, D. (1975). Survey of eye movement recording methods. *Behavior Research Methods & Instrumentation*, 7(5), 397–429.
- Yuan, W., & Semmlow, J. L. (2000). The influence of repetitive eye movements on vergence performance. *Vision Research*, 40(22), 3089–3098.
- Yuan, W., Semmlow, J. L., & Munoz, P. (2000). Effects of prediction on timing and dynamics of vergence eye movements. *Ophthalmic and Physiological Optics*, 20(4), 298–305.

## References

---

- Yuille, A. L., Hallinan, P. W., & Cohen, D. S. (1992). Feature extraction from faces using deformable templates. *International Journal of Computer Vision*, 8(2), 99–111.
- Zambarbieri, D. (2002). The latency of saccades toward auditory targets in humans. *Progress in Brain Research*, 140, 51–59.
- Zee, D. S., Fitzgibbon, E. J., & Optican, L. M. (1992). Saccade-vergence interactions in humans. *Journal of Neurophysiology*, 68(5), 1624–1641.
- Zee, D. S., & Levi, L. (1989). Neurological aspects of vergence eye movements. *Revue Neurologique*, 145(8–9), 613–620.
- Zhang, Z., & Cai, Q. (2014). Improving cross-ratio-based eye tracking techniques by leveraging the binocular fixation constraint. In *Proceedings of the Symposium on Eye Tracking Research and Applications* (pp. 267–270). ACM.
- Zhou, D., Ni, N., Ni, A., Chen, Q., Hu, D.-N., & Zhou, J. (2017). Association of visual acuity with ocular dominance in 2045 myopic patients. *Current Eye Research*, 42(8), 1155–1159.
- Zhu, M., Hertle, R. W., & Yang, D. (2008). Relationships between versional and vergent quick phases of the involuntary version-vergence nystagmus. *Journal of Vision*, 8(9), 1–11.
- Zuber, B. L., Stark, L., & Cook, G. (1965). Microsaccades and the velocity-amplitude relationship for saccadic eye movements. *Science*, 150(3702), 1459–1460.

